Buckling behaviour of stiffened steel plates under shear stress and normal stress

Author: Matthijs Blankendaal
Date: June 23, 2025

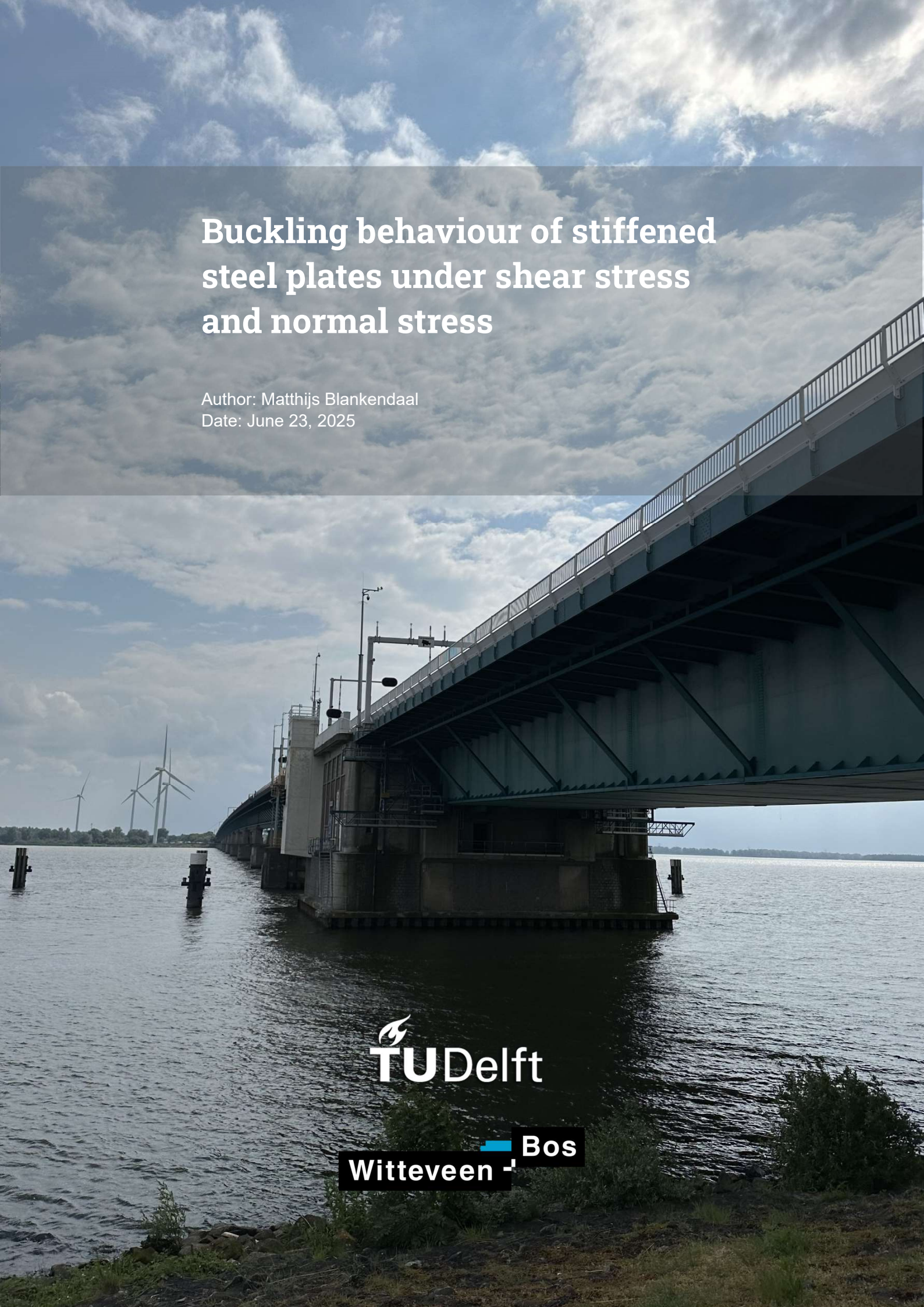

TU Delft

Witteveen + Bos

Buckling behaviour of stiffened steel plates under shear stress and normal stress

By

Matthijs Blankendaal

In partial fulfilment of the requirements for the degree of:

Master of Science
in Civil Engineering

at the Delft University of Technology,
to be defended publicly on Monday June 30, 2025

Student number:	5187389	
Thesis committee:	Prof. dr. M. Veljkovic	TU Delft, Chair
	Dr. T. Tankova	TU Delft, Daily supervisor
	Dr. ir. P.C.J. Hoogenboom	TU Delft, Committee member
	Ing. B.S. Hylkema MSEng. RC	Witteveen+Bos, Daily supervisor
	M. Aarsen MSc	Witteveen+Bos, Daily supervisor
Faculty:	Faculty of Civil Engineering and Geosciences, Delft	
Track:	Structural Engineering - Steel and Timber Construction	
Company:	Witteveen+Bos, Amsterdam	
Date	June 23, 2025	

“It always seems impossible until it’s done”
- Nelson Mandela -

Preface

Since I started studying my master Structural Engineering at the TU Delft, I have been fascinated by large steel structures of bridges. When I drove over one, I was impressed of the structure's scale, complexity and elegance. Steel bridges have not only captured my attention in recent years, but also that of a wider audience. The reason therefore is that steel bridges have frequently appeared in the news due to their age. Many bridges in the Netherlands are subjected to heavier loads than they were designed for. As a result it is necessary to recalculate and update the structural construction of these steel bridges.

My Master's thesis was carried out in partnership with the engineering firm Witteveen+Bos. This engineering firm is one of the companies that is working on the evaluation and recalculation of structurally outdated bridges. These structures often contain (un)stiffened steel plates that are subjected simultaneously by several internal forces. The following research topic in collaboration with my supervisors at Witteveen+Bos is defined as follows: the influence of tensile stress on the shear buckling of stiffened steel plates.

Hopefully, this thesis will contribute to improving our understanding of how tensile stresses influence the shear buckling behaviour of stiffened and unstiffened steel plates, which may support engineers in the structural evaluation of outdated steel bridges.

M.M.J.M. Blankendaal
Amsterdam, June 2025

Acknowledgements

I would like to express my gratitude to my graduation committee: Milan Veljkovic, Trayana Tankova and Pierre Hoogenboom for their valuable time and feedback during my thesis project. Special thanks to Trayana, who was always available to offer her insights and assistance during challenging moments.

In addition, I would like to praise the engineers from Witteveen+Bos for their time and for sharing their knowledge. Particularly, I am extremely grateful to my two Witteveen+Bos supervisors: Björn Hylkema and Mark Aarsen, who monitored my progress weekly, offered valuable insights and always tried to give me alternative solutions when I got stuck.

I would also like to thank my fellow students and friends Mike Mellaard and Adil Ayi at TU Delft. Our education journey started at the University of Applied Sciences in Amsterdam and now ends at TU Delft. I found our education far from easy, but having each other's as support helped me to successfully complete my Master's degree in Structural Engineering.

Finally, I would like to express my gratitude to my parents, who have supported me not only throughout my entire educational journey but also in my personal life. They provided me with the time and space to be in a position to successfully finish my education as a M.Sc. Structural Engineer. For this, I am truly grateful.

Abstract

In the Netherlands many existing steel bridges are being recalculated because they are, among other things, subjected to heavier loads than they were originally designed for. A lot of these steel bridges contain (un)stiffened steel plates that are simultaneously subjected to multiple internal forces. The combined shear-bending stress state is critical for the recalculation, as bending introduces both tensile and compressive stresses, which, in combination with shear, govern the buckling resistance of the (un)stiffened steel plates.

The aim of this thesis is to get a better insight of the influence of tensile stress, induced by bending, in combination with shear stress on the buckling resistance of (un)stiffened steel plates. To achieve this, a literature review (Part 1) and a parametric study (Part 2) were carried out in this thesis. Literature findings show that tensile stresses can potentially increase the buckling resistance of steel plates. The Eurocode provides a verification method, which is called the reduced stress method, to calculate plate buckling resistance. However, results of the parametric study in this thesis show that the reduces stress method does not take into account the positive contribution of tensile stresses on the buckling resistance.

An alternative method to calculate the buckling resistance of steel plates is to use the calculation software EBPlate, which computes several parameters that are used in the reduced stress method. When the reduced stress method is performed with the parameters that EBPlate has computed, the results change. The results show that EBPlate does take the positive influence of tensile stress into account, as evidenced by increased buckling resistance when tensile stress is introduced.

Finally, FEM calculations were made in RFEM for the same plate cases and stress states. The results also confirmed the positive influence of tensile stress on the buckling resistance. However, the calculations that were made with the reduced stress method in combination with EBPlate gave higher buckling resistance values compared to the RFEM calculations. Despite this, RFEM is considered to provide more accurate results due to its more refined modelling capabilities. Therefore, RFEM is assumed as the benchmark for realistic structural behaviour in this study. However, because FEM simulations take long, EBPlate remains a preferred tool in engineering practice due to its efficiency and ease of use.

To align EBPlate results with the results from RFEM, reduction formulas are developed in Chapter 9. These reduction formulas can be used in combination with EBPlate to offer conservative and safe estimates of the buckling resistance, thus matching or conservatively underestimating the buckling resistance compared to FEM results.

Contents

Nomenclature

Symbol	Definition
a	Distance between transverse stiffeners
a_c	Critical length for elastic buckling
a_{mn}	Displacement parameters or degrees of freedom
$A_{sl,1}$	Gross area of the stiffener
b	Height of the plate
b_{eff}	Effective height of the plate
b_1, b_2	Distances from plate edges to stiffener
c_s, c_i	Distance from plastic hinges to top and bottom flanges
D	Flexural rigidity of the plate
E	Young's modulus
F_{Ed}	Design load
F_{Rd}	Design resistance
f_y	Yield strength
f_{yw}	Yield strength in the web
h_f	Height of the plate
I_s	Second moment of area of the stiffener
k_σ	Plate buckling coefficient
k_τ	Shear buckling factor
m	Number of half sine waves in the plate
m_{max}	Maximum number of half-waves in x direction
n_{max}	Maximum number of half-waves in y direction
R_0	Initial stiffness matrix
R_G	Geometrical stiffness matrix
S	Stresses
S_{cr}	Critical stresses
t	Plate thickness
t_w	Web thickness
V_{cr}	Elastic buckling resistance
V_{pc}	Post-buckling resistance of plate girder
V_{pl}	Plastic shear resistance
V_u	Ultimate shear resistance
w_1	Amplitude of global imperfection
w_2	Amplitude of local imperfection
x	Longitudinal coordinate along the length of the plate
z	Vertical coordinate along the height of the plate
α	Aspect ratio
α_{cr}	Load amplifier factor for elastic critical state
$\alpha_{cr,x}$, $\alpha_{cr,z}$	Critical factors for longitudinal and transverse stresses
$\alpha_{cr,\tau}$	Critical factor for shear stress
α_u	Load amplification factor
$\alpha_{ult,k}$	Load amplifier factor for characteristic resistance
γ	Relative flexural stiffness of the stiffener
γ_{M1}	Partial safety factor
ΔU	Variation of strain energy of the plate

ΔW_{int}	Variation of internal work of critical stresses S_{cr}
η	Steel hardening factor
θ	Inclination of the web panel diagonal
λ_{rel}	Relative slenderness of the plate
$\overline{\lambda_p}$	Plate slenderness
ν	Poisson's ratio
ρ	Plate buckling reduction factor
ρ_{min}	Minimum reduction factor of ρ_x, ρ_z or χ_w
ρ_x, ρ_z	Reduction factors for longitudinal and transverse stresses
σ_{cr}	Critical plate buckling stress
$\sigma_{cr,sl}$	Elastic critical buckling stress of the stiffener
$\sigma_{cr,x}$, $\sigma_{cr,z}$	Critical longitudinal and transverse plate buckling stresses respectively
$\sigma_{eq,Ed}$	Equivalent stress
$\sigma_{x,Ed}$, $\sigma_{z,Ed}$	Design longitudinal and transverse stresses respectively
σ_t	Diagonal tension field stress
τ_{Ed}	Design shear stress
τ_{cr}	Critical shear buckling stress
φ	Inclination of the tension field
χ_w	Shear buckling factor of the web
ψ_x, ψ_z	Stress ratios for longitudinal and transverse respectively

1 Research framework

1.1 Context

Steel bridges that are built in the past need to be recalculated because nowadays more and heavier traffic is using these steel bridges. Slender steel plated structures are often used for long span box girder bridges. This is done because slender steel plated structures lead to low material consumption, optimization of their fabrication, low dead loads and a high utilization. Due to this high slenderness the steel plates tend to buckle[1].

On the cross section of these slender steel plated structures several internal forces are acting simultaneously. As a result, multiple multiaxial stress states can develop. Examples of this multiaxial stress state is the shear stress in combination with compression or tension stress. Often, during the recalculation of steel bridges the buckling due to shear of the steel plates do not satisfy the requirements that are described in the European standards. Therefore engineers needs to reinforce the existing structure with the use of new stiffeners. This represents a significant undertaking and involves substantial costs. Therefore, it may be worthwhile to explore alternative solutions.

Steel plates under shear stresses show reduced buckling resistance when also subjected to compression stresses and improved buckling resistance when also subjected to tensile stresses. As a result, a stiffened steel plate that is subjected to compression and shear does not fulfil the buckling requirements, unlike a stiffened steel plate that is subjected to tension and shear, see Figure 2 and Figure 1. This positive influence of tensile stresses on shear stress might be used improve the design rules in the current European standards[1].

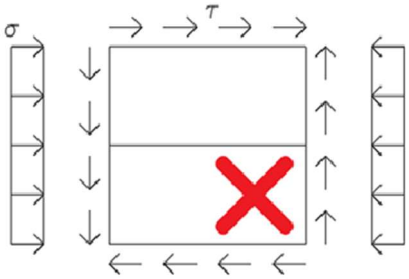

Figure 2 Stiffened steel plate under a shear-compression multiaxial stress state, which does not meet buckling requirements.

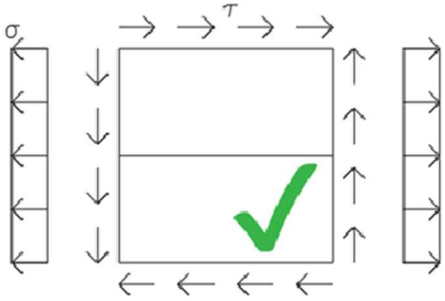

Figure 1 Stiffened steel plate under a shear-tension multiaxial stress state, which does meet buckling requirements.

1.2 Problem description

Based on recalculations and engineering assessments performed by Witteveen+Bos, there is evidence that the positive influence of tensile stresses on the plate buckling resistance under shear is not (fully) incorporated in the current design rules of the Eurocode. Steel plated structures are designed according to EN 1993-1-5 within the Netherlands. The EN 1993-1-5 states that steel plate structures can be designed by using the finite element method, the effective width method and the reduced stress method. In order to understand why the design methods provided in the Eurocode do not take into account the influence of tensile stresses on the shear buckling resistance of steel plates, the background and theoretical assumptions behind these methods are examined in this report. In this thesis the main focus is on steel plates subjected to tension stress and shear stress. The effective width method does not take the influence of tensile stresses in a cross-section into account when a cross-section is loaded due to tensile stress and shear stress.

In contrast to the effective width method, the reduced stress method does take into account the combined effect of tensile and shear stress in the verification process. This theoretically allows for taking into account the positive effect of tensile stress on the buckling behaviour. In addition to the reduced stress method, calculation tools such as EBPlate in combination with the reduced stress method and FEM models can also be used to determine the buckling resistance of steel plates.

This phenomenon came to light with the recalculation of existing bridges, but can be drawn more broadly to new steel bridges as well. If the positive influence of the tensile stress on the shear plate buckling resistance of steel plate structures are substantial, then there is a possibility that the steel plate structures can be designed more economical whereby the slenderness of the plates can be reduced and/or no stiffeners are needed in the steel plate design. Which lead to economic and environmental advantages in new and existing steel structures.

1.3 Research questions

Based on the problem description, the main research question is formulated as follows:

"How to consider the effect of tensile stress on the shear buckling resistance of stiffened steel plates with varying normal stress distributions and geometric parameters in an accurate analytical approach."

Sub-questions are formulated in order to answer the main research question:

1. What is the influence of tensile stress due to bending on the shear buckling of stiffened steel plates?
2. How does the Eurocode and literature studies take the impact of tensile stress due to bending into account on the shear buckling resistance of steel plates?
3. How does EBPlate, in combination with the reduced stress method and FEM models, compare to the reduced stress method alone in accounting for the influence of tensile stresses on the buckling resistance of steel plates?
4. What model parameters influence the buckling behaviour of (un)stiffened steel plates?

The first two sub-questions will be dealt with in the literature review. The second part of this thesis, parametric study, will focus on the last two sub-questions.

1.4 Structure of the thesis

This thesis is subdivided into three parts: Literature review - Parametric study - Research outcome. For each part, a description is provided below. The corresponding outline of the thesis is shown in Figure 3.

Part I – Literature Review
A literature review is performed to obtain state-of-the-art knowledge about buckling behaviour of steel plates. First, the influence of tensile stress on steel plate buckling is researched more in-depth. Second, three methods for calculating the buckling resistance of steel plates are discussed: the reduced stress method according to the Eurocode, the reduced stress method in combination with EBPlate and FEM models."

Part II - Parametric Study
The second part of this thesis is dedicated to a parametric study focusing on the buckling resistance of unstiffened and stiffened steel plates. The buckling resistance is calculated using three different approaches previously described in the literature review: the reduced stress method, the reduced stress method in combination with EBPlate and FEM. A separate chapter is provided for each approach where a brief introduction and methodology is presented. Part 2 starts with a chapter outlining the parameters used in the

study, followed by three chapters that address each approach separately.

Part III – Research Outcome

The third part of this thesis starts with chapter 8, where the results from all three approaches are presented side by side for comparison. In chapter 9 a new design approach is developed based on the results in chapter 8. Next, the interpretation of the results, application and limitations are discussed. At last, conclusions are drawn and recommendations are given.

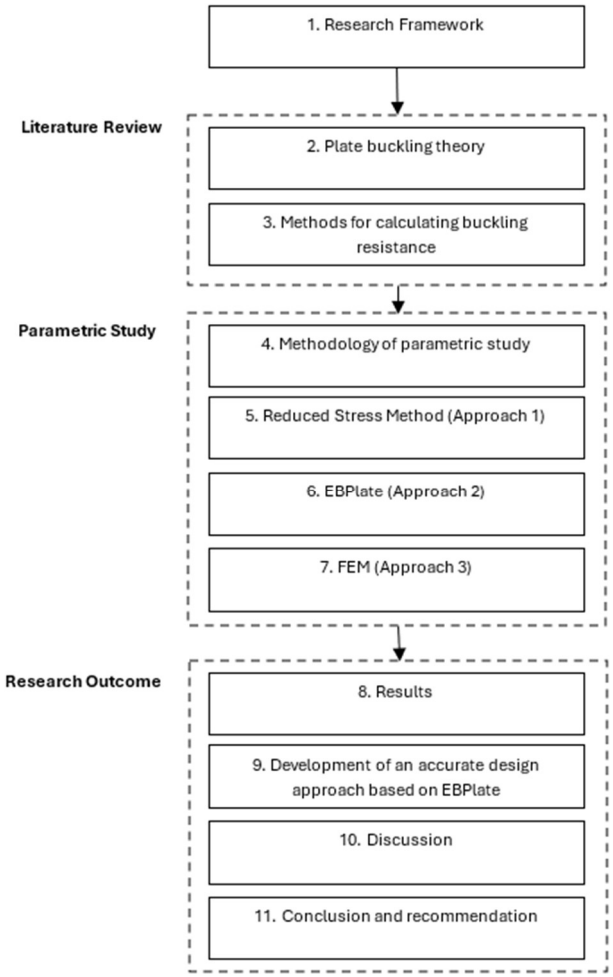

Figure 3 Thesis outline.

Part 1
Literature review

2 Plate buckling theory

2.1 Introduction

Buckling is a type of failure that occurs in structures that have high stiffness in one direction and relative low stiffness in the other direction. When a load is applied in the stiff direction, the structure shows sudden instability or failure in the weaker direction. This is a phenomenon, which is commonly observed in slender structures such as columns and plates.

Plate buckling is a failure mode that can occur when a plate is subjected to compressive and/or shear loads, which results in an out-of-plane deformation. The Eurocode provides guidelines on how to account for plate buckling and how to incorporate it into design calculations. The underlying principles behind the design rules are first in this chapter addressed prior to the next chapter, where is described on how the Eurocode takes into account plate buckling failure. First the buckling behaviour of plates under compressive loads will be discussed in Section 2.2 and second the behaviour of plates subjected to shear loads will be discussed in Section 2.3.

2.2 Plates loaded in compression

2.2.1 Plate vs column-like behaviour

Plate buckling is a complex phenomenon, characterized by nonlinear stress behaviour, load shedding effects and effects of boundary conditions. A distinction is made between plate-like behaviour and column-like behaviour when looking into the post-buckling behaviour of steel plates that are subjected to longitudinal stresses. In contrast to column-like behaviour, where the ultimate load equals the critical load, plate-like behaviour in steel plates may have a post-buckling strength reserve, which allows the ultimate load to exceed the critical load, see Figure 4.

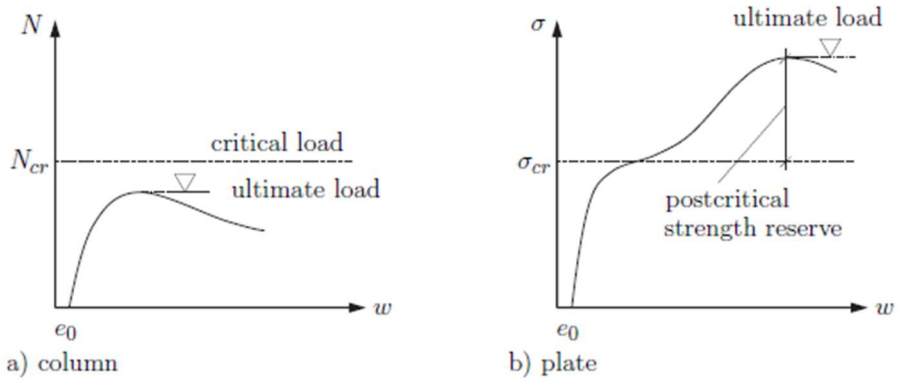

Figure 4 Comparison of column and plate buckling[1].

An analogy to a grillage model is used to explain the postcritical strength reserve, which is displayed in Figure 5. In the grillage model, the continuous plate is replaced by columns in x-direction and ties in y-direction. Under loading on the x – edges, the columns will buckle. The ties are stretched as the columns buckle outward, thus restraining the motion and providing post buckling reserve. The plate can continue to carry loads around the buckle through the edges that are parallel to the applied load. The grillage model effectively illustrates the source of post-buckling strength and how longitudinal stresses are redistributed as a result[2].

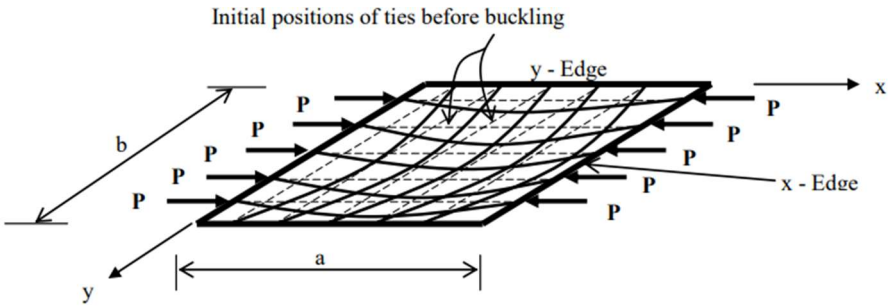

Figure 5 Post-buckling model of a thin plate under in-plane loads[2].

Building upon this grillage model, a more detailed explanation of the actual stress redistribution by illustrating the effect of edge stiffness and boundary conditions, is shown in Figure 6. Before buckling of the plate occurs, the compressive stresses are equally distributed over the plate width, see Figure 6a. As illustrated by the earlier explanation of the grillage model, it can be seen that due to higher stiffness near the edges, the applied stresses redistribute nonlinearly and reach higher stress values near the edges. Tensile membrane stresses occur perpendicular to the loading direction but the amount of these stabilizing membrane stresses depends on the edge boundary conditions. In Figure 6b the stress distribution is shown with unconstrained edges. An unconstrained edge boundary condition defines an edge which is free to move in-plane. In Figure 6c the stress distribution is shown with constrained edges. A constrained edge boundary condition defines an edge which remains straight[3].

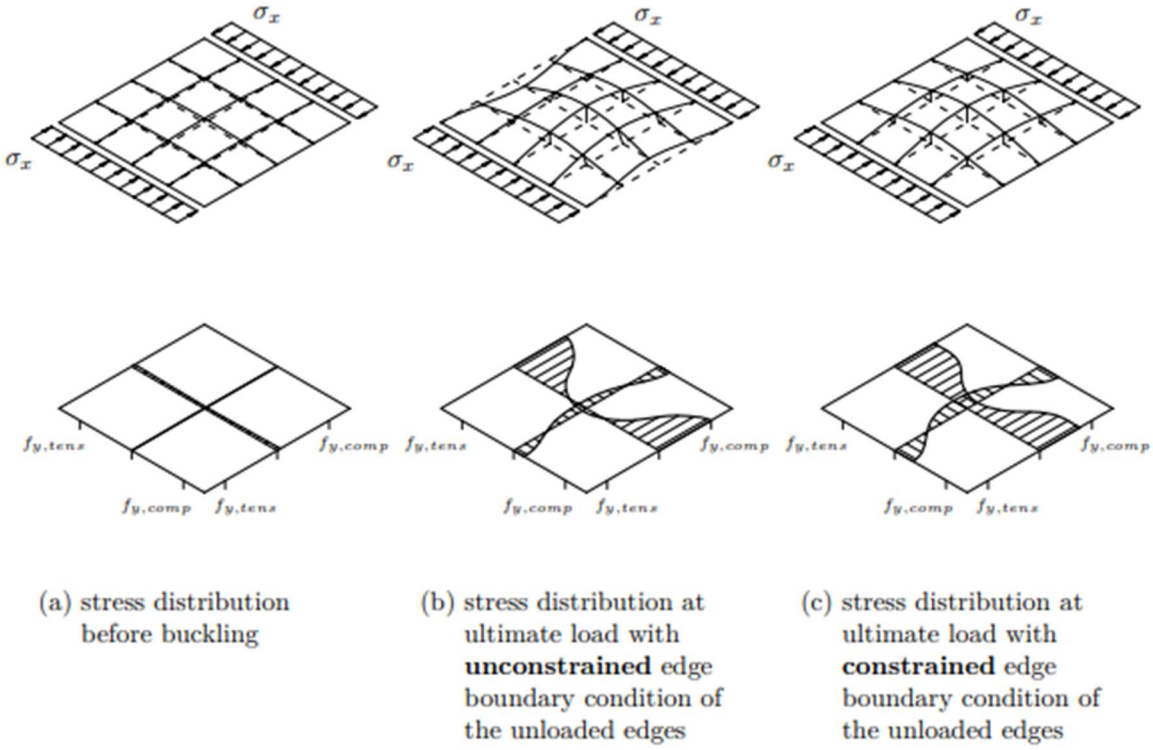

(a) stress distribution before buckling

(b) stress distribution at ultimate load with **unconstrained** edge boundary condition of the unloaded edges

(c) stress distribution at ultimate load with **constrained** edge boundary condition of the unloaded edges

Figure 6 Stability behaviour of a single plate subjected to longitudinal stresses[3].

As can be seen in Figure 6 the boundary conditions of the plate play a major role in governing column or plate-like behaviour. Apart from the boundary conditions, the aspect ratio a/b also decides if a plate behaves column-like or plate-like buckling behaviour. Plates with a low aspect ratio would behave more column-like behaviour. The EN 1993-1-5[4] states that for aspect ratios a/b < 1 column type of buckling may occur and the column behaviour check must be performed. Figure 7 shows in which cases column type buckling may occur. It must be noted that postcritical strength reserve only occurs when plate-like behaviour is dominating. When there is column like behaviour dominating, the plate is behaving like a column, therefore benefits of postcritical strength reserves are not taken into account. To determine if column-like behaviour, plate like behaviour or an interaction between plate-like and column-like behaviour is governing in a plate an interpolation formula is used. This formula is presented in Section 3.3.3.

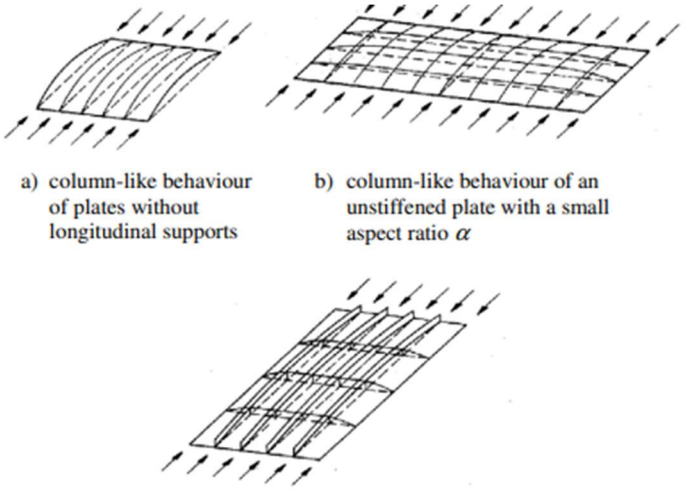

Figure 7 Column-like behaviour[4].

2.2.2 Euler plate buckling

In structural design, it is necessary to check if the plate under compression will buckle before reaching its maximum material strength. This is particularly important for slender elements, such as thin steel plates, which are very sensitive to buckling. The concept is that although the material might be able to carry a stress up the yield strength, a thin plate will usually buckle before at a lower stress level known as the critical buckling stress. To take this into account, no check is done against the yield strength but instead a reduced value is therefore used that depends on the plate's geometry and material. This done by using a reduction factor, which reduces the yield stress based on how slender the plate is. This means the plate is only allowed to carry a lower stress, which is safe against buckling.

$$\sigma_{cr} = \rho * f_y \tag{2.1}$$

Where

- σ_{cr} is the critical plate buckling stress
- ρ is the plate buckling reduction factor
- f_y is the yield stress

The reduction factor depends on the relative slenderness of the plate, which is a way to describe how 'thin and long' the plate is compared to its strength.

$$\lambda_{rel} = \sqrt{\frac{f_y}{\sigma_{cr}}} \tag{2.2}$$

Where

- λ_{rel} is the relative slenderness of the plate

Eq. (2.1) and Eq. (2.2) can be combined to express the reduction factor as a function of the plate relative slenderness, see Eq. (2.3). If a plate is very slender, the relative slenderness is high, which results in a small reduction factor and therefore a lower allowable stress.

$$\rho = \frac{\sigma_{cr}}{f_y} = \frac{1}{{\lambda_{rel}}^2} \tag{2.3}$$

The first contribution to buckling theory was made by Euler, who derived the linear elastic buckling load for an ideal, axially compressed column[5]. This fundamental concept can be extended to the buckling behaviour of plates. The critical plate buckling stress of a plate that is subjected to longitudinal compression stresses, see Figure 8[6], can be described by the Euler based formula shown in Eq. (2.4).

$$\sigma_{cr,p} = k_\sigma * \frac{\pi^2 * E}{12 * (1 - \nu^2)} * \left(\frac{t}{b}\right)^2 \tag{2.4}$$

Where

- $\sigma_{cr,p}$ is the critical plate buckling stress
- k_σ is the buckling coefficient
- E is the elastic modulus
- ν is the Poisson's ratio
- t is the thickness of the plate
- b is the height of the plate

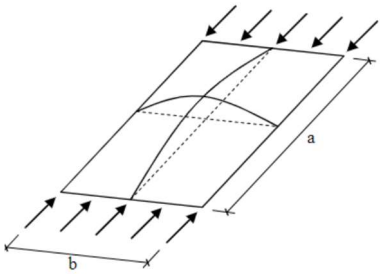

Figure 8 Definition of a single plate subjected to longitudinal compression stresses[6].

The buckling factor depends on the support condition, stress ratio and aspect ratio, and is given in Eq. (2.5). However, the aspect ratio of the plate is not considered in the Eurocode. Instead a minimum value of 4 is assumed. This is a conservative simplification because for both low and high aspect ratios the buckling factor can be significantly higher, as illustrated in Figure 9[7].

$$k_\sigma = \left(\frac{m}{\alpha} + \frac{\alpha}{m}\right)^2 \tag{2.5}$$

Where

- m is the amount of half sine waves in the plate
- α is the aspect ratio

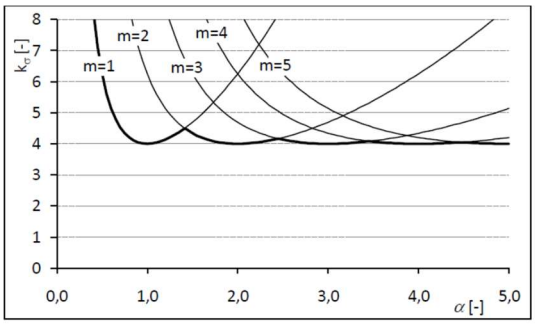

Figure 9 Buckling factor for a simply supported plate as a function of aspect ratio[7].

2.2.3 Von Kármán plate buckling

As described in Section 2.2.1, the stress distribution in a plate subjected to compressive stresses is nonlinear and complex. The critical plate buckling stress, which is based on Euler's formula is an approximation that assumes a linear stress distribution across the plate width as the load increases. To take this phenomenon of redistribution of stresses into account, the effective width method was introduced by Von Kármán in 1932[8]. This method simplifies the complex nonlinear stress distribution of a plate that is subjected to compression stresses. The method models the plate as an idealized strip with a specific thickness and an effective width, in which the critical stress reaches the yield strength of the steel[7]. The real stress distribution is approximated by the two outer strips that carry the yield stress. The total width of these strips defines the plate's effective width, which is shown in Figure 10. The reduction factor in this method is derived by equating the critical buckling stress of the plate calculated using the standard width to the yield strength of the steel calculated using the effective width. By replacing the standard width with the effective width in the buckling formula, we obtain the following expression:

$$f_y * \left(\frac{b_{eff}}{t}\right)^2 = k_\sigma * \frac{\pi^2 * E}{12 * (1 - \nu^2)} = \sigma_{cr} * \left(\frac{b}{t}\right)^2 \quad (2.6)$$

Where

- b_{eff} is the effective height of the plate

Equation (2.6) can be simplified into Equation (2.7), which can then be further simplified to Equation (2.8).

$$\frac{b_{eff}}{b} = \sqrt{\frac{\sigma_{cr}}{\lambda_{rel}}} \quad (2.7)$$

$$\rho = \frac{1}{\lambda_{rel}} \quad (2.8)$$

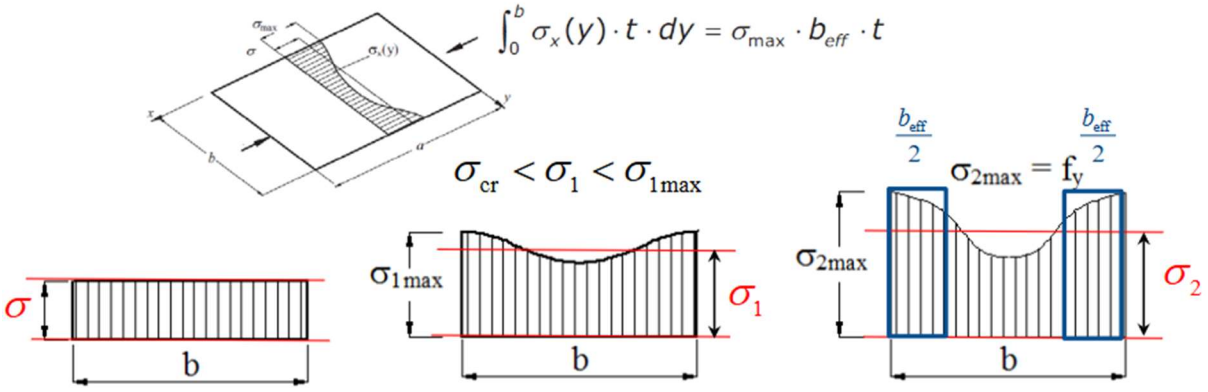

Figure 10 Effective width concept[6].

2.2.4 Winter plate buckling

The effective width method that Von Kármán proposed did not take into account the effect of initial imperfections of the plate, such as residual stresses[7]. The effective width method based on Von Kármán theory showed different results in comparison with experimental results for small b/t ratios. The initial imperfections for plates with small b/t ratios do have a high impact on the buckling behaviour. Therefore, Winter developed a new formula to calculate the effective width, that does take into account the initial imperfections, see Eq. (2.9).

$$\frac{b_{eff}}{b} = \sqrt{\frac{\sigma_{cr}}{\lambda_{rel}}} * \left(1 - 0{,}22 * \sqrt{\frac{\sigma_{cr}}{f_y}}\right) = \frac{\lambda_{rel} - 0.22}{\lambda_{rel}^2} \qquad (2.9)$$

The Winter reduction factor is used in EN 1993–1-5:2006 for plate buckling calculations.

2.3 Plates loaded in shear

In the previous chapter, the buckling behaviour of a plate subjected to longitudinal compressive stresses was described. The plate tends to buckle which is a well-known phenomenon in structural engineering. A similar instability can occur when the plate is loaded in shear, often referred to as shear buckling. A square element in the plate, whose edges are oriented at 45° to the plate edges, experiences tensile stresses on two opposite edges and compressive stresses on the other two edges. The compressive stresses lead to local buckling of the element. As a result, the plate deforms out of plane in a wave-like pattern perpendicular to the compressive stress direction. The resulting wave formation is typical for plates that have buckled under shear loading[9], see Figure 11.

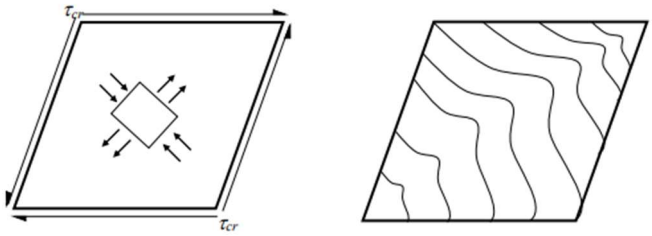

Figure 11 Shear buckling of a plate[9].

Although plates may buckle under shear, this does not necessarily mean they have failed. If we draw imaginary diagonals on the plate, the diagonal which gets loaded in compression buckles and cannot support

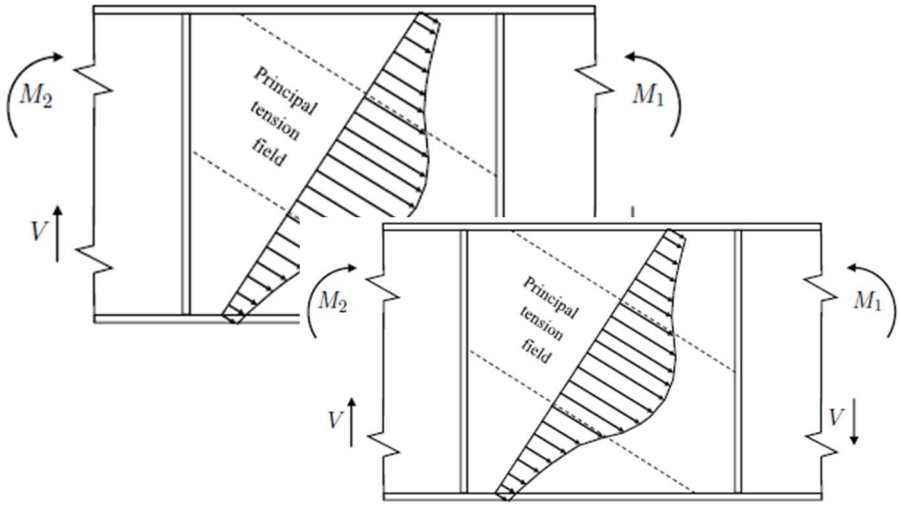

Figure 12 Tension field action[10].

additional load. However, the diagonal in tension continues to take more load and the plate becomes like a

triangular truss with only tension diagonals[9]. This is called tension field action and can be shown with the use of Figure 12[10]. After a plate experiences elastic shear buckling, compressive stresses decrease, and tensile stresses (or tension fields) take over. These tension fields redistribute the load, enhancing the post-buckling strength of the plate. As a result, the plates subjected to combined tension and shear have improved stability because the tensile forces counteract the destabilizing effects of shear-induced compressive stresses.

Three phases can be identified in the shear loading of a plate girder to failure[11], see Figure 13. First is the linear elastic stage, where the web resists the shear through small deformations and exhibits linear stiffness. Second is Post-buckling Stage I, where the web begins to buckle and deform along the compression diagonal and the shear stiffness reduces progressively. Lastly, in Post-buckling Stage II, the web yields and the stiffness drops significantly as plastic mechanisms develop. In this stage, three different responses may occur based on how the flanges, stiffeners and post-yield web behaviour contribute to the resistance.

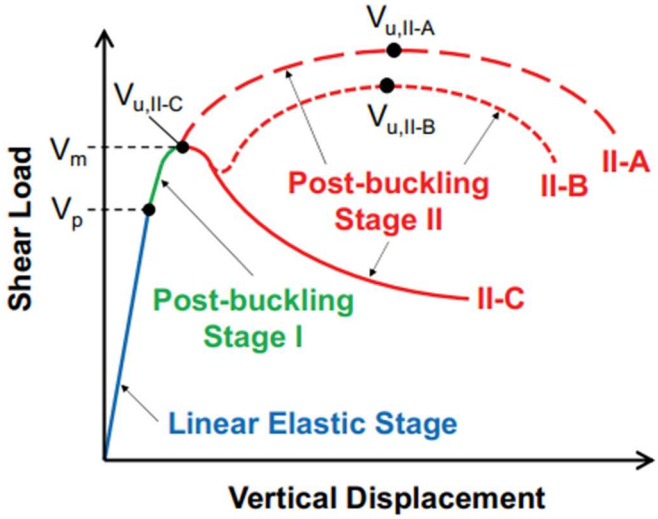

Figure 13 Typical vertical load-displacement of slender plate girders up to shear failure[11].

In Stage II-A, shear resistance keeps increasing but at a lower rate because of the ongoing activation of the flanges and stiffeners after yielding, which is a type of positive hardening. In stage II-B resistance falls off at first upon yielding but increases once more as the web experiences strain hardening and stiffeners or flanges become more resistant. In stage II-C is where there can no longer be any additional resistance that is built up after there has been yielding because stiffeners and flanges are no longer able to offer enough support. This results in a steady drop in resistance as deformation continues and failure is achieved.

2.3.1 Basler model

Basler confirmed with experiments for the first time the stress distribution of the tension field that develops in a thin plate girder with transverse stiffeners[12]. The Basler model is displayed in Figure 14 and is based on two assumptions. The first assumption is that the flanges are not able to anchor the tension field because the flanges are assumed to be too flexible. The second assumption is that the buckling shear stress even after elastic buckling is uniformly distributed over the web. In the stage of elastic buckling the flat web plate loaded in pure shear will have principal stresses that are equal to the critical shear stress acting at a 45◦ angle[13]. The critical stress for a simple supported web panel is given by Eq. (2.10). Where the shear buckling factor depends on the aspect ratio of the web panel.

$$\tau_{cr} = k_\tau * \sigma_e = k_\tau * \frac{\pi^2 * E}{12 * (1 - \nu^2)} * \left(\frac{t}{b}\right)^2 \quad (2.10)$$

Where

- τ_{cr} is the critical shear buckling stress
- k_τ is the shear buckling factor
- E is the elastic modulus
- ν is the Poisson's ratio
- t is the thickness of the plate
- b is the height of the plate

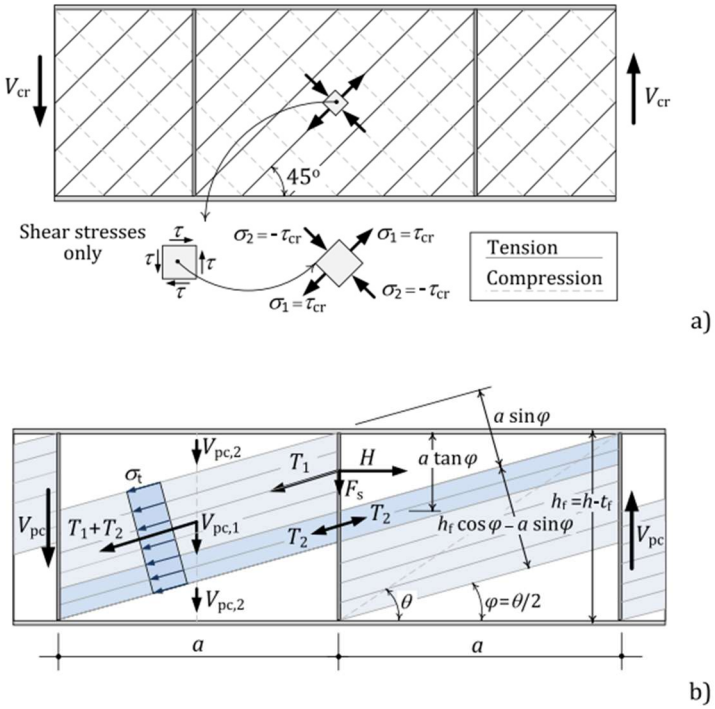

Figure 14 Basler model: a) pre-buckling stage – pure shear stress state of the web plate, and b) post-buckling stage – tension field action at an angle φ = θ/2 to maximize the post buckling resistance[13].

The flanges have practically no influence of the shear buckling resistance in the Basler model. Therefore, the post-buckling resistance is calculated using a tension field action which is only anchored in the transverse stiffener. As a result, the maximum post-buckling shear resistance can be calculated as a function of the diagonal tension field stress, which can be evaluated using the von Mises yield criterion. This post-buckling resistance combined with the elastic buckling resistance gives the ultimate shear resistance of a plate girder according to the Basler model[13], see Eq. (2.11).

$$V_u = V_{cr} + V_{pc} = \left(\tau_{cr} + \frac{(f_y - \sqrt{3} * \tau_{cr})}{2 * \sqrt{1 + \alpha^2 + \alpha}} \right) * h_f * t_w \qquad (2.11)$$

Where

- V_u is the ultimate shear resistance
- V_{cr} is the elastic buckling resistance
- V_{pc} is the post-buckling resistance of the plate girder
- f_y is the yield stress
- α is the aspect ratio of the web
- h_f is the height of the plate
- t_w is the thickness of the web

2.3.2 Cardiff model

Later experimental research at Cardiff University demonstrated that plate girder flanges can participate in

localized bending , which lead to contributions of the flanges to the post buckling resistance of slender webs[14]. The Cardiff model, which is shown in Figure 15, states that the tension field is anchored to both the stiffener and the flange, and that the formation of plastic hinges at the flange-to-stiffener joints and in the flanges, at the tension field width's edge, impacts the ultimate post-buckling resistance[15].

When the web panel is subjected to the critical shear stress it can no langer resist any additional compressive loading and web load carrying system changes. In this case, the shear load is redistributed and is carried by a diagonal tension field σ_t in the web, see Figure 15. This tension field is anchored in the flanges an acts as a membrane, which results in causing the flanges to bend inward. This process is depended by the stiffness

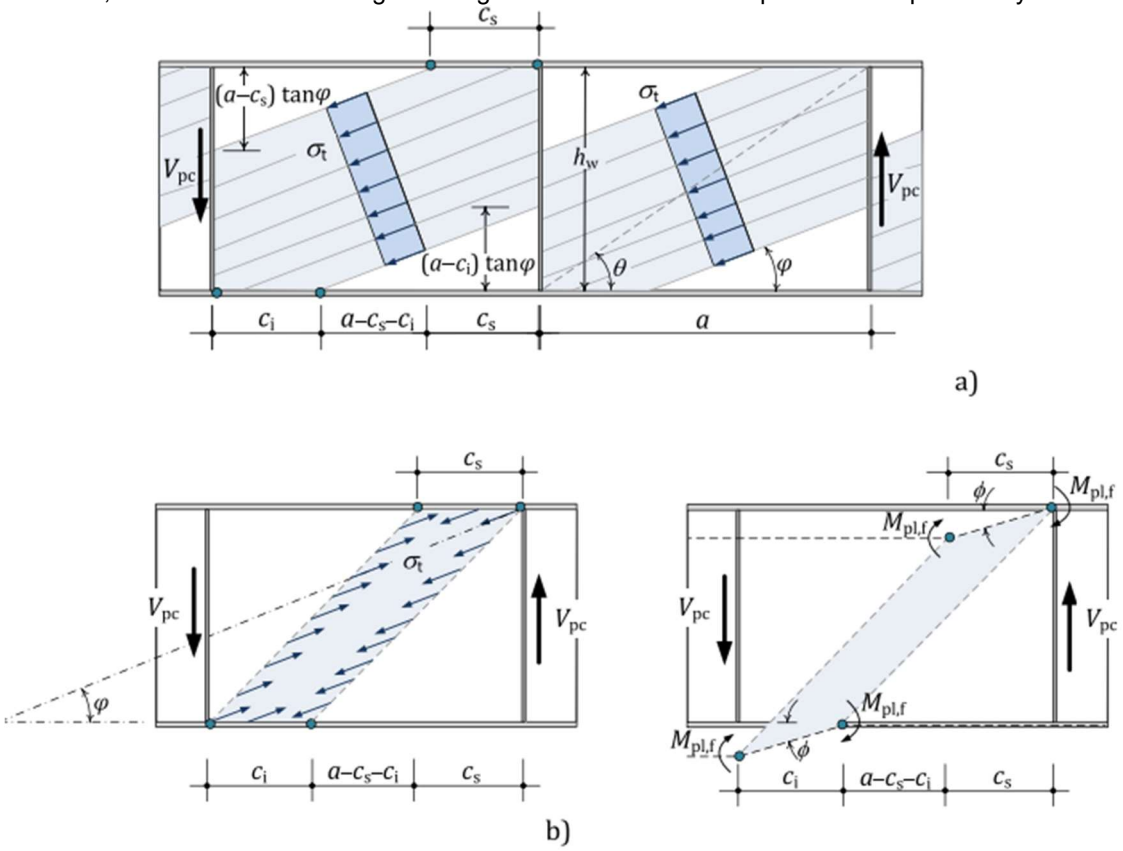

Figure 15 Cardiff model: a) post-buckling stage – tension field action at an angle φ to be determined, and b) failure mode of the plate girder panel for pure shear[13].

of the flanges.

The girder will fail because of yielding in the web in combination with the formation of four hinges in the flanges. As a result, the ultimate shear resistance of a plate girder according to the Cardiff model is given by Eq. (2.12). In the equation can be seen that the ultimate resistance of the plate girder consist out of three contributions, which are the pre-buckling resistance, the web post-buckling resistance and the flange contribution to shear resistance.

$$V_u = V_{cr} + V_{pc} = \left[\tau_{cr} + \sigma_t * (\sin\varphi)^2 + \left((cot\varphi - \cot\theta) + \frac{1}{h_w}(c_s + c_i)\right)\right] * h_w * t_w \qquad (2.12)$$

Where

- σ_t is the diagonal tension field stress
- φ is the inclination of the tension field
- θ is the inclination of the web panel diagonal
- c_s and c_i is the distance of plastic hinges on the top and bottom flange

2.3.3 Höglund model

Basler and Cardiff models determine the ultimate shear resistance by adding the elastic shear buckling resistance and the post-buckling resistance, which is defined differently in each model. Therefore both models assume the presence of two simultaneously stress fields acting in the web panel with different inkling angles,

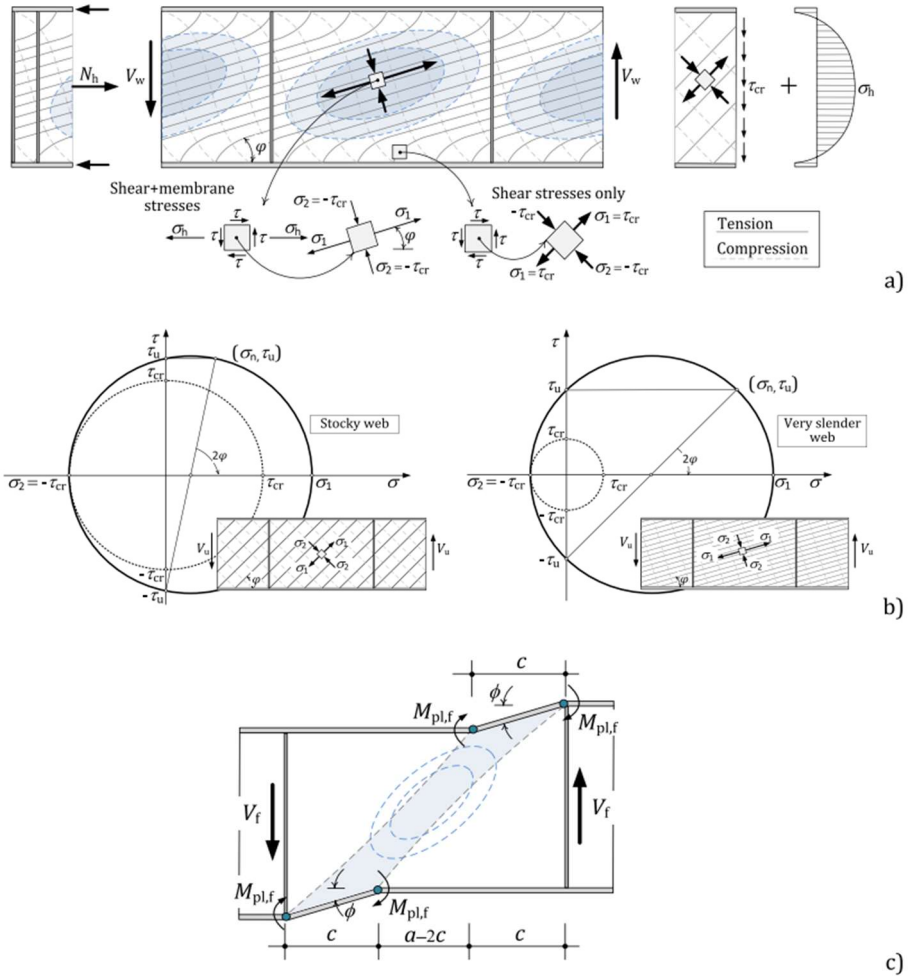

Figure 16 Höglund model: a) post-buckling stage – rotated stress field action; b) Mohr circle of the stress state at the middle of the web plate at failure; and c) plastic mechanism assumed at failure[13].

which is a physically unrealistic assumption. To solve this unrealistic assumption, Höglund proposed a model where the Cardiff tension field model was replaced by the rotated stress field model, which led to good agreement with experimental tests[16], see Figure 16.

Höglund replaced the Cardiff tension field model with the rotated stress field model, which assumes only one consistent stress field throughout the web panel after buckling. The compressive stress remains equal to the critical shear buckling stress but is considered as part of a rotated principal stress state. The post-buckling resistance of the web is therefore calculated based on this rotated stress field, which satisfies the von Mises yield criterion using a single set of principal stresses with a consistent orientation13[13]. As a result, the web shear resistance according to the Höglund model using the web modified slenderness is given in Eq. (2.13).

$$V_u = \tau_{cr} * h_w * t_w = \chi_w * h_w * t_w * f_{yw}/\sqrt{3} \qquad (2.13)$$

Where

- χ_w is the shear buckling factor of the web
- f_{yw} is the yield stress in the web

The ultimate shear resistance is limited to the web's plastic shear resistance to ensure that the calculated capacity does not exceed the actual material strength of the web. Although post-buckling effects and tension field actions can increase the shear resistance beyond the elastic buckling load, the web cannot sustain shear stresses beyond its plastic limit without failure. Therefore, the shear resistance is limited at the plastic shear capacity to reflect the true load-carrying capacity of the web panel, see Eq. (2.14).

$$V_w = V_w + V_f \leq V_{pl} = \frac{\eta * f_{yw} * h_w * t_w}{\sqrt{3}} \tag{2.14}$$

Where

- V_{pl} is the plastic shear resistance
- η is the steel hardening factor

Höglund's rotated stress field model is used in EN 1993–1-5:2006 for web shear buckling calculations.

2.4 Global vs local buckling

Stiffened plate buckling can be divided into two types of buckling: global buckling and local buckling. Global buckling involves the entire plate deforming as a single entity. Local buckling occurs in small sections, such as individual panels within a larger structure, where parts buckle independently. Figure 17 and Figure 18 illustrates the difference between global buckling and local buckling using the example of a stiffened plate[17]. When buckling occurs, the structural member's capacity depends whether the buckling is global or local, and whether the structure provides any post-critical load capacity[18].

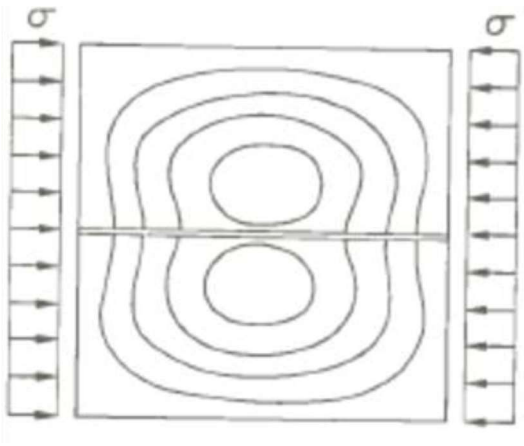

Figure 17 Global buckling of stiffened steel plate subjected to compression[17].

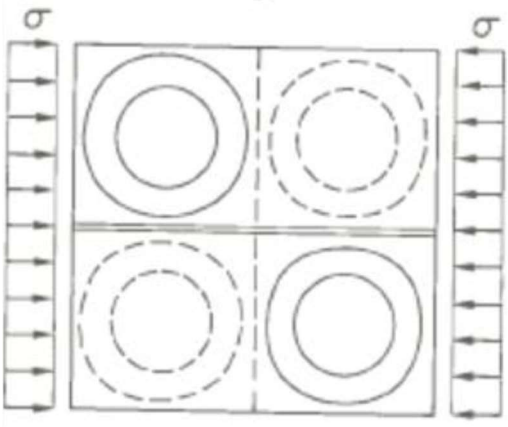

Figure 18 Local buckling of stiffened steel plate subjected to compression[17].

3 Methods for calculating buckling resistance

3.1 Introduction

In the Netherlands, the EN 1993-1-5[4] is used for calculating plate buckling in steel structures because the standard is part of the Eurocodes, which is a set of standardized European design rules. The standard is legally required under the Dutch Building Code to meet Dutch construction regulations and ensure the safety and reliability of structural designs in the Netherlands. The EN 1993-1-5 provides a reliable and efficient design method for steel structures because it is based on extensive research, offers standardized calculations for plate buckling, and is widely recognized and implemented in engineering practices, ensuring consistency and safety in structural design.

The EN 1993-1-5 provide two different methods for the design of slender plates, in addition to the option of using the finite element method. The first method is called the effective width method and is described in great detail in the Eurocode. The second method is called the reduced stress method, which is less commonly used in the engineering community. In Section 3.2, the differences between these two methods are discussed, and then in Section 3.3, a more detailed explanation of the reduced stress method is provided, because it is the method applied throughout this thesis. The reasoning for this choice is also presented in Section 3.2.

For the calculation of the buckling resistance of steel plates using the reduced stress method, the minimum load amplifier, is used in the calculation. This factor represents the minimum load amplifier for the design loads to reach the elastic critical load of the plate and can be calculated for very common cases obtained from formulas or specific charts found in EN 1993-1-5, which are based on simplified assumptions. However, these assumptions are often far from reality and tend to be conservative. Furthermore, these charts may not be applicable to more complicated situations because they are restricted to a limited number of configurations, such as particular geometries, stiffener properties and stress distributions[19].

Nowadays, specialized software tools can be used to calculate the critical buckling coefficient with greater accuracy. EBPlate is a tool that offers values for elastic critical stresses in a far wider range of real-world situations than traditional design aids. EBPlate is a popular tool in the engineering community because it has an user-friendly graphical interface and is free of charge. Section 3.4 offers a more thorough description of the EBPlate software and how it was used in this thesis.

The buckling resistance of steel plates can be determined as well using the finite element method (FEM), in addition to analytical techniques and software programs such as EBPlate. This numerical approach allows for detailed modelling of complex geometries, boundary conditions, and loading situations, offering a high level of accuracy. In Section 3.5 the application of FEM for this purpose is further discussed.

3.2 Difference between effective width method and reduced stress method

The effective width method and the reduced stress method do have a fundamental difference in the approach for determining an approximation for the real stress distribution. The reduced stress method checks at which stress level individual plate parts within a cross-section begin to buckle. When a cross-section consists of multiple plate parts, the lowest critical buckling stress governs the behaviour of the entire cross-section. As long as the applied stress does not exceed this critical stress, the section can be treated as Class 3. Class 3

cross-sections are defined as those in which the stress in the extreme compression fibre, under an assumed elastic stress distribution, can reach the yield strength, but local buckling may still prevent the full development of the plastic moment resistance. The usual cross-section verifications can be used, only with the yield stress multiplied by a reduction factor[7]. The reduction of the allowable stresses in comparison with the full strength is a function of the slenderness of the regarded plate. For the reduced stress method according to EN 1993-1-5 the determination of the plate slenderness is based on the complete stress field, resulting in a unique plate slenderness without the differentiation for the single acting forces. Figure 19 shows the assumed stress-distribution for an I-shaped cross-section loaded by a bending moment for both methods[20].

In contrast to the reduced stress method, the effective width method assumes that load shedding between cross-section elements is possible[22]. Load shedding refers to the redistribution of the load that was previously carried by a buckled part of the plate to other, non-buckled parts of the plate. As a result, other parts of the plate may also reach their buckled state[7]. The effective width method is founded on the reduction of the cross section due to local buckling of the subpanels between the stiffeners and global buckling. This verification is performed for axial force, shear force, bending moment and transverse force separately. In case multiple forces are acting simultaneously on the cross section, interaction formulas are used. The advantage of this method is that the method takes into account the stress redistribution between the panels. The disadvantage of this method is that it does not provide an option for verifying steel plates that are subjected to tension and shear stress simultaneously because the individual loads are in the first step considered separately[1].

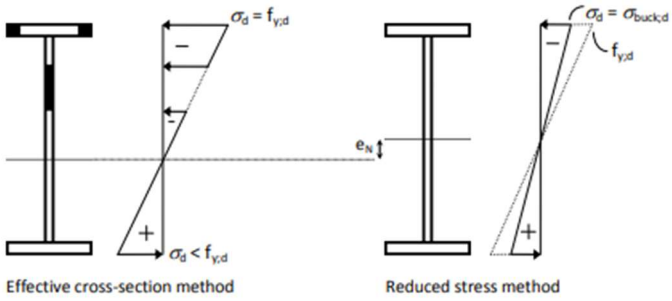

Figure 19 Assumed stress distribution for Effective width method and reduced stress method[7].

In this thesis the main focus is on steel plates subjected to tension stress and shear stress. In contrast to the effective width method, the reduced stress method accounts for the combined effects of these loads in the verification process. Therefore the reduced stress method is used in this thesis and is described in detail in the next chapter.

3.3 Reduced stress method

3.3.1 Introduction

The Eurocode EN 1993-1-5 provides the formulas used in the Reduced Stress Method, which forms the basis for the stress distribution and design rules of plated structural elements. With the use of the two following books: Commentary and Worked Examples to EN 1993-1-5 Plated Structural Elements[21] and Design of Plated Structures[22], the methodology of the reduced stress method is shown below, including how it should be applied and which formulas are required to calculate the buckling resistance of a steel plate.

3.3.2 Global vs local buckling

In Section 2.4 the distinction between global and local buckling was described. The reduced stress method can be used to determine both the local buckling resistance and the global buckling resistance of a stiffened plate. In the case of a stiffened plate, where a stiffener divides the entire plate into two subpanels, the reduced

stress method must be applied to each subpanel individually to evaluate their local reduction factors. Furthermore, the global reduction factor must be determined by applying the method to the full stiffened plate as a whole, treating it as a single structural system. The normative reduction factors are then used to determine to buckling resistance of the stiffened steel plate. For example, a stiffened steel plate with one longitudinal stiffener yields three reduction factors: one for the upper subplate, one for the lower subplate, and one for the global system. In the verification process, the lowest of these reduction factors is used.

3.3.3 Methodology and implementation of the reduced stress method

The basis of the reduced stress method is that, to reach the characteristic value of the ultimate resistance F_{Rk}, an amplification factor α_u is applied to the design load F_{Ed}. This amplification factor is derived using Eq. (3.1).

$$\alpha_u = \rho * \alpha_{ult,k} \tag{3.1}$$

Where

- α_u is the amplification factor
- ρ is the plate buckling reduction factor depending on the plate slenderness to take account of out-of-plane buckling
- $\alpha_{ult,k}$ is the minimum load amplifier to reach the characteristic value of resistance without taking into account the out-of-plane instability

The unity check of a structure system can now be displayed as Eq. (3.2).

$$\frac{F_{Ed}}{F_{Rd}} = \frac{F_{Ed}}{\rho * \frac{\alpha_{ult,k} * F_{Ed}}{\gamma_{M1}}} \leq 1 \tag{3.2}$$

Where

- F_{Ed} is the design load
- F_{Rd} is the design resistance
- γ_{M1} is the partial factor

Eq. (3.2) can now be rewritten as Eq. (3.3).

$$\frac{\rho * \alpha_{ult,k}}{\gamma_{M1}} \geq 1 \tag{3.3}$$

The yield criterion can be used to determine the minimum load amplifier $\alpha_{ult,k}$ which may be obtained from the Von Mises criterion, as shown in Eq. (3.4).

$$\frac{1}{{\alpha_{ult,k}}^2} = \left(\frac{\sigma_{x,Ed}}{f_y}\right)^2 + \left(\frac{\sigma_{z,Ed}}{f_y}\right)^2 - \left(\frac{\sigma_{x,Ed}}{f_y}\right)\left(\frac{\sigma_{z,Ed}}{f_y}\right) + 3\left(\frac{\tau_{Ed}}{f_y}\right)^2 \tag{3.4}$$

Where

- $\sigma_{x,Ed}$ and $\sigma_{z,Ed}$ are the design longitudinal and transverse stresses respectively
- τ_{Ed} is the design shear stress
- f_y is the yield stress

Now, Eq. (3.1) and Eq. (3.4) can be combined into a single equation. The relevant plate buckling reduction factor ρ may be obtained as either ρ_{min} as the minimum reduction factor of ρ_x, ρ_z or χ_w, which is displayed as Eq. (3.5).

$$\left(\frac{\sigma_{x,Ed}}{\frac{f_y}{\gamma_{M1}}}\right)^2 + \left(\frac{\sigma_{z,Ed}}{\frac{f_y}{\gamma_{M1}}}\right)^2 - \left(\frac{\sigma_{x,Ed}}{\frac{f_y}{\gamma_{M1}}}\right)\left(\frac{\sigma_{z,Ed}}{\frac{f_y}{\gamma_{M1}}}\right) + 3\left(\frac{\tau_{Ed}}{\frac{f_y}{\gamma_{M1}}}\right)^2 \leq \rho_{min}^2 \tag{3.5}$$

Where

- ρ_{min} is as the minimum reduction factor of ρ_x, ρ_z or χ_w

Or by a value interpolated between the values of ρ_x, ρ_z or χ_w by using the formula for $\alpha_{ult,k}$ as interpolation formula, which is displayed as Eq. (3.6).

$$\left(\frac{\sigma_{x,Ed}}{\frac{\rho_x * f_y}{\gamma_{M1}}}\right)^2 + \left(\frac{\sigma_{z,Ed}}{\frac{\rho_z * f_y}{\gamma_{M1}}}\right)^2 - \left(\frac{\sigma_{x,Ed}}{\frac{\rho_x * f_y}{\gamma_{M1}}}\right)\left(\frac{\sigma_{z,Ed}}{\frac{\rho_z * f_y}{\gamma_{M1}}}\right) + 3\left(\frac{\tau_{Ed}}{\frac{\chi_w * f_y}{\gamma_{M1}}}\right)^2 \leq 1 \tag{3.6}$$

Where

- ρ_x and ρ_z are the reduction factors for longitudinal and transverse stresses respectively taking into account column-like behaviour where relevant
- χ_w is the reduction factor for shear stress

In Eq. (3.6) is shown that the reduction factors reduced the yield stress due to plate buckling taking into account column-like behaviour. The determination of the plate slenderness is based on the complete stress field, resulting in a unique plate slenderness without the differentiation for the single acting forces. The reduction factors are determined only with one plate slenderness. The plate slenderness depends on the minimum load amplifier $\alpha_{ult,k}$ for the design loads to reach the characteristic value of resistance of the most critical point of the plate and on the minimum load amplifier α_{cr} for the design loads to reach the elastic critical load of the plate, under the complete stress field. Eq. (3.7) shows the determination of the plate slenderness.

$$\overline{\lambda_p} = \sqrt{\frac{\alpha_{ult,k}}{\alpha_{cr}}} \tag{3.7}$$

Where

- $\overline{\lambda_p}$ is the plate slenderness
- α_{cr} is the minimum load amplifier for the design loads to reach the elastic critical load of the plate, under the complete stress field

The load amplifiers $\alpha_{ult,k}$ and α_{cr} can be determined by hand calculations or α_{cr} may be obtained from relevant computer simulations like EBPlate. Assuming a plane stress field the equivalent stress $\sigma_{eq,Ed}$ can be shown as Eq. (3.8) and is used to illustrate the procedure.

$$\sigma_{eq,Ed} = \sqrt{\sigma_{x,Ed}^2 + \sigma_{z,Ed}^2 - \sigma_{x,Ed} * \sigma_{z,Ed} + 3 * \tau_{Ed}^2} \tag{3.8}$$

Where

- $\sigma_{eq,Ed}$ is the equivalent stress

The load amplifier $\alpha_{ult,k}$ is het smallest factor for which the design equivalent stress has to be increased to reach the characteristic yield strength and can be written according to Eq. (3.4). Now, Eq. (3.4) and Eq. (3.8). can be combined into Eq. (3.9).

$$\alpha_{ult,k} = \frac{f_y}{\sigma_{eq,Ed}} \tag{3.9}$$

The load amplifier α_{cr} is the smallest factor for which the design equivalent stress has to be increased to reach the elastic critical equivalent stress. It can be written according to Eq. (3.10).

$$\alpha_{cr} = \frac{1}{\frac{1+\psi_x}{4*\alpha_{cr,x}} + \frac{1+\psi_z}{4*\alpha_{cr,z}} + \sqrt{\left(\frac{1+\psi_x}{4*\alpha_{cr,x}} + \frac{1+\psi_z}{4*\alpha_{cr,z}}\right)^2 + \frac{1-\psi_x}{2*\alpha_{cr,x}^2} + \frac{1-\psi_z}{2*\alpha_{cr,z}^2} + \frac{1}{\alpha_{cr,\tau}^2}}} \tag{3.10}$$

Where

- ψ_x and ψ_z are the stress ratios for longitudinal and transverse respectively
- $\alpha_{cr,x}$ and $\alpha_{cr,z}$ are the critical factors for longitudinal and transverse stresses respectively
- $\alpha_{cr,\tau}$ is the critical factor for shear stress

The minimum load amplifier $\alpha_{cr,x}$, $\alpha_{cr,z}$ and $\alpha_{cr,\tau}$ can be calculated for each component individually according to Eq. (3.11a, 3.11b and 3.11c)

$$\alpha_{cr,x} = \frac{\sigma_{cr,x}}{\sigma_{x,Ed}} \tag{3.11a}$$

$$\alpha_{cr,z} = \frac{\sigma_{cr,z}}{\sigma_{z,Ed}} \tag{3.11b}$$

$$\alpha_{cr,\tau} = \frac{\tau_{cr,\tau}}{\tau_{\tau,Ed}} \tag{3.11c}$$

Where

- $\sigma_{cr,x}$ and $\sigma_{cr,z}$ are the critical longitudinal and transverse plate buckling stresses respectively
- $\tau_{cr,\tau}$ is the critical shear stress

The critical plate buckling stress of an unstiffened steel plate is calculated by multiplying the buckling factor with the Euler critical stress, as shown in Eq. (3.12). The buckling factor is dependent on the support condition and the stress ratio. The table used by the Eurocode to calculate the buckling factor for internal compression elements is shown below as Table 1. The Euler critical stress is the stress at which an ideal, thin plate would buckle elastically under compressive loading, assuming no imperfections or plasticity.

$$\sigma_{cr,p} = k_\sigma * \frac{\pi^2 * E}{12 * (1-\nu^2)} * \left(\frac{t}{b}\right)^2 \tag{3.12}$$

Where

- $\sigma_{cr,p}$ is the critical plate buckling stress
- k_σ is the buckling coefficient
- E is the elastic modulus
- ν is the Poisson's ratio
- t is the thickness of the plate
- b is the height of the plate

$\psi = \sigma_2/\sigma_1$	1	$1 > \psi > 0$	0	$0 > \psi > -1$	-1	$-1 > \psi > -3$
Buckling factor k_σ	4,0	$8,2 / (1,05 + \psi)$	7,81	$7,81 - 6,29\psi + 9,78\psi^2$	23,9	$5,98 (1 - \psi)^2$

Table 1 Buckling factors for internal compression elements[4].

For a stiffened steel plate with one stiffener the following method can be used to calculate the elastic critical plate buckling stress. The stiffened plate is substituted by a fictive column on a continuous elastic support. The column represents a stiffener with the contributing part of the plate according to Figure 20 and the elastic support represents the flexural stiffness of the plate. With this method the elastic critical buckling stress of the stiffener can be calculated according to Eq. (3.13)

$$\sigma_{cr,sl} = \frac{1.05 * E}{A_{sl,1}} * \frac{\sqrt{I_{sl,1} * b * t^3}}{b_1 * b_2} \; if \; a \geq a_c$$
$$\sigma_{cr,sl} = \frac{\pi^2 * E * I_{sl,1}}{A_{sl,1} * a^2} + \frac{E * a^2 * b * t^3}{4 * \pi^2 * (1 - \nu^2) * A_{sl,1} * b_1^2 * b_2^2} \; if \; a < a_c \qquad (3.13)$$
$$a_c = 4.33 * \sqrt[4]{\frac{b_1^2 * b_2^2 * I_{sl,1}}{b * t^3}}$$

Where

- $\sigma_{cr,sl}$ is the elastic critical buckling stress of the stiffener
- $A_{sl,1}$ is the gross area of the column
- $I_{sl,1}$ is the second moment of area of the gross cross-section of the column
- b_1, b_2 are the distances from the longitudinal edges of the web of the stiffener ($b_1 + b_2 = b$)
- a is the distance between transverse stiffeners
- a_c is the threshold length that determines which of the two formulas is used to calculate the elastic critical plate buckling stress

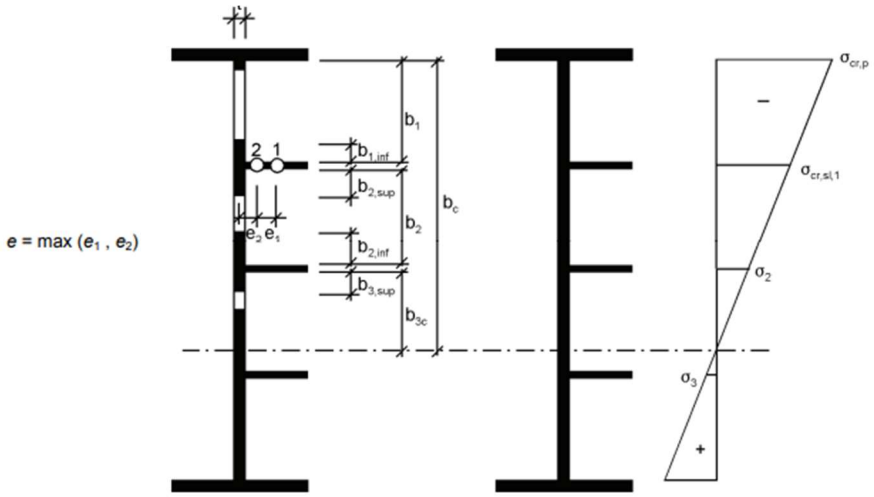

	Breedte voor de bruto-oppervlakte	Breedte voor de effectieve doorsnede volgens tabel 4.1	Voorwaarde voor ψ_i
$b_{1,inf}$	$\frac{3-\psi_1}{5-\psi_1} b_1$	$\frac{3-\psi_1}{5-\psi_1} b_{1,eff}$	$\psi_1 = \frac{\sigma_{cr,sl,1}}{\sigma_{cr,p}} > 0$
$b_{2,sup}$	$\frac{2}{5-\psi_2} b_2$	$\frac{2}{5-\psi_2} b_{2,eff}$	$\psi_2 = \frac{\sigma_2}{\sigma_{cr,sl,1}} > 0$
$b_{2,inf}$	$\frac{3-\psi_2}{5-\psi_2} b_2$	$\frac{3-\psi_2}{5-\psi_2} b_{2,eff}$	$\psi_2 > 0$
$b_{3,sup}$	0,4 b_{3c}	0,4 $b_{3c,eff}$	$\psi_3 = \frac{\sigma_3}{\sigma_2} < 0$

Figure 20 Notations for longitudinally stiffened plates[4].

The parameters $A_{sl,1}$ and $I_{sl,1}$ are the gross area and gross second moment area of the stiffener, which can be calculated with the use of Figure 20. To determine the relevant elastic plate buckling stress $\sigma_{cr,p}$, defined at the most stressed compression part of the plate, $\sigma_{cr,sl}$ should be extrapolated to this edge.

The plate buckling reduction factor ρ for internal compression elements can be calculated according to Eq. (3.14).

$$\begin{aligned} &\rho = 1{,}0 && \text{for } \overline{\lambda_p} \leq 0{,}5 + \sqrt{0{,}085 - 0{,}055 * \psi} \\ &\rho = \frac{\lambda_p - 0{,}055(3+\psi)}{(\lambda_p)^2} && \text{for } \overline{\lambda_p} < 0{,}5 + \sqrt{0{,}085 - 0{,}055 * \psi} \end{aligned} \tag{3.14}$$

The critical column buckling stress of an unstiffened steel plate is calculated according to Eq. (3.15) with the assumption that the plate is complete unsupported along the longitudinal edges.

$$\sigma_{cr,c} = \frac{\pi^2 * E * t^2}{12 * (1 - \nu^2) * a^2} \tag{3.15}$$

The elastic critical column buckling stress of a stiffened steel plate is calculated by extrapolating $\sigma_{cr,sl}$, which is the buckling stress of a single stiffener closest to the panel edge having the highest compression, to the edge of the stiffened panel. The buckling stress of the stiffener can be calculated with the use of Eq. (3.16).

$$\sigma_{cr,sl} = \frac{\pi^2 * E * I_{sl,1}}{A_{sl,1} * a^2} \tag{3.16}$$

The column buckling reduction factor for unstiffened compression elements can be calculated according to Eq. (3.17) by selecting buckling curve a ($\alpha = 0{,}21$).

$$\chi_c = \frac{1}{\phi + \sqrt{\phi^2 - \overline{\lambda_p}^2}} \qquad \text{but } \overline{\chi_c} \leq 1{,}0 \tag{3.17}$$

Where

- $\phi = 0{,}5 * (1 + \alpha * (\lambda_p - 0.2) + \overline{\lambda_p}^2)$

For stiffened compression elements the imperfection parameter α must be increased according to Eq. (3.18) with $\alpha = 0{,}34$ for closed stiffeners.

$$\alpha_e = \alpha + \frac{0{,}09}{i/e} \tag{3.18}$$

Where

- $i = \sqrt{\frac{I_{sl,1}}{A_{sl,1}}}$

Section 2.2.1 introduced the distinction between plate-like and column-like buckling behaviour. This interaction is taken into account through the interpolation formula given in Eq. (3.30), which is used to calculate the final reduction factor ρ_c as presented in Eq. (3.19). Figure 21 shows the interactions between plate and column like behaviour.

$$\rho_c = (\rho - \chi_c) * \xi * (2 - \xi) + \chi_c \tag{3.19}$$

$$\xi = \frac{\sigma_{cr,p}}{\sigma_{cr,c}} - 1, \text{ but } 0 \leq \xi \leq 1 \tag{3.20}$$

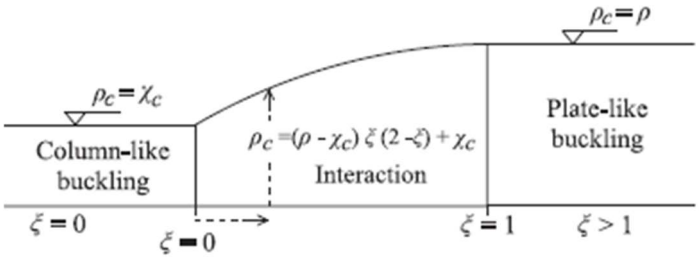

Figure 21 Interaction between plate and column buckling[4].

The critical shear buckling stress of an unstiffened steel plate is calculated by multiplying the shear buckling factor with the Euler critical stress, as shown in Eq. (3.21).

$$\tau_{cr} = k_\tau * \sigma_E \tag{3.21}$$

Where

- τ_{cr} is the critical shear buckling stress
- k_τ is the shear buckling factor

The shear buckling factor of unstiffened panels is dependent on the length and the height of the panels and can be calculated according to Eq. (3.22).

$$k_\tau = 5{,}34 + 4{,}00 * \left(\frac{h_w}{a}\right)^2 \text{ for } \frac{a}{h_w} \geq 1 \tag{3.22}$$

For stiffened panels the shear buckling stiffened panels with one longitudinal stiffener and where $\alpha = \frac{a}{h_w} < 3$ can be calculated according to Eq. (3.23).

$$k_\tau = 4{,}1 + \frac{6{,}3 + 0{,}18 * \frac{I_{sl}}{t^3 * h_w}}{\alpha^2} + 2{,}2 * \sqrt[3]{\frac{I_{sl}}{t^3 * h_w}} \tag{3.23}$$

The second moment of area I_{sl} is determined with an effective plate width of $15 * \varepsilon * t$ on each side of the stiffener.

The table used by the Eurocode to calculate the shear buckling reduction factor χ_w is shown below as Table 2. A distinguish is made between rigid end post and non-rigid end post because the axial and flexural stiffness of the end post influence the post-critical reserve. The recommended value for the coefficient that includes the increase of shear resistance at smaller web slenderness (η) according to EN1993-1-5 for $f_y \leq 460\ N/mm^2$ is equal to 1,2. This coefficient is derived from tests and depends on the strain hardening of the steel and on the contribution from the flanges.

	Rigid end post	Non-rigid end post
$\bar{\lambda}_w < 0{,}83/\eta$	η	η
$0{,}83/\eta \leq \bar{\lambda}_w < 1{,}08$	$0{,}83/\bar{\lambda}_w$	$0{,}83/\bar{\lambda}_w$
$\bar{\lambda}_w \geq 1{,}08$	$1{,}37/(0{,}7 + \bar{\lambda}_w)$	$0{,}83/\bar{\lambda}_w$

Table 2 Contribution from the web χ_w to shear buckling resistance[4].

In the case of stiffened steel plates, stiffeners should be dimensioned in such a way that the buckling failure occurs in the plate itself, before it occurs in the stiffener. The design of longitudinal stiffeners subject to direct stresses is fully incorporated into the design procedures for longitudinally stiffened panels and an additional check of the stiffeners alone is not necessary. Also when stiffened plates are loaded in shear, no special design checks are needed for longitudinal stiffeners. The influence of longitudinal stiffeners is reflected in the

calculation of the shear buckling coefficient of a stiffened panel[22].

The relative flexural stiffness of the stiffener is defined as the ratio between the flexural rigidity of the stiffener and that of the plate and it influences the plate's buckling behaviour. The formula on how to determine the relative flexural stiffness of a stiffener is shown in Eq. (3.24), where the reference flexural stiffness D of the plate is defined as given in Eq. (3.25).

$$\gamma = \frac{E * I_s}{b * D} \tag{3.24}$$

Where

- γ is the relative flexural stiffness of the stiffener
- E is the elastic modulus
- I_s is the second moment of area of the gross cross-section of the column
- b is the height of the plate
- D is the reference flexural stiffness of the plate

$$\mathrm{D} = \frac{E * t^3}{12(1 - \nu^2)} \tag{3.25}$$

Where

- t is the thickness of the plate
- ν is the Poisson's ratio

3.4 Reduced stress method with EBPlate

3.4.1 Introduction

In the previous section is described in which way the EN 1993-1-5 deals with the plate buckling resistance of steel plates. It was shown that the calculation of plate buckling involves determining the critical elastic buckling stress or associated parameters such as plate buckling factors and minimum load amplifiers. These parameters can be difficult to determine accurately due to variations in stress distribution and stiffening configurations. For this reason, a computer tool has been developed: a piece of software called EBPlate, which stands for Elastic Buckling of Plates.

When calculating the critical stress the designer may feel relatively helpless because Annex A of EN 1993-1-5 gives a few analytical formulas, but their field of application only covers a restricted number of stiffened plate configurations. These formulas neglect some favourable effects, such as the presence of stiffeners in the tension zone of the plate, which in reality enhance the global stiffness and stability of the structure. In some cases, the formulas may even prove to be inconsistent. EBPlate can be used in combination with the reduced stress method to calculate the buckling resistance of a plate. Instead of using Eq. (3.10) to calculate the minimum load amplifier with a complex formula, EBPlate can be used to calculate this minimum load amplifier for the design loads to reach the elastic critical load of the plat under the complete stress field. An alternative way to determine the critical buckling stress is to use a Finite Element Method program. But this is more time-consuming, sometimes difficult to perform and gives different results[23].

EBPlate can be used in combination with the reduced stress method to calculate the buckling resistance of a plate. EBPlate is able to calculate the minimum load amplifier for the design loads to reach the elastic critical load of the plat under the complete stress field.

EBPlate is a semi-analytical calculation tool that uses classical plate theories, such as Kirchhoff's theory or first-order shear deformation theory, in combination with the Rayleigh-Ritz method. It is designed for

structured plate problems, typically rectangular plates with uniform thickness and standard boundary conditions and provides results for buckling, load capacity, eigenvalues and deformations. Unlike FEM software such as RFEM or Abaqus, EBPlate does not use finite elements, does not support free geometry or complex material behaviour and is not a general purpose differential equation solver. While some of its results may resemble those from FEM, EBPlate is best described as an analytical tool with a numerical solution technique, rather than a true FEM program.

3.4.2 Methodology used by EBPlate

The general methodology employed by EBPlate in calculating critical stresses is explained with the use of the Presentation Manual EBPlate[19]. EBPlate computes the minimum load amplifier, which must be applied to the reference stresses (σ_x and τ_x) defined by the user and acting within the plate to reach the elastic buckling point. The critical stresses are then calculated according to Eq. (3.26) and Eq. (3.27).

$$\sigma_{x,cr} = \alpha_{cr} * \sigma_x \tag{3.26}$$

$$\tau_{cr} = \alpha_{cr} * \tau \tag{3.27}$$

At the buckling level point, the deformation shape of the plate is expressed by a Fourier series, which describes the deformations of the plate as sinusoidal functions.

$$w(x,y) = \sum_{m=1}^{m_{max}} \sum_{n=1}^{n_{max}} \left(a_{mn} * \sin\left(\frac{m * \pi * x}{a}\right) * \sin\left(\frac{n * \pi * y}{b}\right)\right) \tag{3.28}$$

Where

- m_{max} is the maximum number of half-waves considered in the x direction
- n_{max} is the maximum number of half-waves considered in the y direction
- a_{mn} are the displacement parameters or degrees of freedom of the system

The minimum load amplifier is calculated using the Rayleigh-Ritz Method (energy method). According to this method, a plate will buckle when the deformation energy (ΔU) equals the internal energy generated by the applied stresses (ΔW_{int}). At the buckling point, the following condition holds:

$$\Delta U - \Delta W_{int}(S_{cr}) = 0 = minimum \tag{3.29}$$

Where

- ΔU is the variation of strain energy of the plate
- ΔW_{int} is the variation of internal work of critical stresses S_{cr}
- $S_{cr} = \alpha_{cr} * S$ are the critical stresses

This equation represents the equilibrium point at which the system energetically favors a "buckling shape."

EBPlate calculates the energy variations in the system, and then uses these variations to derive the stiffness matrices. Subsequently EBPlate solves an eigenvalue problem to calculate the minimum load amplifier. The equation for this eigenvalue problem is as follows:

$$det[R_0 - \alpha_{cr} * R_G(S)] = 0 \tag{3.30}$$

Where

- R_0 is the initial stiffness matrix (from strain energy)
- R_G is the geometrical stiffness matrix (from internal work of stresses)
- S are the stresses

This is a standard form in stability analysis, and the smallest value of α_{cr} that satisfies this equation corresponds to the minimum load amplifier. Once the minimum load amplifier is determined, EBPlate can calculate the critical stresses for the plate, see Eq. (3.26) and (3.27).

3.5 FEM

3.5.1 Introduction

As previously mentioned, EN 1993-1-5 provides two main design methods for (un)stiffened steel plates: the effective width method and the reduced stress method. In addition to these, an alternative verification approach based on the Finite Element Method (FEM) is presented in the informative Annex C of EN 1993-1-5. Compared to the two main design methods the Finite Element Method is much more universal and can be applied on a larger scale. However, this increases flexibility comes at the cost of greater complexity, requiring specialized software and a solid understanding of numerical modelling[26].

Steel structures behave in a nonlinear way because of structural and geometric imperfections that arise from fabrication and due to nonlinear material behaviour. There are different possible FEM-based approaches to asses structural performance. Two of those approaches are the Linear Buckling Analysis (LBA) and the Geometric and Material Nonlinear Analysis including Imperfections (GMNIA), which will be further explained and used in this thesis.

Linear Buckling Analysis treats the system as a bifurcation problem using the stresses caused by the applied load, resulting in the determination of eigenvalues and their corresponding buckling modes. However, LBA does not account for geometric imperfections, residual stresses and material nonlinearity, all of which can significantly influence the actual buckling behaviour. The GMNIA considers initial imperfections and material nonlinearity, therefore it is not a bifurcation problem like in the case of the LBA, but a nonlinear stress problem that must be solved stepwise.

3.5.2 Imperfections

As previously described, GMNIA makes use of initial imperfections. There are two sources of initial imperfections in steel structures: geometric imperfections and residual stresses. These initial imperfections develop during the production and treatment processes of the plate elements. Both imperfections can be modelled together by using equivalent geometric imperfections. Equivalent geometric imperfections account for both effects by increasing the amplitude of the geometric imperfection.

Type of imperfection	Component	Shape	Magnitude
global	member with length ℓ	bow	see EN 1993-1-1, Table 5.1
global	longitudinal stiffener with length a	bow	min (a/400, b/400)
local	panel or subpanel with short span a or b	buckling shape	min (a/200, b/200)
local	stiffener or flange subject to twist	bow twist	1 / 50

Table 3 Equivalent geometric imperfections[4].

The EN 1993-1-5 give recommendations for defining the deformed shapes(Figure 26 Modelling of equivalent geometric imperfections[4].Figure 26) and the corresponding amplitudes(Table 3) of these equivalent imperfections. Imperfection shapes can be based either on the buckling shapes obtained from eigenmodes or on predefined sinusoidal shapes described by Eq. (3.31), (3.32), and (3.33) and is explained in combination with Figure 22.

$$w_1 = \min\left(\frac{a}{400}, \frac{b}{400}\right) * \cos\left(\frac{\pi * x}{b}\right) * \sin\left(\frac{\pi * z}{b}\right) \quad (3.31)$$

$$w_2 = \min\left(\frac{a}{200}, \frac{b_1}{200}\right) * \cos\left(\frac{\pi * x}{b_1}\right) * \sin\left(\frac{\pi * z}{b_1}\right) \quad (3.32)$$

$$v = \frac{y}{50} * \sin\left(\frac{\pi * z}{b}\right) \quad (3.33)$$

Where

- w_1 is the imperfection amplitude of the global buckling shape of the plate
- w_2 is the imperfection amplitude of the local buckling shape of the plate
- v is the imperfection amplitude of the local buckling shape of the stiffener
- a is the length of the plate
- b is the height of the plate
- x is the longitudinal coordinate along the length of the plate
- z is the vertical coordinate along the height of the plate

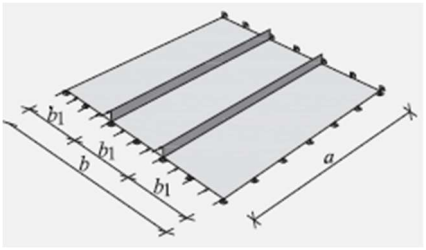

Figure 22 Stiffened steel plate[22].

These predefined shapes represent the global and local buckling modes of the plate and the stiffener and are shown in Figure 23, Figure 24 and Figure 25. Any one of these sinusoidal shapes may be taken as the leading imperfection (applied at 100% amplitude), while the others may be included as accompanying imperfections (applied at 70% amplitude)10[10].

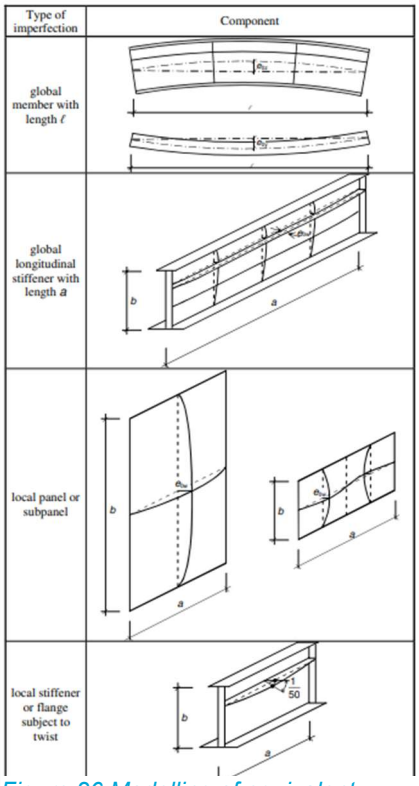

Figure 26 Modelling of equivalent geometric imperfections[4].

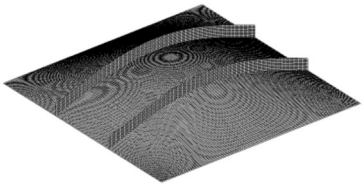

Figure 25 Sinusoidal buckling shape plate w_1[22].

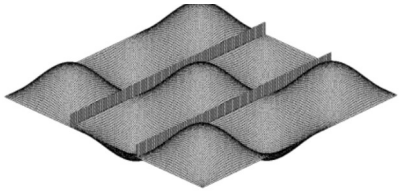

Figure 24 Sinusoidal buckling shape plate w_2[22].

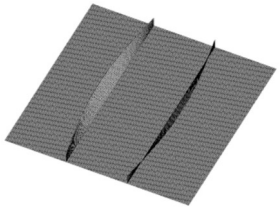

Figure 23 Sinusoidal buckling shape stiffene [22].

Part 2
Parametric study

4 Methodology of parametric study

4.1 Introduction

In the second part of this thesis, a parametric study is conducted. The parametric study will focus on unstiffened and stiffened steel plates. The buckling resistance of various steel plates will be calculated using three different approaches: the reduced stress method (Chapter 5), the reduced stress method in combination with EBPlate (Chapter 6) and RFEM (Chapter 7). These three approaches are already explained in more detail in the literature study. A separate chapter is dedicated to each method, including a brief introduction, the methodology and specific topics relevant to that particular method.

In Chapter 8, an individual analysis of the results per method is done. Afterwards, the three methods are compared and analysed side by side. This includes an analysis of the main findings and evaluation of differences in results among the reduced stress method, the EBPlate method, and RFEM method. These differences form the basis for the development of a new conservative design approach, which is presented in Chapter 9.

Chapter 9 presents the development of a new design approach for stiffened steel plates, based on insights gained from the results of the EBPlate method and the RFEM method. This newly proposed approach aims to provide safe and practical design guidance for engineering applications when using EBPlate to calculate the buckling resistance of stiffened steel plates.

This approach makes it possible to determine if the reduced stress method and the reduced stress method in combination with EBPlate takes into account the positive effect of tensile stresses on the plate buckling resistance. Both approaches are semi-analytical and require significantly less computational effort compared to a FEM analysis. The results of these approaches are compared to the results of a validated RFEM model, which forms the basis for answering the main research question.

First the parameters of the steel plates that will be investigated, along with the different loading conditions will be presented in the next section.

4.2 Material and parameters

The buckling resistance calculations are carried out with nominal values for structural steel S355 with an elastic modulus $E = 210000N/mm^2$; Poisson's Ratio $\nu = 0{,}3$; and a yield strength $f_y = 355N/mm^2$. The height of each steel plate is equal to 1500mm. The focus of the parametric study is on single steel plates, which means that the plate does not have flanges or is surrounded by surrounding plates. Therefore is the coefficient that includes the increase of shear resistance at smaller web slenderness (η) equal to 1,0. Reasoning for why η is equal to 1,0 for single steel plates is in more detail explained in Section 3.3.3. Moreover, for both the reduced stress method and the EBPlate method, the calculations were performed assuming both a rigid and a non-rigid end post

4.2.1 Unstiffened steel plates

In the parametric study, rectangular and square steel plates are considered corresponding to $\alpha = 1$ and $\alpha = 2$ with a plate thickness that is equal to 6mm; 10mm; 15mm or 21,4mm. The plates are subjected to compressive and tensile loading with stress ratios (ψ) equal to 1,0; 0,5; 0,0 and -0,5. The applied shear-to-normal stress ratios (τ/σ), as well as the rest of the parameters, are presented in Table 4. In total, 512 different cases have been analysed. Figure 28 and Figure 27 provides a clear overview of all parameters used in the parametric study for unstiffened steel plates. These parameters are chosen in order to give a broad and representative range of geometric and loading conditions, allowing the buckling resistance to be investigated across a broad variety of practical cases.

Parameter	Symbol	Values
Aspect ratio	α	1; 2
Plate thickness	t (mm)	6; 10; 15; 21.4
Stress ratio	ψ	1; 0.5; 0.0; -0.5
Shear-to-normal stress ratio	τ/σ	0; 0.25; 0.5; 0.67; 1; 2; 4; 9; 10000; -9; -4; -2; -1; -0.67; -0.5; -0.25

Table 4 Input parameters for the unstiffened parametric study.

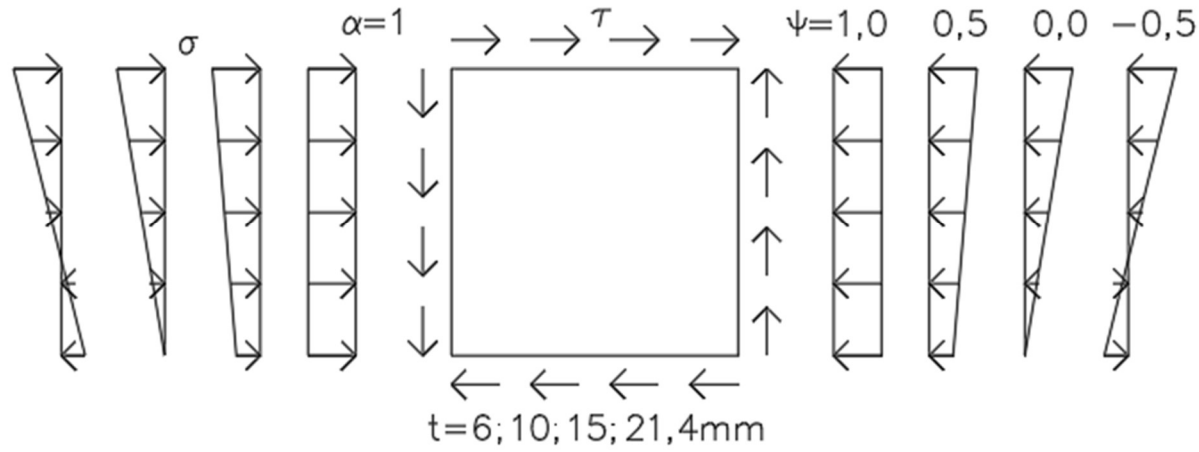

Figure 27 Graphical representation of analysed parameter combinations for unstiffened plates with α =1 , shown here under compressive loading conditions. Equivalent tensile loading combinations are also part of the study.

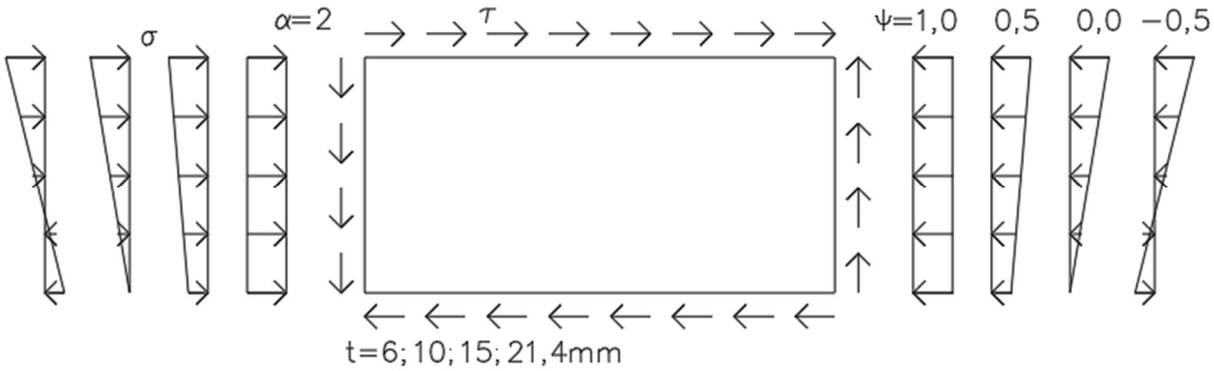

Figure 28Graphical representation of analysed parameter combinations for unstiffened plates with α =2, shown here under compressive loading conditions. Equivalent tensile loading combinations are also part of the study.

4.2.2 Stiffened steel plates

For stiffened steel plates, the same parameters for the aspect ratio, plate thickness and stress ratio are used. Less shear-to-normal stress ratios values are used in comparison to unstiffened steel plates to reduce the number of calculations, while still providing a comprehensive and clear overview of the buckling resistance of the plates. The relative flexural stiffness (γ) of the stiffeners in the stiffened plates is also considered as a parameter, with values equal to be 10, 25, 50, 75 and 100. A γ value of 10 represents a very flexible non-stiff stiffener, while a γ value of 100 represents a very stiff stiffener. Relevant properties of the stiffeners are defined on the following page. All the different parameters considered for the stiffened plates in the parametric study are shown in Table 5. In total, 1600 different cases have been analysed. Figure 29 and Figure 30 provides a clear overview of all parameters used in the parametric study for stiffened steel plates.

Parameter	Symbol	Values
Aspect ratio	α	1; 2
Plate thickness	t (mm)	6; 10; 15; 21,5
Relative flexural stiffness	γ	10; 25; 50; 75; 100
Stress ratio	ψ	1; 0,5; 0,0; -0,5
Shear-to-normal stress ratio	τ/σ	0; 0,5; 1; 2; 4; 6000; -2; -1; -0,5; -0,25

Table 5 Input parameters for the stiffened parametric study.

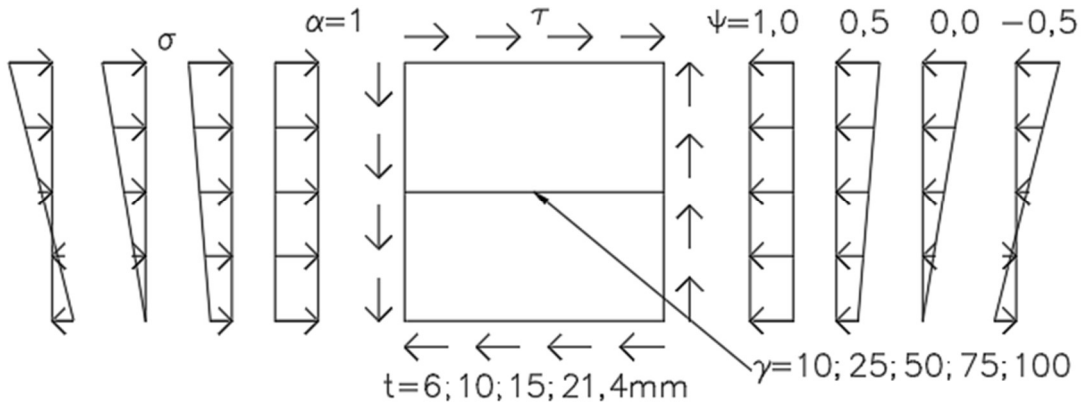

Figure 30 Graphical representation of analysed parameter combinations for stiffened plates with α =1, shown here under compressive loading conditions. Equivalent tensile loading combinations are also part of the study.

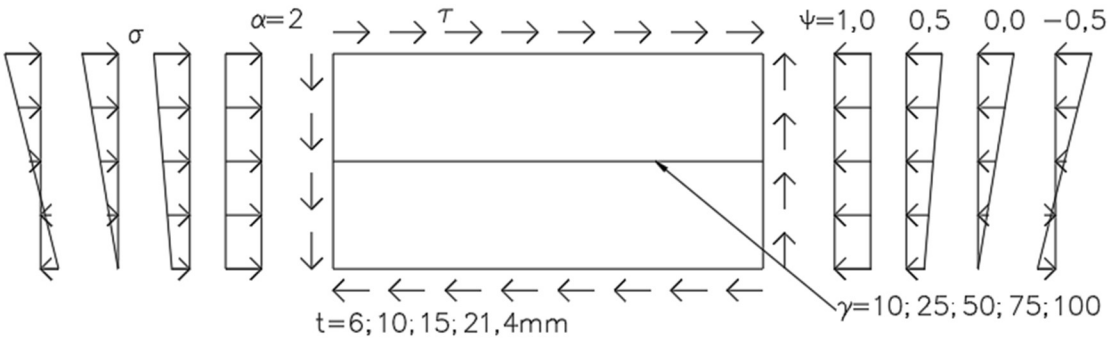

Figure 29 Graphical representation of analysed parameter combinations for stiffened plates with α =2, shown here under compressive loading conditions. Equivalent tensile loading combinations are also part of the study.

In the case of stiffened steel plates, parameters for longitudinal stiffeners must be selected. In the parametric study, only single-sided flat bar stiffeners are used. This choice is motivated by their simplicity, frequent use in practice and suitability for studying a wide range of configurations by varying the relative flexural stiffness. In Section 3.3.3 is described on how the relative flexural stiffness is defined.

Table 6 shows maximal width-to-thickness ratios for flat longitudinal stiffeners to prevent torsional buckling. In the parametric study, single-sided flat bar stiffeners made of S355 steel are used. The table shows that if the b/t ratio of the stiffener is equal to 10.6 or lower, the torsional buckling can be excluded for the longitudinal stiffener. As a result, the b/t ratio used for the single-sided flat bar stiffeners in the parametric study are equal to 10.

Steel grade	235	275	355	420	460
$b_{st} / t_{st} \leq$	13.0	12.0	10.6	9.7	9.3

Table 6 Limit ratio b/t for flat stiffeners to prevent torsional buckling[22].

For the parametric study, five values were considered for the relative flexural stiffness (γ) of the stiffeners. These values are 10, 25, 50, 75 and 100, where a value of 10 represents a weak stiffener and a value of 100 represents a very strong stiffener. These values were chosen with the objective to capture the transition from global buckling behaviour, typical for weak stiffeners, to local buckling behaviour, which occurs when using strong stiffeners.

With the use of Eq. (3.24), Eq. (3.25) and Table 6 the dimensions of the stiffeners for the parametric study are determined and are presented in Table 7.

Dimension Stiffener (mm)	γ = 10	γ = 25	γ = 50	γ = 75	γ = 100
t = 6,0mm	56,0 x 5,6	74,0 x 7,4	91,0 x 9,1	103,0 x 10,3	113,0 x 11,3
t = 10,0mm	81,0 x 8,1	105,0 x 10,5	130,0 x 13,0	147,0 x 14,7	161,0 x 16,1
t = 15,0mm	107,0 x 10,7	140,0 x 14,0	172,0 x 17,2	195,0 x 19,5	213,0 x 21,3
t = 21,4mm	138,0 x 13,8	179,0 x 17,9	221,0 x 22,1	250,0 x 25,0	273,0 x 27,3

Table 7 Dimensions of the longitudinal stiffeners used in the parametric study.

The location of the stiffener plays an important role in the buckling resistance of the stiffened steel plates. The optimal position of the stiffener depends on the stress ratio and the shear stress acting on the steel plate[24]. The optimal ratios of the stiffener placement height to the total plate height for various normal stress ratios and for pure shear are shown in Figure 32 and Figure 31. However, no research has yet done on the optimal stiffener location for the combination of various stress ratios and shear. The focus of this thesis is on shear stress, therefore the optimal stiffener position for shear loading is used, rather than the one based on the stress ratio. As a result, the location of all longitudinal stiffeners are located at the middle of the plate, regardless of the applied normal stress ratio.

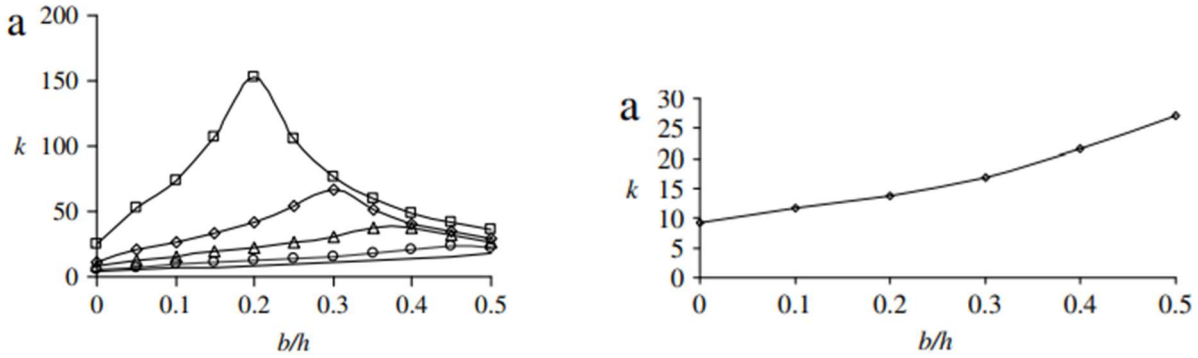

Figure 31 Buckling factor vs b/h diagram for various normal stress ratios and flat stiffeners[24].

Figure 32 Buckling factor vs b/h diagram for flat stiffeners in panels subjected to pure shear[24].

5 Reduced stress method (Approach 1)

5.1 Introduction

The reduced stress method has already been extensively addressed in the literature study. This chapter aims to clarify how the reduced stress method is being applied in the parametric study for both the unstiffened and stiffened steel plates. The focus is on the practical application of the method and calculation steps. In Section Methodology5.2 the methodology and the corresponding workflows are discussed.

5.2 Methodology

5.2.1 Unstiffened steel plates

On the next page, a workflow is presented that illustrates how the reduced stress method is applied to each case of the parametric study for unstiffened steel plates. In the workflow the most important steps of the calculation are shown and briefly described. A comprehensive explanation of the full calculation, including all formulas used, can be found in the literature study in part 1 of this thesis.

The workflow starts with a case consisting of an unstiffened steel plate, including its corresponding properties and stress state(1). The critical plate buckling stress(2.1), critical column buckling stress(2.2) and the critical shear buckling stress(2.3) are calculated for the unstiffened steel plate with the use of formulas that are given in the Eurocode. The weighting factor(5.0) can be determined with the use of the critical plate buckling stress(2.1) and critical column buckling stress(2.2). With the use of the critical plate buckling stress(2.1) and the critical shear buckling stress(2.3) the load amplifiers(3) are computed, which are then used to calculate the plate slenderness(4). This plate slenderness allows for the calculation of the plate (5.1), column (5.2), and shear (5.3) reduction factors. While the shear reduction factor(5.3) can be used directly in the verification formula(7), the plate(5.1) and column(5.2) reduction factors have to be converted into the interpolation factor (6) first using the weighting factor(5.0). This interpolation factor(6) is then also used in the verification formula(7). The verification formula provides a maximum shear and normal stress, which represents the buckling resistance of the corresponding case.

Workflow: RSM (Approach 1) - non stiffened steel plate buckling resistance

1. Stress state

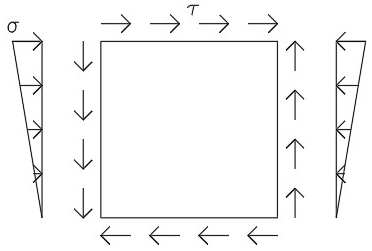

2.1 Critical plate buckling stress

$$\sigma_{cr,p} = k_\sigma * \frac{\pi^2 * E}{12 * (1-\nu^2)} * \left(\frac{t}{b}\right)^2$$

2.2 Critical column buckling stress

$$\sigma_{cr,c} = \frac{\pi^2 * E * t^2}{12 * (1-\nu^2) * a^2}$$

2.3 Critical shear buckling stress

$$\tau_{cr} = k_\tau * \frac{\pi^2 * E}{12 * (1-\nu^2)} * \left(\frac{t}{b}\right)^2$$

3. Load amplifiers

$$\alpha_{ult,k} = \frac{f_y}{\sqrt{\sigma_{x,Ed}^2 + 3 * \tau_{Ed}^2}}$$

$$\alpha_{cr} = \frac{1}{\frac{1+\psi_x}{4*\alpha_{cr,x}} + \sqrt{\left(\frac{1+\psi_x}{4*\alpha_{cr,x}}\right)^2 + \frac{1-\psi_x}{2*\alpha_{cr,x}^2} + \frac{1}{\alpha_{cr,\tau}^2}}} \quad \text{with} \quad \alpha_{cr,x} = \frac{\sigma_{cr,p}}{\sigma_{x,Ed}}, \; \alpha_{cr,\tau} = \frac{\tau_{cr}}{\tau_{\tau,Ed}}$$

4. Plate slenderness

$$\overline{\lambda_p} = \sqrt{\frac{\alpha_{ult,k}}{\alpha_{cr}}}$$

5.3 Shear reduction factors
For calculation $\chi_w(\overline{\lambda_p})$, see Table 2 in Section 3.3.3

5.0 Weighting factor

$\xi = 1$ if $a/b \geq 1$

$$\xi = \frac{\sigma_{cr,p}}{\sigma_{cr,c}} - 1 \; if \; a/b < 1$$

5.1 Plate reduction factors

$$\rho_x = \frac{\lambda_p - 0{,}055(3+\psi)}{(\lambda_p)^2} \leq 1$$

5.2 Column reduction factors

$$\chi_c = \frac{1}{\phi + \sqrt{\phi^2 - \overline{\lambda_p}^2}} \leq 1$$

With $\phi = 0{,}5 * (1 + \alpha * (\lambda_p - 0.2) + \overline{\lambda_p}^2)$ and $\alpha = 0{,}21$ for unstiffened steel plates

6. Interpolation factor

$$\rho_c = (\rho_x - \chi_c) * \xi * (2 - \xi) + \chi_c$$

7. Verification

$$\left(\frac{\sigma_{x,Ed}}{\frac{\rho_c * f_y}{\gamma_{M1}}}\right)^2 + 3\left(\frac{\tau_{Ed}}{\frac{\chi_w * f_y}{\gamma_{M1}}}\right)^2 \leq 1$$

5.2.2 Stiffened steel plates

On the next page, a workflow is presented that illustrates how the reduced stress method is applied to each case of the parametric study for stiffened steel plates. The workflow for stiffened steel plates has a lot of similarities with the workflow for unstiffened steel plates, but a few additional steps are required. Instead of two reduction factors, one shear reduction factor and one normal reduction factor, now six reduction factors are calculated. Two reduction factors for the upper subplate, two for the lower subplate and two for the total stiffened plate.

The workflow starts with a case consisting of a stiffened steel plate, including its corresponding properties and stress state(1). This stiffened steel plate is analysed in three different ways: the plate as a whole(1.3), the upper subplate(1.1) and the lower subplate(1.2). For both the upper and lower subplates, the workflow for unstiffened steel plates can now be followed. This results in a shear reduction factor and a final reduction factor for each subplate (6.1 and 6.2).

For the complete stiffened steel plate (1.3), the critical plate buckling stress (2.1), critical column buckling stress (2.2), and critical shear buckling stress (2.3) are calculated. The formulas that are used in these steps are different from the formulas that are applied in the calculation for unstiffened plates. From that point onward, the same steps and formulas are used to determine the shear reduction factor(5.3) and final reduction factor(6.3) for the total stiffened plate. The minimum of the reduction factors of the upper subplate, lower subplate and total stiffened plate are the normative reduction factors(6.4) and are used in the final verification formula(7). As a result the buckling resistance of the corresponding stiffened steel plate can be calculated.

Workflow: RSM (Approach 1) - stiffened steel plate buckling resistance

1. Stress state

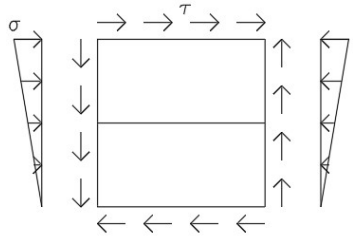

1.1 Upper subplate

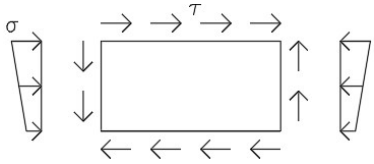

Follow workflow "Eurocode non stiffened steel plate buckling resistance calculation"

1.2 Lower subplate

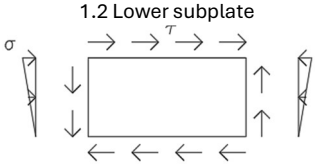

Follow workflow "Eurocode non stiffened steel plate buckling resistance calculation"

1.3 Total stiffened plate

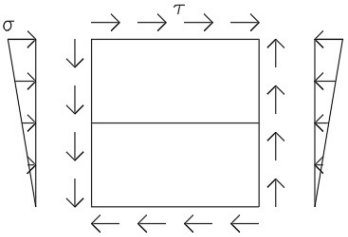

2.1 Critical plate buckling stress

$$\sigma_{cr,p,sl} = \frac{\pi^2 * E * I_{sl,1}}{A_{sl,1} * a^2} + \frac{E * a^2 * b * t^3}{4 * \pi^2 * (1 - \nu^2) * A_{sl,1} * b_1^2 * b_2^2}$$

$$\sigma_{cr,p} = Extrap(\sigma_{cr,p,sl})$$

2.2 Critical column buckling stress

$$\sigma_{cr,c,sl} = \frac{\pi^2 * E * I_{sl,1}}{A_{sl,1} * a^2}$$

$$\sigma_{cr,c} = Extrap(\sigma_{cr,c,sl})$$

2.2 Critical shear buckling stress

$$\tau_{cr} = \left(4{,}1 + \frac{6{,}3 + 0{,}18 * \frac{I_{sl}}{t^3 * h_w}}{\alpha^2} + 2{,}2 * \sqrt[3]{\frac{I_{sl}}{t^3 * h_w}}\right) * \sigma_E$$

3. Load amplifiers

$$\alpha_{ult,k} = \frac{f_y}{\sqrt{\sigma_{x,Ed}^2 + 3 * \tau_{Ed}^2}}$$

$$\alpha_{cr} = \frac{1}{\frac{1+\psi_x}{4*\alpha_{cr,x}} + \sqrt{\left(\frac{1+\psi_x}{4*\alpha_{cr,x}}\right)^2 + \frac{1-\psi_x}{2*\alpha_{cr,x}^2} + \frac{1}{\alpha_{cr,\tau}^2}}} \text{ with } \begin{matrix} \alpha_{cr,x} = \frac{\sigma_{cr,p}}{\sigma_{x,Ed}} \\ \alpha_{cr,\tau} = \frac{\tau_{cr}}{\tau_{\tau,Ed}} \end{matrix}$$

4. Plate slenderness

$$\overline{\lambda_p} = \sqrt{\frac{\alpha_{ult,k}}{\alpha_{cr}}}$$

5.3 Shear reduction factors
For calculation $\chi_{w,total}(\overline{\lambda_p})$, see Table 2 in Section 3.3.3

5.0 Weighting factor

$$\xi = \frac{\sigma_{cr,p}}{\sigma_{cr,c}} - 1$$

5.1 Plate reduction factors

$$\rho_x = \frac{\lambda_p - 0{,}055(3 + \psi)}{(\lambda_p)^2} \leq 1$$

5.2 Column reduction factors

$$\chi_c = \frac{1}{\phi + \sqrt{\phi^2 - \overline{\lambda_p}^2}} \leq 1$$

With $\phi = 0{,}5 * (1 + \alpha_e * (\lambda_p - 0.2) + \overline{\lambda_p}^2)$
and $\alpha_e = 0{,}49 + \frac{0{,}09}{i/e}$ for stiffened steel

6.1 Final reduction factors

$\rho_{c,upper}$

χ_{upper}

6.2 Final reduction factors

$\rho_{c,lower}$

χ_{lower}

6.3 Interpolation factor

$$\rho_{c,total} = (\rho_x - \chi_c) * \xi * (2 - \xi) + \chi_c$$

6.4 Normative reduction factors

$$\rho_c = \min(\rho_{c,upper}; \rho_{c,lower}; \rho_{c,total})$$

$$\chi_w = \min(\chi_{w,upper}; \chi_{w,lower}; \chi_{w,total})$$

7. Verification

$$\left(\frac{\sigma_{x,Ed}}{\frac{\rho_c * f_y}{\gamma_{M1}}}\right)^2 + 3\left(\frac{\tau_{Ed}}{\frac{\chi_w * f_y}{\gamma_{M1}}}\right)^2 \leq 1$$

6 EBPlate (Approach 2)

6.1 Introduction

In this chapter, the methodology is presented for how EBPlate is used in combination with the reduced stress method in the parametric study to determine the buckling resistance of both unstiffened and stiffened steel plates. The material properties and boundary conditions used in the EBPlate calculations are also described.

6.2 Material properties and boundary conditions

Standard linear elastic material properties are used for the buckling analysis in EBPlate. The elastic modulus is taken as $E = 210000 N/mm^2$ and the Poisson's Ratio is taken as $\nu = 0{,}3$. The effective width of the plate to be considered in the calculation of the stiffeners flexural inertia is taken as ten times the plate thickness, see Figure 33 Effective width of plate for stiffener inertia calculation19[19].

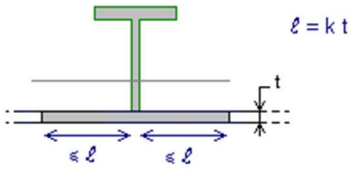

Figure 33 Effective width of plate for stiffener inertia calculation19[19].

The rotational restraints of all four edges of the plate are hinged supports. This means that the edges are simply supported, allowing rotation but not moment transfer. EBPlate does not provide options for additional boundary conditions, for example custom constraints, because EBPlate is specifically designed for elastic buckling analysis with predefined supports and loading options.

6.3 Methodology

6.3.1 Unstiffened steel plates

On the next page, a workflow is presented that illustrates how the reduced stress method in combination with EBPlate is applied to each case of the parametric study for unstiffened steel plates. The workflow is, apart from one adjustment, identical to the one used for calculating the buckling resistance of unstiffened steel plates using the reduced stress method. The load amplifier α_{cr} (3) is calculated by the program EBPlate, corresponding to the first global buckling mode, instead of Eq. (3.10). Figure 34 shows the first global buckling mode, with the corresponding load amplification factor for a case of the parametric study.

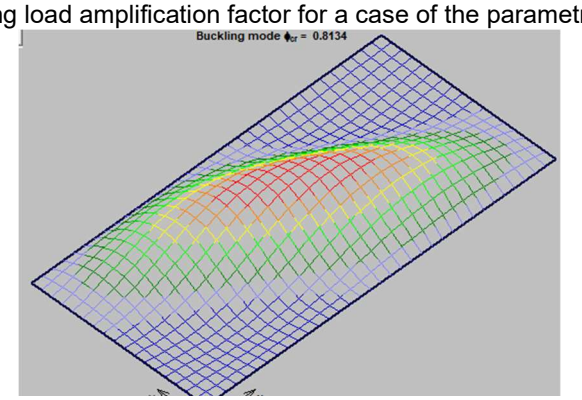

Figure 34 First global buckling mode of a steel plate from the parametric study (α = 2, t = 6 mm, ψ = 1 and τ/σ = -1), showing the corresponding load amplification factor[19].

Workflow: EBPlate (Approach 2) - non stiffened steel plate buckling resistance

1. Stress state

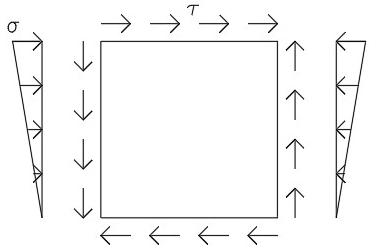

2.1 Critical plate buckling stress

$$\sigma_{cr,p} = k_\sigma * \frac{\pi^2 * E}{12 * (1 - \nu^2)} * \left(\frac{t}{b}\right)^2$$

2.2 Critical column buckling stress

$$\sigma_{cr,c} = \frac{\pi^2 * E * t^2}{12 * (1 - \nu^2) * a^2}$$

2.3 Critical shear buckling stress

$$\tau_{cr} = k_\tau * \frac{\pi^2 * E}{12 * (1 - \nu^2)} * \left(\frac{t}{b}\right)^2$$

3. Load amplifiers

$$\alpha_{ult,k} = \frac{f_y}{\sqrt{\sigma_{x,Ed}^2 + 3 * \tau_{Ed}^2}}$$

$$\alpha_{cr} = EBplate$$

4. Plate slenderness

$$\overline{\lambda_p} = \sqrt{\frac{\alpha_{ult,k}}{\alpha_{cr}}}$$

5.3 Shear reduction factors
For calculation $\chi_w(\overline{\lambda_p})$, see Table 2 in Section 3.3.3

5.0 Weighting factor

$\xi = 1$ if $a/b \geq 1$

$$\xi = \frac{\sigma_{cr,p}}{\sigma_{cr,c}} - 1 \; if \; a/b < 1$$

5.1 Plate reduction factors

$$\rho_x = \frac{\lambda_p - 0{,}055(3 + \psi)}{(\lambda_p)^2} \leq 1$$

5.2 Column reduction factors

$$\chi_c = \frac{1}{\phi + \sqrt{\phi^2 - \overline{\lambda_p}^2}} \leq 1$$

With $\phi = 0{,}5 * (1 + \alpha * (\lambda_p - 0.2) + \overline{\lambda_p}^2)$ and $\alpha = 0{,}21$ for unstiffened steel plates

6. Interpolation factor

$$\rho_c = (\rho_x - \chi_c) * \xi * (2 - \xi) + \chi_c$$

7. Verification

$$\left(\frac{\frac{\sigma_{x,Ed}}{\rho_c * f_y}}{\gamma_{M1}}\right)^2 + 3\left(\frac{\frac{\tau_{Ed}}{\chi_w * f_y}}{\gamma_{M1}}\right)^2 \leq 1$$

6.3.2 Stiffened steel plates

On the next page, a workflow is presented that illustrates how the reduced stress method in combination with EBPlate is applied to each case of the parametric study for stiffened steel plates. The workflow for stiffened steel plates has a lot of similarities with the workflow for unstiffened steel plates, but a few additional steps are required. Instead of two reduction factors, one shear reduction factor and one normal reduction factor, now four reduction factors are calculated. Two reduction factors for the global buckling of the total stiffened plate and two reduction factors for the local buckling of the total stiffened plate.

The workflow starts with a case consisting of a stiffened steel plate, including its corresponding properties and stress state(1). For the complete stiffened plate, a distinction is made between global and local buckling. For both types of buckling, a final reduction factor and a shear reduction factor are determined. First of all, for the complete stiffened steel plate (1), the critical plate buckling stress (2.1), critical column buckling stress (2.2), and critical shear buckling stress (2.3) are calculated. The formulas that are used in these steps are different from the formulas that are applied in the calculation for unstiffened plates. The weighting factor(5.0) can be determined with the use of the critical plate buckling stress(2.1) and critical column buckling stress(2.2) and will be used later on to calculate the interpolation factor for global buckling(6.1). For both global and local buckling are the load amplifiers(3.1 and 3.2) α_{cr} calculated by the program EBPlate, as described in the following paragraph, while the load amplifiers(3.1 and 3.2) $\alpha_{ult,k}$ are calculated according to the given formulas. As a result, two plate slendernesses are determined, one for global buckling(4.1) and one for local buckling(4.2). With the use of these two plate slendernesses the final reduction factors and shear reduction factors are determined for global and local buckling. The minimum of the reduction factors of the upper subplate, lower subplate, global total plate and local total plate are the normative reduction factors(6.2) and are used in the final verification formula(7). As a result the buckling resistance of the corresponding stiffened steel plate can be calculated.

EBPlate performs a linear buckling analysis for each case of the parametric study. EBPlate computes for the first 10 buckling modes the load amplifiers. However, EBPlate itself does not distinguish between global and local buckling modes. An additional step is therefore required to determine if a buckling mode and its corresponding load amplifier classifies as global or local. This extra step must also be done during the RFEM approach. In Section 7.4.2 the procedure used in the RFEM method on how a buckling mode is classified as global or local buckling is described. The same classification of buckling modes, so whether a buckling mode is classified as global or local, obtained from the RFEM analysis is also used in the EBPlate method. Figure 35 shows the first global buckling mode and Figure 36 shows the first local buckling mode, both with their corresponding load amplification factors, for a case from the parametric study.

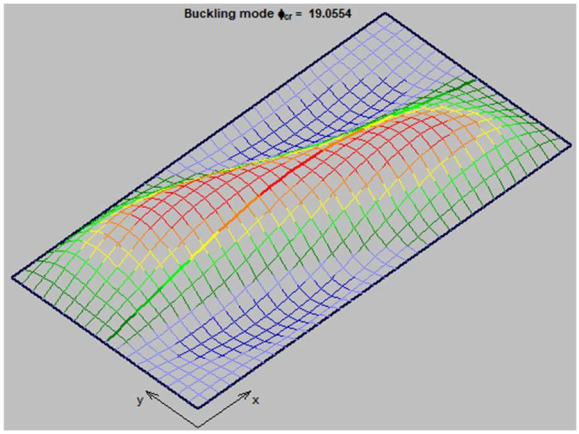

Figure 35 First global buckling mode of a steel plate from the parametric study (α = 2, t = 6 mm, ψ = 1, τ/σ = -1 and γ=50), showing the corresponding load amplification factor[19].

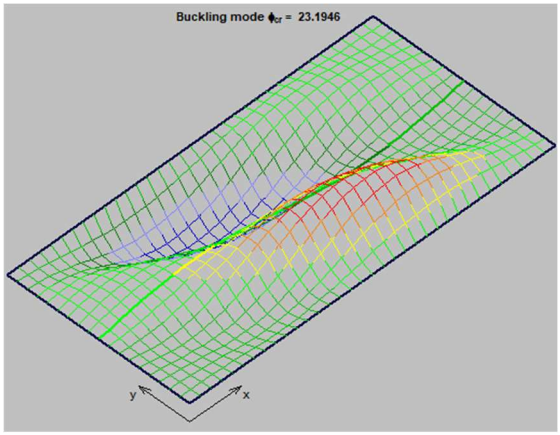

Figure 36 First local buckling mode of a steel plate from the parametric study (α = 2, t = 6 mm, ψ = 1, τ/σ = -1 and γ=50), showing the corresponding load amplification factor[19].

Workflow: EBPlate (Approach 2) - stiffened steel plate buckling resistance

1. Stress state

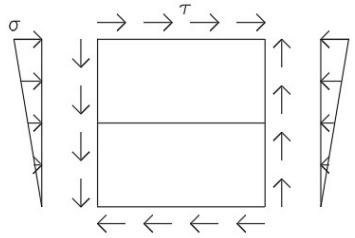

2.1 Critical plate buckling stress

$$\sigma_{cr,p} = k_\sigma * \frac{\pi^2 * E}{12 * (1-\nu^2)} * \left(\frac{t}{b}\right)^2$$

2.2 Critical column buckling stress

$$\sigma_{cr,c,sl} = \frac{\pi^2 * E * I_{sl,1}}{A_{sl,1} * a^2}$$

$$\sigma_{cr,c} = Extrap\left(\sigma_{cr,c,sl}\right)$$

2.3 Critical shear buckling stress

$$\tau_{cr} = \left(4{,}1 + \frac{6{,}3 + 0{,}18 * \frac{I_{sl}}{t^3 * h_w}}{\alpha^2} + 2{,}2 * \sqrt[3]{\frac{I_{sl}}{t^3 * h_w}}\right) * \sigma_E$$

5.0 Weighting factor

$$\xi = \frac{\sigma_{cr,p}}{\sigma_{cr,c}} - 1$$

3.1 Load amplifiers global

$$\alpha_{ult,k} = \frac{f_y}{\sqrt{\sigma_{x,Ed}^2 + 3 * \tau_{Ed}^2}}$$

$$\alpha_{cr,global} = EBPlate$$

3.2 Load amplifiers local

$$\alpha_{ult,k} = \frac{f_y}{\sqrt{\sigma_{x,Ed}^2 + 3 * \tau_{Ed}^2}}$$

$$\alpha_{cr,local} = EBPlate$$

4.1 Plate slenderness global

$$\overline{\lambda_{p,global}} = \sqrt{\frac{\alpha_{ult,k}}{\alpha_{cr,global}}}$$

4.2 Plate slenderness local

$$\overline{\lambda_{p,local}} = \sqrt{\frac{\alpha_{ult,k}}{\alpha_{cr,local}}}$$

5.3.1 Shear reduction factors global
For calculation $\chi_{w,global}\left(\overline{\lambda_{p,global}}\right)$, see Table 3.2 in chapter 3.3.3

5.3.2 Shear reduction factors local
For calculation $\chi_{w,local}\left(\overline{\lambda_{p,local}}\right)$, see Table 3.2 in section 3.3.3

5.2.1 Column reduction factors global

$$\chi_{c,global} = \frac{1}{\phi + \sqrt{\phi^2 - \overline{\lambda_p}^{-2}}} \leq 1$$

With $\phi = 0{,}5 * \left(1 + \alpha_e * \left(\lambda_{p,global} - 0.2\right) + \overline{\lambda_{p,global}}^2\right)$
and $\alpha_e = 0{,}49 + \frac{0{,}09}{i/e}$ for stiffened steel plates

5.1.1 Plate reduction factor global

$$\rho_{x,global} = \frac{\lambda_p - 0{,}055(3+\psi)}{\left(\lambda_p\right)^2} \leq 1$$

5.1.2 Plate reduction factors local

$$\rho_{c,local} = \frac{\lambda_p - 0{,}055(3+\psi)}{\left(\lambda_p\right)^2} \leq 1$$

6.1 Interpolation factor

$$\rho_{c,global} = \left(\rho_{x,global} - \chi_{c,global}\right) * \xi * (2 - \xi) + \chi_{c,global}$$

6.2 Normative reduction factors

$$\rho_c = \min\left(\rho_{c,global}; \rho_{c,local}\right)$$

$$\chi_w = \min\left(\chi_{w,globall}; \chi_{w,local}\right)$$

7. Verification

$$\left(\frac{\sigma_{x,Ed}}{\frac{\rho_c * f_y}{\gamma_{M1}}}\right)^2 + 3\left(\frac{\tau_{Ed}}{\frac{\chi_w * f_y}{\gamma_{M1}}}\right)^2 \leq 1$$

7 FEM (Approach 3)

7.1 Introduction

In this chapter, the methodology is presented on how RFEM is used in the parametric study to determine the buckling resistance of both unstiffened and stiffened steel plates. The material properties, imperfections, mesh, boundary conditions, solving method, and validation are discussed as well in this chapter.

7.2 Methodology

7.2.1 Unstiffened steel plates

To determine the buckling resistance of unstiffened steel plates using FEM, a parametric workflow was created using RFEM in combination with a Python script. The process begins with a RFEM model of a standard steel plate without any applied loads. A Python script is then run, which contains all the input parameters: aspect ratio, plate thickness, stress ratio and tau-sigma ratios. For each combination of these parameters, the script performs the following steps:

1. Linear Buckling Analysis (LBA):
   RFEM first performs an LBA to determine the first eigenmode of the plate under the given load parameters.
2. Application of Initial Imperfections:
   The buckling shape of the first eigenmode obtained from the LBA is used as the initial imperfection. More details about the imperfections are discussed in Section 7.4.
3. Geometrically and Materially Nonlinear Analysis with Imperfections (GMNIA):
   After the initial imperfection is applied, the script initiate that RFEM performs a GMNIA. The GMNIA takes into account: second-order effects (geometrical nonlinearity), initial geometric imperfections and material inelasticity (e.g., yielding and plastic behaviour).
4. Retrieval of Critical Load Step:
   The Python script saves this critical load increment, which is determined with the GMNIA in RFEM. The critical load increment is the last successfully converged load step in the analysis, this point represents at which the plate can no longer sustain additional loading. Beyond this increment, convergence fails due to instability, plastic failure or a combination of both.
5. Calculation of Buckling Resistance:
   Next, the critical load increment is multiplied by the initial applied load to calculate the buckling resistance of the plate for the current set of parameters.
6. Parameter Iteration:
   Now the script automatically updates the model with a new set of input parameters and repeats the entire process.

7.2.2 Stiffened steel plates

Stiffened steel plates have an extra parameter (the dimension of the stiffener), which is added to the Python script. In addition, not one but two GMNIA analyses are performed for stiffened steel plates. One GMNIA analyse is performed with the first global eigenmode shape as imperfection and the second one with the first local eigenmode shape as imperfection. If an eigenmode shape is classified as a local buckling shape or a global buckling shape is explained in Section 7.4.2.

So instead of only calculating the first eigenmode, what was done for unstiffened steel plates, the first ten eigenmodes are determined using a LBA in RFEM. After the LBA is performed, the results of these LBA are

read by the python script which identifies each eigenmode shape as either local or global buckling shape. The first eigenmode shape that identifies as local and the first eigenmode shape that identifies as global are then used as imperfection for the GMNIA analyse. As a result, two buckling resistances are determined for each stiffened steel plate. The lower of the two is considered the normative value and is presented in the results. Once this is done, the workflow continues in the same way as for the unstiffened steel plates.

Here a workflow is shown on how the buckling resistance is calculated for stiffened steel plates using RFEM.

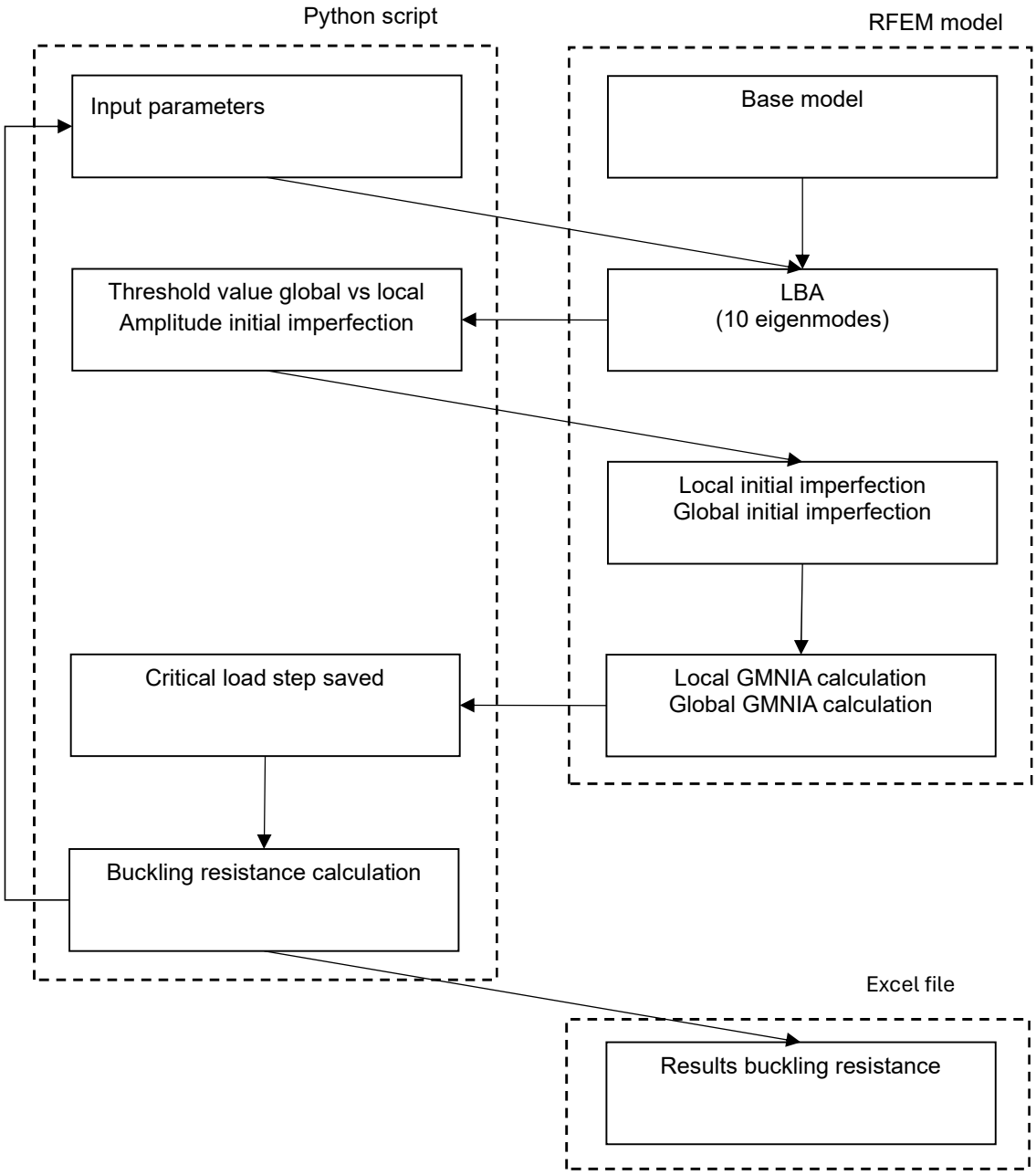

Workflow on how to calculate the buckling resistance of stiffened steel plates using RFEM.

7.3 Material properties

In the parametric study that is performed in RFEM, structural steel S355 is used as the material. The material is defined with an elastic modulus of E = 210000 N/mm²; Poisson's Ratio $\nu = 0{,}3$; yield strength $f_y = 355N/mm^2$ and to avoid numerical instabilities in the analysis, a small plastic plateau is introduced with a slope of E/10000, resulting in a bi-linear material model without strain hardening.

7.4 Imperfections

7.4.1 Number of imperfection shapes

In the literature review in Section 3.5.2, the handling of imperfections applied for GMNIA was discussed according to EN 1993-1-5. The following imperfection shapes for a stiffened plate must be considered: global eigenmode, local eigenmode, global sinusoidal buckling shape (plate), local sinusoidal buckling shape (plate), local sinusoidal buckling shape (stiffener) and various combinations of the last three shapes. For a stiffened plate with one stiffener, this results in 14 buckling shapes that must be used for the GMNIA, see Figure 37.

In this parametric study, only the first global eigenmode for unstiffened steel plates and only the first global eigenmode and the first local eigenmode for stiffened steel plates are considered as equivalent imperfections. These two imperfection shapes typically represent the most critical and fundamental instability patterns for stiffened steel plates. In practice, using the eigenmodes as imperfection shapes is common, as they effectively capture the dominant effects of geometric imperfections. Including all 14 imperfection shapes defined in the Eurocode would significantly increase computational effort and complexity, which is not the main focus of this study. Since the objective is to identify general trends in buckling resistance rather than to perform a full design verification, the selected imperfection shapes, based on the eigenmodes, are deemed sufficient to capture the essential structural behaviour.

No.	Imperfection Type
IMP1	Global eigenmode
IMP2	Local eigenmode
IMP3	Global sinusoidal plate shape
IMP4	Local sinusoidal plate shape
IMP5	Local sinusoidal stiffener shape
IMP6	IMP3 + 70% of IMP4
IMP7	IMP3 + 70% of IMP5
IMP8	IMP3 + 70% of (IMP4 + IMP5)
IMP9	IMP4 + 70% of IMP3
IMP10	IMP4 + 70% of IMP5
IMP11	IMP4 + 70% of (IMP3 + IMP5)
IMP12	IMP5 + 70% of IMP3
IMP13	IMP5 + 70% of IMP4

Figure 37 Number of imperfections shapes for buckling verification.

7.4.2 Global vs local buckling

As described before, in case of stiffened plates two GMNIA analyses are performed in RFEM for the stiffened plate: one with the first global eigenmode shape as imperfection and one with the first local eigenmode shape as imperfection. The classification of which eigenmode shape corresponds to a global or a local buckling shape is explained below.

For each stiffened steel plate case, the first ten eigenmodes are determined using a LBA. In the RFEM model 19 nodes are placed at mid height of the plate, which is the same location of the stiffener. From the LBA results, the deformation amplitude of the out of plane direction is known and normalized between 0 and 1, where 1 represent the maximum deformation observed. The normalized deformation amplitudes of the 19 nodes that are placed at mid height of the plate are also computed.

If any of these nodes exceeds a normalized amplitude exceeding the threshold of 0.35, the corresponding eigenmode shape is classified as a global buckling mode. If none of the node amplitudes exceed this threshold, the eigenmode shape is considered as a local buckling mode. The choice to make this threshold value equal to 0.35 is based on several examples demonstrating a clear distinction between local and global buckling behaviour.

Annex D provides the full analysis of the plate with parameters α=2, t=6mm, ψ=-0.5, γ=10, and τ/σ=0.5, where the first 10 eigenmodes along with their corresponding out-of-plane normalized amplitudes for the 19 mid-height nodes are shown. The first four eigenmodes are shown in the figures below, where the normalized out of plane displacements of the stiffener are plotted along the plate length. Eigenmode 1 has a maximum normalized displacement of 0.97001 at one of the 19 nodes and is therefore classified as a global eigenmode. Eigenmode 2 has a maximum normalized displacement of 0.5594 at one of the nodes and is therefore also classified as global buckling. Eigenmode 3 has a maximum normalized displacement of 0.20404 at one of the nodes and is thus classified as local buckling. As a result, the buckling shapes of the eigenmodes 1 and 3 are selected as imperfection shapes for the GMNIA analyses.

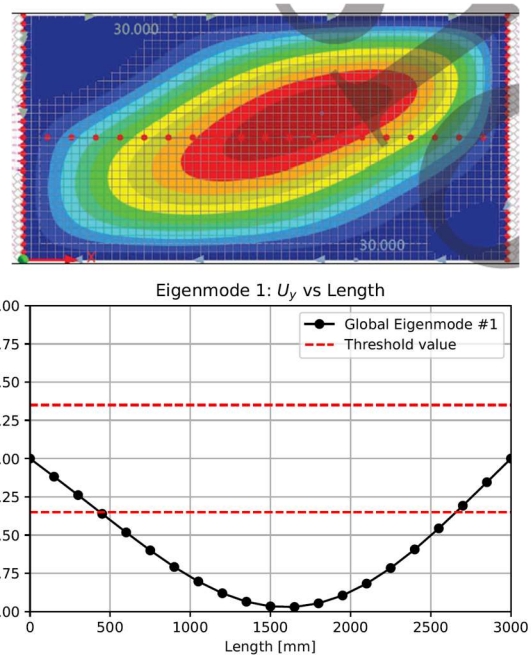

Figure 39 First eigenmode shape with u=0.97001, which results in first global eigenmode.

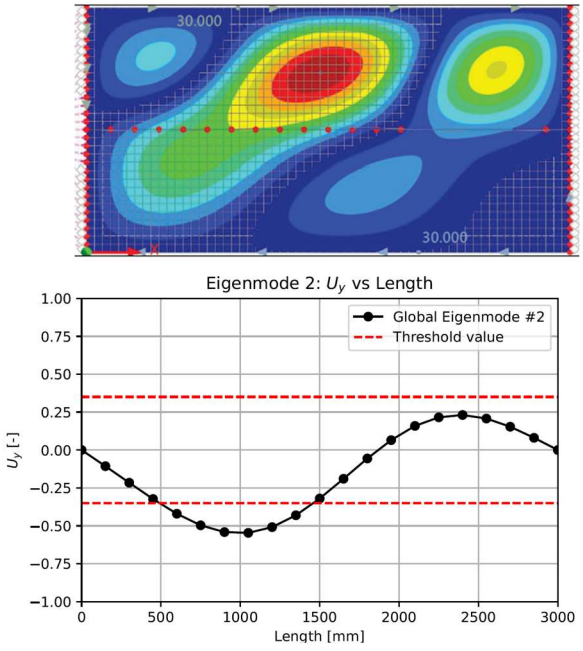

Figure 38 Second eigenmode shape with u=0. 5594, which results in second global eigenmode.

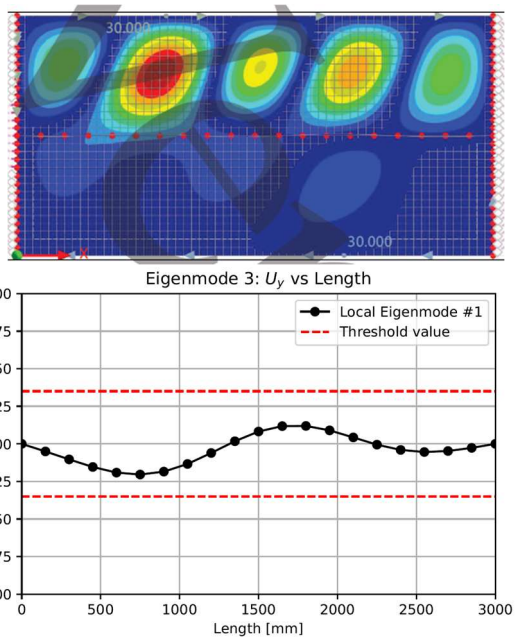

Figure 41 Third eigenmode shape with u=0.20404, which results in first local eigenmode.

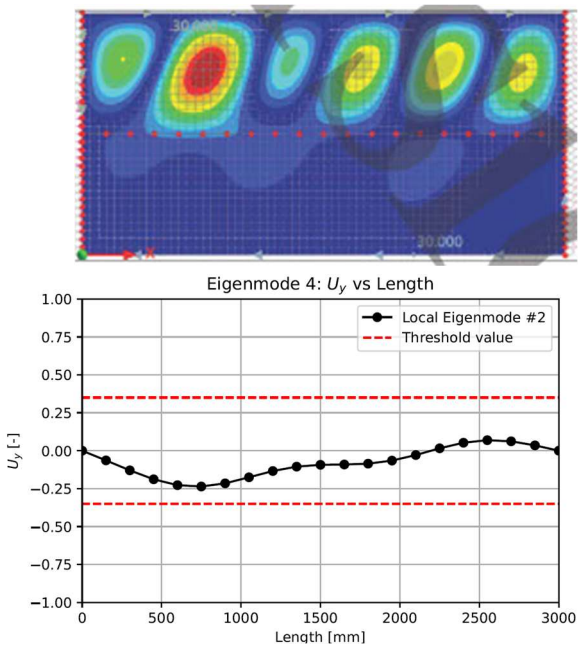

Figure 40 Fourth eigenmode shape with u=0.2360, which results in second local eigenmode.

7.4.3 Unstiffened steel plates

In the case of unstiffened plates only global buckling exist and no local buckling exist because no stiffener is present. Therefore, only the first global eigenmode shape is used as the imperfection shape. The amplitude of this imperfection shape according to EN 1993-1-5 is equal to $\min(a/400;\ b/400)$. Table 8 shows the amplitude used for the first global eigenmode shape in the GMNIA analysis of unstiffened plates.

α	a (mm)	b (mm)	magnitude	amplitude (mm)
1	1500	1500	min(a/400; b/400)	3.75
2	3000	1500	min(a/400; b/400)	3.75

Table 8 Imperfection amplitude for global eigenmode.

7.4.4 Stiffened steel plates

In the case of stiffened plates, two imperfection shapes are considered for two GMNIA analyses (global and local). The imperfection amplitude that belongs to the global eigenmode shape does have the same amplitude as the global eigenmode shape of unstiffened steel plates, see Table 8. The amplitude of the local eigenmode shape according to EN 1993-1-5 [6] is equal to $\min(a/200;\ 0{,}5b/200)$. Table 9 shows the amplitude used for the first local eigenmode shape as imperfection shape in the GMNIA analysis of stiffened plates.

α	a (mm)	0.5b (mm)	magnitude	amplitude (mm)
1	1500	750	min(a/200; 0.5b/200)	3.75
2	3000	750	min(a/200; 0.5b/200)	3.75

Table 9 Imperfection amplitude for global eigenmode.

7.5 Mesh

Two dimensional shell elements are used to represent the steel plate for the discretization of the finite element model in RFEM. The shape of the finite elements are triangles and quadrangles, where the quadrangles shapes are used wherever possible to ensure mesh regularity. The shell elements that are used in RFEM are based on the Reissner-Mindlin theory, which takes bending and transverse shear deformation into account. Therefore are the shell elements suitable for modelling thin and thick plates. RFEM generates the mesh automatic, which ensures appropriate element shape and aspect ratios.

The Mindlin-Reissner plate theory requires that the m_{xy} approaches zero at the edges. Larger mesh size can result in edge warping and inaccurate stress distributions. Normally small elements near the plate edges are generated to capture this behaviour. However, in this study, no local mesh refinement near the edges was applied due to the global mesh size constraints and to avoid inconsistencies in the model's mesh pattern.

This choice may influence the accuracy of the shear stress distribution near the edges and could slightly affect the computed buckling resistance. A sensitivity check was performed using a uniformly refined mesh across the entire plate. The difference in critical buckling load was found to be 3.35%, which is relatively small. However, it cannot be conclusively stated that this difference is solely due to the absence of refined edge elements or the inaccurate enforcement of $m_{xy} = 0$ at the edges.

The mesh size of approximately 50 x 50 mm is applied for the model to balance computational efficient with solution accuracy. Additionally, a finer mesh of 25 x 25 mm was analysed for comparison for one of the cases of the parametric study. The table below shows the resulting buckling resistance and out of plane deflection obtained from the GMNIA analysis for both mesh sizes, as well as the percentage difference between the two. A mesh density corresponding with less than a 5% difference within the obtained result compared to the larger mesh, generally provides a good approximation of the results[25].

Mesh size (mm)	Buckling resistance (N/mm²)	% Difference (Buckling)	Deflection (mm)	% Difference (Deflection)
50 × 50	37.08	—	28.81	—
25 × 25	35.84	-3.35 %	28.53	-0.97 %

Table 10 Mesh sensitivity analysis.

7.6 Boundary conditions

7.6.1 Modelling of “straight edges” boundary conditions in RFEM

An important parameter in the analysis of plate buckling effects is the applied boundary condition. Several type of boundary conditions can be used, one of which consist of hinged boundary conditions, where the edges that are loaded due to normal stress remain straight in plane (constrained) and the edges that are not loaded due to normal stress are free to move in plane (unconstrained)[3] . This particular boundary condition provides accurate results for plates that are subjected to normal and shear stress[1].

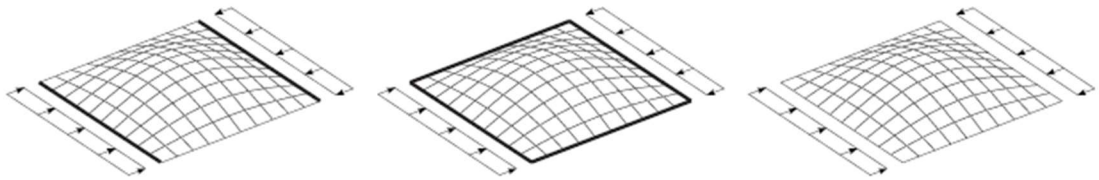

Figure 42 Different type of boundary conditions, left one is used in parametric study[1].

In Section 8.2,the buckling resistance of a steel plate with straight-edge boundary conditions is compared to that of the same steel plate positioned between two adjacent steel plates.

In some finite element software, like Abaqus, the boundary condition “edges remain straight” can be easily realised using constraint equations. These equations link the displacements of nodes along the edge to ensure they stay aligned, preventing the edge from bending[25].

However, RFEM is commonly used in engineering firms, whereas Abaqus is more often used in research institutions. Because of this, it is important that the model can also be implemented in RFEM. Unfortunately, RFEM does not have a straightforward way to model this type of boundary condition. Therefore, in RFEM an alternative modelling approach is needed to achieve the same boundary condition.

In RFEM the boundary condition “edges remain straight” are modelled as follows. All edges of the plate are supported with line supports that prevent out-of-plane deformation. A fully fixed nodal support is located on the right side of the steel plate. From this support, multiple rigid members are extended to the plate and are connected to the plate with the use of hinges. The fully fixed nodal support prevents both translation and rotation, serving as a stiff reference point. The rigid members ensure that the nodes along the plate edge move together, maintaining a straight edge, maintaining a straight edge, while the hinge connections allow for rotational freedom at the connection points, preventing artificial constraints and allowing realistic deformation of the plate.

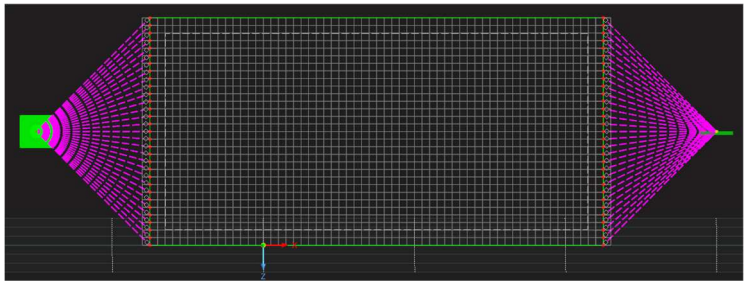

Figure 43 Edges remain straight modelled in RFEM.

Another nodal support is located on the left side of the plate. From this support, rigid members also extend towards the plate again connected with hinges. The hinged rigid members in combination with the nodal support, ensure that the edge remains straight while still permitting in-plane movement along the edge. The nodal support prevents out-of-plane displacement and movement perpendicular to the edge, but allows translation along the edge and local rotations through the hinges. In Figure 43 is shown how the steel plate is modelled in RFEM.

In Figure 44, the $u_x$displacement plot is shown of a plate that is subjected to both normal and shear stress. The consistent colour along the left and right edges indicate that the nodes along these edges experience nearly identical in-plane displacements. This uniform displacement distribution confirms that the edges remain straight and do not deform individually.

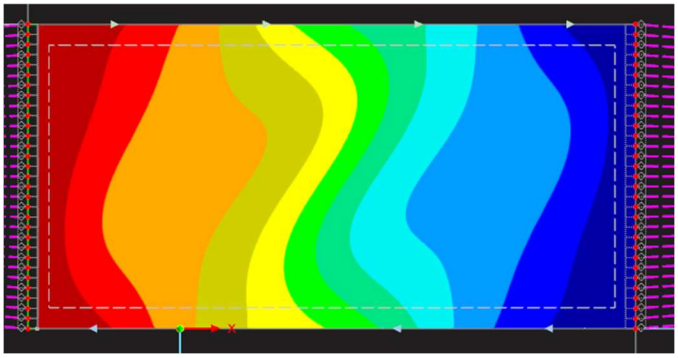

Figure 44 u_x displacement for edges remain straight (left and right side).

An important aspect of this modelling approach is that the mesh size is aligned with the spacing between the hinge connections, ensuring that nodes along the supported edges move collectively. This modelling approach does not exactly replicate the constraint equations used in software like Abaqus, but it has been validated against Abaqus results in Section 7.6.2 and proven to produce equivalent behaviour.

7.6.2 Validation boundary conditions

To validate if the boundary condition “edges remain straight” have been correctly modelled in RFEM, multiple cases of the parametric study were also calculated using a geometrically and materially nonlinear analysis with imperfections (GMNIA) in Abaqus. The buckling resistance calculated from both software programs were then compared with each other. The cases with their corresponding parameters and buckling results are shown in the Table 11. The table shows that the highest percentage difference between the results from Abaqus and RFEM is 1,53%, which is considered as acceptable.

α	b/t	ψ	tau/sigma	RFEM Normal stress (N/mm2)	RFEM Shear stress (N/mm2)	ABAQUS Normal stress (N/mm2)	ABAQUS Shear stress (N/mm2)	Percentage difference
2	250	1	0.0	71.67	0.0	70.58	0.0	1.53
2	70	1	0.0	194.39	0.0	192.54	0.0	0.96
2	250	1	10000.0	0.0	54.17	0.0	53.97	0.37
2	70	1	10000.0	0.0	174.53	0.0	174.1	0.25
2	70	1	1.0	112.15	112.15	110.715	110.715	1.29
2	70	0	0.0	297.2	0.0	297.068	0.0	0.04
2	70	1	-4.0	-46.15	184.48	-46.0	184.0	0.26
2	150	1	-0.67	-205.88	137.25	-205.19	136.79	0.34

Table 11 Comparison between ABAQUS GMNIA and RFEM GMNIA calculations.

7.7 Solving method

In RFEM the iterative method for nonlinear analysis is conducted using the Newton-Raphson method, which iteratively solves thee equilibrium equations for each load increment. In this study is the load increase in steps of 1, which enables a steady and systematic increase toward the critical state. This method captures the point where the steel plate loses its stability and buckling of the plate begins. At this point the critical load can be determined. The analysis uses load control, where the load is the driving parameter during each step. This is in contrast to arc-length control (e.g., the Riks method used in software such as Abaqus), which follows the entire post-buckling path by controlling a combination of load and displacement. Both approaches rely on the Newton-Raphson iteration method to solve the nonlinear equations. However, the research focuses on the maximum buckling resistance and not on the post-buckling behaviour of the plates. The load controlled Newton-Raphson approach used in RFEM is therefore sufficient for the scope of the study.

7.8 Validation

Validation is comparing the obtained results with experimental data or with known accurate numerical models. For unstiffened and stiffened steel plates two validations have been performed which are described in Section 7.8.1 for unstiffened steel plates and in Section 7.8.2 for stiffened steel plates.

7.8.1 Unstiffened steel plates

The RFEM model for unstiffened plates that has been used in the parametric study of this thesis has been validated against numerical models presented in [1]. These numerical models were validated by experimental data. Although the parametric study that was performed in [1] was smaller compared to this thesis, it can be used for validation. To validate the RFEM model, the numerical results of an unstiffened steel plate from the parametric study are compared to the numerical results from [1], which is shown in Figure 45. The unstiffened steel plate that is used to validate has the following parameters: α=2, b/t=150 and ψ=0. The results from both studies have been overlaid in the graph. On how to interpretate the graph is described in detail in Section 8.1. In the graph, the red triangles represent the plate buckling resistance results obtained from the parametric

study which was performed in this thesis. The black triangles correspond to the results from the numerical models in [1]. The graph shows that the results align closely, which indicates that the RFEM model used in this study accurately determines the buckling resistance of unstiffened steel plates and can therefore be considered validated.

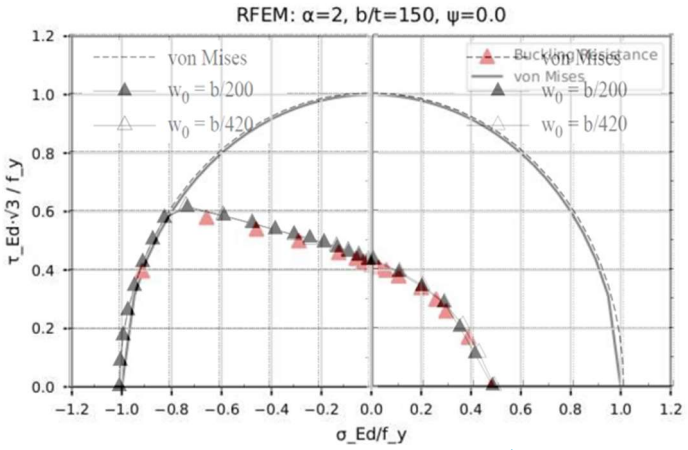

Figure 45 Validation RFEM model with [1].

Additionally, the RFEM model was as well validated by comparing it with an example from the book: Design of Steel Plated Structure with Finite Elements[26]. In this book a numerical model is used to calculate the plate buckling resistance of an unstiffened steel plate, which showed good alignment with the buckling resistance calculated with the use of EN 19993-1-5. This same unstiffened steel plate was modelled using the RFEM approach of this study. The parameters of the plate are as follows: a=1200mm, b=1000mm, t_w=12mm and f_y=355MPa. The first global eigenmode was selected as the shape for the initial geometric imperfection, with an amplitude of min(a/400,b/400) and applied to the RFEM model. In Table 12 the results are shown, which show good alignment to each other.

	Design of Steel Plated Structure with Finite Elements[26].	Own RFEM analysis	% Difference
First buckling mode	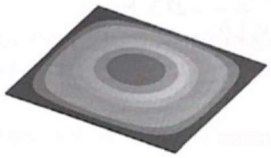	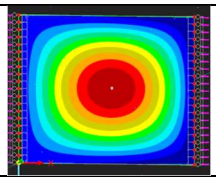	
Eigenvalue	1.12	1.13	0.88
Resistance (MPa)	176	178	1.12

Table 12 Validation of the model for unstiffened steel plate with [26].

7.8.2 Stiffened steel plates

For the validation of stiffened steel plates, the results from the RFEM model were compared with an example from the book: Design of Plated Structures[22]. The example is shown in Figure 46 and has the following parameters: a=1200mm, b=1000mm, t_w=12mm, b_{sl}=100mm , t_{sl}=10mm and f_y=355MPa. The first global

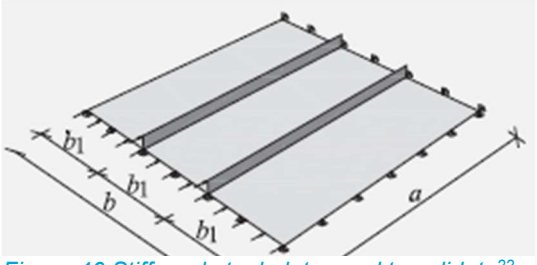

Figure 46 Stiffened steel plate used to validate[22].

eigenmode was selected as the shape for the initial geometric imperfection, with an amplitude of min(a/400,b/400) and applied to the RFEM model. In Table 13 the results are shown, which show good alignment to each other.

	Design of Steel Plated Structure[22]	Own RFEM analysis	% Difference
First buckling mode	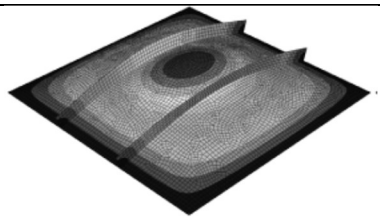	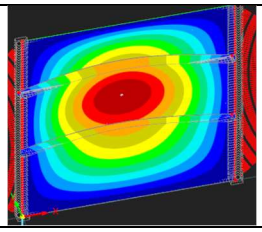	
Ultimate Force (kN)	443	452	2.03

Table 13 Validation of the model for stiffened steel plate with [22].

Additionally, experimental data was used to validate the stiffened steel plates which are subjected to shear stress. This study in [27] conducted a series of experiments on stiffened steel plates loaded in shear. One of these experiments was reproduced using the RFEM approach that is used in this study. The girder that was used in the experiment has the following parameters: a=360mm, h_w=750mm, t_w=3.3mm, b_f=125mm, t_f=10mm, b_{sl}=125mm, t_{sl}=10mm and h_{sl}=360, see Figure 48. The same girder was modelled in RFEM, see Figure 47. The exact imperfection of the girder that was used in the experiment could not be found, therefore, the first eigenmode was chosen as the imperfection shape, with an amplitude of min(a/200, h_{sl}/200).

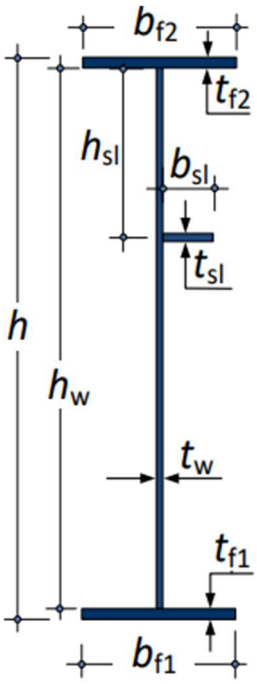

Figure 48 Girder parameters used in [27].

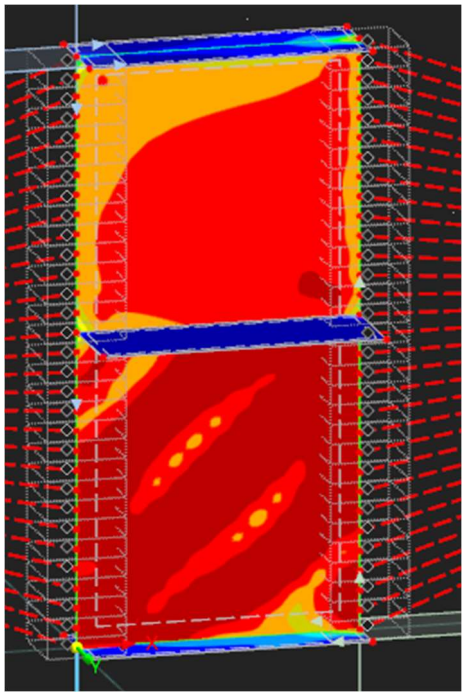

Figure 47 RFEM model with the same parameters as [27].

Table 14 presents the results, which show good agreement between the experimental data and the RFEM model.

	Ultimate Strength of Stiffened Plate Girders Subjected to Shear[27]	Own RFEM analysis	% Difference
Ultimate Force (kN)	564	537	4.79

Table 14 Validation of the model for stiffened steel plate with[27] .

Part 3
Research outcome

8 Results

8.1 Introduction to the buckling resistance results

In this chapter, the buckling resistance of a plate with a rigid end post and a non-rigid end post is compared in Section 8.2. Section 8.3 presents the results, which are the buckling resistances, obtained from all three approaches and compares them for both unstiffened and stiffened steel plates. Subsequently, Section 8.4 investigates the influence of individual parameters on the difference in results between approach 2 and approach 3. Finally, Section 8.5 examines the outliers observed in approach 3.

The results of the parametric study, which is the buckling resistance of steel plates, are visualized with the use of a normalized interaction diagram. The horizontal axis represents the normal stress divided by the yield stress (σ_{Ed}/f_y) and the vertical axis represents the shear stress multiplied by $\sqrt{3}$ and divided by the yield stress $(\tau_{Ed} * \sqrt{3}/f_y)$. In the graph, the negative side of the horizontal axis corresponds to tensile stresses and the positive side right side of the horizontal axis corresponds to compressive stresses.

In each graph, a circular boundary is plotted, representing the Von Mises yield criterion. To obtain a circular shape, the shear stress axis is scaled by a factor of $\sqrt{3}$. The resulting criterion can be written as: $\left(\frac{\sigma_{Ed}}{f_y}\right)^2 + \left(\frac{\tau_{Ed}*\sqrt{3}}{f_y}\right)^2 = 1$. This transformation allows the yield surface to appear as a circle in the graph, making comparison with the buckling resistance curve more intuitive. The Von Mises circle represents the material's yielding limit under combined normal and shear loading, assuming an ideal elastic-plastic behaviour without strain hardening. Besides the Von Mises criterium, the buckling resistance of a steel plate is also plotted. It shows the combinations of normalized normal and shear stresses at which the plate becomes unstable due to elastic buckling. This representation is chosen because it allows for a clear comparison between the buckling resistance of the plate and the material's yielding limit under the combined loading conditions.

RFEM is considered to provide the most accurate results due to its ability to model geometric imperfections, boundary conditions, and material nonlinearities in greater detail. Therefore, RFEM is assumed as the benchmark for realistic structural behaviour. As a result, the results of Approach 1 and Approach 2 are compared with those of Approach 3 (RFEM). This is done with the use of a parity plot, where the buckling factors of Approach 1 and 2 are plotted against the buckling factors of Approach 3. This is done as follows: in the parity plots, the buckling factors of Approach 1 or Approach 2 (y-axis) are plotted against the results of RFEM (x-axis). A 1:1 line, which is called the identity line, is also included in the figure, representing perfect agreement with the RFEM buckling factors. If the data points in the graph are above the identity line, it means that the buckling resistance from approach 1 or approach 2 are higher than those from RFEM.

To gain an understanding of the accuracy and reliability of Approach 1 and Approach 2 compared to the RFEM results, three statistical indicators are used: the coefficient of determination (R^2), the mean absolute error (MAE) and the root mean square error (RMSE). These three statistical indicators provide a detailed analysis of how well Approach 1 and Approach 2 calculates the buckling resistance in comparison to the RFEM Approach.

The coefficient of determination (R^2) indicates how well the calculated buckling resistance from Approach 1 or 2 corresponds to the calculated buckling resistance from RFEM. It shows the degree in which Approach 1 or 2 follows the same trend or pattern in comparison with RFEM. R^2 value equal to 1.0 represents perfect correlation and a value of 0.0 represents no correlation at all. However, R^2 does not reveal whether the

predictions are systematically too high or too low. The R^2 is calculated according to Eq. (8.1).

$$R^2 = 1 - \frac{\sum(y_i - \hat{y}_i)^2}{\sum(y_i - \hat{y})^2} \tag{8.1}$$

Where

- R^2 is the coefficient of determination
- y_i is the RFEM buckling resistance
- $\hat{y}_i$ is the buckling resistance calculated from method 1 or 2
- $\hat{y}$ İs the mean of the RFEM results

The mean absolute error (MAE) is the average of the absolute differences between the results from Approach 1 or 2 and the results from RFEM. The MAE indicates how far off, on average, the results from Approach 1 or 2 are from the RFEM results. MAE value equal to 0.0 indicates the best accuracy. The MAE is calculated according to Eq. (8.2).

$$MAE = \frac{1}{n}\sum_{i=1}^{n}|y_i - \hat{y}_i| \tag{8.2}$$

The root mean square error (RMSE) has the same idea as the MAE but it gives more weight to larger errors due to the squaring differences in the formulas. Therefore, it is more sensitive to outliners. RMSE value equal to 0.0 indicates that Approach 1 or 2 does not have large differences in results in comparison with RFEM. The RMSE is calculated according to Eq. (8.3).

$$RMSE = \sqrt{\frac{1}{n}\sum_{i=1}^{n}|y_i - \hat{y}_i|} \tag{8.3}$$

8.2 Rigid vs non-rigid end post

The parametric study assumes that the edges of the plate, which are subjected to normal stress, remain straight RFEM model. In the reduced stress method, the calculation of the shear buckling reduction factor depends whether the end posts of the plate are assumed to be rigid or non-rigid. For both assumptions (rigid and non-rigid), the buckling resistance was calculated using approach 2 for a steel plate with parameters equal to α=1, b/t=250 and ψ=1. The blue line in Figure 49 represents the rigid assumption and the orange line represents the non-rigid assumption.

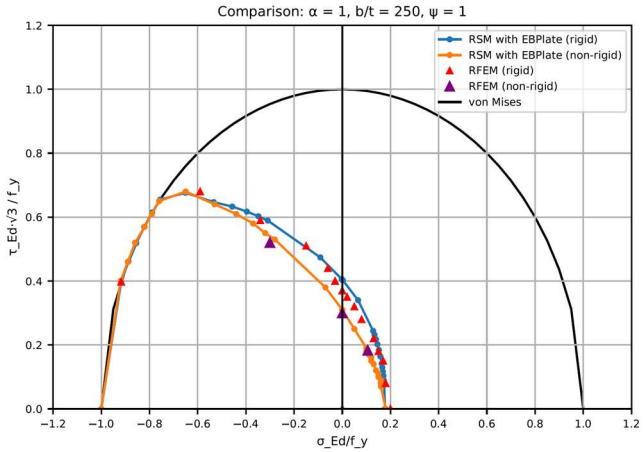

Figure 49 Buckling resistance stiffened steel plate: α=1; b/t=250; ψ=1.

In addition, the buckling resistance was also determined according to approach 3 (RFEM) with the assumption that the edges remain straight. These results are plotted as red triangles in Figure 49 and in Figure 50 can be seen how the boundary conditions are modelled in RFEM. In order to illustrate the influence of non-rigid edges, which are when the edges do not remain straight, the buckling resistance was also determined for three different values for τ / σ, using a model in which the steel plate is surrounded by other steel plates, see Figure 51. This is opposed to the "edges remain straight" scenario shown in Figure 50.

The results of these three cases are plotted in purple in Figure 49 and show a strong alignment with the non-rigid assumption.

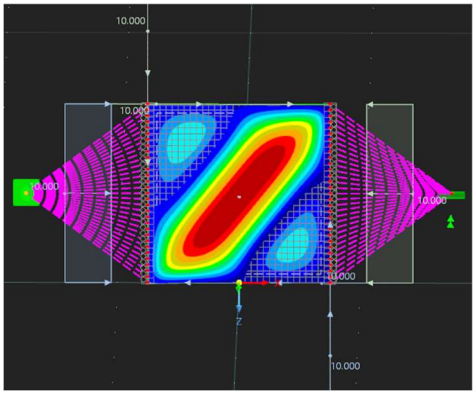

Figure 50 Unstiffened steel plate modelled with edges remain straight (α=1; b/t=250; ψ=1).

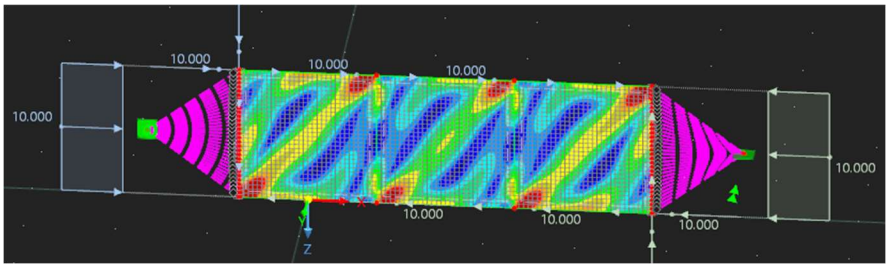

Figure 51 Unstiffened steel plate surrounded by other steel plates (α=1; b/t=250; ψ=1).

8.3 Comparison of RSM, RSM with EBPlate and RFEM results

8.3.1 Unstiffened steel plates

In Annex A, the buckling resistance results for unstiffened plates calculated with Approach 1, Approach 2 and Approach 3 are combined in one graph for comparison. Figure 52, taken from Annex A, shows the same trends observed in all the other plots from Annex A. When the unstiffened plate is subjected to compression and shear all three approaches calculates similar results for the buckling resistance. However, when the plate is subjected to tension and shear the EBPlate and RFEM method give similar results and clearly show an increase in the buckling resistance as tensile stresses increase.

In contrast, the reduced stress method does not capture this effect. From the reduced stress method graph, it can be observed that increasing the tensile stresses does not lead to higher buckling resistance, the curve remains nearly horizontal on the tension side. As a result, the reduced stress method underestimate the buckling resistance by a wide margin compared to the other two methods.

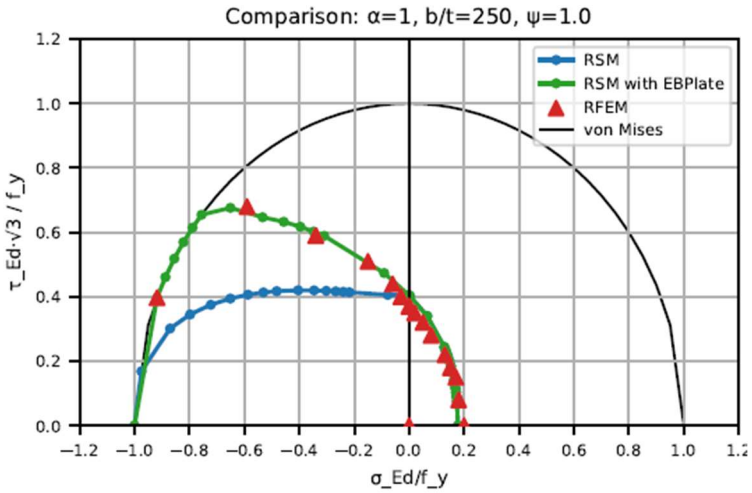

Figure 52 Buckling resistance unstiffened steel plate: α=1; b/t=250; ψ=1.0

8.3.2 Stiffened steel plates

In Annex B, the buckling resistance results for stiffened plates calculated with Approach 1, Approach 2 and Approach 3 are combined in one graph for comparison. Figure 53, taken from Annex B, shows the same trends observed in all the other plots from Annex B. Figure 53 and the remaining plots in Annex B illustrates that the reduced stress method consistently calculates lower buckling resistances in comparison with RFEM, while the EBPlate method calculates consistently higher buckling resistances in comparison with RFEM.

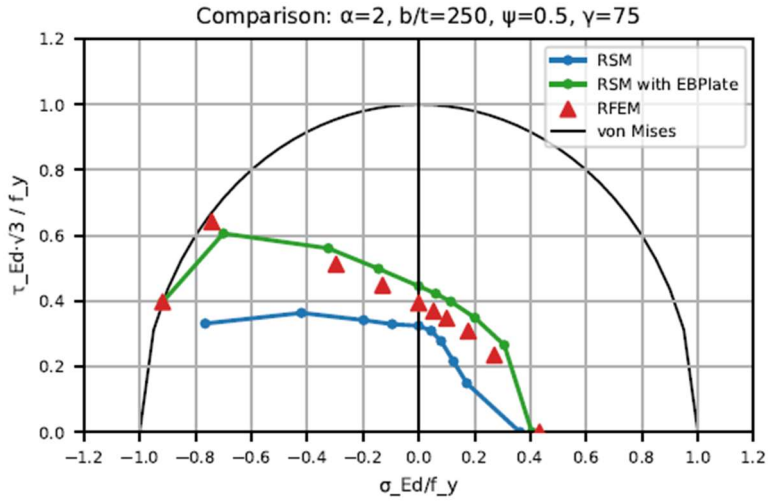

Figure 53 Buckling resistance stiffened steel plate: α=2; b/t=250; ψ=0.5; γ=75

The buckling factors for both Approach 1 and 2 are compared to the RFEM buckling factors using the three statistical indicators that are determined and shown in the corresponding figures. In each figure the results of Approach 1 or 2 (y-axis) is plotted against the results of RFEM (x-axis). The identity line is also plotted in the figure which represents the RFEM results.

In Figure 54 is the buckling factor of the reduced stress method (Approach 1) compared to the results of RFEM. Almost all datapoints lie below the identity, which indicates that the buckling resistance determined with the reduced stress method results are consistently lower in comparison with the RFEM results.

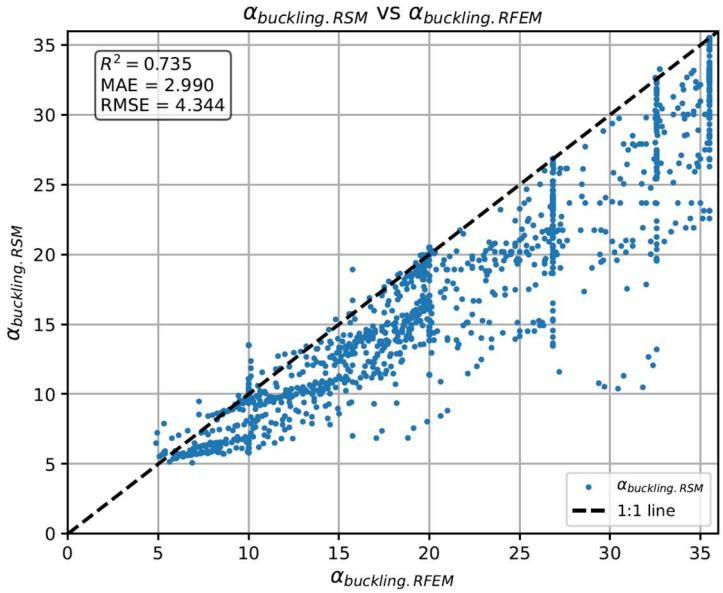

Figure 54 Parity plot: RFEM vs Reduced stress method.

In the plot vertical groupings of data points are shown at specific locations. These represent cases where RFEM has determined that the buckling resistance is equal to the Von Mises criterium However, Approach 1 determines a lower buckling resistance for the same shear-normal stress ratio. As a result, the data points share the same horizontal position but differ in vertical value, forming vertical lines in the plot.

In Figure 55, the buckling factor of the reduced stress method with EBPlate (Approach 2) are compared with the buckling factors obtained from the RFEM approach. A lot of the datapoints are found above the identity line, which indicates that the EBPlate approach finds higher bucking resistance of the stiffened plates than the RFEM approach does. However, there are as well datapoints below the identity line. When in buckling factor is increased the datapoints in the graph tend to be randomly scattered with both points above and below the identity line.

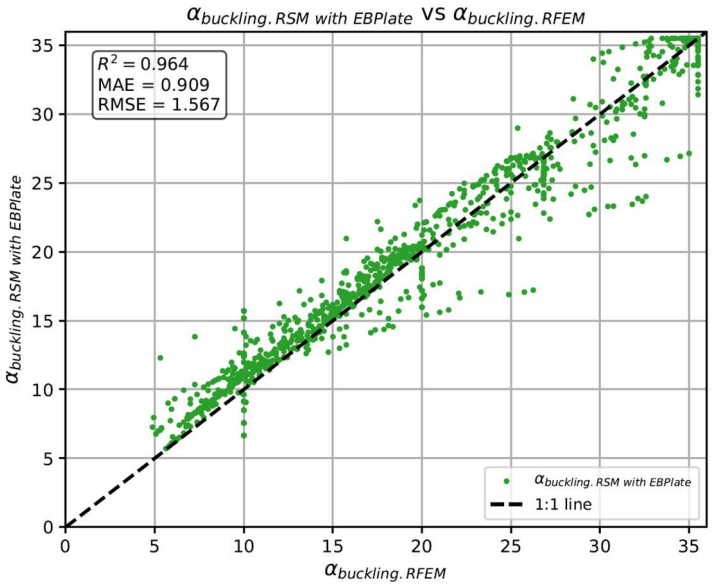

Figure 55 Parity plot: RFEM vs Reduced stress method with EBPlate.

Compared to Approach 1, the datapoints of Approach 2 lie closer to the identity line, indicating a better overall agreement with the RFEM results. Table 15 shows that approach 2 indeed outperforms approach 1 in calculating the buckling resistance if RFEM is assumed to be the benchmark for realistic structural behaviour. All statistical indicators demonstrate significantly better agreement with the RFEM results when using the reduced stress method with EBPlate compared to the reduced stress method. The higher accuracy of the statistical indicators was expected, based on the findings of the parametric study.

Methode	R^2	MAE	RMSE
RSM	0.735	2.99	4.344
RSM with EBPlate	0.964	0.909	1.567

Table 15 Statistical indicators RSM and RSM with EBPlate.

To explain the differences in the buckling factors between the approaches, all parameters that influence these difference are looked into in Section 8.4. Since Approach 2 takes the positive influence of tensile stress into account and consistently predicts higher buckling resistance values than RFEM, the following analysis specifically focuses on the differences between the results of Approach 2 and RFEM in order to clarify this variation.

8.4 Influence of parameters on the buckling resistance

To illustrate the systematic difference between reduced stress method with EBPlate and RFEM, the buckling factors calculated with RFEM are plotted on the x-axis, and those calculated with reduced stress method with EBPlate are plotted on the y-axis. The identity line is also included to indicate perfect agreement between the two approaches. However, the data points are now color-coded according to the parameter under investigation, allowing for a clear visual comparison of how the differences depend on this parameter.

8.4.1 Influence of the shear-to-normal stress ratio on buckling resistance

From Figure 56, a pattern can be observed with respect to the shear-to-normal stress ratio. When the plate is subjected to pure compression stress, tau/sigma equal to 0.0001, approach 2 consistently predicts lower buckling resistance values compared to RFEM. This is illustrated by the data points that lie below the identity line which indicates that RFEM gives higher buckling resistances in comparison with reduced stress method with EBPlate approach.

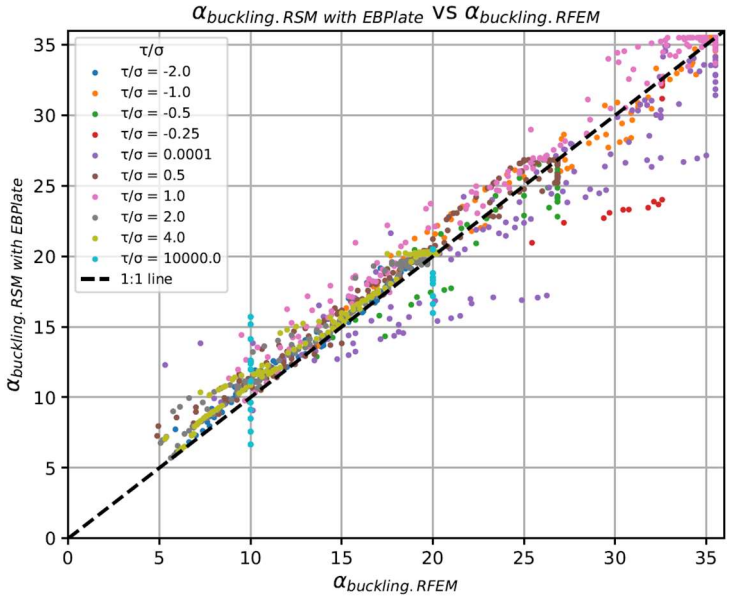

Figure 56 Parity plot: RFEM vs Reduced stress method witb EBPlate (τ/σ coloured).

8.4.2 Influence of the α-ratio on buckling resistance

From Figure 57, it is observed that no clear trend is visible with respect to the α-ratio. The data points corresponding to α = 1 and α = 2 are scattered and overlap throughout the graphs, indicating that the difference between reduced stress method with EBPlate and RFEM does not systematically depend on the α-ratio..

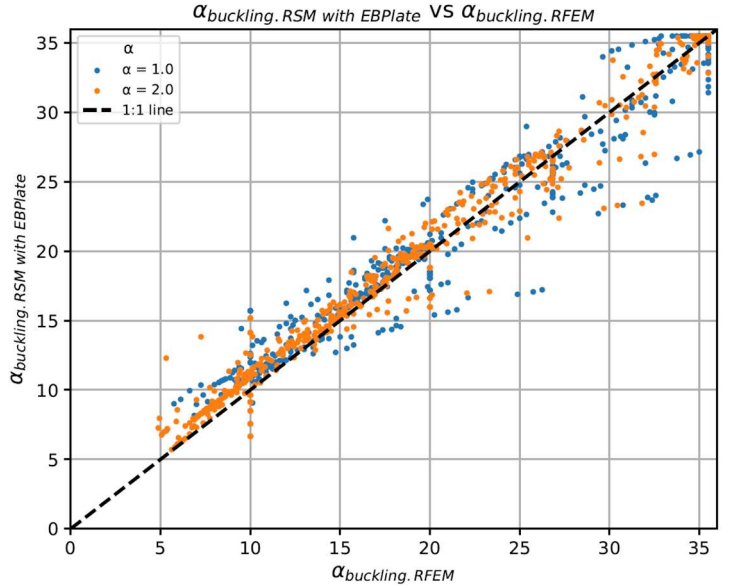

Figure 57 Parity plot: RFEM vs Reduced stress method witb EBPlate (aspect ratio coloured).

In addition to the comparison between the reduced stress method with EBPlate and RFEM results, the influence of the α-ratio on the buckling resistance is also investigated. From the outcome of all three calculation approaches, and for both unstiffened and stiffened steel plates, it is observed that the plate with aspect ratio equal to 1 has a higher buckling resistance than the plate with aspect ratio equal to 2 for any shear-to-normal stress ratio. This trend is illustrated in Figure 58. Plates with a higher aspect ratio are more prone to buckling. The increased length reduces the lateral support of the plate, increasing its slenderness and makes it easier for out-of-plane deformations to develop. As a result, the plate reaches at a lower stress level its buckling resistance.

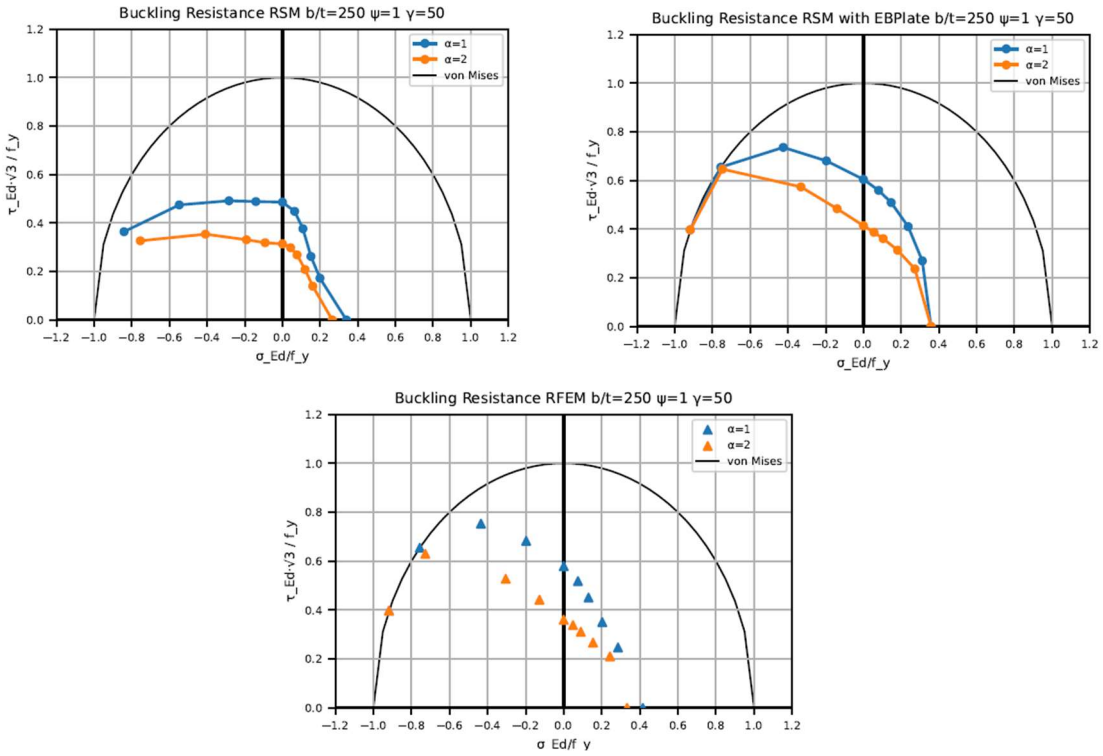

Figure 58 Buckling resistance - influence of aspect ratio
Left: Approach 1, right: Approach 2, bottom: Approach 3

8.4.3 Influence of the plate thickness on buckling resistance

Figure 59 do not indicate a clear pattern in the different results between the reduced stress method with EBPlate and RFEM results as a function of the plate thickness. The datapoints for the different plate thicknesses scatter and overlap on the graph. However, it is observed that the results of plates with smaller thicknesses are more often on the safe side in comparison than plates with larger thicknesses. However, reduced stress method with EBPlate results do still often give higher buckling resistance results as the RFEM approach for thinner plates.

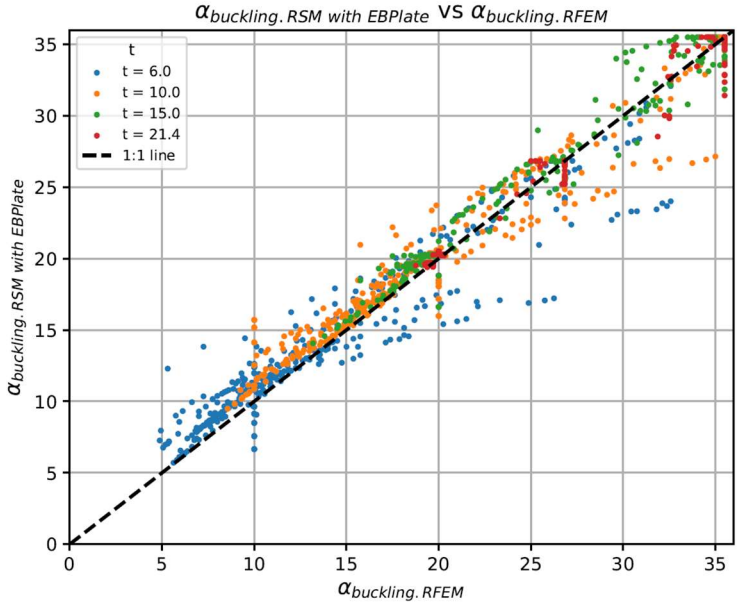

Figure 59 Parity plot: RFEM vs Reduced stress method witb EBPlate (plate thickness coloured).

In addition to the comparison between the reduced stress method with EBPlate and RFEM results, the influence of plate thickness on buckling resistance is also investigated. From the outcomes of all three calculation approaches, and for both unstiffened and stiffened steel plates, it can be observed that the buckling resistance increases as the plate slenderness decreases. Thicker plates do have higher bending stiffness and therefore greater resistance to deformation when subjected to normal and shear loads, which lead to higher buckling resistance, see Figure 60.

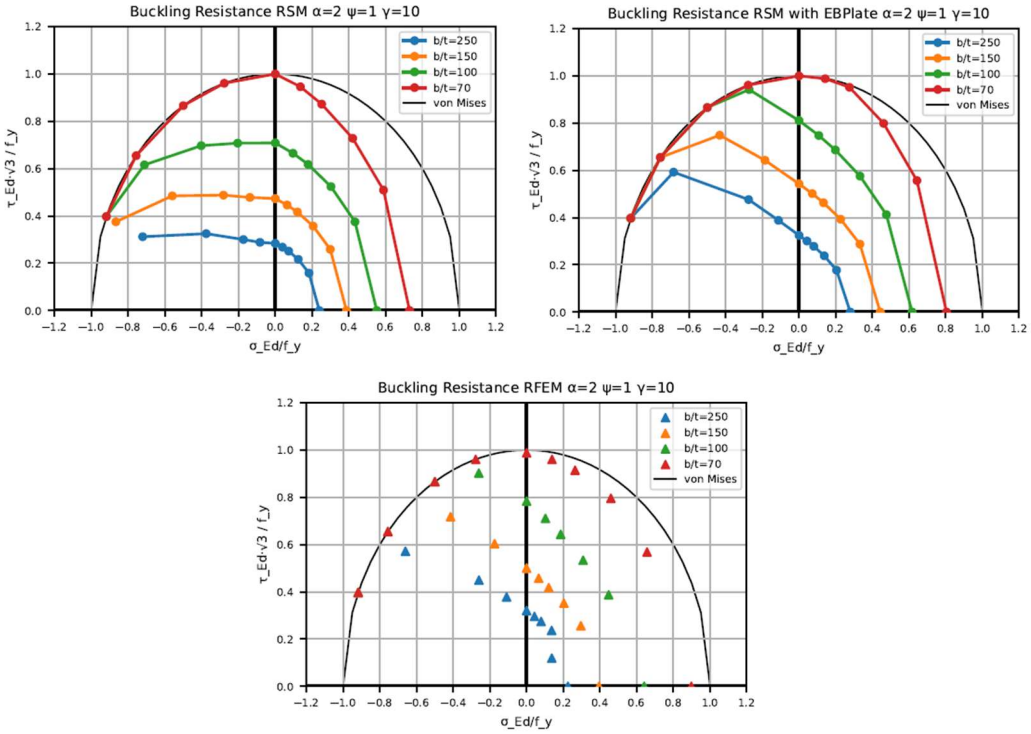

Figure 60 Buckling resistance - influence of plate thickness
Left: Approach 1, right: Approach 2, bottom: Approach 3

8.4.4 Influence of the stress ratio on buckling resistance

Figure 61 do not indicate a clear pattern in the different results between the reduced stress method with EBPlate approach and RFEM results as a function of the stress ratio. The datapoints for the different stress ratios scatter and overlap on the graph. Nevertheless, the results of approach 2 for a stress ratio equal to -0.5 are lower than the results of the RFEM approach than for the other stress ratios. Still, it is frequently observed that reduced stress method with EBPlate approach calculates a higher buckling resistance than RFEM for a stress ratio equal to -0.5.

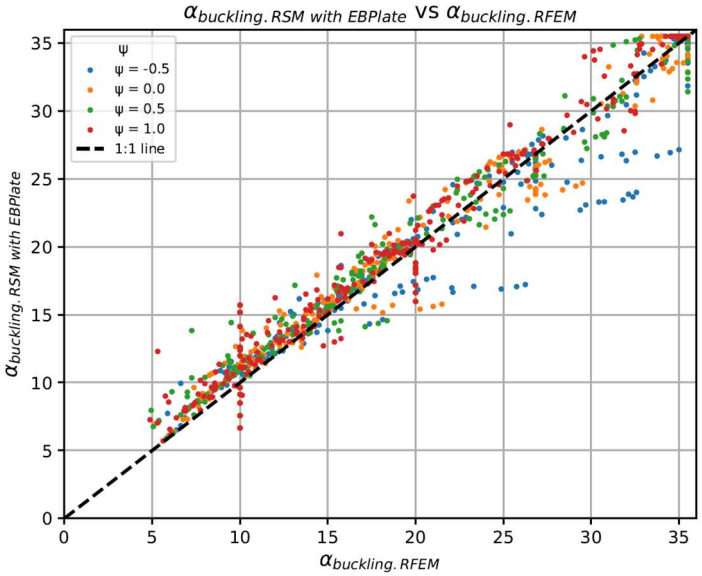

Figure 61 Parity plot: RFEM vs Reduced stress method witb EBPlate (stress ratio coloured).

In addition to the comparison between the reduced stress method with EBPlate approach and RFEM results, the influence of the stress ratio on buckling resistance is also investigated. Based on the outcomes of all three calculation methods, and for both unstiffened and stiffened steel plates, it can be observed that the buckling resistance increases as the stress ratio decreases on the positive side of the graph, when the plate is subjected to combined shear and compressive stresses because lowering the stress ratio results in lower compression stress.

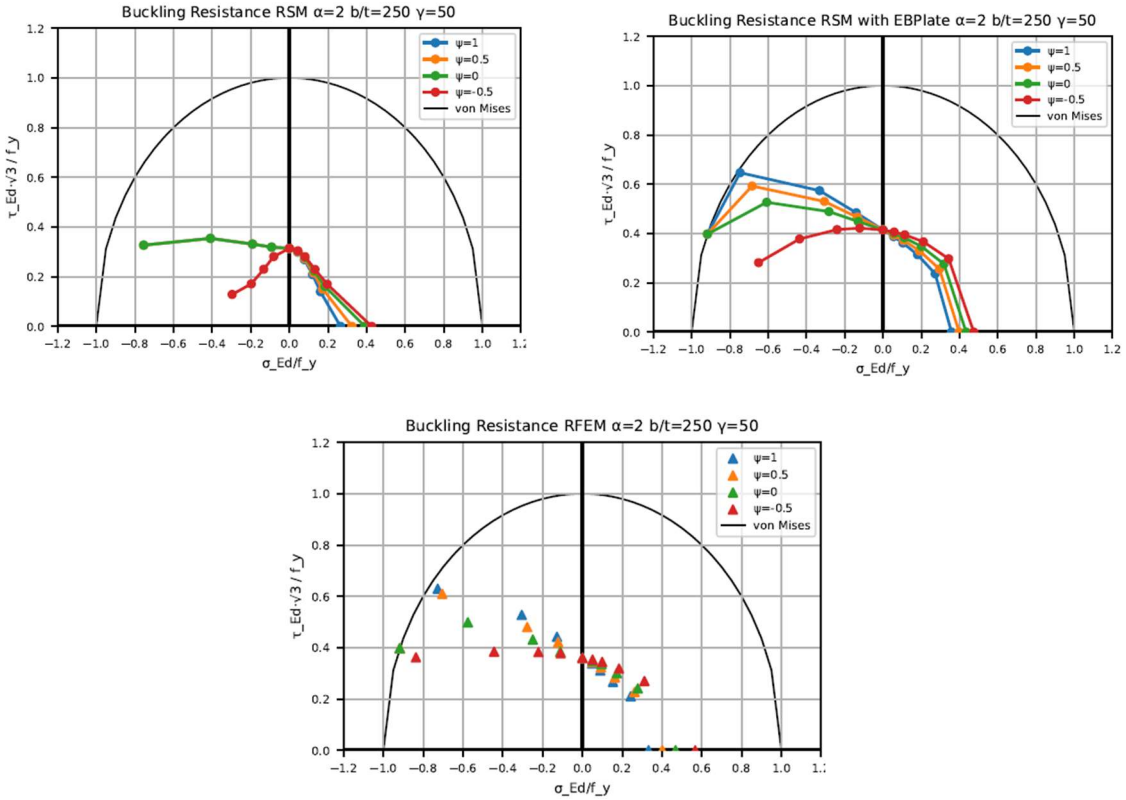

Figure 62 Buckling resistance - influence of stress ratio
Left: Approach 1, right: Approach 2, bottom: Approach 3

When the plate is subjected to combined shear and tension stresses, the negative side of the graph, the opposite trend is observed. The buckling resistance decreases as the stress ratio decreases because a lower stress ratio results in less tensile stresses acting on the steel plate.

The reduced stress method calculates the same buckling resistance for stress ratios equal to 1; 0,5 and 0 in case of a steel plate subjected to tension and shear. This is because $\alpha_{cr,x}$ (Eq. (3.11a)) is assumed as infinite, for stress ratio 1; 0,5 and 0, because only tension stress acts on the steel plate and therefore α_{cr} (Eq. (3.10)) will only depend on the shear stress acting on the steel plate. The shear stress is for all three stress ratios the same which leads to the same buckling resistance.

8.4.5 Influence of the relative flexural stiffness of the stiffener on buckling resistance

From Figure 63, it is observed that no clear trend is visible with respect to the relative flexural stiffness of the stiffener. The data points corresponding to different values of the relative flexural stiffness are scattered and overlap throughout the graphs, indicating that the difference between reduced stress method with EBPlate approach and RFEM results does not systematically depend on this parameter.

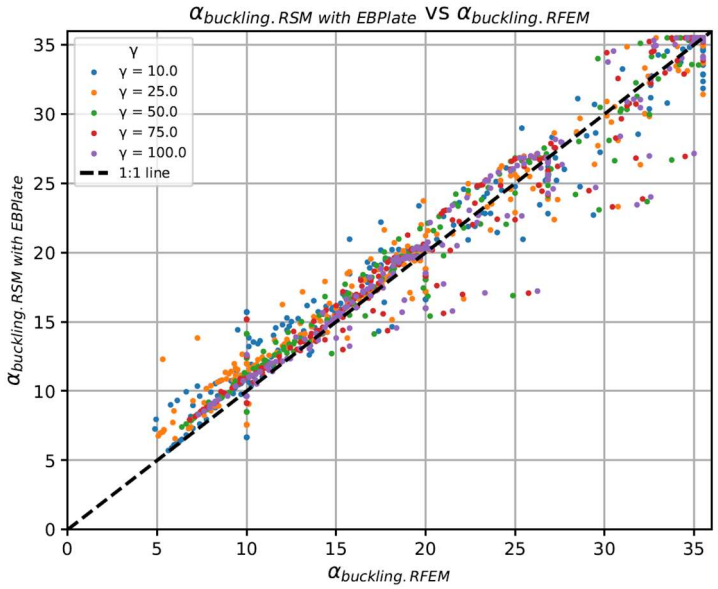

Figure 63 Parity plot: RFEM vs Reduced stress method witb EBPlate (relative flexural stiffness coloured).

In addition to the comparison between the reduced stress method with EBPlate approach and RFEM results, the influence of the relative flexural stiffness on buckling resistance is also investigated. Based on the outcomes of all three calculation methods, and for both unstiffened and stiffened steel plates, it can be observed that the buckling resistance increases as the relative flexural stiffnesses of the stiffener increases. How stiffer the longitudinal stiffener, how greater the restraint against out-of-plane deformation, which lead to an improvement of the structural stability of the plane.

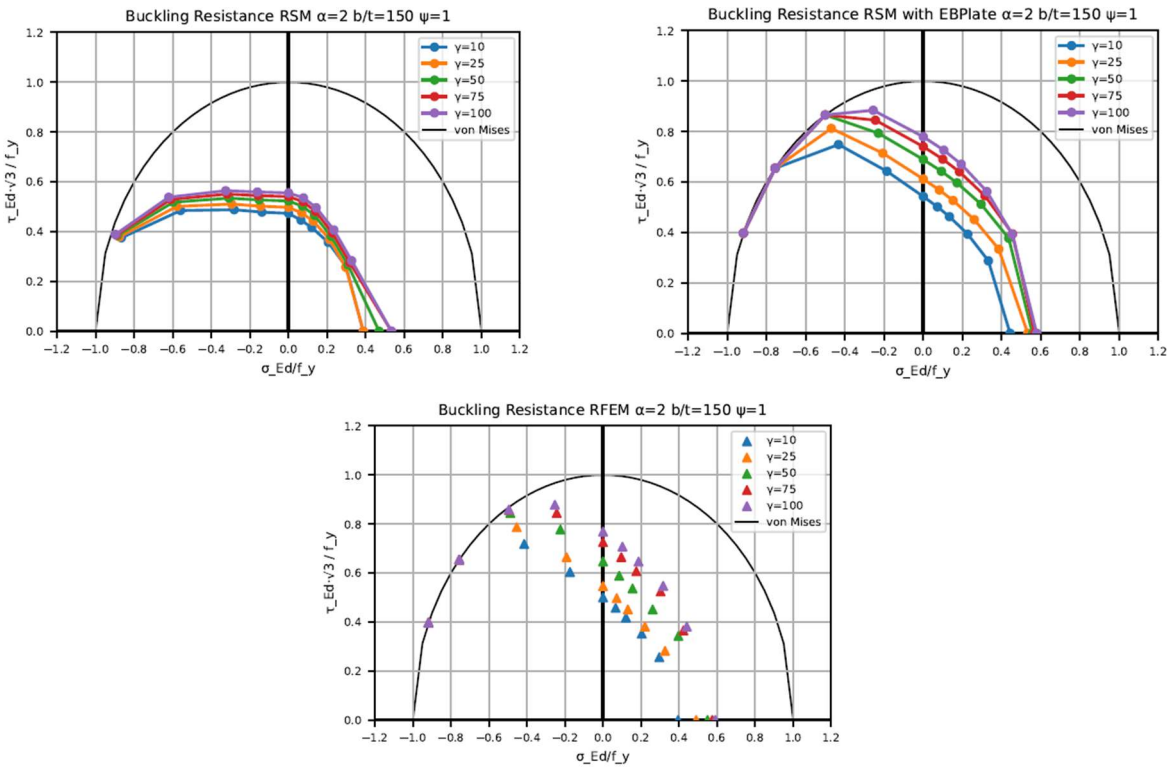

Figure 64 Buckling resistance - influence of relative flexural stiffness
Left: Approach 1, right: Approach 2, bottom: Approach 3

8.5 Analysis of RFEM Outliers

In rare cases, the buckling resistance obtained from RFEM shows a clear deviation from the general trend observed in the other RFEM results. This deviation can be observed in Figure 65 and Figure 66, where the RFEM results, indicated by the red triangles, drop below the expected trend line. These outliners are only present for steel plates with weak stiffeners. It is observed that in these specific cases, the failure is governed by local buckling of the stiffener instead of failure in the plate. As a result, the computed buckling resistance is significantly lower than the buckling resistance would have been, if the failure mode was not in the stiffener but in the plate.

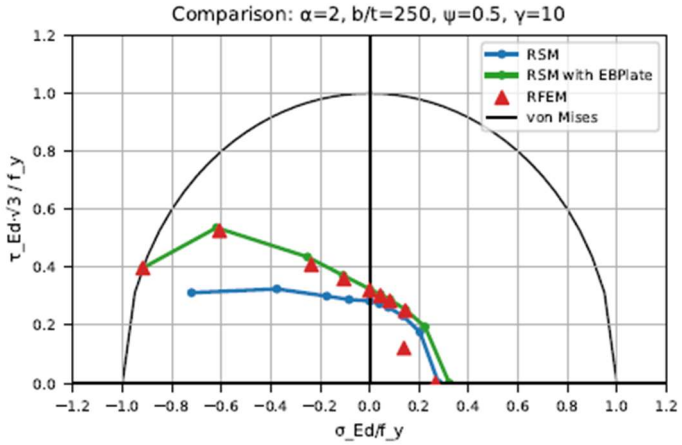

Figure 65 Buckling resistance stiffened steel plate: α=2; b/t=250; ψ=0.5; γ=10

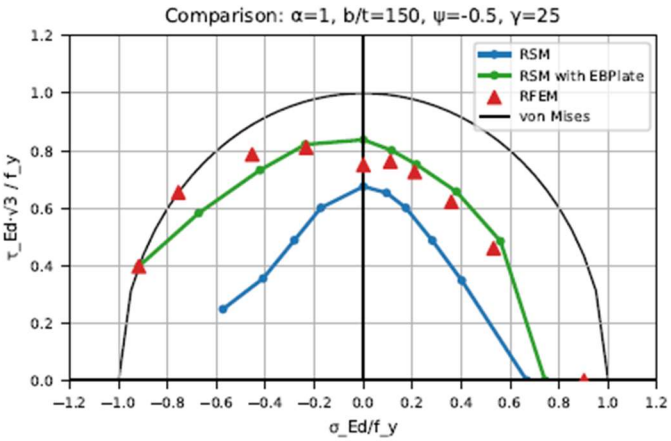

Figure 66 Buckling resistance stiffened steel plate: α=1; b/t=150; ψ=-0.5; γ=25

9 Development of an accurate design approach based on EBPlate

9.1 Introduction

In the previous chapter is shown that for stiffened steel plates the EBPlate approach generally calculates higher buckling resistance values compared to the RFEM approach. In this thesis, RFEM is assumed as the benchmark for realistic structural behaviour, as it is considered to provide more accurate results due to its refined modelling capabilities. However, because FEM simulations take long, EBPlate remains a preferred tool in engineering practice due to its efficiency and ease of use. However, the consistent overestimation of buckling resistance by the EBPlate approach raises concerns regarding safety.

To tackle this issue, this chapter proposes the development of new reduction formulas that can be applied in the EBPlate approach. As a result the buckling resistance of stiffened steel plates calculated with the EBPlate approach in combination with the reduction formulas will be equal to, or lower, than the buckling resistance values obtained with RFEM. In Section 9.2 the methodology used to derive this correction is discussed, while Section 9.3 presents the application of the reduction formulas and compares the adjusted EBPlate results to RFEM results.

9.2 Methodology

The verification formula that is used in the EBPlate approach is shown below as Eq. (9.1). In order to obtain more conservative buckling resistance results using the EBPlate approach, a modification to this formula is proposed. Instead of applying a constant exponent value of 2 to the shear stress term, this value of 2 is replaced with a factor E3, see Eq. (9.2). By reducing the exponent applied to the shear term, so E3 is lower than 2, the buckling resistance will be lower than it was calculated with E3 value equal to 2. The choice to reduce the shear stress term and not the normal stress term is because the RFEM results compared to the EBPlate approach results were lower when there was only normal stress applied, see Section 8.4.1. However, when shear is involved, EBPlate approach tends to overestimate the buckling resistance compared to RFEM.

$$\left(\frac{\sigma_{x,Ed}}{\frac{\rho_x * f_y}{\gamma_{M1}}}\right)^2 + 3\left(\frac{\tau_{Ed}}{\frac{\chi_w * f_y}{\gamma_{M1}}}\right)^2 \leq 1 \tag{9.1}$$

$$\left(\frac{\sigma_{x,Ed}}{\frac{\rho_x * f_y}{\gamma_{M1}}}\right)^2 + 3\left(\frac{\tau_{Ed}}{\frac{\chi_w * f_y}{\gamma_{M1}}}\right)^{E3} \leq 1 \tag{9.2}$$

For each case in the parametric study the factor E3 is calculated, such that the buckling resistance derived from the EBPlate approach match the RFEM results. The buckling resistance calculated with RFEM are used as values for $\sigma_{x,Ed}$ and τ_{Ed} in Eq. (9.2) and the reduction factors calculated with the EBPlate approach are used as values for ρ_x and χ_w in Eq. (9.2), which results in factor E3 being the only unknown. The factor E3 can now be solved for each case to match the buckling resistance of EBPlate approach to that of RFEM. The calculated E3 values are plotted against their corresponding relative slenderness λ_{rel} values, which is shown in Figure 67.

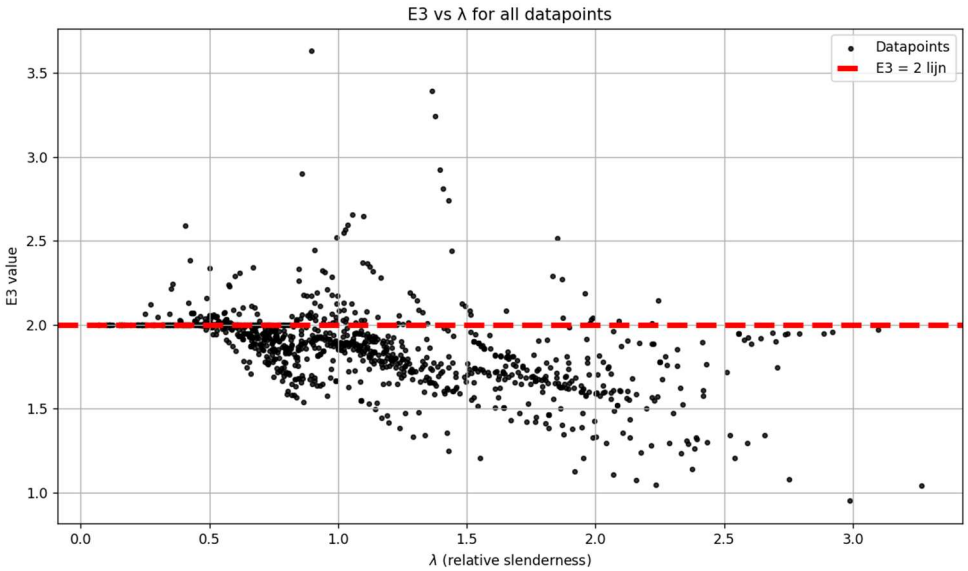

Figure 67 λ_{rel} values vs E3 values for all stiffened plate cases.

Eq (9.3) provides the formula for the relative plate slenderness. The E3 values were plotted against the relative plate slenderness because no clear trend was identified in Section 8.4 regarding which individual parameter influences the difference between the results of Approach 2 and the RFEM approach. The relative plate slenderness includes α_{cr}, which is the minimum load amplifier for the design loads to reach the elastic critical load of the plate, under the complete stress field. This minimum load amplifier depends on all investigated parameters, such as the aspect ratio, plate thickness, stress ratio, and the relative stiffness of the stiffener.

$$\lambda_{rel} = \sqrt{\frac{N_{pl}}{N_{cr}}} = \sqrt{\frac{\alpha_{ult}}{\alpha_{cr}}} \tag{9.3}$$

Three reduction formulas will be introduced to guarantee conservative design results when the EBPlate approach is used. Reduction Formula 1 (RF1) is formulated so that, when applied in combination with the EBPlate approach, only 1% of the resulting buckling resistance values are higher than the corresponding values calculated using RFEM. Similarly, Reduction Formula 5 (RF5) and Reduction Formula 10 (RF10) guarantee that only 5% and 10% of the results from the EBPlate approach in combination with the new reduction formulas, are higher than the RFEM results.

The percentile method is used in order to compute these new reduction formulas. The dataset is divided into bins, each bin contains 10% of the cases of the total datapoints. As a result there are 10 bins each containing 160 cases of the parametric study. For each bin, the 1st, 5th and 10th percentiles of the required E3 reduction factor is calculated and plotted in Figure 68.

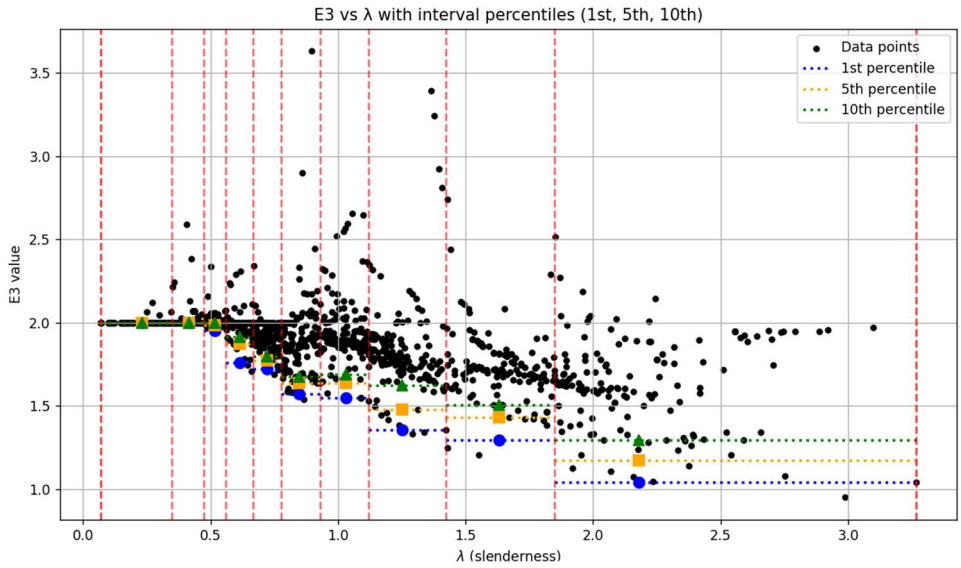

Figure 68 λ_{rel} values vs E3 values for all stiffened plate cases with interval percentiles.

The 1st, 5th and 10th percentiles of the first three bins is equal or close to a value of 2. These cases show already good agreement between Approach 2 and the RFEM results. Therefore, no reduction is needed when the relative plate slenderness λ_{rel} is less than or equal to 0.559. As a result, a curve will be fitted starting from bin number 4. Six polynomial curves are fitted in total, two for each percentile, using either the form $x^2 + bx + c$ or $ax^2 + b$. These fits are based on the calculated percentile values, excluding the first three bins.

This results in two different set of reduction formulas, each set containing three reduction formulas. In Figure 69 the three reduction formulas, with the form $ax^2 + b$, are plotted in the $E3\ vs\ \lambda_{rel}$ plot. In Figure 70 the three reduction formulas, with the form $ax^2 + bx + c$, are plotted in the $E3\ vs\ \lambda_{rel}$ plot. The reduction formulas with the form $ax^2 + bx + c$ are chosen to be used because it resulted in fitted reduction formulas that more closely matched the targeted 1%, 5%, and 10% thresholds, see Table 16.

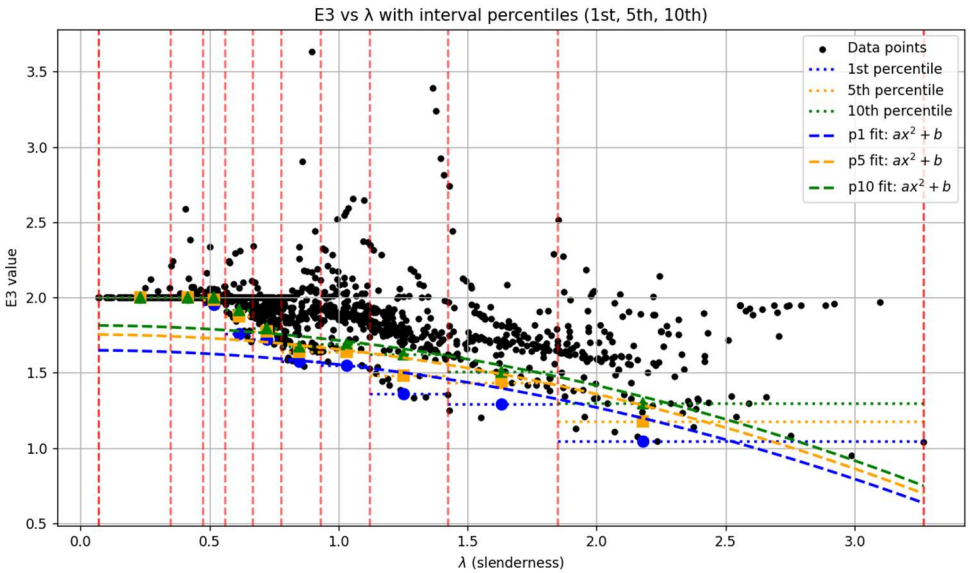

Figure 69 λ_{rel} values vs E3 values with new RF (ax^2+c)

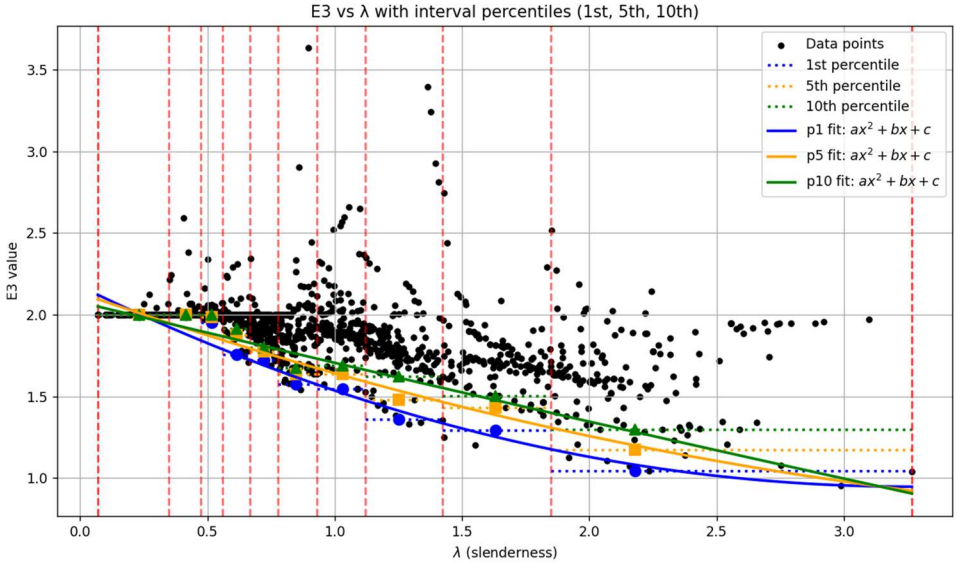

Figure 70 λ_{rel} values vs E3 values with new RF (ax^2+bx+c)

Formula Form	Target Safety Margin	Resulting Formula	Resulting Safety Margin
ax² + b	1%	$E_3 = 2 \quad \text{voor } \lambda_{rel} \leq 0.559$ $E_3 = -0.0951\lambda_{rel}^2 + 1.6496 \quad \text{voor } \lambda_{rel} > 0.559$	2.28%
ax² + b	5%	$E_3 = 2 \quad \text{voor } \lambda_{rel} \leq 0.559$ $E_3 = -0.0991\lambda_{rel}^2 + 1.7543 \quad \text{voor } \lambda_{rel} > 0.559$	6.15%
ax² + b	10%	$E_3 = 2 \quad \text{voor } \lambda_{rel} \leq 0.559$ $E_3 = -0.0998\lambda_{rel}^2 + 1.8147 \quad \text{voor } \lambda_{rel} > 0.559$	10.81%
ax² + bx + c	1%	$E_3 = 2 \quad \text{voor } \lambda_{rel} \leq 0.559$ $E_3 = 0.1034\lambda_{rel}^2 - 0.7322\lambda_{rel} + 2.1627 \quad \text{voor } \lambda_{rel} > 0.559$	1.88%
ax² + bx + c	5%	$E_3 = 2 \quad \text{voor } \lambda_{rel} \leq 0.559$ $E_3 = 0.0596\lambda_{rel}^2 - 0.588\lambda_{rel} + 2.1634 \quad \text{voor } \lambda_{rel} > 0.559$	6.25%
ax² + bx + c	10%	$E_3 = 2 \quad \text{voor } \lambda_{rel} \leq 0.559$ $E_3 = 0.0595\lambda_{rel}^2 - 0.5204\lambda_{rel} + 2.1599 \quad \text{voor } \lambda_{rel} > 0.559$	9.82%

Table 16 Overview new fitted reduction formulas.

In Table 17 the new proposed reduction formulas are shown with their corresponding abbreviation and percentage indicating the safety margin, which must be used in combination with the verification formula, which is Eq. (9.2).

$$\left(\frac{\sigma_{x,Ed}}{\frac{\rho_x * f_y}{\gamma_{M1}}}\right)^2 + 3\left(\frac{\tau_{Ed}}{\frac{\chi_w * f_y}{\gamma_{M1}}}\right)^{E3} \leq 1 \qquad (9.2)$$

Abbreviation	Formula	Safety Margin
RF1	$E_3 = 2 \quad \text{voor } \lambda_{rel} \leq 0.559$ $E_3 = 0.1034\lambda_{rel}^2 - 0.7322\lambda_{rel} + 2.1627 \quad \text{voor } \lambda_{rel} > 0.559$	1%
RF5	$E_3 = 2 \quad \text{voor } \lambda_{rel} \leq 0.559$ $E_3 = 0.0596\lambda_{rel}^2 - 0.588\lambda_{rel} + 2.1634 \quad \text{voor } \lambda_{rel} > 0.559$	5%
RF10	$E_3 = 2 \quad \text{voor } \lambda_{rel} \leq 0.559$ $E_3 = 0.0595\lambda_{rel}^2 - 0.5204\lambda_{rel} + 2.1599 \quad \text{voor } \lambda_{rel} > 0.559$	10%

Table 17 New proposed reduction formulas in combination with Eq. (9.2).

9.3 Implementation

The new reduction formulas have been applied to calculate the buckling resistance of the same steel plates that were investigated in the parametric study. The results of these calculations are displayed in plots and provided in Annex C. One of these plots is shown below as Figure 71. From this figure, it can be seen that the buckling resistance, if calculated using one of the new reduction formulas, is indeed lower than the buckling resistance calculated with RFEM. The reduction formulas do not have any impact on the buckling resistance if only normal stress is applied on the steel plates.

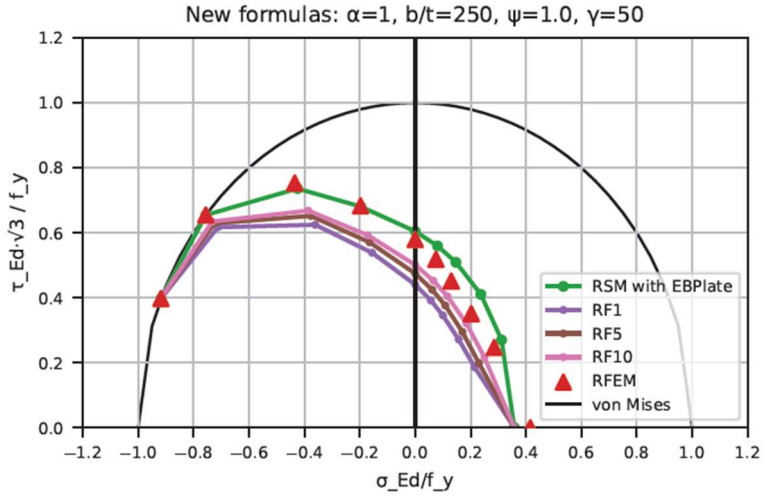

Figure 71 Buckling resistance stiffened steel plate with new RF: α=1; b/t=250; ψ=1; γ=50

The results obtained with the use of the new reduction formulas are plotted against the RFEM results. The same statistical indicators as those in Chapter 8 have also been calculated for each new reduction formula and can be found in each corresponding plot. In this way a good comparison can be made between the new reduction formulas and against the results of approach 1 and 2. In figure 73 the NF1 is plotted 74 nf5 en 75 nf10

The results obtained using the newly developed reduction formulas are plotted against the RFEM results in Figure 72 for NF1, Figure 74 for NF5 and Figure 73 for NF10. The same statistical indicators as those presented in Chapter 8 have been calculated for the results obtained with the new reduction formula and are included in the corresponding plots. This allows for a clear comparison between the newly obtained results from the new reduction formulas and for the results of Approach 1 and Approach 2.

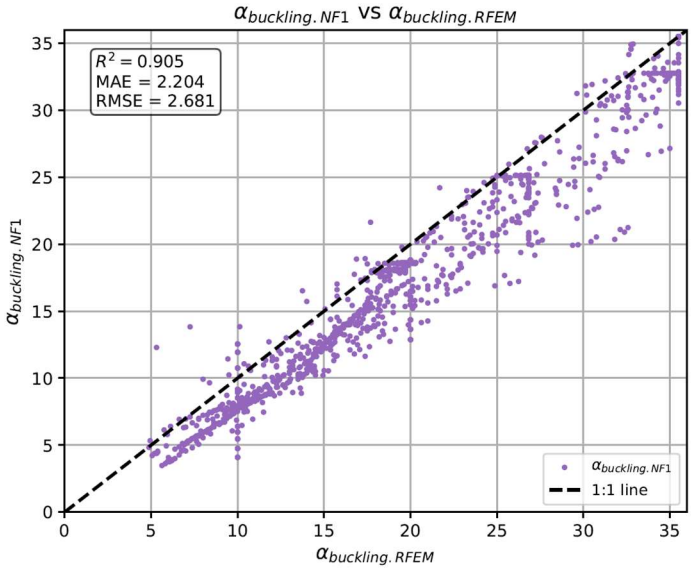

Figure 72 Parity plot: RFEM vs NF1.

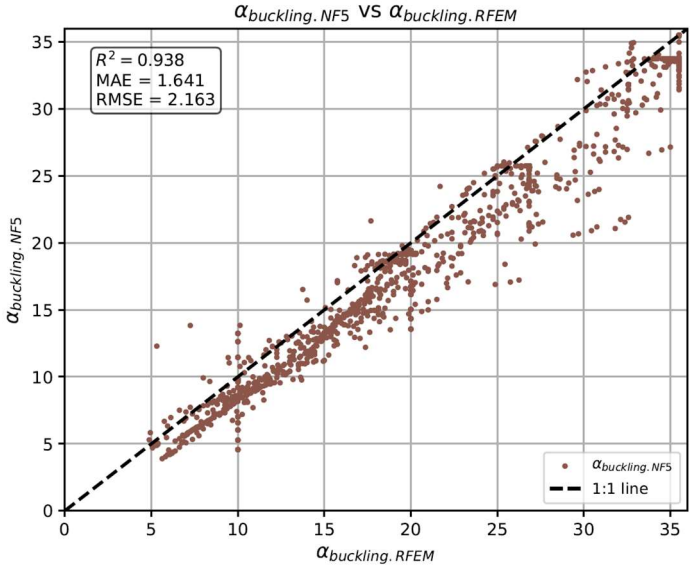

Figure 74 Parity plot: RFEM vs NF5.

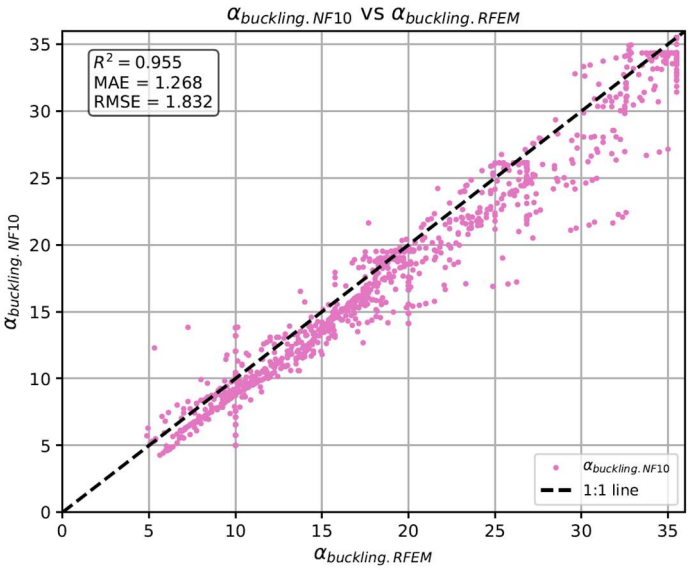

Figure 73 Parity plot: RFEM vs NF10.

If we compare these figures with Figure 55, it can be seen that the datapoints are now plotted on the safe side of the 1:1 line, which was not the case with Figure 55 where the EBPlate approach without reduction was compared to the RFEM results. In Figure 72, it can be seen that for NF1 almost no datapoints (around 1% of all datapoints) are plotted on the unsafe side of the identity line. However, as the NF values increase, more and more datapoints are plotted on the unsafe side of the identity line.

From the statistical indicators that are shown in Table 18 it can be seen that the EBPlate approach still provides results that are the closest to the RFEM results. However, it was observed that the EBPlate approach calculates higher buckling resistances compared to the RFEM calculations. Therefore, new reduction formulas are developed, which calculates more conservative buckling resistances and provide results that align more closely with RFEM than the reduced stress method. The statistical indicators show that all three new reduction formulas demonstrate better agreement with RFEM than the reduced stress method. Among these new reduction formulas, NF10 is the one that is closest to the RFEM results, offering a safer and more reliable approach in comparison with the EBPlate method.

Methode	R^2 (σ/f_y)	MAE (σ/f_y)	RMSE (σ/f_y)
RSM	0.735	2.99	4.344
RSM with EBPlate	0.964	0.909	1.567
NF1	0.905	2.204	2.681
NF5	0.938	1.641	2.163
NF10	0.955	1.268	1.832

Table 18 Statistical indicators of the new reduction formulas.

10 Discussion

10.1 Interpretation of the results

For unstiffened steel plates that are subjected to compression and shear all three approaches gave roughly the same results. This consistency is due to the relatively straightforward buckling behaviour of unstiffened plates under compression and shear stresses. The governing buckling shapes are global and well understood. Without stiffeners, there are no additional localized effects or stiffness variations that can cause divergence between simplified analytical methods and more advanced numerical methods.

When an unstiffened plate is subjected to tension and shear Approach 2 (EBplate) en Approach 3 (RFEM) also gave roughly the same results. However, Approach 1 (reduced stress method) did not match the results of the other two methods. The results of Approach 1 showed a horizontal line in the buckling resistance plot when an unstiffened plate was subjected to tension and shear loading. This is because in case of tension, it is assumed that a steel plate does not buckle and therefore the critical plate buckling stress is not defined, which leads to $\alpha_{cr,x}$ (Eq. (3.10a)) to be assumed as infinite. As a result, the minimum load amplifier α_{cr} (Eq. (3.9)) will only depend on the shear stress acting on the steel plate. This leads to a horizontal buckling resistance, independent of the amount of applied tensile stress.

Approach 2 and 3 do not assume the critical plate buckling stress being infinite. The two approaches model the actual stress state and deformations of the plate, including the positive stabilizing effect of tensile stresses on the shear buckling. This trend can also be observed in the results, where the buckling resistance increases when higher tensile stresses are applied.

For stiffened steel plates, the buckling behaviour becomes more complex due to the presence of stiffeners. The stiffeners cause both local and global buckling modes to occur. This complexity leads to stress distributions and deformation behaviours that are not possible for simplified methods to model. The reduced stress method assume linear-elastic material behaviour, neglect of post-buckling strength and simplified stress redistribution. Moreover, stabilizing effects are not taken into account, such as the beneficial interaction between tensile and shear stresses or the support provided by adjacent stiffeners. As a result, the buckling resistance is calculated lower compared to the buckling resistances determined with RFEM.

The EBPlate approach also consistently calculates buckling resistances higher than the reduced stress method because the load amplifier that EBPlate calculates is consistently higher. This is because EBPlate models the actual stress distribution and deformation shape of the plate using classical plate theory combined with the Rayleigh-Ritz method, which is more accurate in comparison with the simplified formulas used in the reduced stress method. However, the EBPlate approach still relies on many simplified formulas to convert the load amplifier into the final buckling resistance, for example the interaction between plate-like and column-like behaviour is still treated using Eurocode based formulas.

In comparison with the EBPlate approach, the RFEM approach calculates lower buckling resistance values. RFEM includes a more detailed and realistic structural behaviour because it considers geometric and material nonlinearities, post-buckling behaviour and imperfections. Unlike the EBPlate approach, RFEM does not use simplified assumptions or Eurocode-based interaction formulas. RFEM instead performs a full numerical analyses, which allows RFEM to take into account the reduction in stiffness after buckling, the redistribution of stresses in the plate and the influence of imperfections on the buckling resistance. Although EBPlate applies the Rayleigh-Ritz method to approximate deformation shapes and calculate the load amplifier, it still simplifies the interaction between different buckling modes and does not take destabilizing effects into

account. As a result, RFEM is assumed as the benchmark for realistic structural behaviour.

However, it is important to note that RFEM is itself a finite element model and therefore subject to its own assumptions and limitations. The results of RFEM depends on model choices such as boundary conditions, mesh size, imperfections and material definitions. The RFEM results should be considered a relative benchmark and not the absolute truth because no experiments were conducted.

No clear trends were observed in the influence of specific parameters, such as plate slenderness, stress ratio and relative flexural stiffness of the stiffener, that could consistently explain why the EBPlate approach obtained higher results than the RFEM approach. However, when plates were subjected to pure compression, the EBPlate results were not higher than those from RFEM but rather showed closer agreement. A possible explanation for this is that under such loading conditions, the buckling behaviour remains relatively global and less prone to local buckling effects. From the results of the parametric study of unstiffened steel plates was found that the EBPlate approach was able to accurately capture the global behaviour of the plate and produce similar results as RFEM. The presence of stiffeners and more complex loading conditions(shear and normal stress) introduce local buckling phenomena and stress redistributions, which increase the complexity of the structural behaviour. The EBPlate approach appears to be unable to fully capture these effects, which could explain the observed overestimation of buckling resistance in those cases.

10.2 Application

The three new proposed reduction formulas are for engineers that need to determine the buckling resistance of stiffened steel plates, but do not have the time or resources to model the stiffened steel plates in a FEM model. With the use of FEM the most accurate buckling resistance can be determined, but they are time-consuming and require significant expertise. On the other hand, the reduced stress method can be used, but it calculates overly conservative buckling resistances for stiffened steel plates. Therefore, the new proposed formulas in combination with EBPlate offer an alternative between the two extremes. The new proposed formulas improve the accuracy of the EBPlate approach without requiring a time-consuming FEM model and avoid the excessive conservatism of the reduced stress method. This ensures broad applicability in practical engineering situations

The new proposed formulas were developed using a large dataset that includes a wide de range of design parameters, including large ranges of slenderness ratios, stress ratios and relative flexural stiffness of the stiffeners. The new proposed reduction formulas may only be used for steel plates that have parameters within the investigated parametric study.

Three predetermined safety margins of 1%, 5% and 10% can be chosen by the user for the desired level of safety, which gives the user flexibility in their design approach. The user can select the desired level of safety margin depending upon the conservatism required. A 1% safety margin will provide a lower buckling resistance, but it is a safer and more conservative solution. On the other hand, a 10% safety margin provides a less conservative solution, with the buckling resistance calculated to be much higher. The trade-off between safety and accuracy must be considered carefully. While stronger resistance values are provided by the increased safety margins, they may also lead to too safe results that do not align with RFEM results. It should be understand that safety is a fundamental consideration in engineering design, but it is equally essential to have realistic predictions with good agreement to real behaviour as provided by RFEM.

10.3 Limitations

The scope of the parametric study is limited to stiffened plates with a single longitudinal stiffener positioned at mid-span. Only single sided flat bar stiffeners were considered, while closed stiffeners are not used in the parametric study. Only for this type of stiffener and location of this stiffener the new proposed formulas can be used with full reliability and cannot be used with full reliability for stiffened steel plates with multiple stiffeners or different kind of stiffeners.

For each case in the parametric study two GMNIA analyses were performed with two different imperfections. The imperfections were based on the buckling shapes from the first local eigenmode and the first global eigenmode. To determine if an eigenmode was classified as local or as global a threshold value for the normalized deformation amplitude was used. The classification threshold of 0.35 for distinguishing between global and local eigenmodes was determined based on visual inspection and multiple examples within this parametric study. The threshold was effective in separating clearly different buckling behaviours, it is important to note that this value was not derived from literature.

The new proposed reduction formulas developed in this study are specifically designed based on the modelling assumptions and computational framework of EBPlate. The formulas are not directly transferable to other engineering software because they are based on the computational methods and boundary conditions of EBPlate, which limits their general applicability.

11 Conclusion and recommendation

The aim of this thesis has been to get a better insight of the influence of tensile stress, in combination with shear stress, on the buckling resistance of unstiffened and stiffened steel plates. The main research question is:

"How to consider the effect of tensile stress on the shear buckling resistance of stiffened steel plates with varying normal stress distributions and geometric parameters in an accurate analytical approach."

11.1 Conclusion

When unstiffened plates are subjected to compression and shear, the buckling resistance that is calculated is the same for the reduced stress method (Approach 1), the reduced stress method combined with EBPlate (Approach 2) and RFEM (Approach 3). Reasoning therefore is that de buckling behaviour of unstiffened steel plates is well understood. Approach 1 does not take into account the positive influence of tensile stresses. As a result, Approach 1 calculates lower buckling resistance for an unstiffened plates that is subjected to tension and shear in comparison to Approaches 2 and 3.

For stiffened plates, the presence of stiffeners leads to a distinction between global and local buckling modes, increasing the complexity of the buckling behaviour of the plate. This buckling behaviour is now also influenced more strongly by column-like behaviour, rather than purely plate-like behaviour. Approach 1 consistently predicts lower buckling resistance for compression-shear and tension-shear than the other two approaches because it is based on simplified analytical formulas that assume uniform stress distribution and do not take into account he interaction between global and local buckling. Furthermore, the reduced stress method assumes a conservative estimation of the critical stress by neglecting post-buckling strength and stress redistribution effects. However, Approach 2 consistently calculates the highest buckling resistance among the three methods. The load amplifier computed by EBPlate which is used in Approach 2 is higher than de load amplifier computed by the reduced stress method. EBPlate models the actual stress distribution and deformation shape of the plate to determine the load amplifier, in contrast to Approach 1 that calculates the load amplifier with simplified formulas.

RFEM is assumed as the benchmark because it uses detailed finite element modelling, including geometrical and material nonlinearities as well as imperfections. This leads to predictions that closely represent actual structural behaviour. No trends were observed in the influence of specific parameters that could explain why the EBPlate Approach consistently obtained higher results than the RFEM method. Except that in cases of pure compression, EBPlate provides equal or lower buckling resistance values compared to RFEM results. This is likely because pure compression involves less complexity, which is dominated by global buckling.

As a result, the verification formula Eq. (9.1) that is used in Approach 2 is modified for the shear stress term, which leads to three new proposed reduction formulas, see Eq. (9.2) in combination with Table 9.2. Each reduction formula has a different safety margin, so that the user is able to select the desired level of safety margin depending upon the conservatism required. A lower safety margin calculates a higher buckling resistance but increases the risk that the EBPlate result exceeds the RFEM result. The reduction formulas were also applied to the parametric study and demonstrated their effectiveness. They ensure that the buckling resistance values calculated with EBPlate fall below the RFEM results while being closer to the RFEM results than the results of the original reduced stress method.

$$\left(\frac{\sigma_{x,Ed}}{\frac{\rho_x * f_y}{\gamma_{M1}}}\right)^2 + 3\left(\frac{\tau_{Ed}}{\frac{\chi_w * f_y}{\gamma_{M1}}}\right)^{E3} \leq 1 \qquad (9.2)$$

Abbreviation	Formula	Safety Margin
RF1	$E_3 = 2$ voor $\lambda_{rel} \leq 0.559$ $E_3 = 0.1034\lambda_{rel}^2 - 0.7322\lambda_{rel} + 2.1627$ voor $\lambda_{rel} > 0.559$	1%
RF5	$E_3 = 2$ voor $\lambda_{rel} \leq 0.559$ $E_3 = 0.0596\lambda_{rel}^2 - 0.588\lambda_{rel} + 2.1634$ voor $\lambda_{rel} > 0.559$	5%
RF10	$E_3 = 2$ voor $\lambda_{rel} \leq 0.559$ $E_3 = 0.0595\lambda_{rel}^2 - 0.5204\lambda_{rel} + 2.1599$ voor $\lambda_{rel} > 0.559$	10%

Table 19 New proposed reduction formulas in combination with Eq. (9.2).

11.2 Recommendations for Modelling

For unstiffened plates subjected to compression and shear the reduced stress method or the EBPlate approach is recommended to use to calculate the buckling resistance of the unstiffened steel plates because the results are in good agreement with the results from RFEM analyses. However, when tensile stresses are subjected to unstiffened steel plates the reduced stress method can be used, but is not recommended. The reduced stress method does not take into account the positive influence of tensile stresses on the shear buckling resistance. However, the EBPlate approach will take into account these positive influence of tensile stresses, which leads to buckling resistances that closely match those obtained from RFEM.

For stiffened plates subjected to pure compression the EBPlate method without reduction formulas is recommended because the buckling resistance calculated with the use of the EBPlate method are similar to the RFEM results. However, if shear is added to the plate the EBPlate approach in combination with the new reduction formulas is recommended. As a result, the buckling resistance will be calculated close to the RFEM results.

11.3 Recommendations for Future Studies

The main focus of this thesis was on the buckling resistance of (un)stiffened steel plates with an aspect ratio of 1 or higher. The stiffened steel plates were stiffened with a single longitudinal stiffener which was located at mid-height of the plate. To broaden the scope and improve the general applicability of the findings, the following points are recommended for future research:

Varying stiffener position: In the parametric study conducted in this thesis, the location of the stiffener was for all cases placed in the middle of the height of the plates. With varying the location of the stiffener, it can be investigated whether the differences in the buckling resistance calculated by the three different methods increase or decrease when the stiffeners are placed, for example, at their optimal position.

Multiple stiffeners: Expand the scope to steel plates with multiple stiffeners instead of only adding one single stiffener. With would allow the influence of both the number of stiffeners and distribution of stiffeners on the buckling resistance of plates that are subjected to normal and shear tress to be explored. In this way it can be assessed whether the new proposed reduction formulas in combination with EBPlate provide safe results for multi-stiffened plates in comparison to RFEM results.

Plates with aspect ratio lower than 1: Expand the study to plates with an aspect ratio lower than 1. These type of plates are also commonly used plates which are found in steel structures in for example steel bridges. Future search should assess whether the same differences between the three methods are observed for these type of plates and whether the new proposed reduction formulas remain applicable and yield safe results for plates with an aspect ratio of 1 or lower.

To expand the scope with the above recommendations, the overall relevance and robustness of the conclusions will increase. It will also further validate the use of the new proposed reduction formulas in combination with EBPlate under a wider range of geometric and structural conditions.

12 Literature and Other sources

[1] Zizza, A. (2016). Buckling behaviour of unstiffened and stiffened steel plates under multiaxial stress states. https://doi.org/10.18419/opus-8994

[2] Oguaghamba, O. A., Ezeh, J. C., Ibearugbulem, M. O., Ettu, L. O., Imo State University, & Federal University of Technology. (2015). *Buckling and postbuckling loads characteristics of all edges clamped thin rectangular plate*. The International Journal of Engineering and Science (IJES), 4(11), 55–61. https://www.theijes.com/papers/v4-i11/Version-2/I041101055061.pdf

[3] Braun, B. (2010). *Stability of steel plates under combined loading*. https://doi.org/10.18419/opus-349

[4] EN 1993-1-5. (2005). Eurocode 3: Design of steel structures – Part 1-5: Plated structural elements. European Committee for Standardization (CEN).

[5] L. Euler, "Euler's calculation of buckling loads for columns of non-uniform section," *In The Rational Mechanics of Flexible or Elastic Bodies,* 1757.

[6] Veljkovic, M. (2020). *CIE4115: Steel Structures 2* [Lecture slides]. Brightspace. Retrieved June 2025, from https://brightspace.tudelft.nl/d2l/le/content/399204/viewContent/2481977/View

[7] Van der Burg, M. J. M. (2011). *Plate buckling in design codes: The difference between NEN 6771 and NEN-EN 1993-1-5* [PhD Thesis, Delft University of Technology].

[8] T. von Karman, "Festigkeitsproblem im Maschinenbau," *Encyk. D. Math. Wiss,* vol. IV, pp. 311-385, 1910.

[9] X, N. (n.d.). *Introduction to plate buckling*. https://www.steel-insdag.org/assets/frontend/trmpdf/Chapter7.pdf

[10] Ziemian, R. D. (2010). *Guide to stability design criteria for metal structures*. Wiley. https://doi.org/10.1002/9780470549087

[11] Augustyn, K. E., Quiel, S. E., & Garlock, M. E. (2022). Post-buckling shear resistance of slender girder webs: Stiffener participation and flange contributions. *Journal Of Constructional Steel Research*, *190*, 107117. https://doi.org/10.1016/j.jcsr.2021.107117

[12] Basler K. Strength of plate girders in shear. J Struct Div 1961;87:151–80.

[13] Pedro, J. J. O., Nascimento, S., & Hendy, C. (2024). Shear buckling resistance models for plate girders – Review and improvements. *Engineering Structures*, *307*, 117857. https://doi.org/10.1016/j.engstruct.2024.117857

[14] Rockey KC, Skaloud M. The Ultimate Behavior of Plate Girders Loaded in Shear. IABSE Colloq Des plate Box girders Ultim Strength 1971:1–19.

[15] Porter DM, Rockey KC, Evans HR. The collapse behaviour of plate girders loaded in shear, the, Struct. Eng 1975;53:313–25.

[16] Hoglund ¨ T. Shear buckling resistance of steel and aluminium plate girders. ThinWalled Struct 1997;29:13–30. https://doi.org/10.1016/S0263-8231(97)00012-8.

[17] Dubas, P., & Gehri, E. (1986). *Behaviour and design of steel plated structures*. http://ci.nii.ac.jp/ncid/BA53772683

[18] Ahlstrand, E., & Johansson, J. (2021). *Steel design of plated structural elements – A comparison of the effective width method and the reduced*. Chalmers University of Technology. https://odr.chalmers.se/items/4e3c8393-9225-41cc-b00c-0c6c7b2d10be

[19] Galéa, Y., & Martin, P. (2006). *Presentation manual of EBPlate* (1st ed.). CTICM – Centre Technique Industriel de la Construction Métallique.

[20] Muller, C. (2003). *Zum Nachweis ebener Tragwerke aus Stahl gegen seitliches Ausweichen* [Dissertation, RWTH Aachen].

[21] Johansson, B., Maquoi, R., Sedlacek, G., Müller, C., Beg, D., Joint Research Centre, & European Convention for Constructional Steelwork. (2007). *Joint report: Commentary and worked examples to EN 1993-1-5 "Plated Structural Elements"*. European Commission. http://www.steelconstruct.com/

[22] Beg, D., Kuhlmann, U., Davaine, L., Braun, B., & ECCS. (2010). *Design of plated structures (*1st ed.). ECCS – European Convention for Constructional Steelwork. https://www.stalforbund.no/wp-content/uploads/2015/07/ECCS_EDM3_table_of_contents.pdf

[23] Galéa, Y., & Martin, P. (2010). *Longitudinally stiffened plates in Eurocode 3: Calculation of the global critical buckling stress*. Journal of Constructional Steel Research, 66(11), 1345–1353.

https://doi.org/10.1016/j.jcsr.2010.05.001

[24] Maiorana, E., Pellegrino, C., & Modena, C. (2010). *Influence of longitudinal stiffeners on elastic stability of girder webs*. Journal of Constructional Steel Research, 67(1), 51–64. https://doi.org/10.1016/j.jcsr.2010.07.005

[25] Simulia. (2011). *Abaqus 6.11 documentation*. Dassault Systèmes.

[26] Braun, B., Chacón, R., Degée, H., Duchêne, Y., Dunai, L., Kövesdi, B., Kuhlmann, U., Lener, G., Pourostad, V., Sinur, F., & Timmers, R. (2023). *Design of steel plated structures with finite elements* (1st ed.). ECCS – European Convention for Constructional Steelwork. https://www.steelconstruct.com

[27] Komatsu, S., "Ultimate Strength of Stiffened Plate Girders Subjected to Shear". IABSE Colloquium on Design on Plate Girders for Ultimate Strength. Mar. 1971, pp. 49-65.

Appendix A: Buckling resistance for unstiffened plates - Approach 1, 2 and 3 side by side

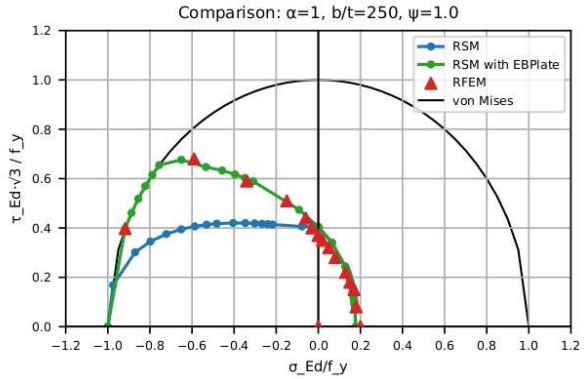
Comparison: α=1, b/t=250, ψ=1.0
RSM
RSM with EBPlate
RFEM
von Mises
τ_Ed·√3 / f_y
σ_Ed/f_y

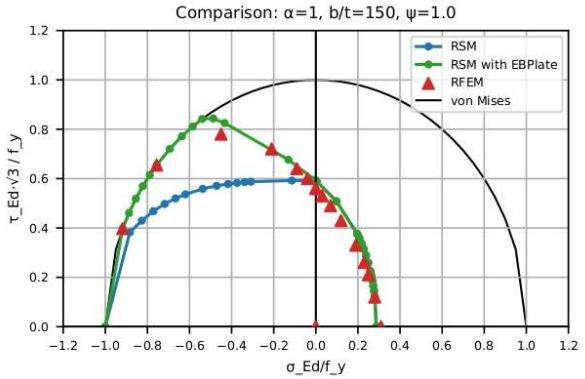
Comparison: α=1, b/t=150, ψ=1.0
RSM
RSM with EBPlate
RFEM
von Mises
τ_Ed·√3 / f_y
σ_Ed/f_y

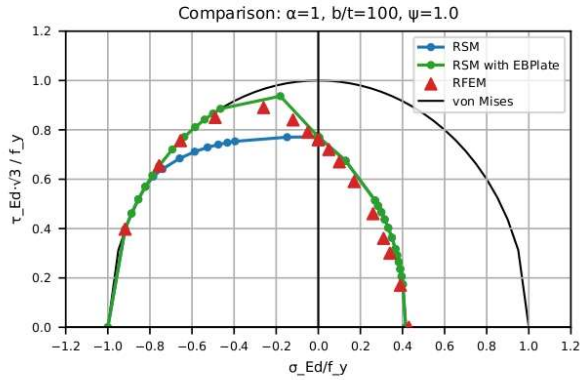
Comparison: α=1, b/t=100, ψ=1.0
RSM
RSM with EBPlate
RFEM
von Mises
τ_Ed·√3 / f_y
σ_Ed/f_y

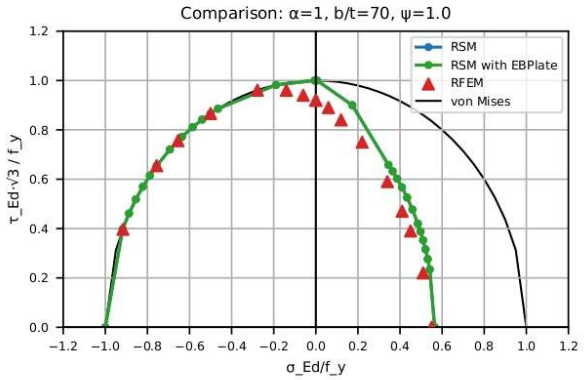
Comparison: α=1, b/t=70, ψ=1.0
RSM
RSM with EBPlate
RFEM
von Mises
τ_Ed·√3 / f_y
σ_Ed/f_y

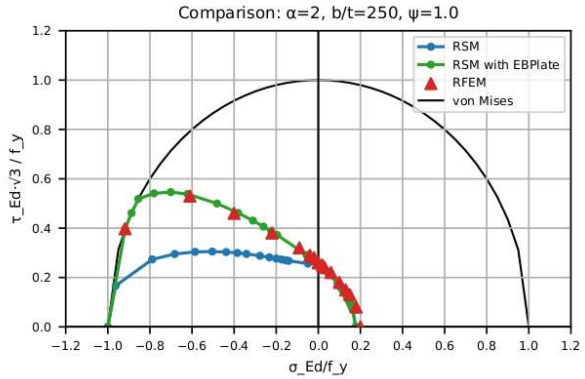
Comparison: α=2, b/t=250, ψ=1.0
RSM
RSM with EBPlate
RFEM
von Mises
τ_Ed·√3 / f_y
σ_Ed/f_y

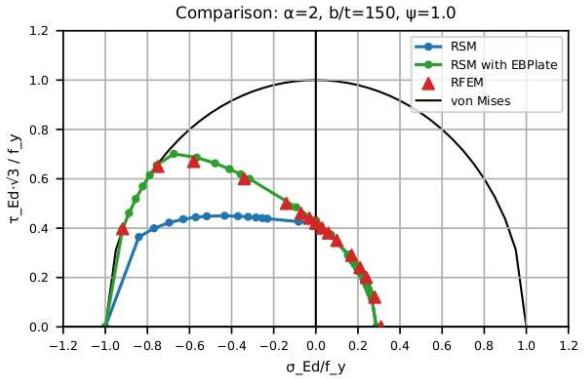
Comparison: α=2, b/t=150, ψ=1.0
RSM
RSM with EBPlate
RFEM
von Mises
τ_Ed·√3 / f_y
σ_Ed/f_y

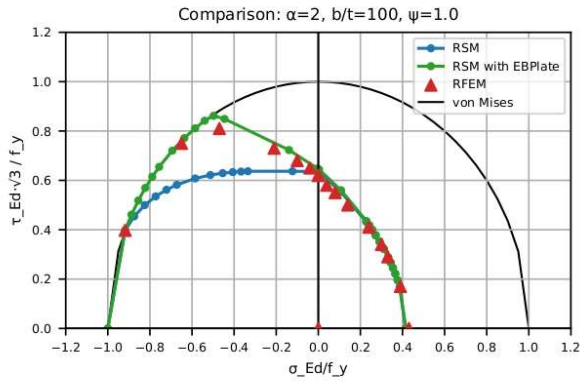
Comparison: α=2, b/t=100, ψ=1.0
RSM
RSM with EBPlate
RFEM
von Mises
τ_Ed·√3 / f_y
σ_Ed/f_y

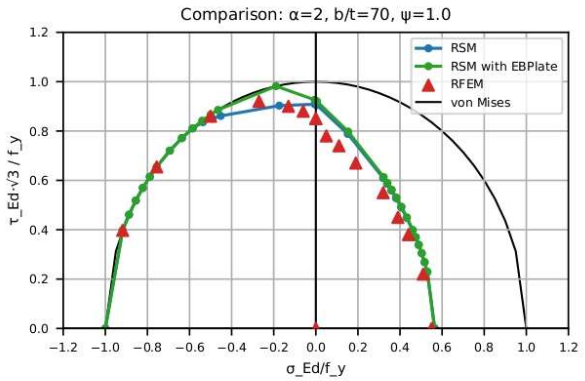
Comparison: α=2, b/t=70, ψ=1.0
RSM
RSM with EBPlate
RFEM
von Mises
τ_Ed·√3 / f_y
σ_Ed/f_y

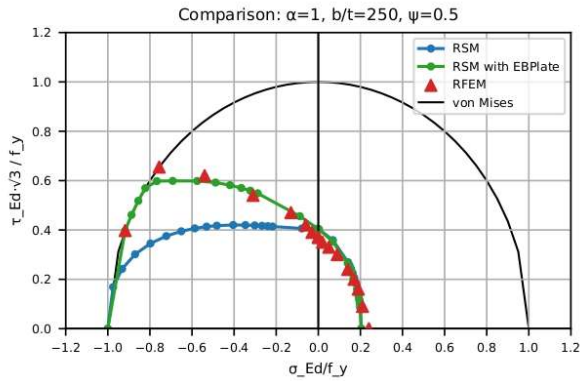
Comparison: α=1, b/t=250, ψ=0.5
RSM
RSM with EBPlate
RFEM
von Mises
τ_Ed·√3 / f_y
σ_Ed/f_y

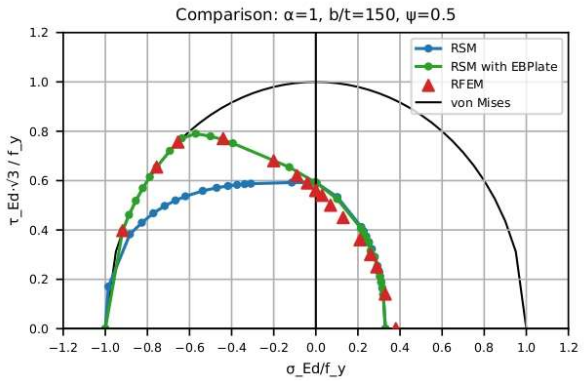
Comparison: α=1, b/t=150, ψ=0.5
RSM
RSM with EBPlate
RFEM
von Mises
τ_Ed·√3 / f_y
σ_Ed/f_y

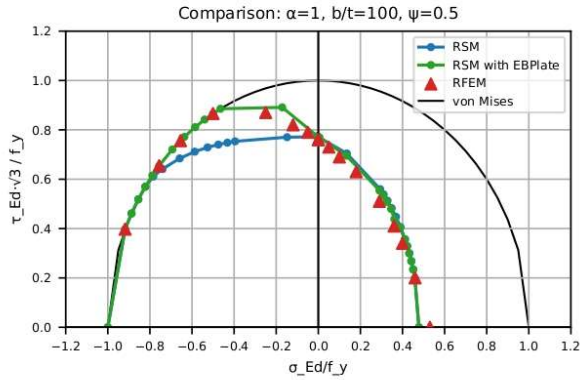
Comparison: α=1, b/t=100, ψ=0.5
RSM
RSM with EBPlate
RFEM
von Mises
τ_Ed·√3 / f_y
σ_Ed/f_y

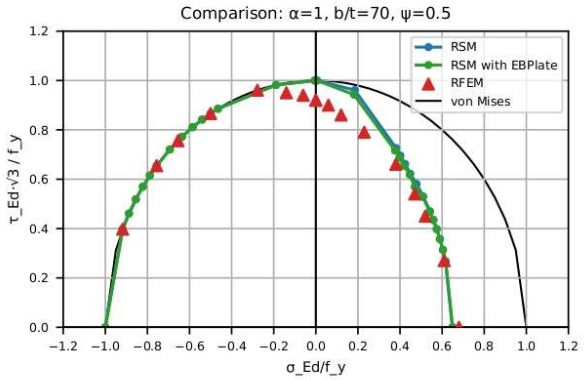
Comparison: α=1, b/t=70, ψ=0.5
RSM
RSM with EBPlate
RFEM
von Mises
τ_Ed·√3 / f_y
σ_Ed/f_y

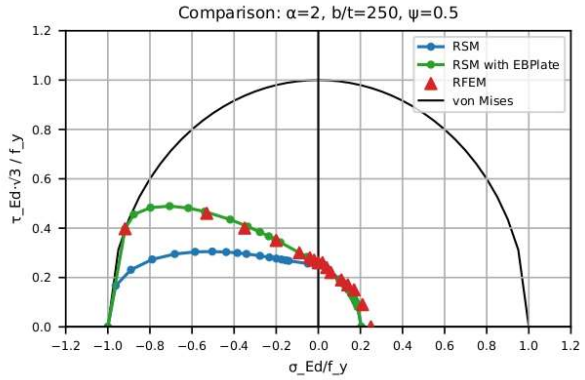
Comparison: α=2, b/t=250, ψ=0.5
RSM
RSM with EBPlate
RFEM
von Mises
τ_Ed·√3 / f_y
σ_Ed/f_y

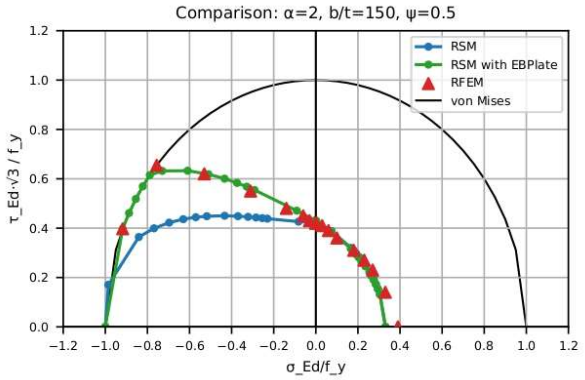
Comparison: α=2, b/t=150, ψ=0.5
RSM
RSM with EBPlate
RFEM
von Mises
τ_Ed·√3 / f_y
σ_Ed/f_y

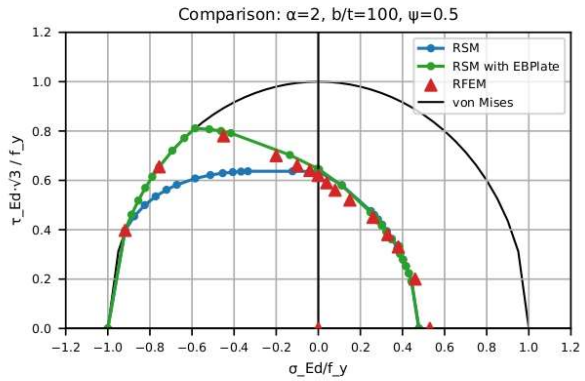
Comparison: α=2, b/t=100, ψ=0.5
RSM
RSM with EBPlate
RFEM
von Mises
τ_Ed·√3 / f_y
σ_Ed/f_y

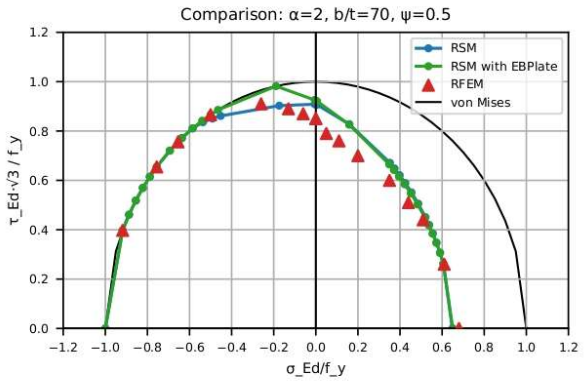
Comparison: α=2, b/t=70, ψ=0.5
RSM
RSM with EBPlate
RFEM
von Mises
τ_Ed·√3 / f_y
σ_Ed/f_y

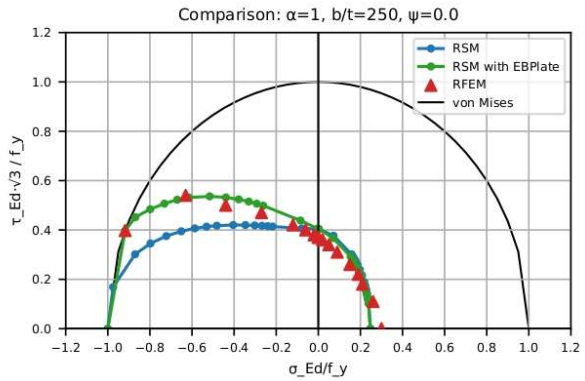
Comparison: α=1, b/t=250, ψ=0.0
RSM
RSM with EBPlate
RFEM
von Mises
τ_Ed·√3 / f_y
σ_Ed/f_y

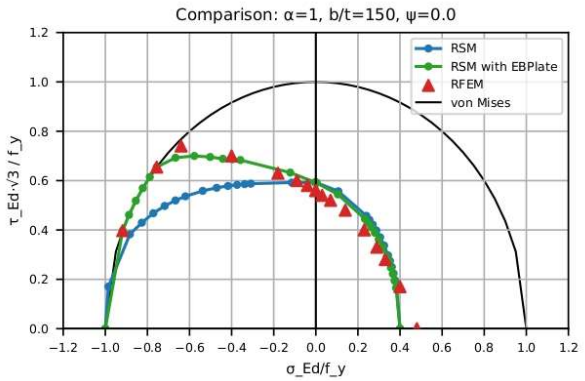
Comparison: α=1, b/t=150, ψ=0.0
RSM
RSM with EBPlate
RFEM
von Mises
τ_Ed·√3 / f_y
σ_Ed/f_y

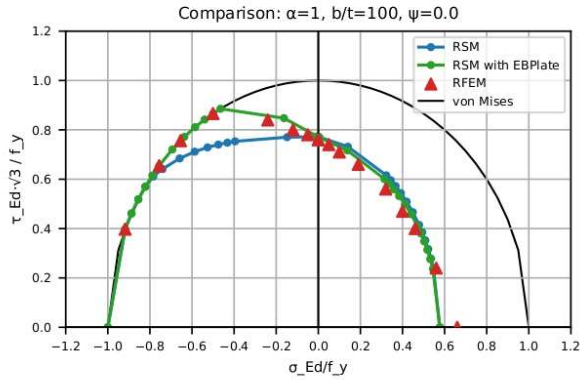
Comparison: α=1, b/t=100, ψ=0.0
RSM
RSM with EBPlate
RFEM
von Mises
τ_Ed·√3 / f_y
σ_Ed/f_y

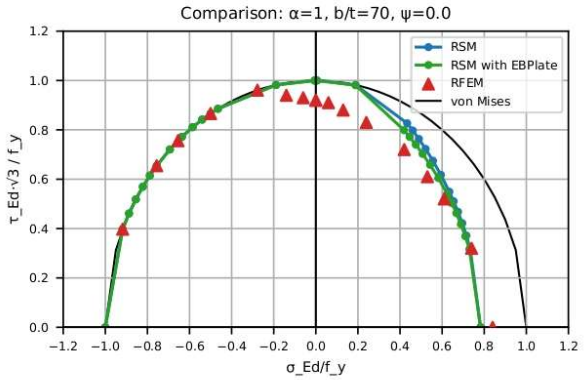
Comparison: α=1, b/t=70, ψ=0.0
RSM
RSM with EBPlate
RFEM
von Mises
τ_Ed·√3 / f_y
σ_Ed/f_y

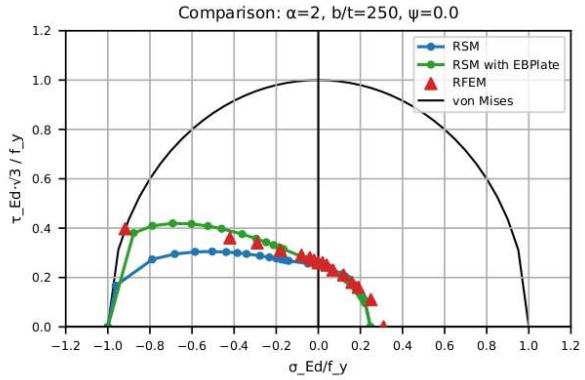
Comparison: α=2, b/t=250, ψ=0.0
RSM
RSM with EBPlate
RFEM
von Mises
τ_Ed·√3 / f_y
σ_Ed/f_y

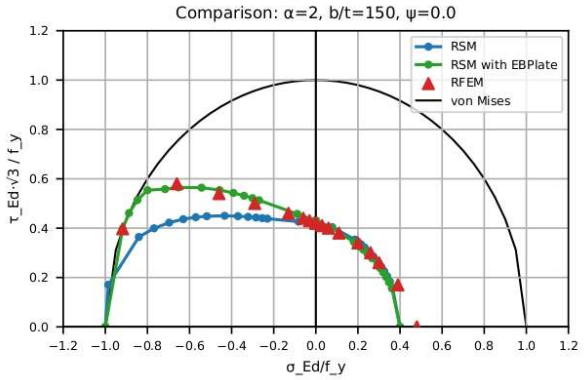
Comparison: α=2, b/t=150, ψ=0.0
RSM
RSM with EBPlate
RFEM
von Mises
τ_Ed·√3 / f_y
σ_Ed/f_y

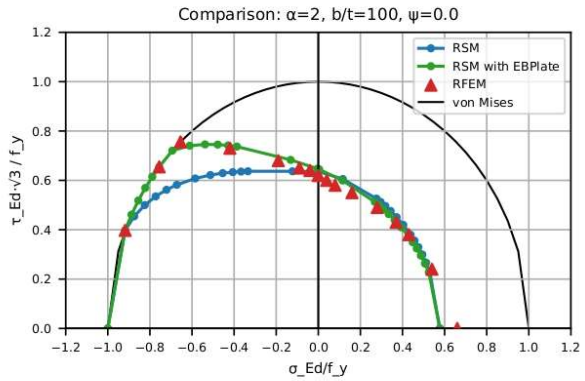
Comparison: α=2, b/t=100, ψ=0.0
RSM
RSM with EBPlate
RFEM
von Mises
τ_Ed·√3 / f_y
σ_Ed/f_y

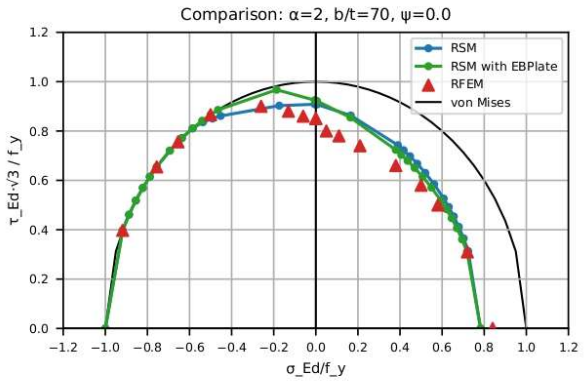
Comparison: α=2, b/t=70, ψ=0.0
RSM
RSM with EBPlate
RFEM
von Mises
τ_Ed·√3 / f_y
σ_Ed/f_y

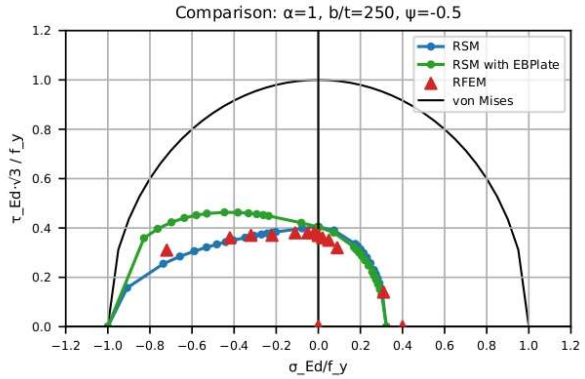
Comparison: α=1, b/t=250, ψ=-0.5
RSM
RSM with EBPlate
RFEM
von Mises
τ_Ed·√3 / f_y
σ_Ed/f_y

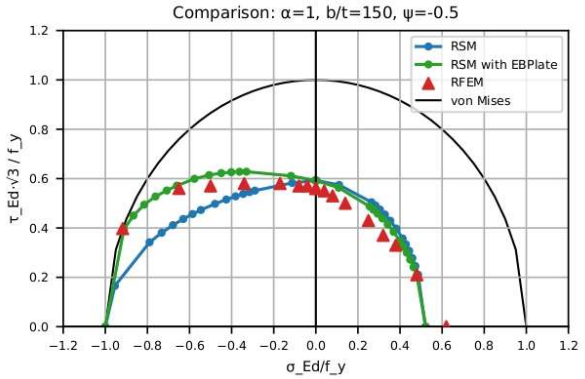
Comparison: α=1, b/t=150, ψ=-0.5
RSM
RSM with EBPlate
RFEM
von Mises
τ_Ed·√3 / f_y
σ_Ed/f_y

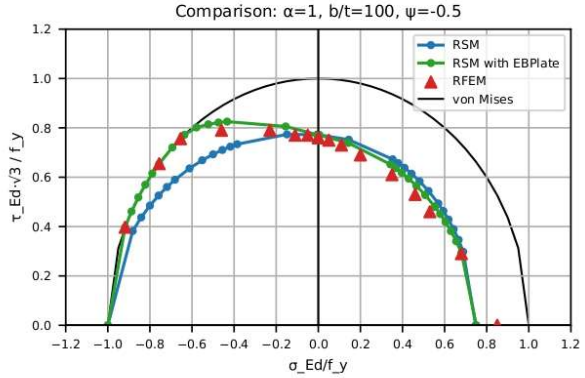
Comparison: α=1, b/t=100, ψ=-0.5
RSM
RSM with EBPlate
RFEM
von Mises
τ_Ed·√3 / f_y
σ_Ed/f_y

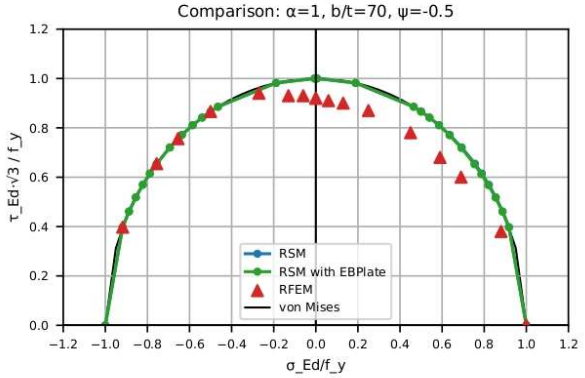
Comparison: α=1, b/t=70, ψ=-0.5
RSM
RSM with EBPlate
RFEM
von Mises
τ_Ed·√3 / f_y
σ_Ed/f_y

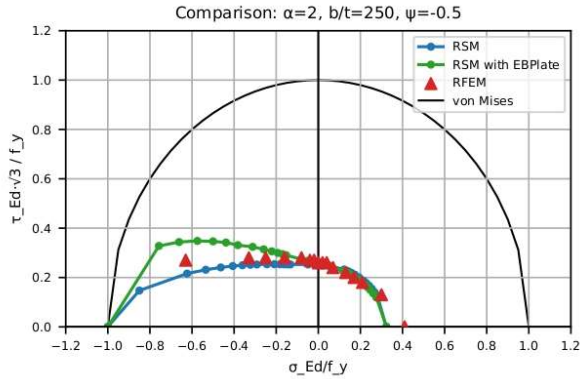
Comparison: α=2, b/t=250, ψ=-0.5
RSM
RSM with EBPlate
RFEM
von Mises
τ_Ed·√3 / f_y
σ_Ed/f_y

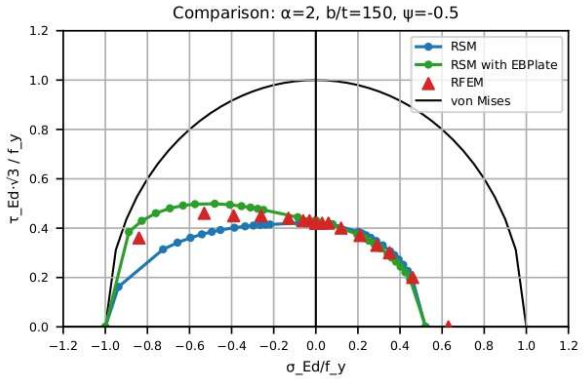
Comparison: α=2, b/t=150, ψ=-0.5
RSM
RSM with EBPlate
RFEM
von Mises
τ_Ed·√3 / f_y
σ_Ed/f_y

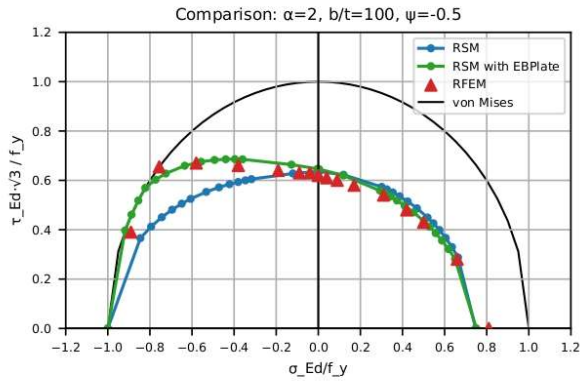
Comparison: α=2, b/t=100, ψ=-0.5
RSM
RSM with EBPlate
RFEM
von Mises
τ_Ed·√3 / f_y
σ_Ed/f_y

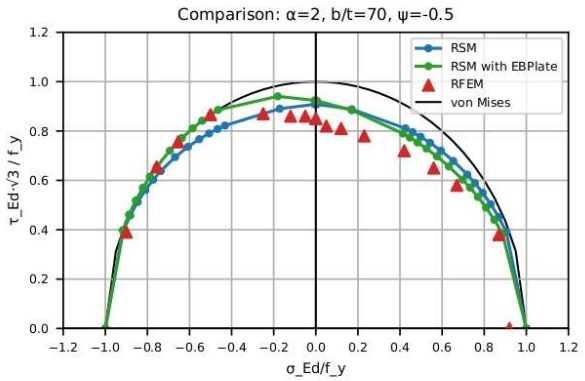
Comparison: α=2, b/t=70, ψ=-0.5
RSM
RSM with EBPlate
RFEM
von Mises
τ_Ed·√3 / f_y
σ_Ed/f_y

Appendix B: Buckling resistance for stiffened plates - Approach 1, 2 and 3 side by side

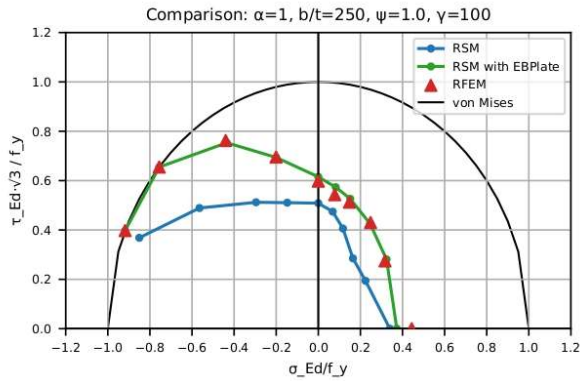
Comparison: α=1, b/t=250, ψ=1.0, γ=100
RSM
RSM with EBPlate
RFEM
von Mises
τ_Ed·√3 / f_y
σ_Ed/f_y

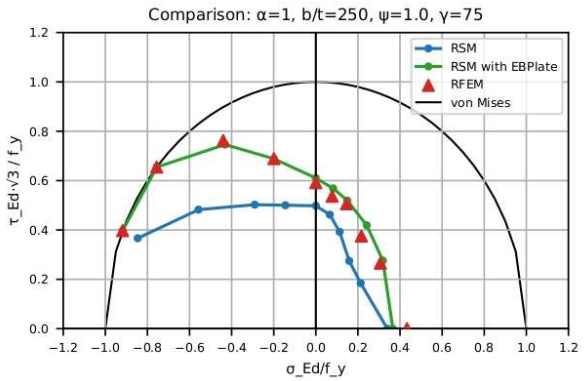
Comparison: α=1, b/t=250, ψ=1.0, γ=75
RSM
RSM with EBPlate
RFEM
von Mises
τ_Ed·√3 / f_y
σ_Ed/f_y

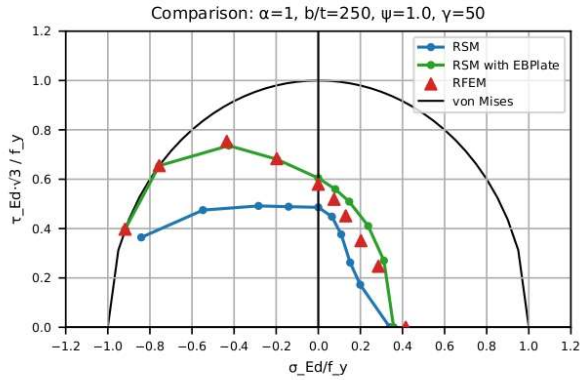
Comparison: α=1, b/t=250, ψ=1.0, γ=50
RSM
RSM with EBPlate
RFEM
von Mises
τ_Ed·√3 / f_y
σ_Ed/f_y

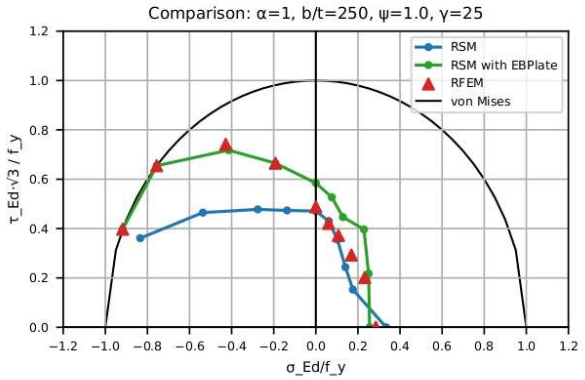
Comparison: α=1, b/t=250, ψ=1.0, γ=25
RSM
RSM with EBPlate
RFEM
von Mises
τ_Ed·√3 / f_y
σ_Ed/f_y

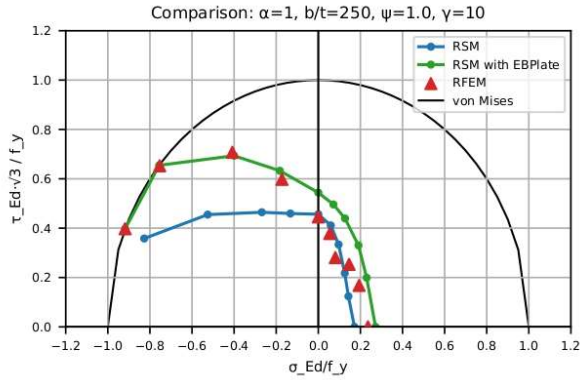
Comparison: α=1, b/t=250, ψ=1.0, γ=10
RSM
RSM with EBPlate
RFEM
von Mises
τ_Ed·√3 / f_y
σ_Ed/f_y

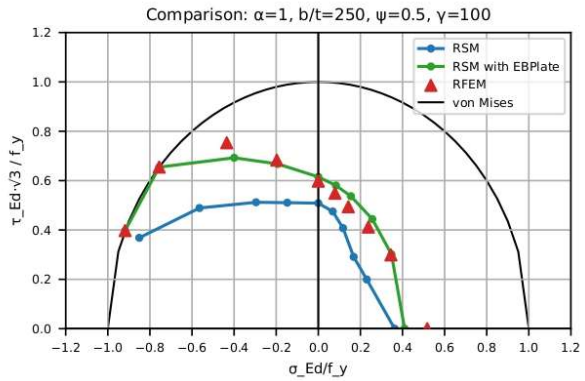
Comparison: α=1, b/t=250, ψ=0.5, γ=100
RSM
RSM with EBPlate
RFEM
von Mises
τ_Ed·√3 / f_y
σ_Ed/f_y

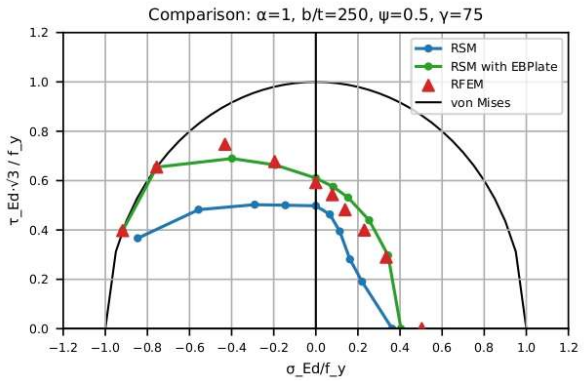
Comparison: α=1, b/t=250, ψ=0.5, γ=75
RSM
RSM with EBPlate
RFEM
von Mises
τ_Ed·√3 / f_y
σ_Ed/f_y

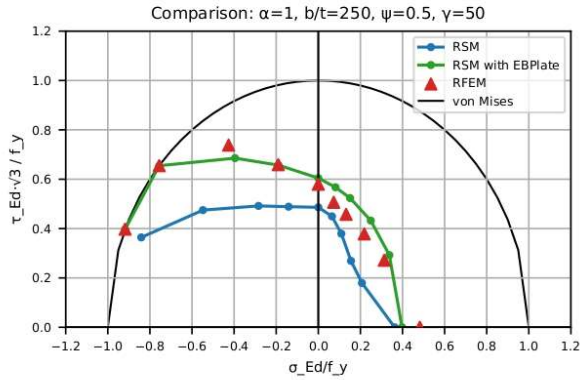
Comparison: α=1, b/t=250, ψ=0.5, γ=50
RSM
RSM with EBPlate
RFEM
von Mises
τ_Ed·√3 / f_y
σ_Ed/f_y

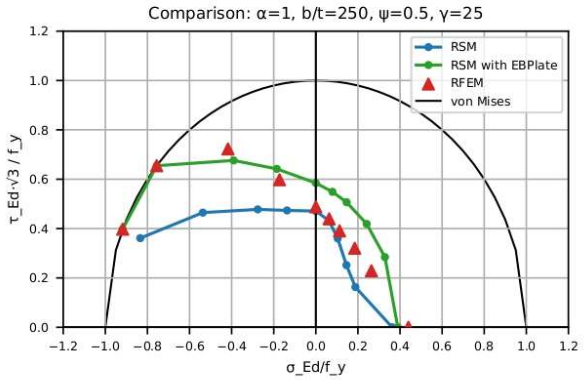
Comparison: α=1, b/t=250, ψ=0.5, γ=25
RSM
RSM with EBPlate
RFEM
von Mises
τ_Ed·√3 / f_y
σ_Ed/f_y

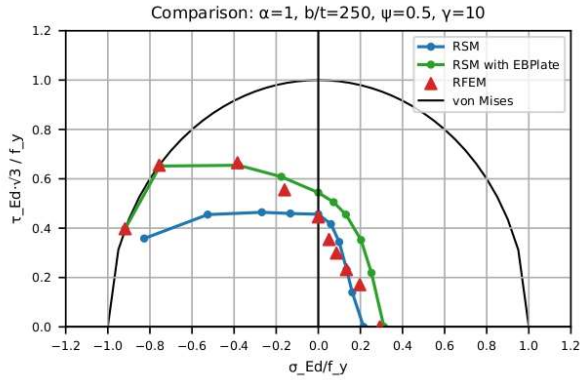
Comparison: α=1, b/t=250, ψ=0.5, γ=10
RSM
RSM with EBPlate
RFEM
von Mises
τ_Ed·√3 / f_y
σ_Ed/f_y

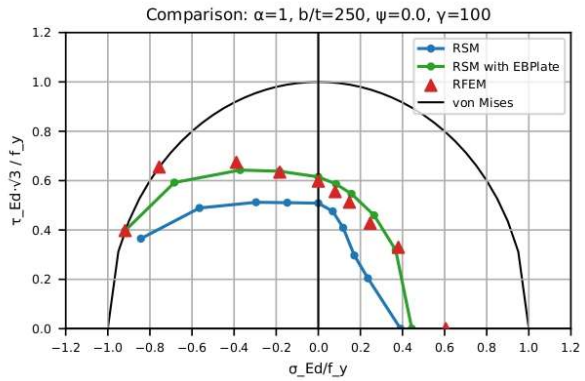
Comparison: α=1, b/t=250, ψ=0.0, γ=100
RSM
RSM with EBPlate
RFEM
von Mises
τ_Ed·√3 / f_y
σ_Ed/f_y

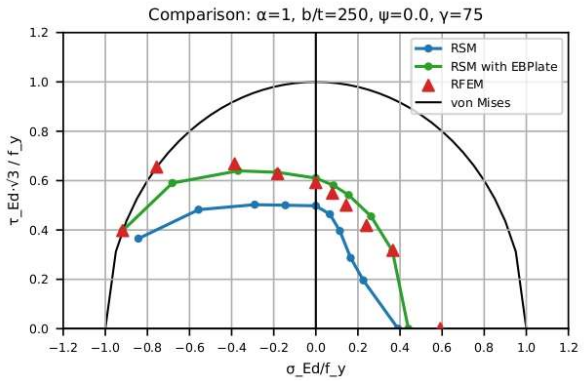
Comparison: α=1, b/t=250, ψ=0.0, γ=75
RSM
RSM with EBPlate
RFEM
von Mises
τ_Ed·√3 / f_y
σ_Ed/f_y

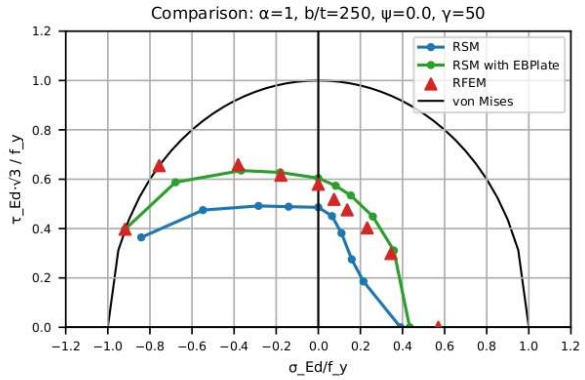
Comparison: α=1, b/t=250, ψ=0.0, γ=50
RSM
RSM with EBPlate
RFEM
von Mises
τ_Ed·√3 / f_y
σ_Ed/f_y

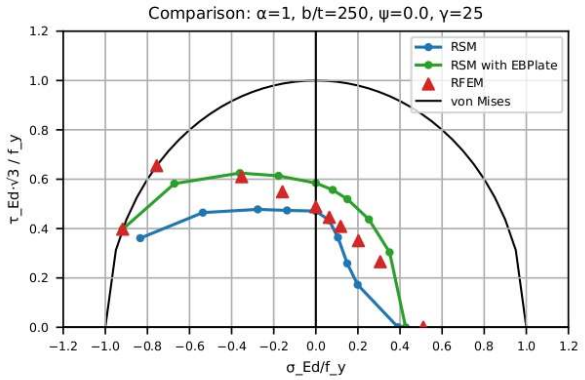
Comparison: α=1, b/t=250, ψ=0.0, γ=25
RSM
RSM with EBPlate
RFEM
von Mises
τ_Ed·√3 / f_y
σ_Ed/f_y

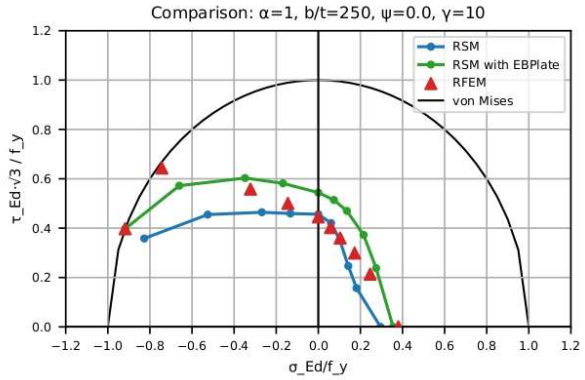
Comparison: α=1, b/t=250, ψ=0.0, γ=10
RSM
RSM with EBPlate
RFEM
von Mises
τ_Ed·√3 / f_y
σ_Ed/f_y

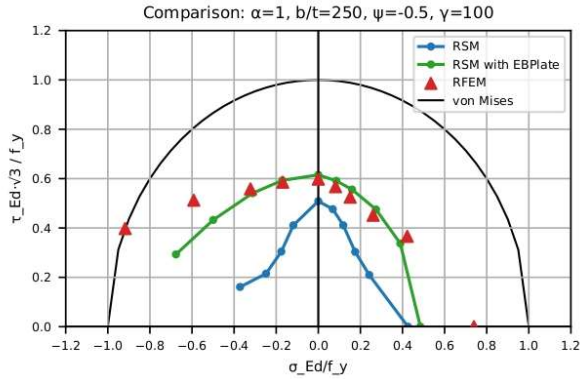
Comparison: α=1, b/t=250, ψ=-0.5, γ=100
RSM
RSM with EBPlate
RFEM
von Mises
τ_Ed·√3 / f_y
σ_Ed/f_y

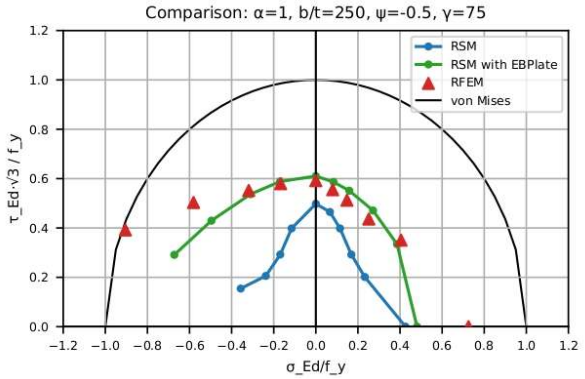
Comparison: α=1, b/t=250, ψ=-0.5, γ=75
RSM
RSM with EBPlate
RFEM
von Mises
τ_Ed·√3 / f_y
σ_Ed/f_y

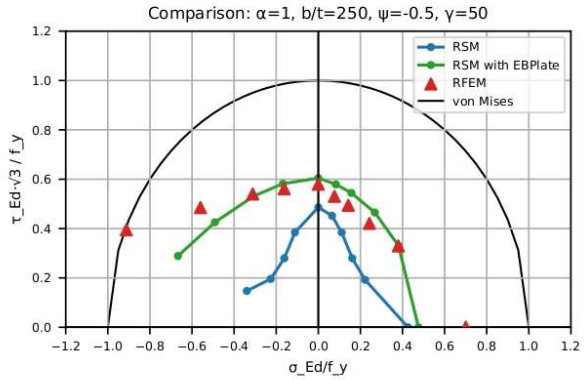
Comparison: α=1, b/t=250, ψ=-0.5, γ=50
RSM
RSM with EBPlate
RFEM
von Mises
τ_Ed·√3 / f_y
σ_Ed/f_y

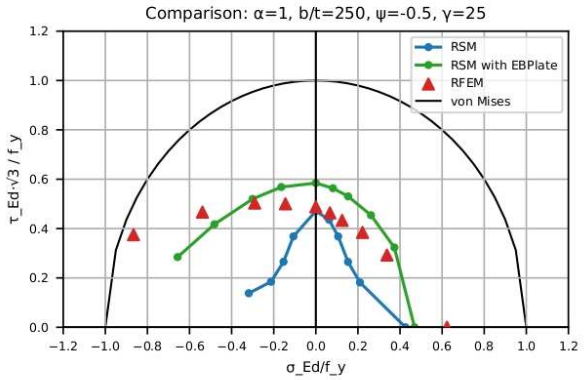
Comparison: α=1, b/t=250, ψ=-0.5, γ=25
RSM
RSM with EBPlate
RFEM
von Mises
τ_Ed·√3 / f_y
σ_Ed/f_y

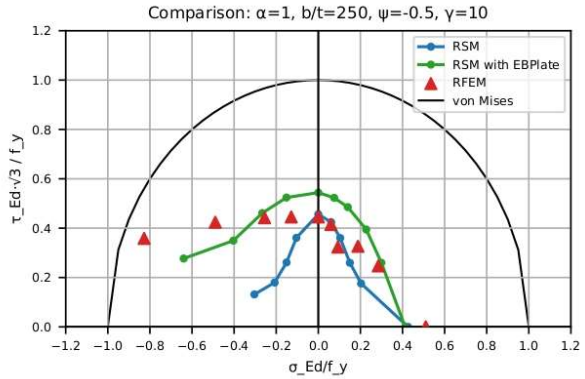
Comparison: α=1, b/t=250, ψ=-0.5, γ=10
RSM
RSM with EBPlate
RFEM
von Mises
τ_Ed·√3 / f_y
σ_Ed/f_y

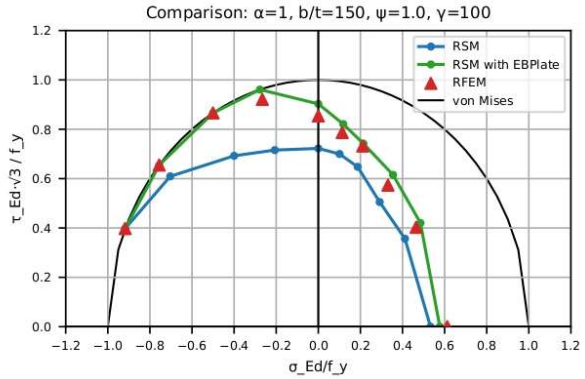
Comparison: α=1, b/t=150, ψ=1.0, γ=100
RSM
RSM with EBPlate
RFEM
von Mises
τ_Ed·√3 / f_y
σ_Ed/f_y

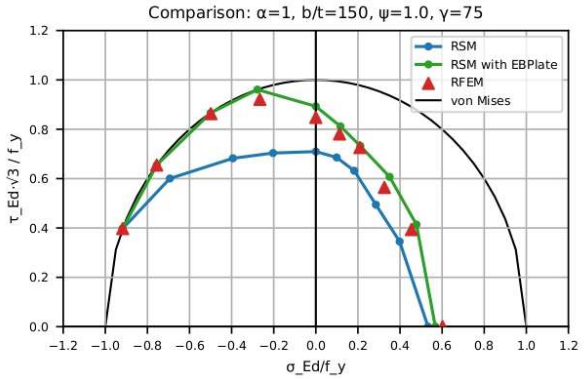
Comparison: α=1, b/t=150, ψ=1.0, γ=75
RSM
RSM with EBPlate
RFEM
von Mises
τ_Ed·√3 / f_y
σ_Ed/f_y

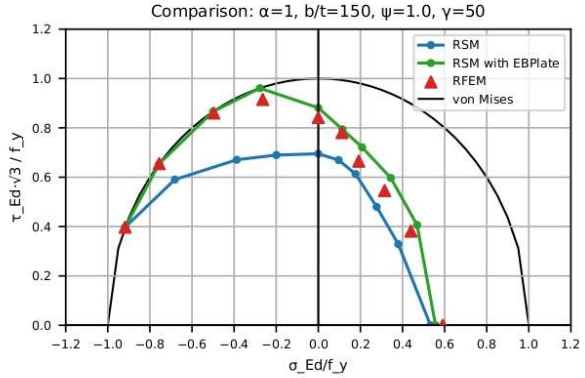
Comparison: α=1, b/t=150, ψ=1.0, γ=50
RSM
RSM with EBPlate
RFEM
von Mises
τ_Ed·√3 / f_y
σ_Ed/f_y

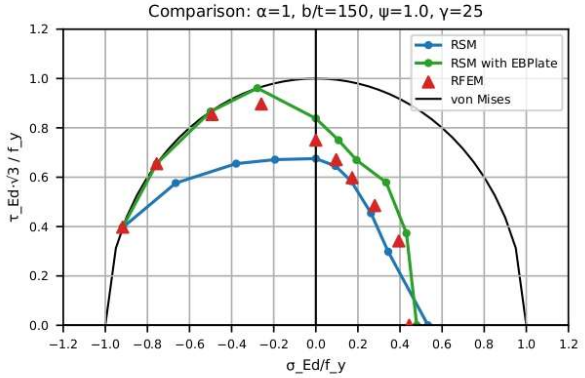
Comparison: α=1, b/t=150, ψ=1.0, γ=25
RSM
RSM with EBPlate
RFEM
von Mises
τ_Ed·√3 / f_y
σ_Ed/f_y

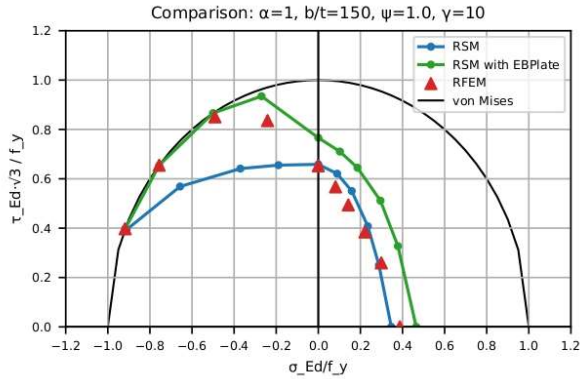
Comparison: α=1, b/t=150, ψ=1.0, γ=10
RSM
RSM with EBPlate
RFEM
von Mises
τ_Ed·√3 / f_y
σ_Ed/f_y

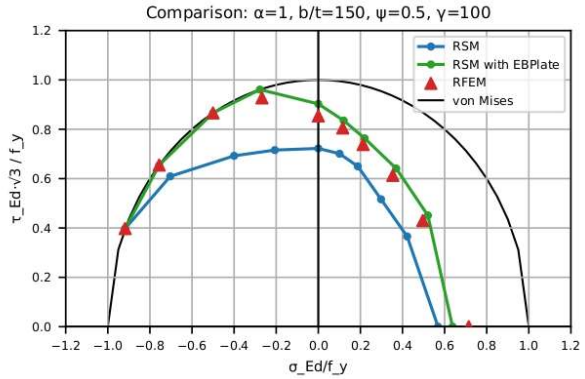
Comparison: α=1, b/t=150, ψ=0.5, γ=100
RSM
RSM with EBPlate
RFEM
von Mises
τ_Ed·√3 / f_y
σ_Ed/f_y

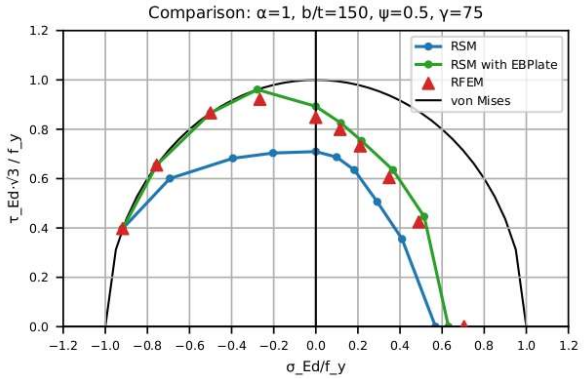
Comparison: α=1, b/t=150, ψ=0.5, γ=75
RSM
RSM with EBPlate
RFEM
von Mises
τ_Ed·√3 / f_y
σ_Ed/f_y

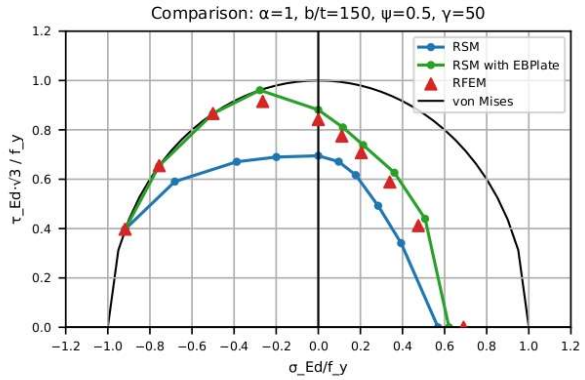
Comparison: α=1, b/t=150, ψ=0.5, γ=50
RSM
RSM with EBPlate
RFEM
von Mises
τ_Ed·√3 / f_y
σ_Ed/f_y

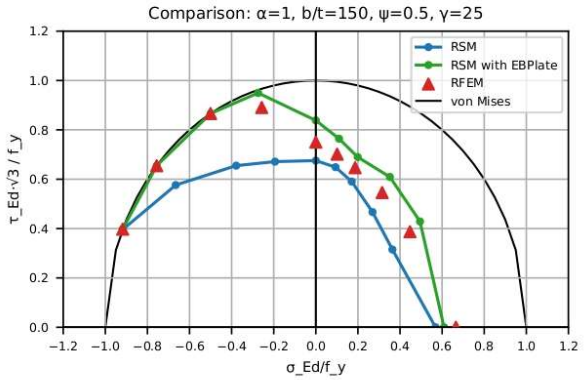
Comparison: α=1, b/t=150, ψ=0.5, γ=25
RSM
RSM with EBPlate
RFEM
von Mises
τ_Ed·√3 / f_y
σ_Ed/f_y

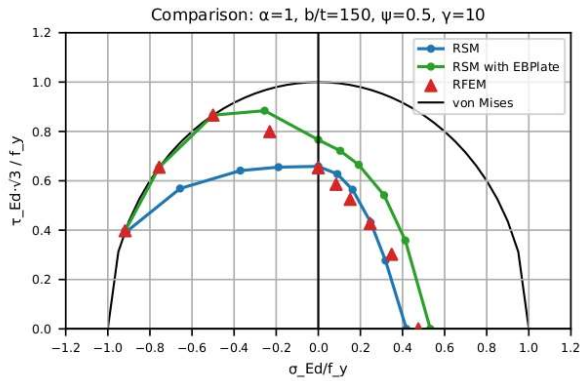
Comparison: α=1, b/t=150, ψ=0.5, γ=10
RSM
RSM with EBPlate
RFEM
von Mises
τ_Ed·√3 / f_y
σ_Ed/f_y

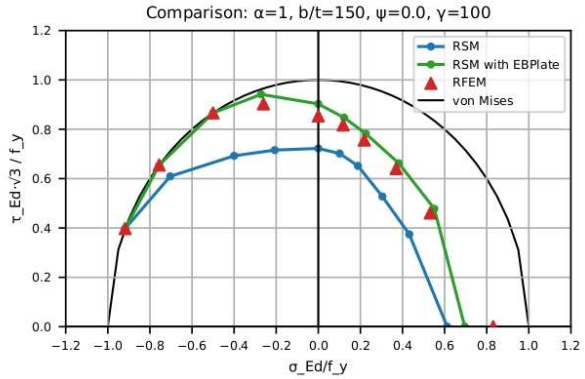
Comparison: α=1, b/t=150, ψ=0.0, γ=100
RSM
RSM with EBPlate
RFEM
von Mises
τ_Ed·√3 / f_y
σ_Ed/f_y

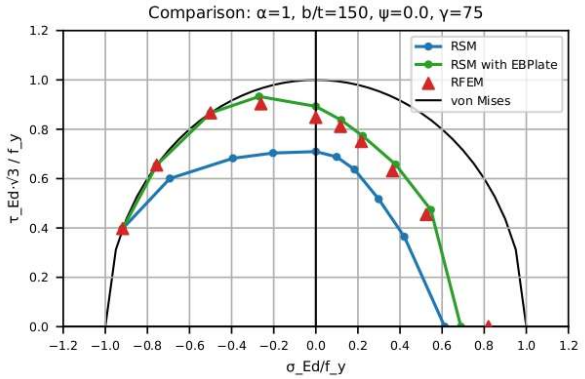
Comparison: α=1, b/t=150, ψ=0.0, γ=75
RSM
RSM with EBPlate
RFEM
von Mises
τ_Ed·√3 / f_y
σ_Ed/f_y

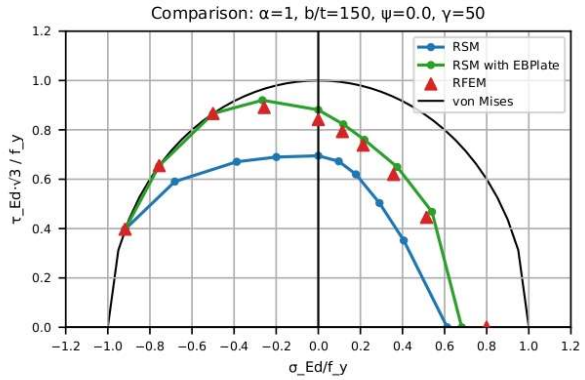
Comparison: α=1, b/t=150, ψ=0.0, γ=50
RSM
RSM with EBPlate
RFEM
von Mises
τ_Ed·√3 / f_y
σ_Ed/f_y

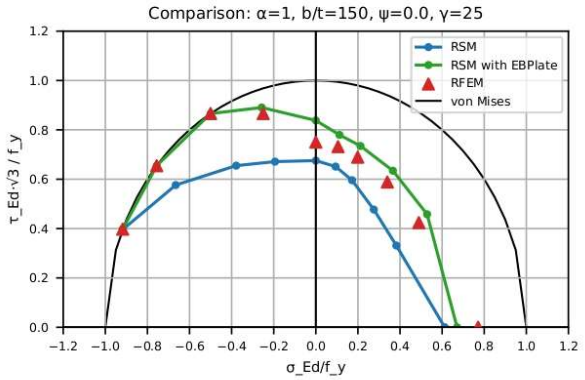
Comparison: α=1, b/t=150, ψ=0.0, γ=25
RSM
RSM with EBPlate
RFEM
von Mises
τ_Ed·√3 / f_y
σ_Ed/f_y

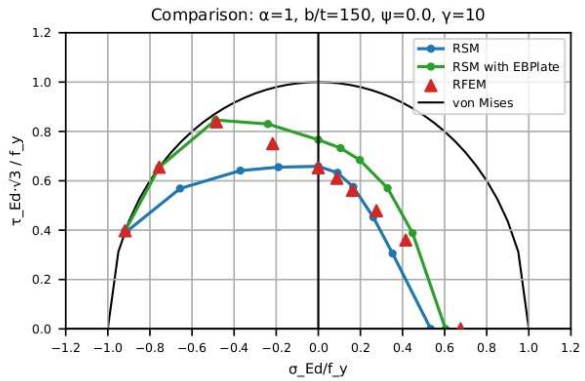
Comparison: α=1, b/t=150, ψ=0.0, γ=10
RSM
RSM with EBPlate
RFEM
von Mises
τ_Ed·√3 / f_y
σ_Ed/f_y

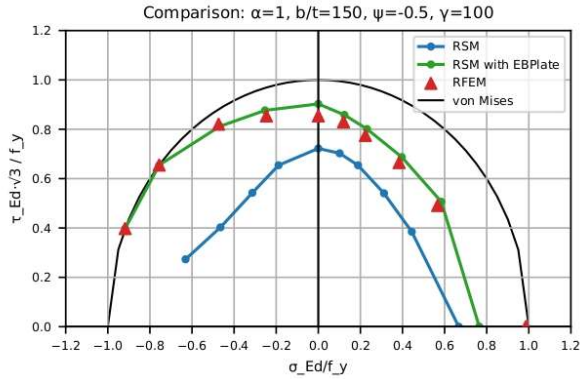
Comparison: α=1, b/t=150, ψ=-0.5, γ=100
RSM
RSM with EBPlate
RFEM
von Mises
τ_Ed·√3 / f_y
σ_Ed/f_y

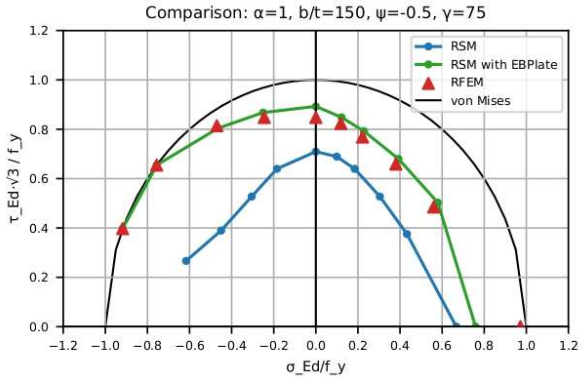
Comparison: α=1, b/t=150, ψ=-0.5, γ=75
RSM
RSM with EBPlate
RFEM
von Mises
τ_Ed·√3 / f_y
σ_Ed/f_y

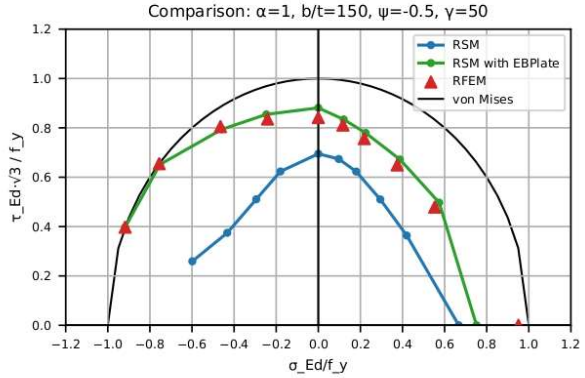
Comparison: α=1, b/t=150, ψ=-0.5, γ=50
RSM
RSM with EBPlate
RFEM
von Mises
τ_Ed·√3 / f_y
σ_Ed/f_y

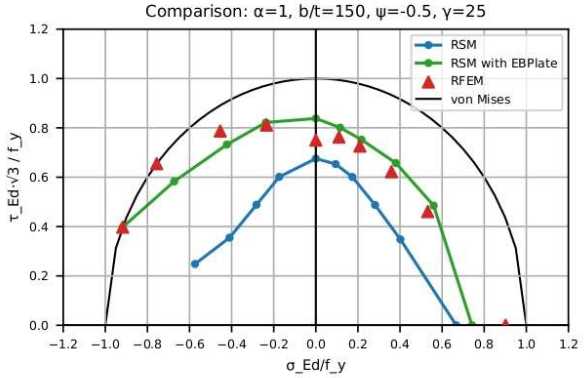
Comparison: α=1, b/t=150, ψ=-0.5, γ=25
RSM
RSM with EBPlate
RFEM
von Mises
τ_Ed·√3 / f_y
σ_Ed/f_y

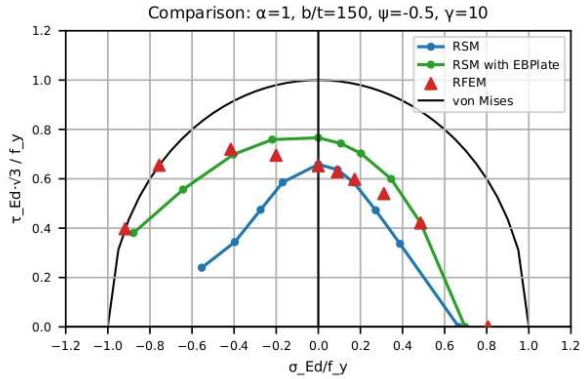
Comparison: α=1, b/t=150, ψ=-0.5, γ=10
RSM
RSM with EBPlate
RFEM
von Mises
τ_Ed·√3 / f_y
σ_Ed/f_y

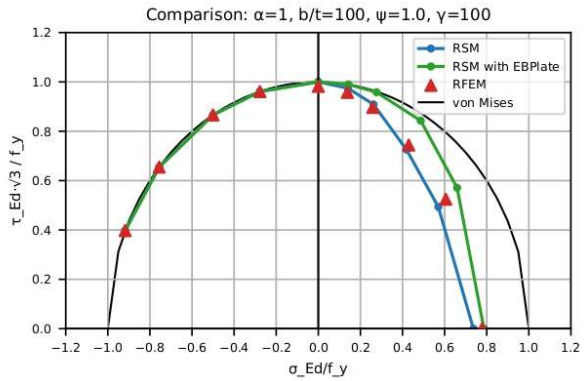
Comparison: α=1, b/t=100, ψ=1.0, γ=100
RSM
RSM with EBPlate
RFEM
von Mises
τ_Ed·√3 / f_y
σ_Ed/f_y

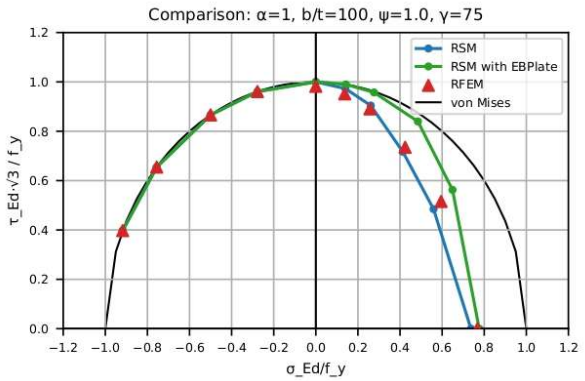
Comparison: α=1, b/t=100, ψ=1.0, γ=75
RSM
RSM with EBPlate
RFEM
von Mises
τ_Ed·√3 / f_y
σ_Ed/f_y

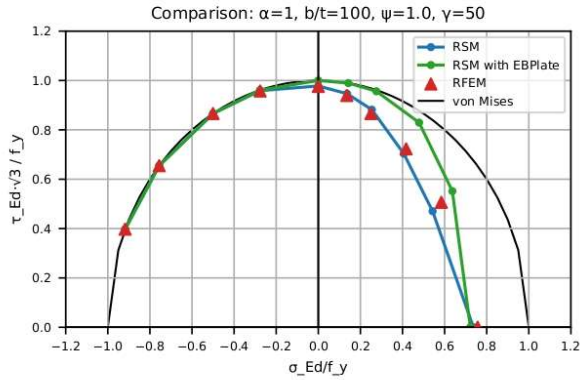
Comparison: α=1, b/t=100, ψ=1.0, γ=50
RSM
RSM with EBPlate
RFEM
von Mises
τ_Ed·√3 / f_y
σ_Ed/f_y

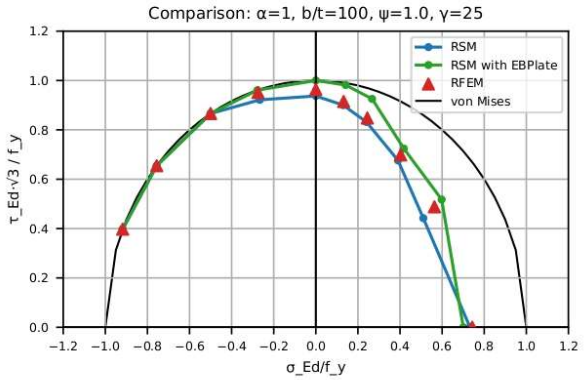
Comparison: α=1, b/t=100, ψ=1.0, γ=25
RSM
RSM with EBPlate
RFEM
von Mises
τ_Ed·√3 / f_y
σ_Ed/f_y

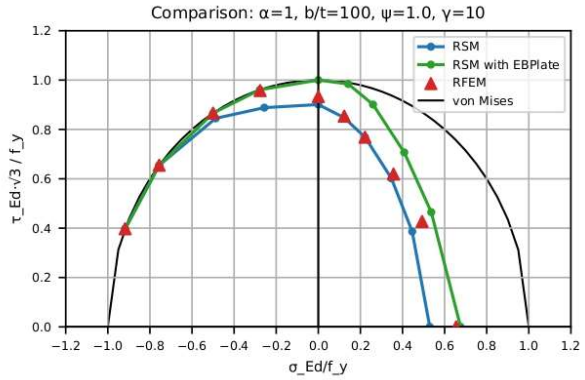
Comparison: α=1, b/t=100, ψ=1.0, γ=10
RSM
RSM with EBPlate
RFEM
von Mises
τ_Ed·√3 / f_y
σ_Ed/f_y

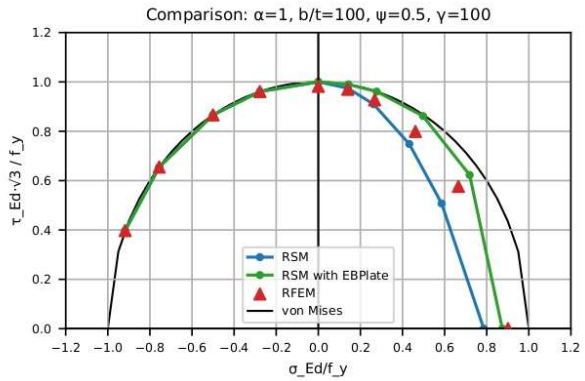
Comparison: α=1, b/t=100, ψ=0.5, γ=100
τ_Ed·√3 / f_y
σ_Ed/f_y
RSM
RSM with EBPlate
RFEM
von Mises

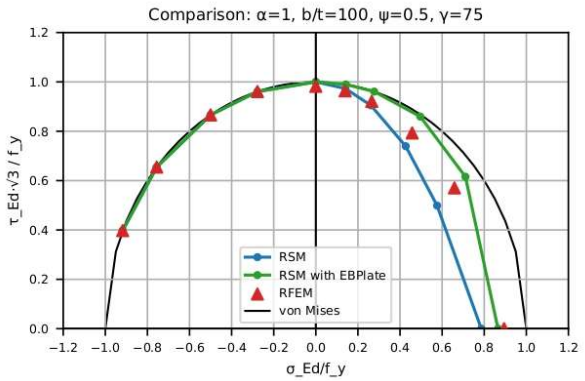
Comparison: α=1, b/t=100, ψ=0.5, γ=75
τ_Ed·√3 / f_y
σ_Ed/f_y
RSM
RSM with EBPlate
RFEM
von Mises

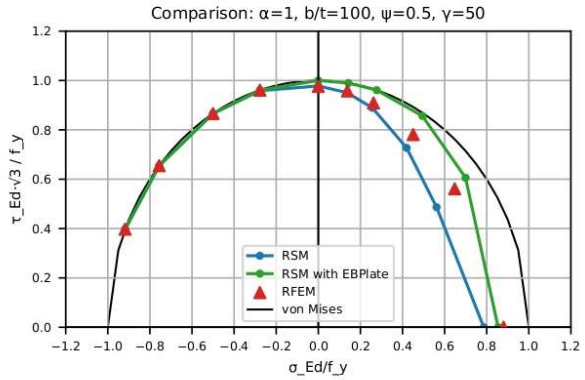
Comparison: α=1, b/t=100, ψ=0.5, γ=50
τ_Ed·√3 / f_y
σ_Ed/f_y
RSM
RSM with EBPlate
RFEM
von Mises

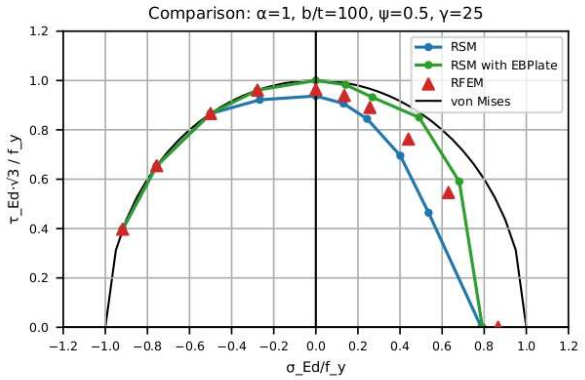
Comparison: α=1, b/t=100, ψ=0.5, γ=25
τ_Ed·√3 / f_y
σ_Ed/f_y
RSM
RSM with EBPlate
RFEM
von Mises

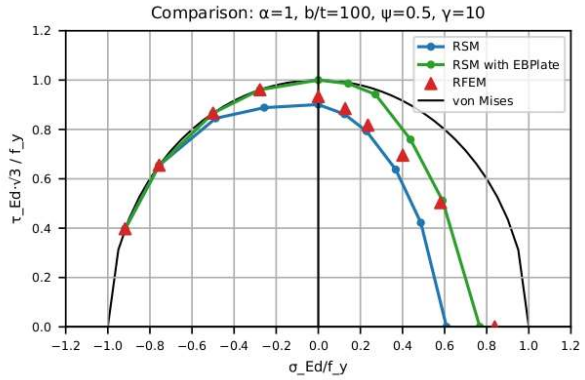
Comparison: α=1, b/t=100, ψ=0.5, γ=10
τ_Ed·√3 / f_y
σ_Ed/f_y
RSM
RSM with EBPlate
RFEM
von Mises

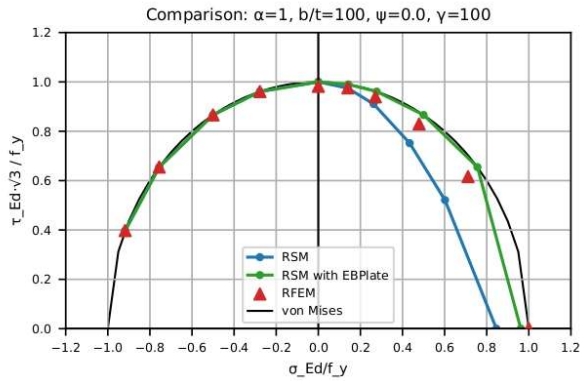
Comparison: α=1, b/t=100, ψ=0.0, γ=100
τ_Ed·√3 / f_y
σ_Ed/f_y
RSM
RSM with EBPlate
RFEM
von Mises

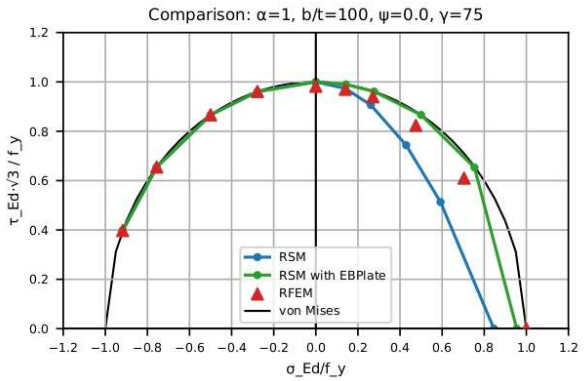
Comparison: α=1, b/t=100, ψ=0.0, γ=75
τ_Ed·√3 / f_y
σ_Ed/f_y
RSM
RSM with EBPlate
RFEM
von Mises

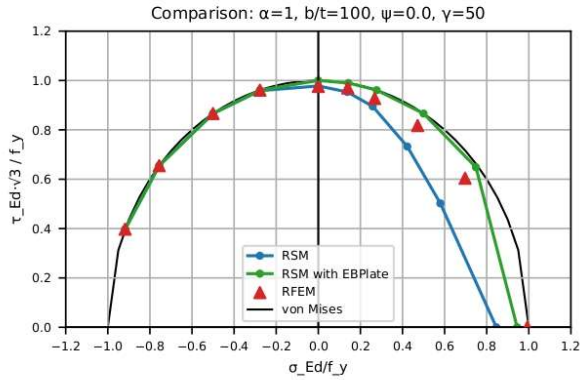
Comparison: α=1, b/t=100, ψ=0.0, γ=50
τ_Ed·√3 / f_y
σ_Ed/f_y
RSM
RSM with EBPlate
RFEM
von Mises

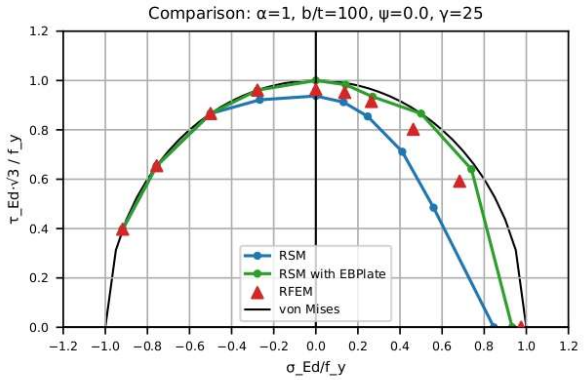
Comparison: α=1, b/t=100, ψ=0.0, γ=25
τ_Ed·√3 / f_y
σ_Ed/f_y
RSM
RSM with EBPlate
RFEM
von Mises

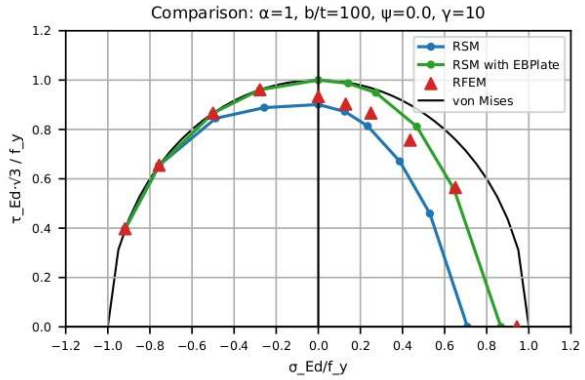
Comparison: α=1, b/t=100, ψ=0.0, γ=10
τ_Ed·√3 / f_y
σ_Ed/f_y
RSM
RSM with EBPlate
RFEM
von Mises

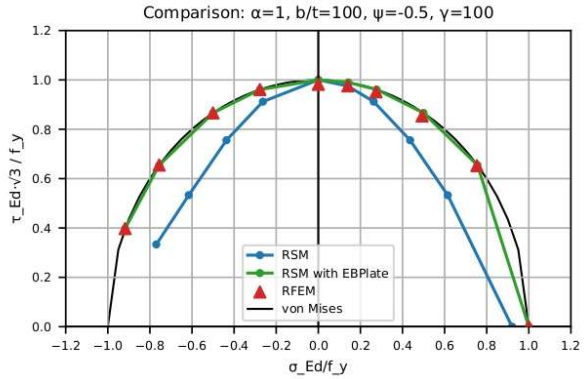
Comparison: α=1, b/t=100, ψ=-0.5, γ=100
τ_Ed·√3 / f_y
σ_Ed/f_y
RSM
RSM with EBPlate
RFEM
von Mises

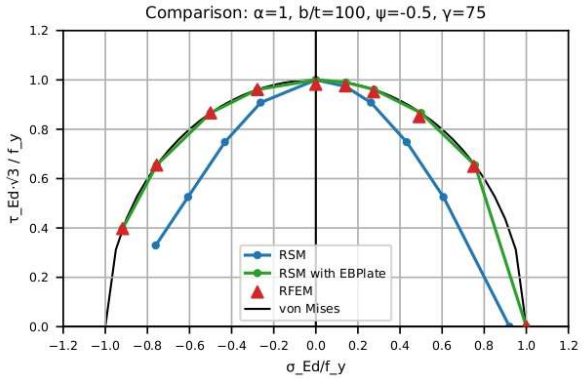
Comparison: α=1, b/t=100, ψ=-0.5, γ=75
τ_Ed·√3 / f_y
σ_Ed/f_y
RSM
RSM with EBPlate
RFEM
von Mises

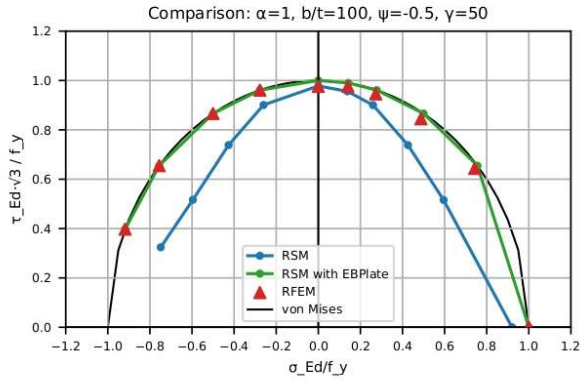
Comparison: α=1, b/t=100, ψ=-0.5, γ=50
τ_Ed·√3 / f_y
σ_Ed/f_y
RSM
RSM with EBPlate
RFEM
von Mises

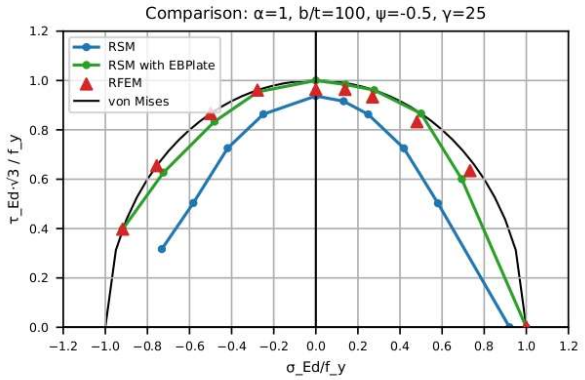
Comparison: α=1, b/t=100, ψ=-0.5, γ=25
τ_Ed·√3 / f_y
σ_Ed/f_y
RSM
RSM with EBPlate
RFEM
von Mises

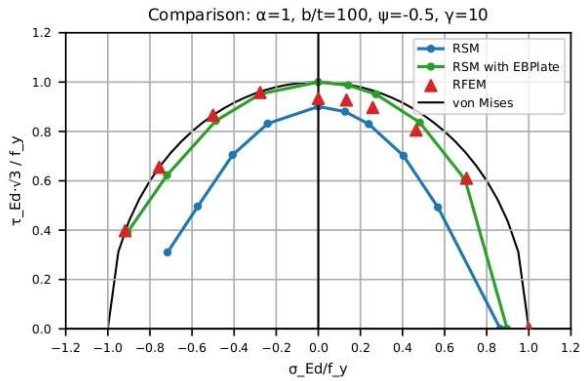
Comparison: α=1, b/t=100, ψ=-0.5, γ=10
τ_Ed·√3 / f_y
σ_Ed/f_y
RSM
RSM with EBPlate
RFEM
von Mises

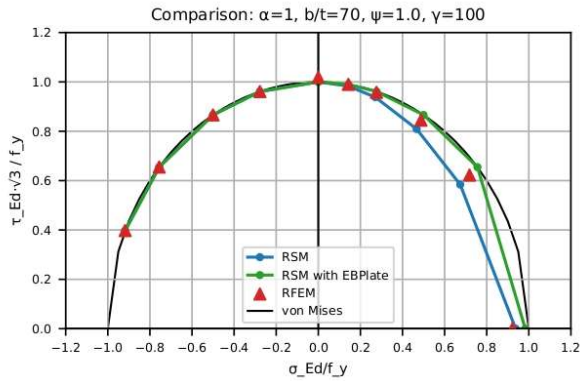
Comparison: α=1, b/t=70, ψ=1.0, γ=100
τ_Ed·√3 / f_y
σ_Ed/f_y
RSM
RSM with EBPlate
RFEM
von Mises

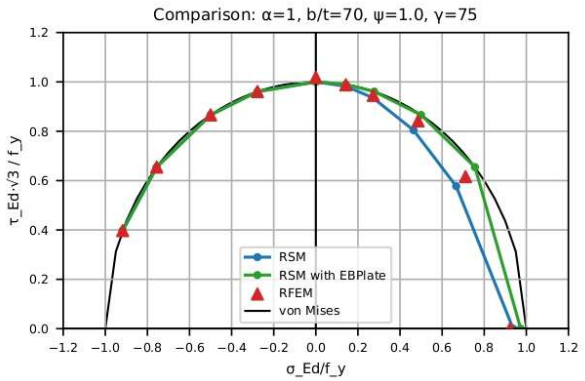
Comparison: α=1, b/t=70, ψ=1.0, γ=75
τ_Ed·√3 / f_y
σ_Ed/f_y
RSM
RSM with EBPlate
RFEM
von Mises

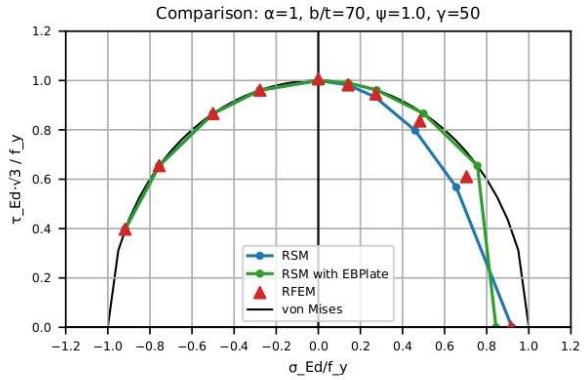
Comparison: α=1, b/t=70, ψ=1.0, γ=50
τ_Ed·√3 / f_y
σ_Ed/f_y
RSM
RSM with EBPlate
RFEM
von Mises

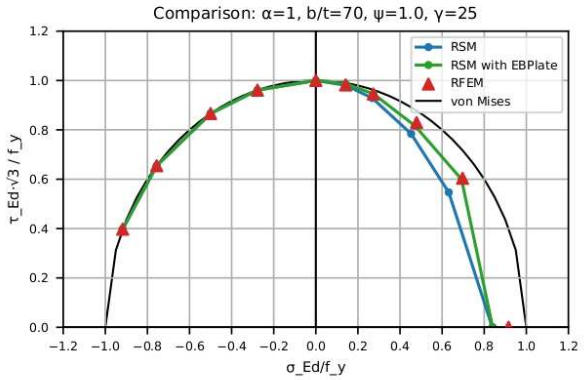
Comparison: α=1, b/t=70, ψ=1.0, γ=25
τ_Ed·√3 / f_y
σ_Ed/f_y
RSM
RSM with EBPlate
RFEM
von Mises

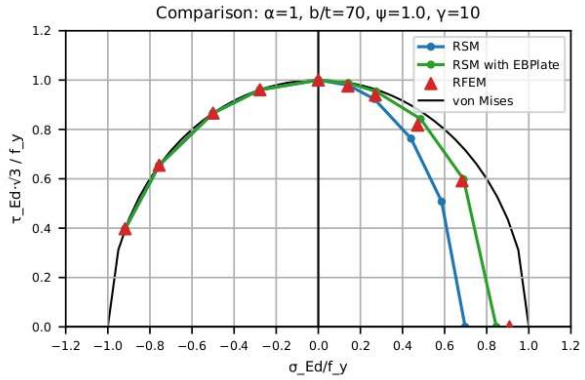
Comparison: α=1, b/t=70, ψ=1.0, γ=10
τ_Ed·√3 / f_y
σ_Ed/f_y
RSM
RSM with EBPlate
RFEM
von Mises

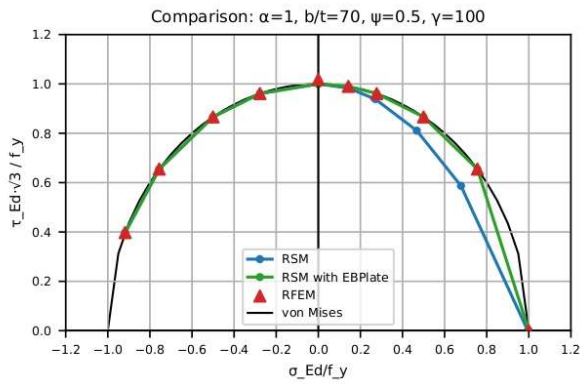
Comparison: α=1, b/t=70, ψ=0.5, γ=100
τ_Ed·√3 / f_y
σ_Ed/f_y
RSM
RSM with EBPlate
RFEM
von Mises

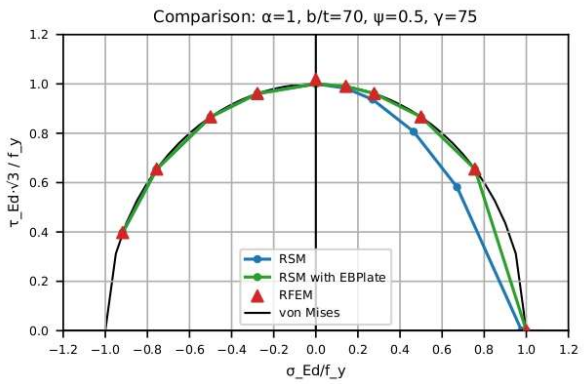
Comparison: α=1, b/t=70, ψ=0.5, γ=75
τ_Ed·√3 / f_y
σ_Ed/f_y
RSM
RSM with EBPlate
RFEM
von Mises

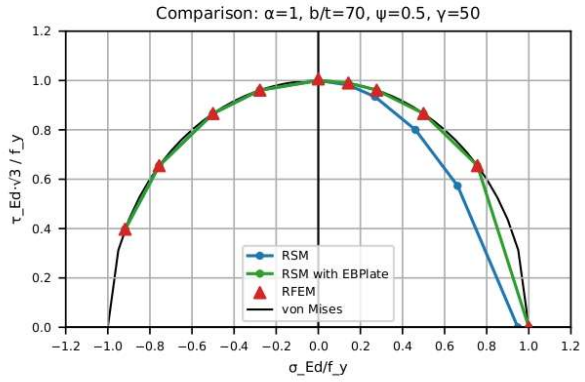
Comparison: α=1, b/t=70, ψ=0.5, γ=50
τ_Ed·√3 / f_y
σ_Ed/f_y
RSM
RSM with EBPlate
RFEM
von Mises

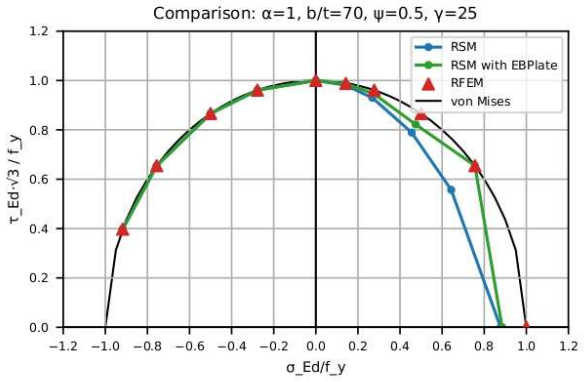
Comparison: α=1, b/t=70, ψ=0.5, γ=25
τ_Ed·√3 / f_y
σ_Ed/f_y
RSM
RSM with EBPlate
RFEM
von Mises

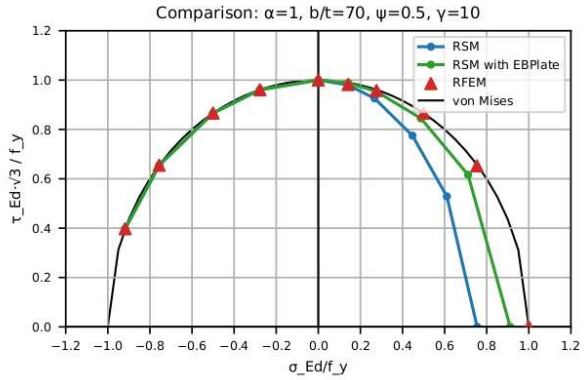
Comparison: α=1, b/t=70, ψ=0.5, γ=10
τ_Ed·√3 / f_y
σ_Ed/f_y
RSM
RSM with EBPlate
RFEM
von Mises

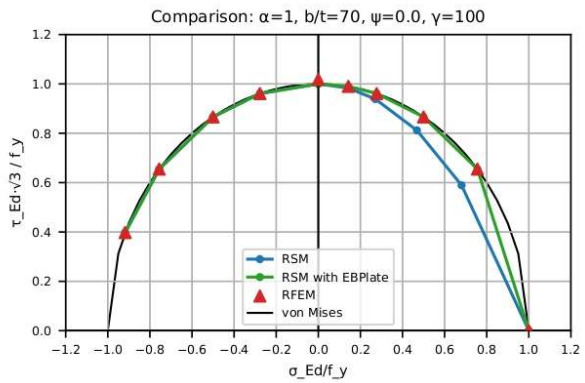
Comparison: α=1, b/t=70, ψ=0.0, γ=100
τ_Ed·√3 / f_y
σ_Ed/f_y
RSM
RSM with EBPlate
RFEM
von Mises

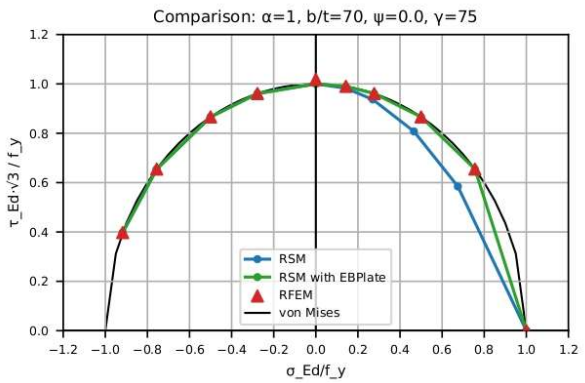
Comparison: α=1, b/t=70, ψ=0.0, γ=75
τ_Ed·√3 / f_y
σ_Ed/f_y
RSM
RSM with EBPlate
RFEM
von Mises

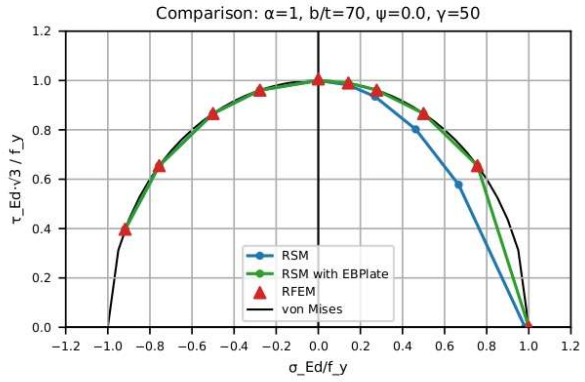
Comparison: α=1, b/t=70, ψ=0.0, γ=50
τ_Ed·√3 / f_y
σ_Ed/f_y
RSM
RSM with EBPlate
RFEM
von Mises

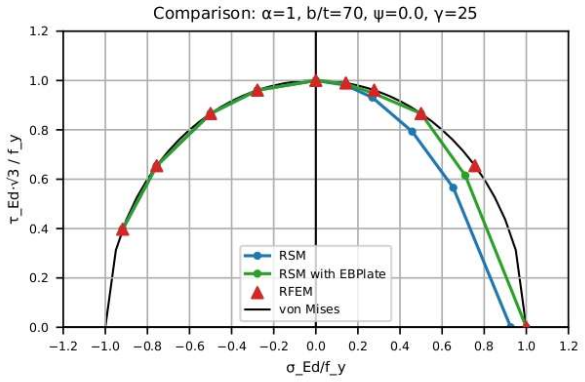
Comparison: α=1, b/t=70, ψ=0.0, γ=25
τ_Ed·√3 / f_y
σ_Ed/f_y
RSM
RSM with EBPlate
RFEM
von Mises

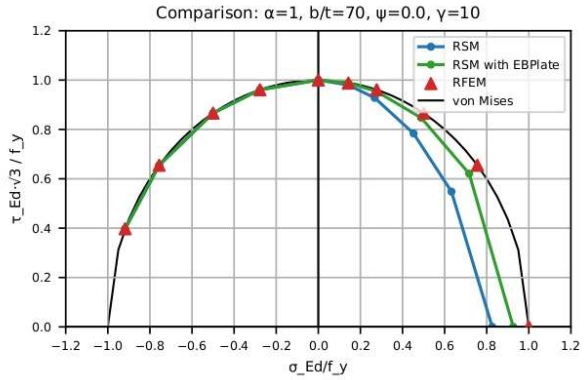
Comparison: α=1, b/t=70, ψ=0.0, γ=10
τ_Ed·√3 / f_y
σ_Ed/f_y
RSM
RSM with EBPlate
RFEM
von Mises

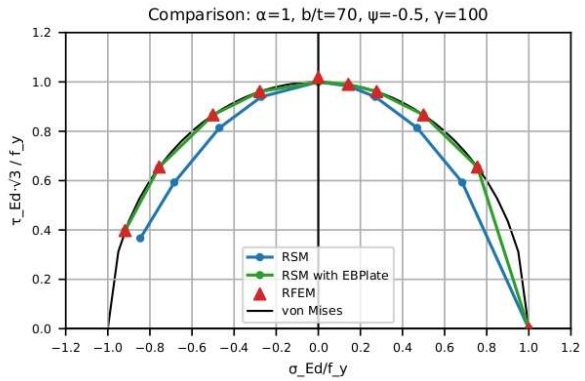
Comparison: α=1, b/t=70, ψ=-0.5, γ=100
τ_Ed·√3 / f_y
σ_Ed/f_y
RSM
RSM with EBPlate
RFEM
von Mises

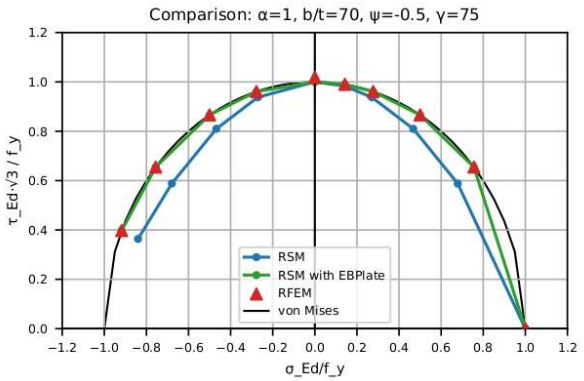
Comparison: α=1, b/t=70, ψ=-0.5, γ=75
τ_Ed·√3 / f_y
σ_Ed/f_y
RSM
RSM with EBPlate
RFEM
von Mises

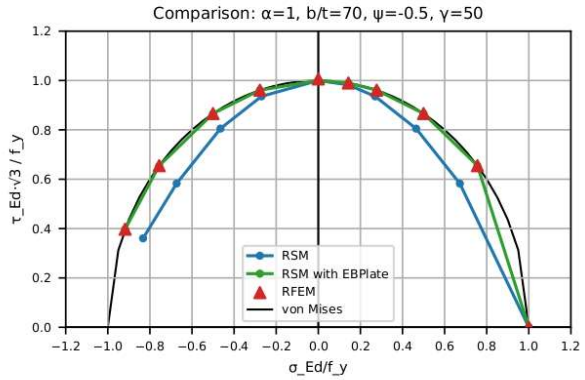
Comparison: α=1, b/t=70, ψ=-0.5, γ=50
τ_Ed·√3 / f_y
σ_Ed/f_y
RSM
RSM with EBPlate
RFEM
von Mises

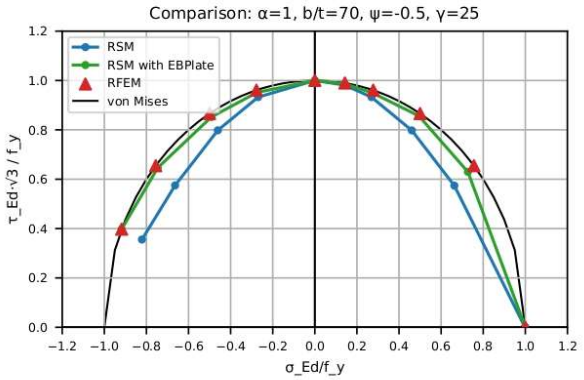
Comparison: α=1, b/t=70, ψ=-0.5, γ=25
τ_Ed·√3 / f_y
σ_Ed/f_y
RSM
RSM with EBPlate
RFEM
von Mises

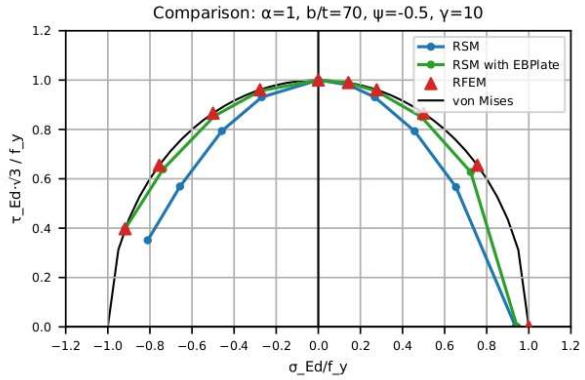
Comparison: α=1, b/t=70, ψ=-0.5, γ=10
τ_Ed·√3 / f_y
σ_Ed/f_y
RSM
RSM with EBPlate
RFEM
von Mises

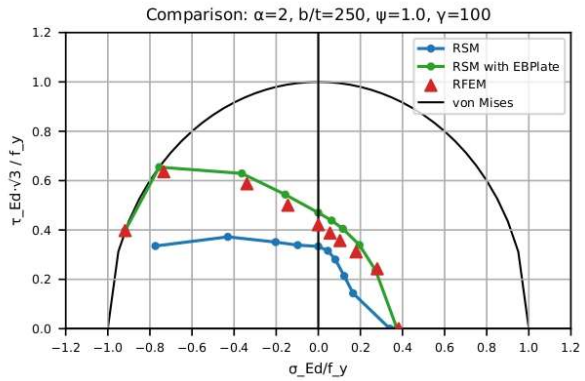
Comparison: α=2, b/t=250, ψ=1.0, γ=100
RSM
RSM with EBPlate
RFEM
von Mises
τ_Ed·√3 / f_y
σ_Ed/f_y

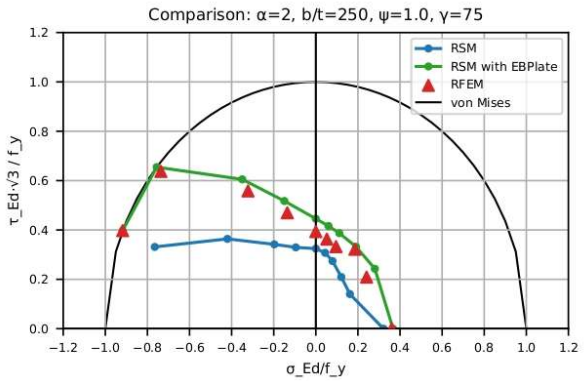
Comparison: α=2, b/t=250, ψ=1.0, γ=75
RSM
RSM with EBPlate
RFEM
von Mises
τ_Ed·√3 / f_y
σ_Ed/f_y

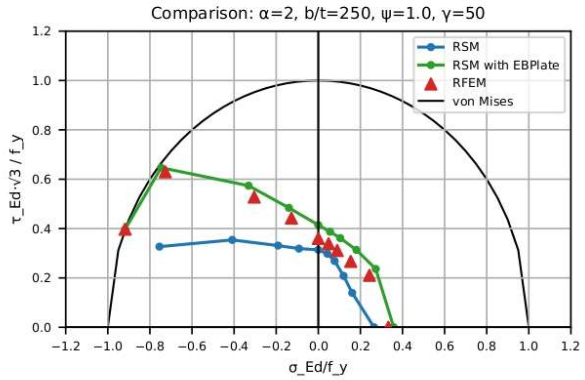
Comparison: α=2, b/t=250, ψ=1.0, γ=50
RSM
RSM with EBPlate
RFEM
von Mises
τ_Ed·√3 / f_y
σ_Ed/f_y

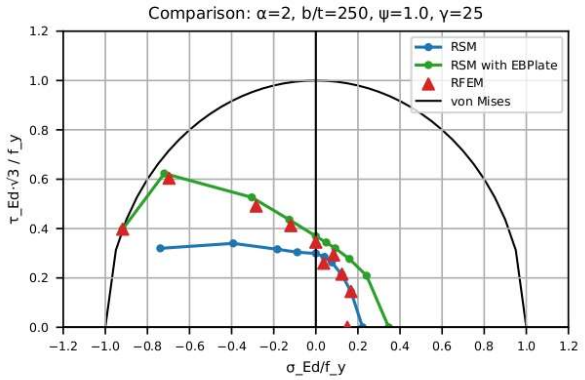
Comparison: α=2, b/t=250, ψ=1.0, γ=25
RSM
RSM with EBPlate
RFEM
von Mises
τ_Ed·√3 / f_y
σ_Ed/f_y

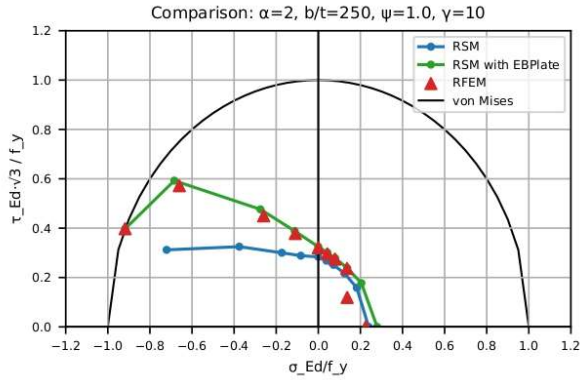
Comparison: α=2, b/t=250, ψ=1.0, γ=10
RSM
RSM with EBPlate
RFEM
von Mises
τ_Ed·√3 / f_y
σ_Ed/f_y

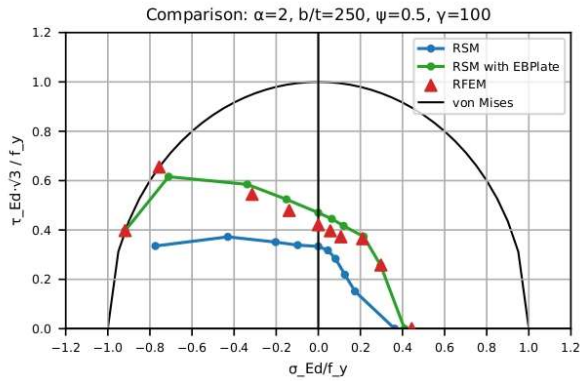
Comparison: α=2, b/t=250, ψ=0.5, γ=100
RSM
RSM with EBPlate
RFEM
von Mises
τ_Ed·√3 / f_y
σ_Ed/f_y

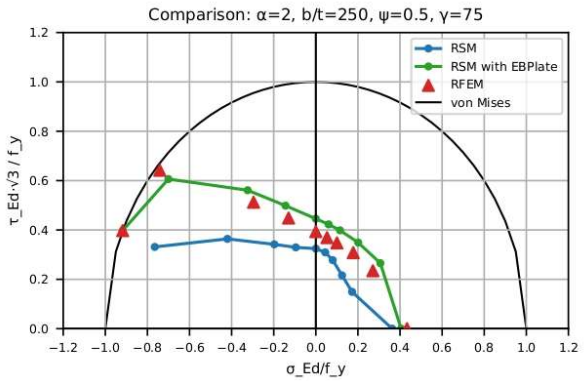
Comparison: α=2, b/t=250, ψ=0.5, γ=75
RSM
RSM with EBPlate
RFEM
von Mises
τ_Ed·√3 / f_y
σ_Ed/f_y

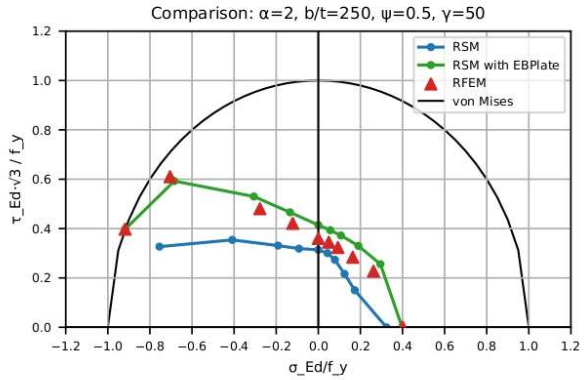
Comparison: α=2, b/t=250, ψ=0.5, γ=50
RSM
RSM with EBPlate
RFEM
von Mises
τ_Ed·√3 / f_y
σ_Ed/f_y

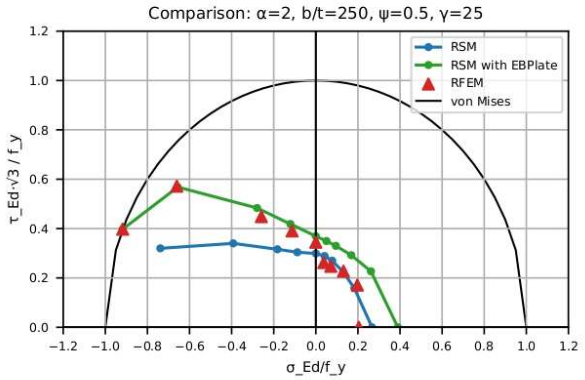
Comparison: α=2, b/t=250, ψ=0.5, γ=25
RSM
RSM with EBPlate
RFEM
von Mises
τ_Ed·√3 / f_y
σ_Ed/f_y

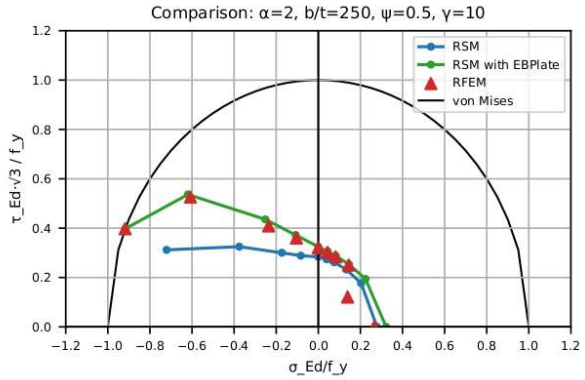
Comparison: α=2, b/t=250, ψ=0.5, γ=10
RSM
RSM with EBPlate
RFEM
von Mises
τ_Ed·√3 / f_y
σ_Ed/f_y

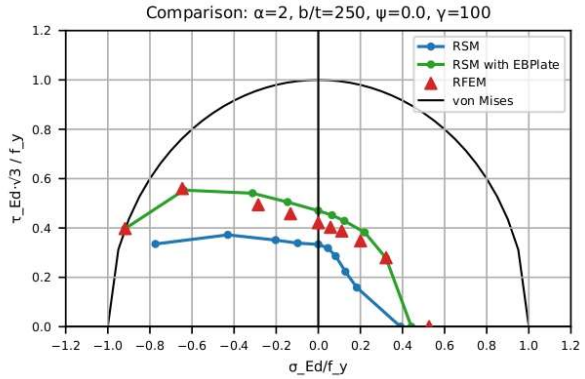
Comparison: α=2, b/t=250, ψ=0.0, γ=100
RSM
RSM with EBPlate
RFEM
von Mises
τ_Ed·√3 / f_y
σ_Ed/f_y

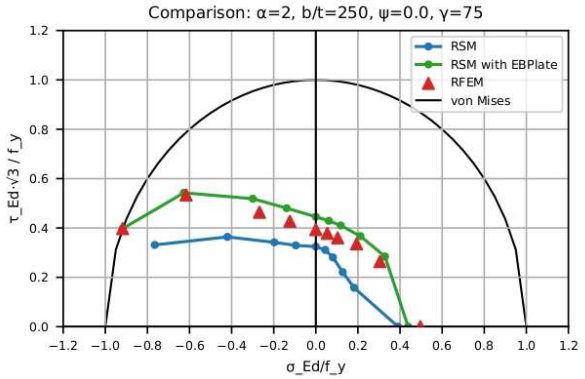
Comparison: α=2, b/t=250, ψ=0.0, γ=75
RSM
RSM with EBPlate
RFEM
von Mises
τ_Ed·√3 / f_y
σ_Ed/f_y

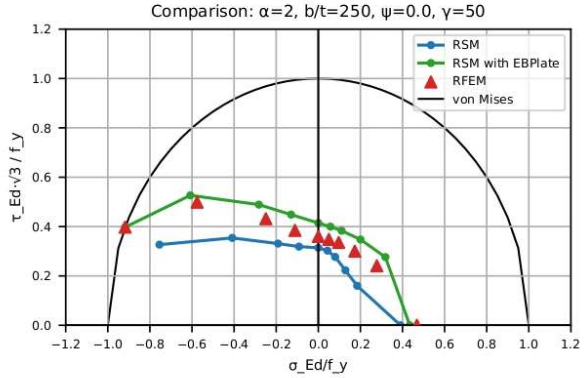
Comparison: α=2, b/t=250, ψ=0.0, γ=50
RSM
RSM with EBPlate
RFEM
von Mises
τ_Ed·√3 / f_y
σ_Ed/f_y

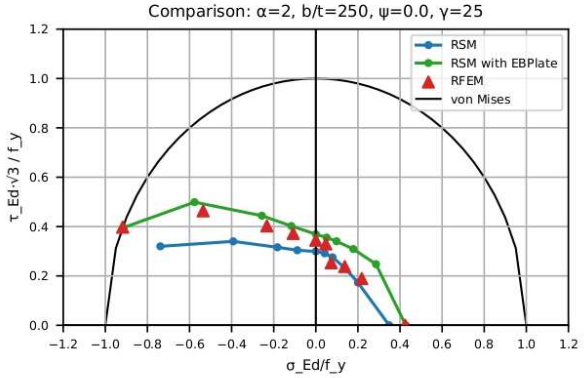
Comparison: α=2, b/t=250, ψ=0.0, γ=25
RSM
RSM with EBPlate
RFEM
von Mises
τ_Ed·√3 / f_y
σ_Ed/f_y

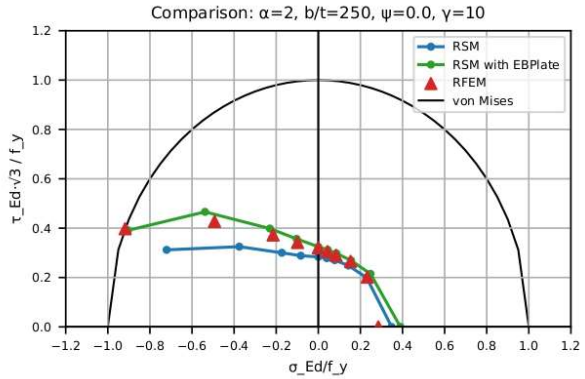
Comparison: α=2, b/t=250, ψ=0.0, γ=10
RSM
RSM with EBPlate
RFEM
von Mises
τ_Ed·√3 / f_y
σ_Ed/f_y

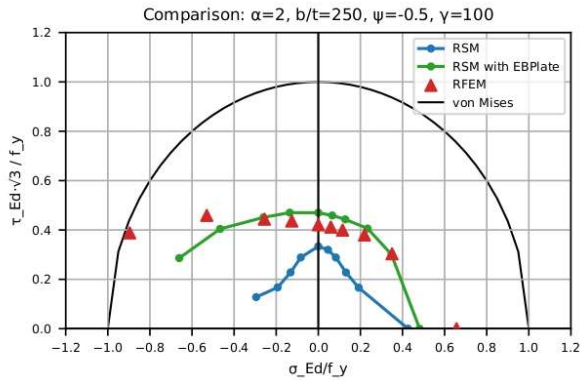
Comparison: α=2, b/t=250, ψ=-0.5, γ=100
RSM
RSM with EBPlate
RFEM
von Mises
τ_Ed·√3 / f_y
σ_Ed/f_y

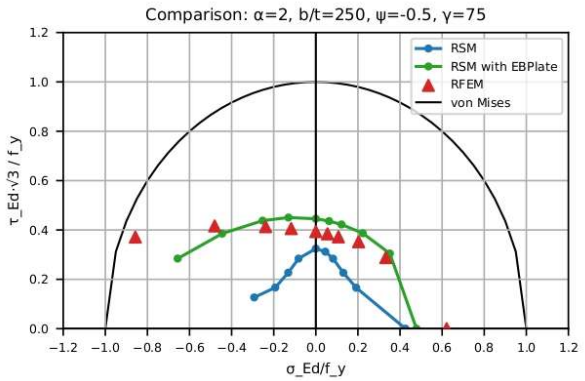
Comparison: α=2, b/t=250, ψ=-0.5, γ=75
RSM
RSM with EBPlate
RFEM
von Mises
τ_Ed·√3 / f_y
σ_Ed/f_y

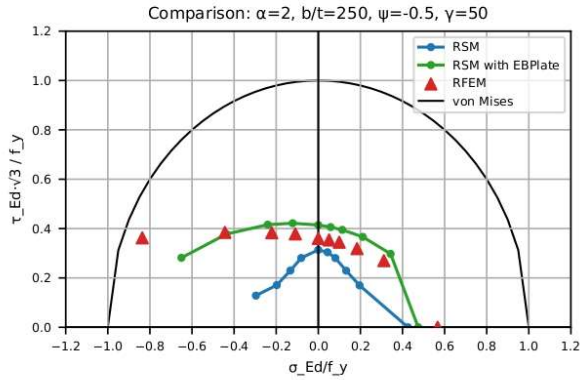
Comparison: α=2, b/t=250, ψ=-0.5, γ=50
RSM
RSM with EBPlate
RFEM
von Mises
τ_Ed·√3 / f_y
σ_Ed/f_y

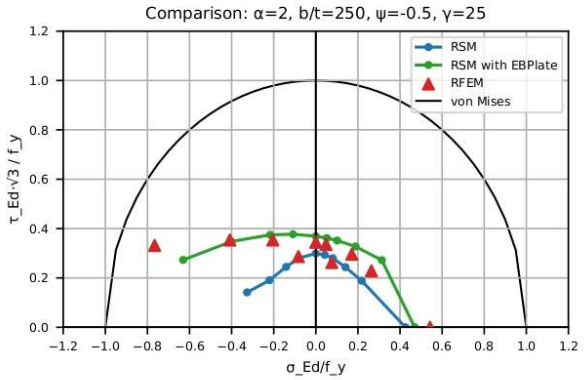
Comparison: α=2, b/t=250, ψ=-0.5, γ=25
RSM
RSM with EBPlate
RFEM
von Mises
τ_Ed·√3 / f_y
σ_Ed/f_y

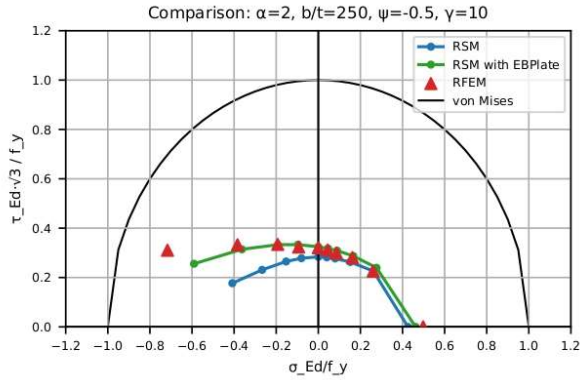
Comparison: α=2, b/t=250, ψ=-0.5, γ=10
RSM
RSM with EBPlate
RFEM
von Mises
τ_Ed·√3 / f_y
σ_Ed/f_y

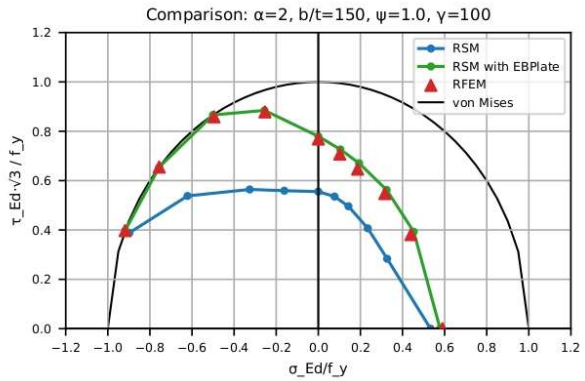
Comparison: α=2, b/t=150, ψ=1.0, γ=100
RSM
RSM with EBPlate
RFEM
von Mises
τ_Ed·√3 / f_y
σ_Ed/f_y

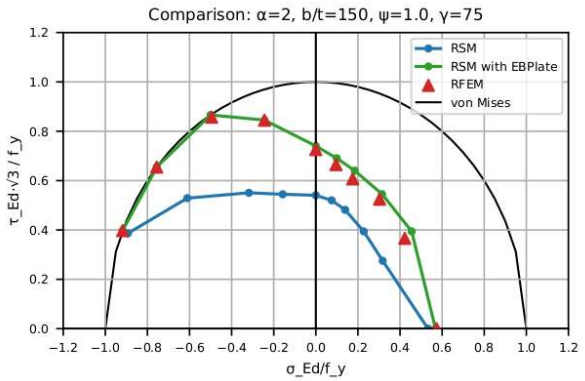
Comparison: α=2, b/t=150, ψ=1.0, γ=75
RSM
RSM with EBPlate
RFEM
von Mises
τ_Ed·√3 / f_y
σ_Ed/f_y

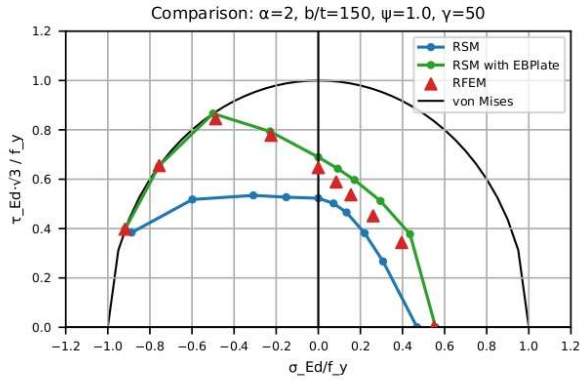
Comparison: α=2, b/t=150, ψ=1.0, γ=50
RSM
RSM with EBPlate
RFEM
von Mises
τ_Ed·√3 / f_y
σ_Ed/f_y

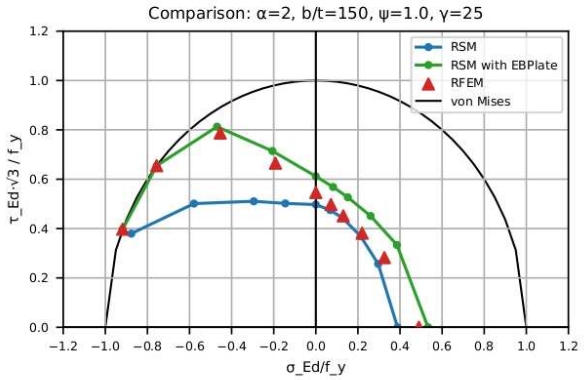
Comparison: α=2, b/t=150, ψ=1.0, γ=25
RSM
RSM with EBPlate
RFEM
von Mises
τ_Ed·√3 / f_y
σ_Ed/f_y

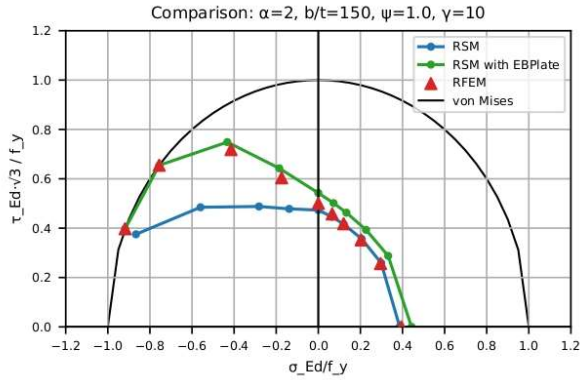
Comparison: α=2, b/t=150, ψ=1.0, γ=10
RSM
RSM with EBPlate
RFEM
von Mises
τ_Ed·√3 / f_y
σ_Ed/f_y

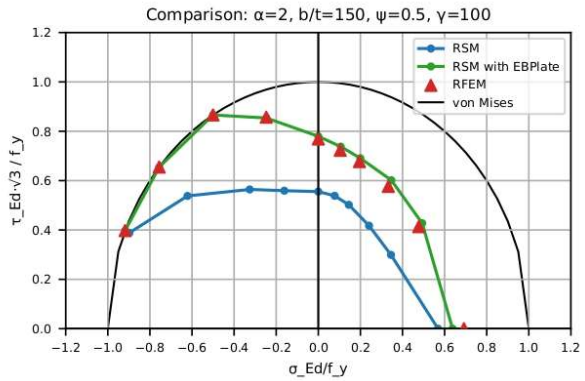
Comparison: α=2, b/t=150, ψ=0.5, γ=100
RSM
RSM with EBPlate
RFEM
von Mises
τ_Ed·√3 / f_y
σ_Ed/f_y

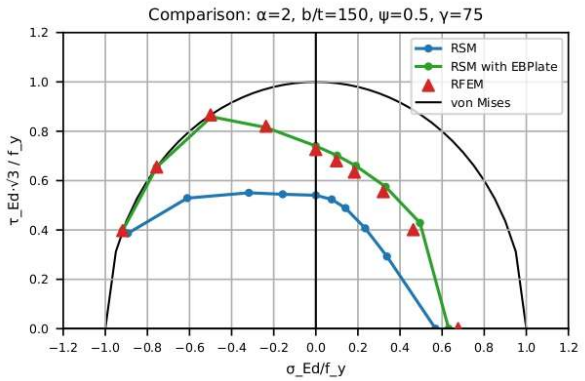
Comparison: α=2, b/t=150, ψ=0.5, γ=75
RSM
RSM with EBPlate
RFEM
von Mises
τ_Ed·√3 / f_y
σ_Ed/f_y

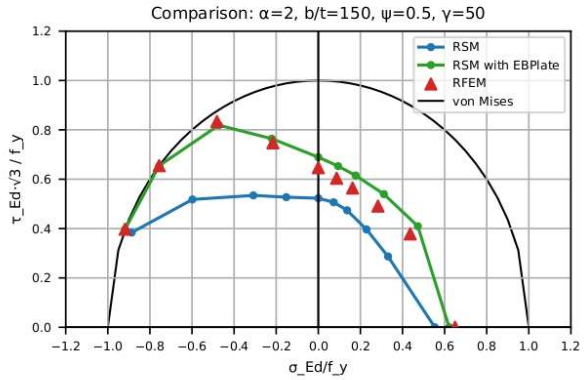
Comparison: α=2, b/t=150, ψ=0.5, γ=50
RSM
RSM with EBPlate
RFEM
von Mises
τ_Ed·√3 / f_y
σ_Ed/f_y

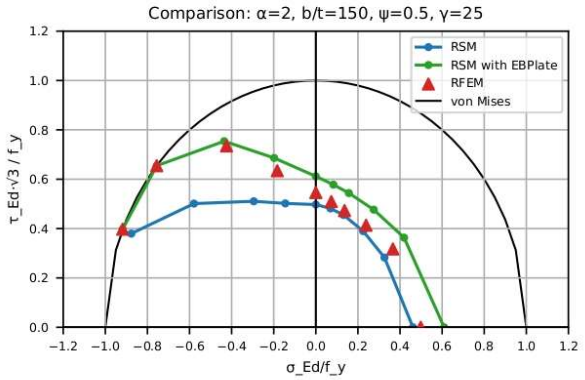
Comparison: α=2, b/t=150, ψ=0.5, γ=25
RSM
RSM with EBPlate
RFEM
von Mises
τ_Ed·√3 / f_y
σ_Ed/f_y

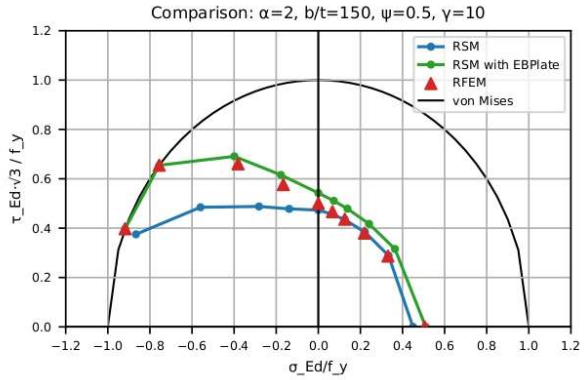
Comparison: α=2, b/t=150, ψ=0.5, γ=10
RSM
RSM with EBPlate
RFEM
von Mises
τ_Ed·√3 / f_y
σ_Ed/f_y

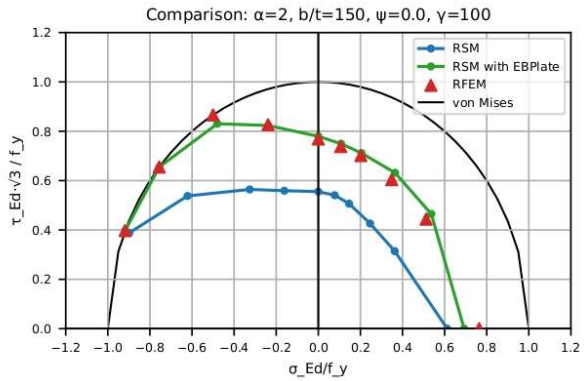
Comparison: α=2, b/t=150, ψ=0.0, γ=100
RSM
RSM with EBPlate
RFEM
von Mises
τ_Ed·√3 / f_y
σ_Ed/f_y

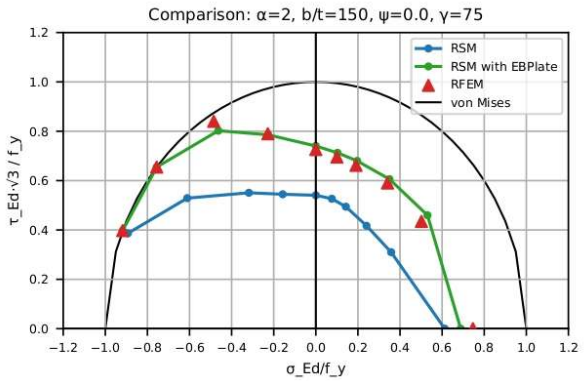
Comparison: α=2, b/t=150, ψ=0.0, γ=75
RSM
RSM with EBPlate
RFEM
von Mises
τ_Ed·√3 / f_y
σ_Ed/f_y

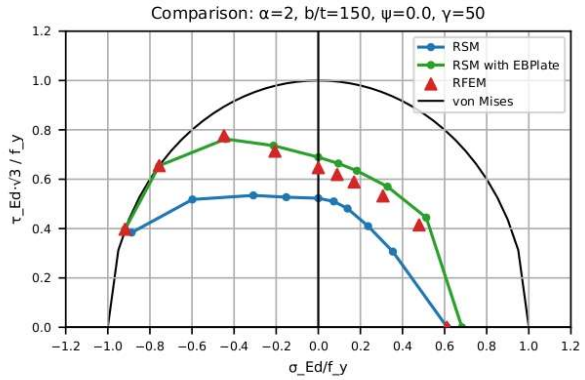
Comparison: α=2, b/t=150, ψ=0.0, γ=50
RSM
RSM with EBPlate
RFEM
von Mises
τ_Ed·√3 / f_y
σ_Ed/f_y

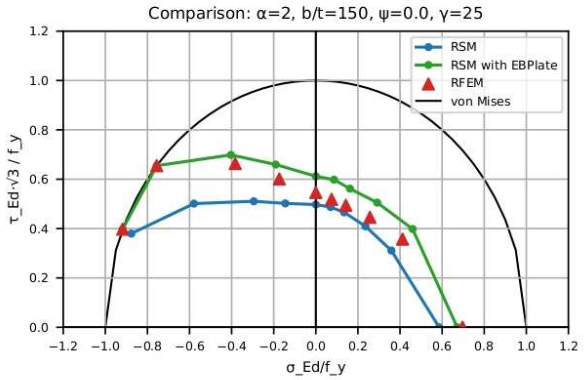
Comparison: α=2, b/t=150, ψ=0.0, γ=25
RSM
RSM with EBPlate
RFEM
von Mises
τ_Ed·√3 / f_y
σ_Ed/f_y

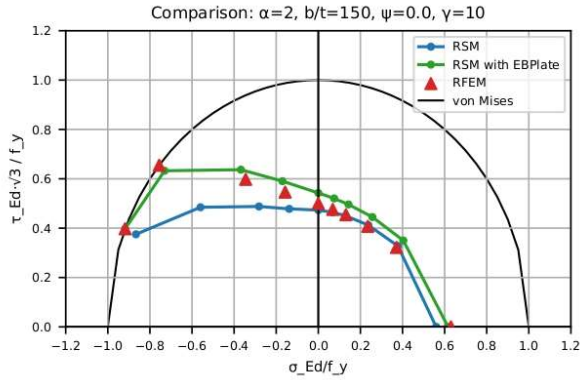
Comparison: α=2, b/t=150, ψ=0.0, γ=10
RSM
RSM with EBPlate
RFEM
von Mises
τ_Ed·√3 / f_y
σ_Ed/f_y

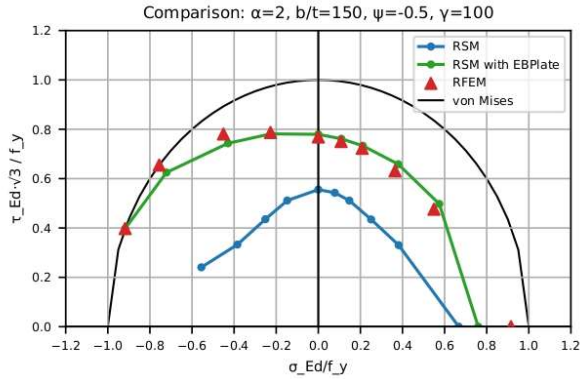
Comparison: α=2, b/t=150, ψ=-0.5, γ=100
RSM
RSM with EBPlate
RFEM
von Mises
τ_Ed·√3 / f_y
σ_Ed/f_y

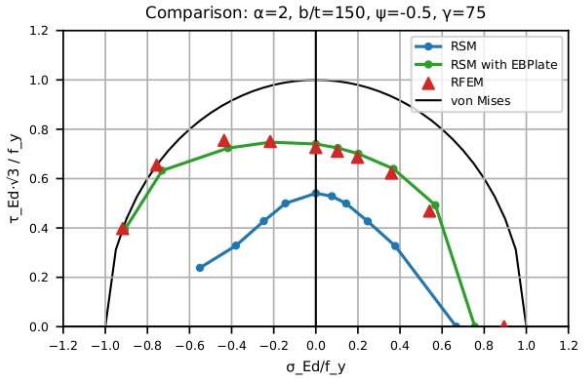
Comparison: α=2, b/t=150, ψ=-0.5, γ=75
RSM
RSM with EBPlate
RFEM
von Mises
τ_Ed·√3 / f_y
σ_Ed/f_y

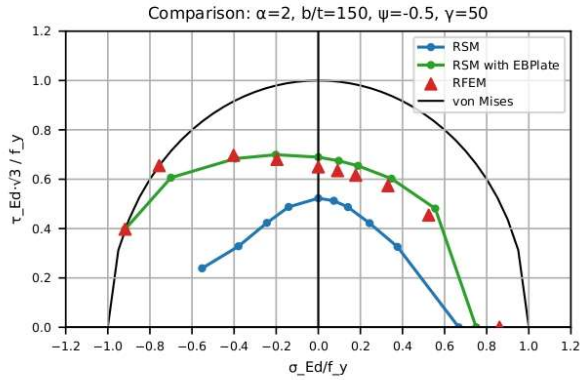
Comparison: α=2, b/t=150, ψ=-0.5, γ=50
RSM
RSM with EBPlate
RFEM
von Mises
τ_Ed·√3 / f_y
σ_Ed/f_y

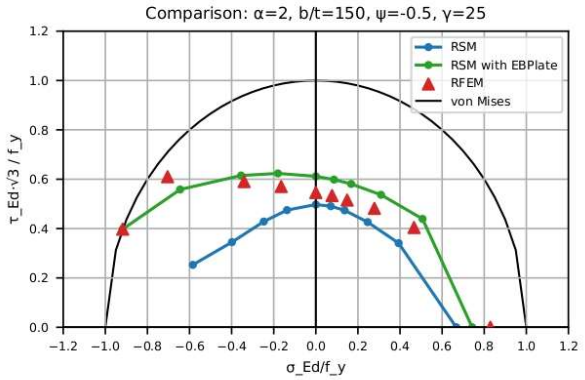
Comparison: α=2, b/t=150, ψ=-0.5, γ=25
RSM
RSM with EBPlate
RFEM
von Mises
τ_Ed·√3 / f_y
σ_Ed/f_y

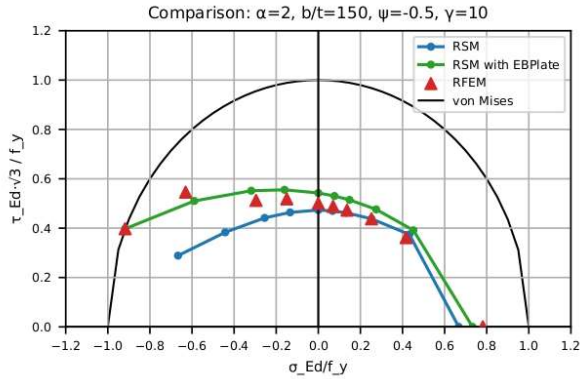
Comparison: α=2, b/t=150, ψ=-0.5, γ=10
RSM
RSM with EBPlate
RFEM
von Mises
τ_Ed·√3 / f_y
σ_Ed/f_y

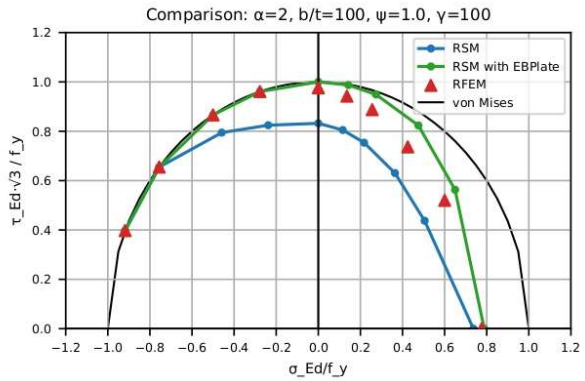
Comparison: α=2, b/t=100, ψ=1.0, γ=100
RSM
RSM with EBPlate
RFEM
von Mises
τ_Ed·√3 / f_y
σ_Ed/f_y

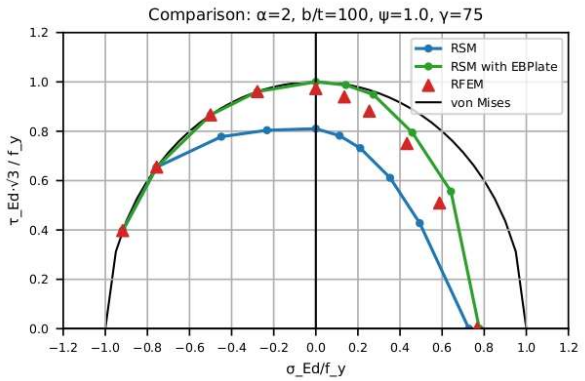
Comparison: α=2, b/t=100, ψ=1.0, γ=75
RSM
RSM with EBPlate
RFEM
von Mises
τ_Ed·√3 / f_y
σ_Ed/f_y

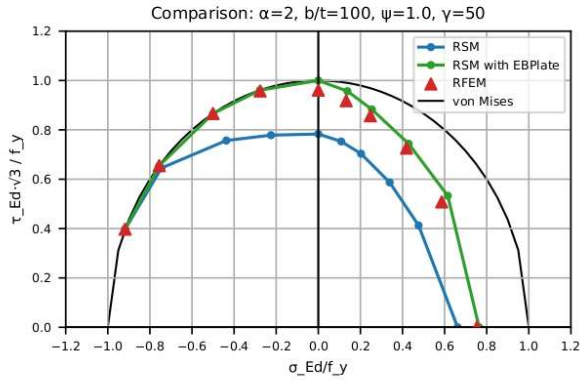
Comparison: α=2, b/t=100, ψ=1.0, γ=50
RSM
RSM with EBPlate
RFEM
von Mises
τ_Ed·√3 / f_y
σ_Ed/f_y

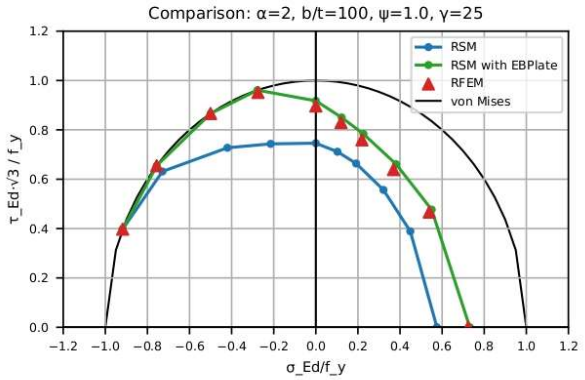
Comparison: α=2, b/t=100, ψ=1.0, γ=25
RSM
RSM with EBPlate
RFEM
von Mises
τ_Ed·√3 / f_y
σ_Ed/f_y

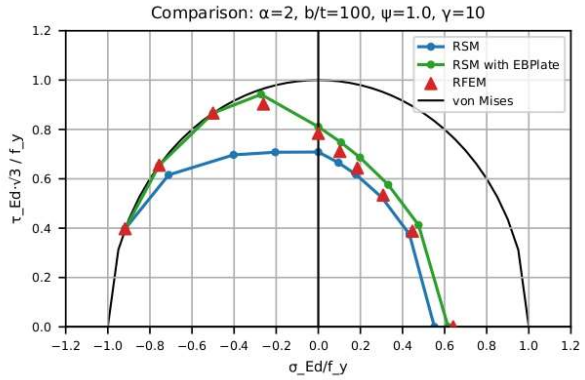
Comparison: α=2, b/t=100, ψ=1.0, γ=10
RSM
RSM with EBPlate
RFEM
von Mises
τ_Ed·√3 / f_y
σ_Ed/f_y

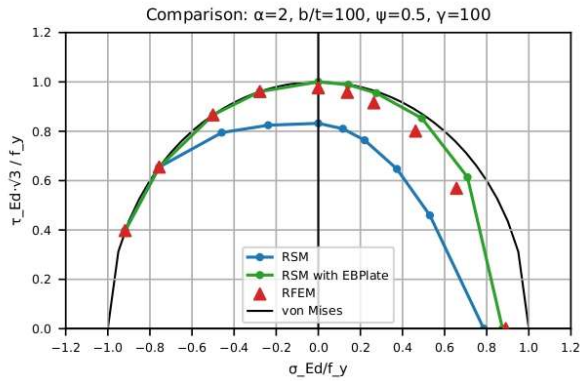
Comparison: α=2, b/t=100, ψ=0.5, γ=100
RSM
RSM with EBPlate
RFEM
von Mises
τ_Ed·√3 / f_y
σ_Ed/f_y

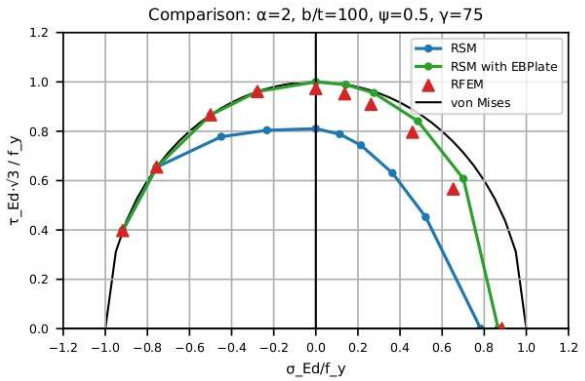
Comparison: α=2, b/t=100, ψ=0.5, γ=75
RSM
RSM with EBPlate
RFEM
von Mises
τ_Ed·√3 / f_y
σ_Ed/f_y

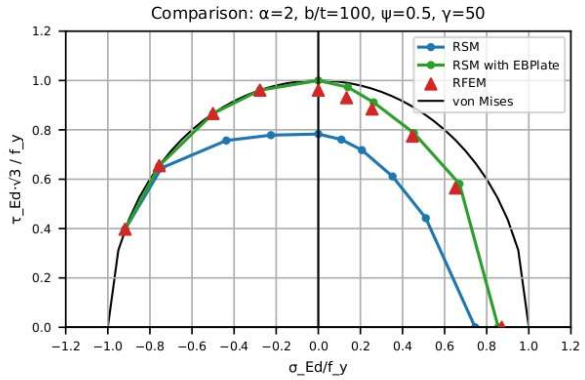
Comparison: α=2, b/t=100, ψ=0.5, γ=50
RSM
RSM with EBPlate
RFEM
von Mises
τ_Ed·√3 / f_y
σ_Ed/f_y

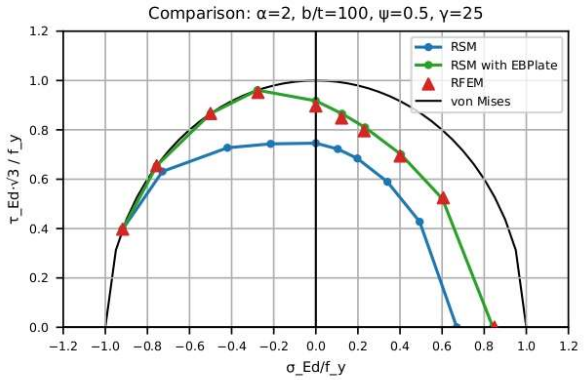
Comparison: α=2, b/t=100, ψ=0.5, γ=25
RSM
RSM with EBPlate
RFEM
von Mises
τ_Ed·√3 / f_y
σ_Ed/f_y

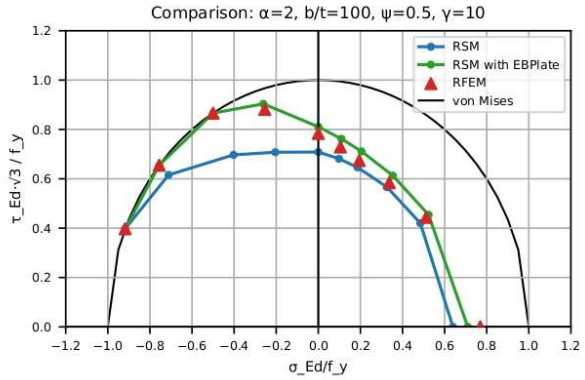
Comparison: α=2, b/t=100, ψ=0.5, γ=10
RSM
RSM with EBPlate
RFEM
von Mises
τ_Ed·√3 / f_y
σ_Ed/f_y

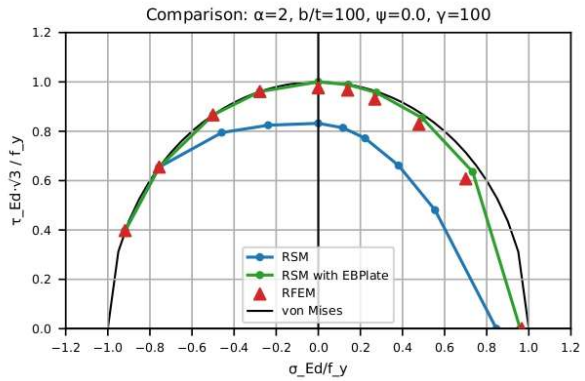
Comparison: α=2, b/t=100, ψ=0.0, γ=100
RSM
RSM with EBPlate
RFEM
von Mises
τ_Ed·√3 / f_y
σ_Ed/f_y

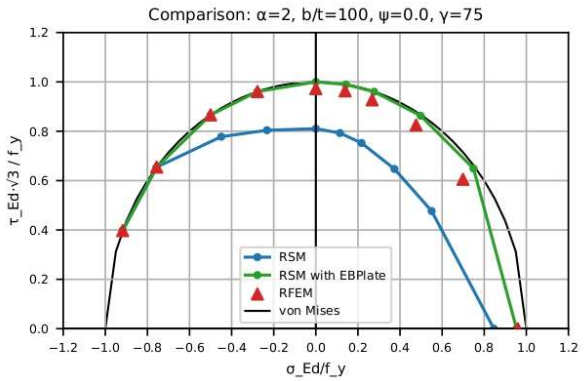
Comparison: α=2, b/t=100, ψ=0.0, γ=75
RSM
RSM with EBPlate
RFEM
von Mises
τ_Ed·√3 / f_y
σ_Ed/f_y

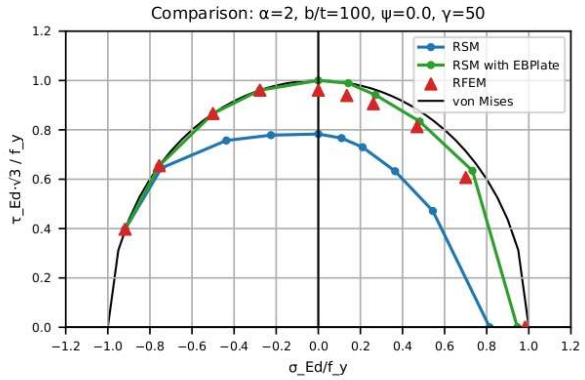
Comparison: α=2, b/t=100, ψ=0.0, γ=50
RSM
RSM with EBPlate
RFEM
von Mises
τ_Ed·√3 / f_y
σ_Ed/f_y

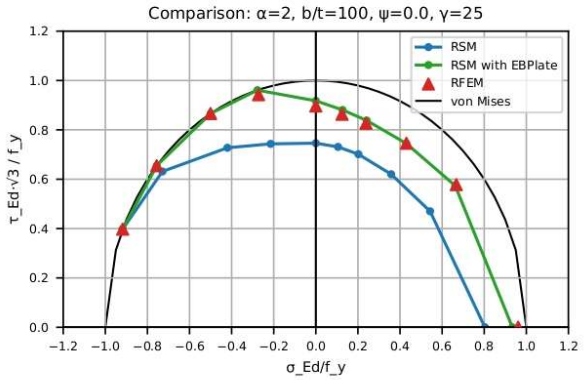
Comparison: α=2, b/t=100, ψ=0.0, γ=25
RSM
RSM with EBPlate
RFEM
von Mises
τ_Ed·√3 / f_y
σ_Ed/f_y

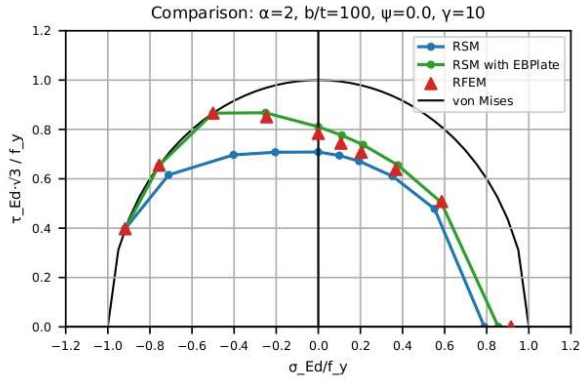
Comparison: α=2, b/t=100, ψ=0.0, γ=10
RSM
RSM with EBPlate
RFEM
von Mises
τ_Ed·√3 / f_y
σ_Ed/f_y

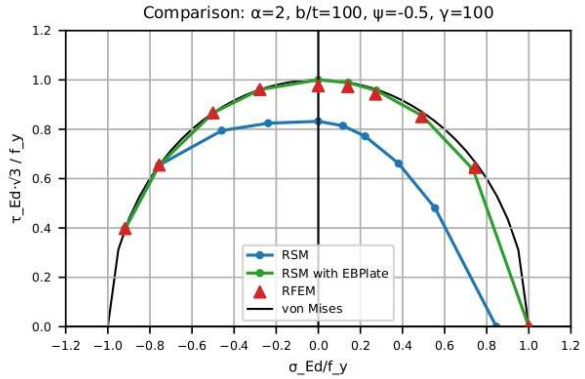
Comparison: α=2, b/t=100, ψ=-0.5, γ=100
RSM
RSM with EBPlate
RFEM
von Mises
τ_Ed·√3 / f_y
σ_Ed/f_y

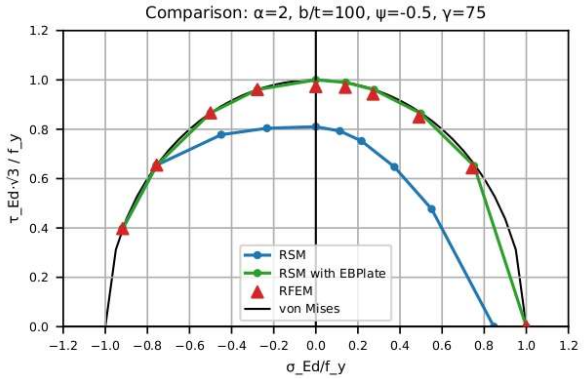
Comparison: α=2, b/t=100, ψ=-0.5, γ=75
RSM
RSM with EBPlate
RFEM
von Mises
τ_Ed·√3 / f_y
σ_Ed/f_y

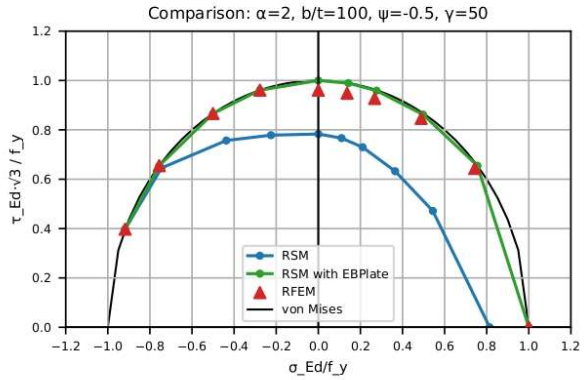
Comparison: α=2, b/t=100, ψ=-0.5, γ=50
RSM
RSM with EBPlate
RFEM
von Mises
τ_Ed·√3 / f_y
σ_Ed/f_y

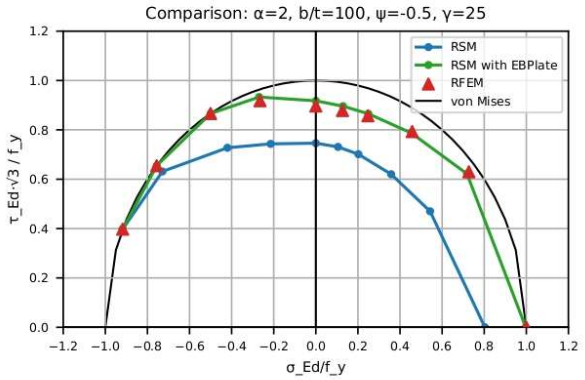
Comparison: α=2, b/t=100, ψ=-0.5, γ=25
RSM
RSM with EBPlate
RFEM
von Mises
τ_Ed·√3 / f_y
σ_Ed/f_y

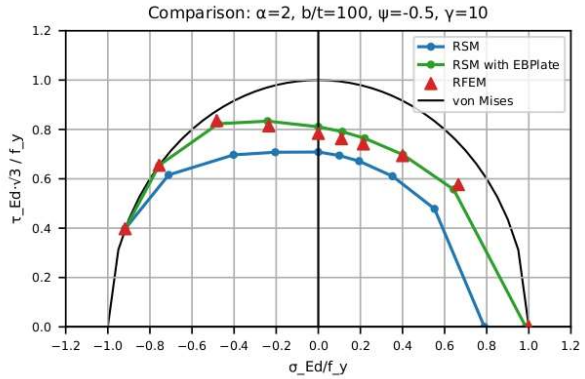
Comparison: α=2, b/t=100, ψ=-0.5, γ=10
RSM
RSM with EBPlate
RFEM
von Mises
τ_Ed·√3 / f_y
σ_Ed/f_y

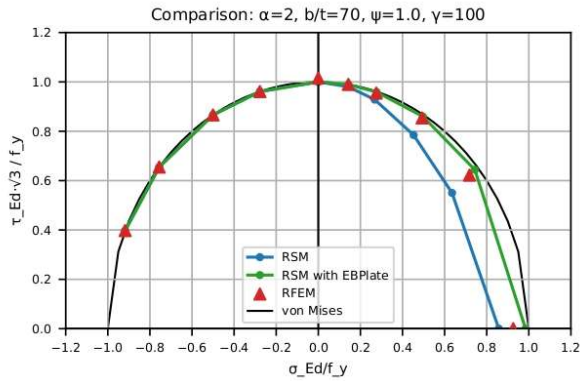
Comparison: α=2, b/t=70, ψ=1.0, γ=100
τ_Ed·√3 / f_y
σ_Ed/f_y
RSM
RSM with EBPlate
RFEM
von Mises

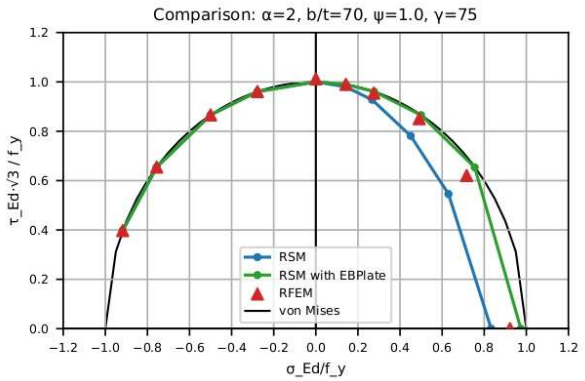
Comparison: α=2, b/t=70, ψ=1.0, γ=75
τ_Ed·√3 / f_y
σ_Ed/f_y
RSM
RSM with EBPlate
RFEM
von Mises

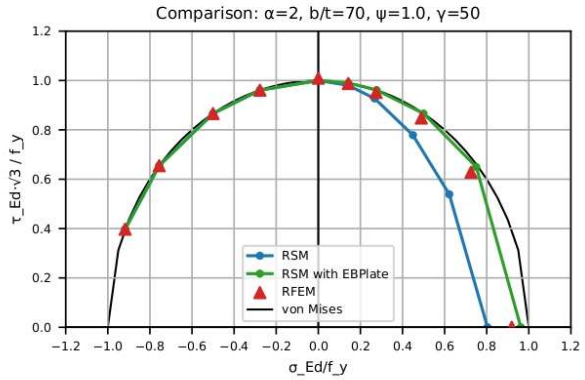
Comparison: α=2, b/t=70, ψ=1.0, γ=50
τ_Ed·√3 / f_y
σ_Ed/f_y
RSM
RSM with EBPlate
RFEM
von Mises

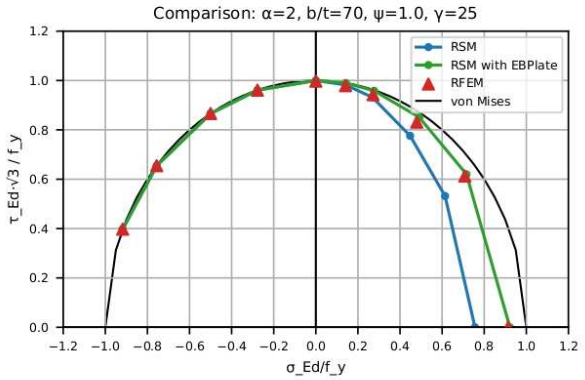
Comparison: α=2, b/t=70, ψ=1.0, γ=25
τ_Ed·√3 / f_y
σ_Ed/f_y
RSM
RSM with EBPlate
RFEM
von Mises

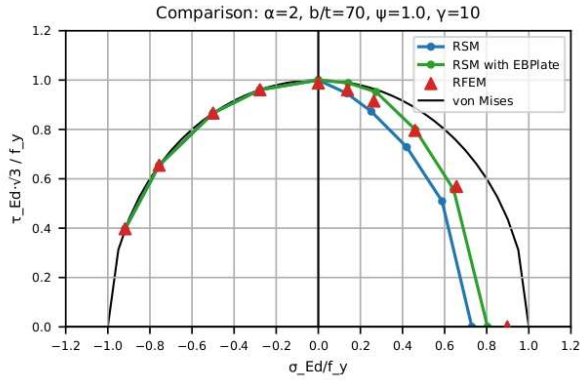
Comparison: α=2, b/t=70, ψ=1.0, γ=10
τ_Ed·√3 / f_y
σ_Ed/f_y
RSM
RSM with EBPlate
RFEM
von Mises

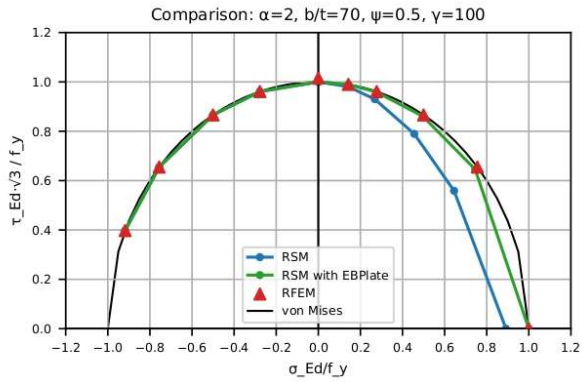
Comparison: α=2, b/t=70, ψ=0.5, γ=100
τ_Ed·√3 / f_y
σ_Ed/f_y
RSM
RSM with EBPlate
RFEM
von Mises

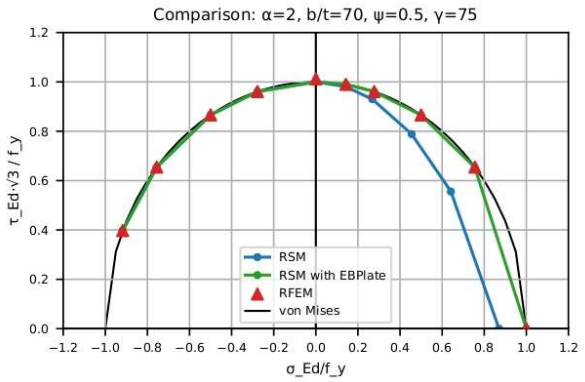
Comparison: α=2, b/t=70, ψ=0.5, γ=75
τ_Ed·√3 / f_y
σ_Ed/f_y
RSM
RSM with EBPlate
RFEM
von Mises

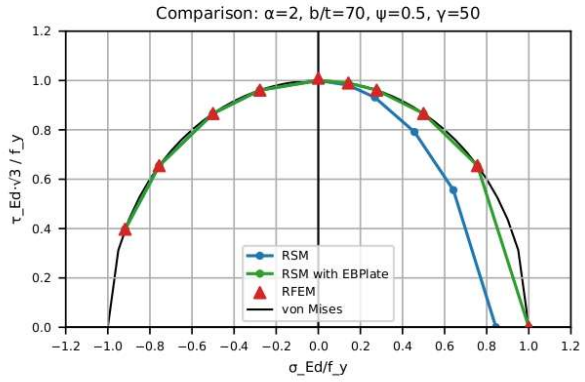
Comparison: α=2, b/t=70, ψ=0.5, γ=50
τ_Ed·√3 / f_y
σ_Ed/f_y
RSM
RSM with EBPlate
RFEM
von Mises

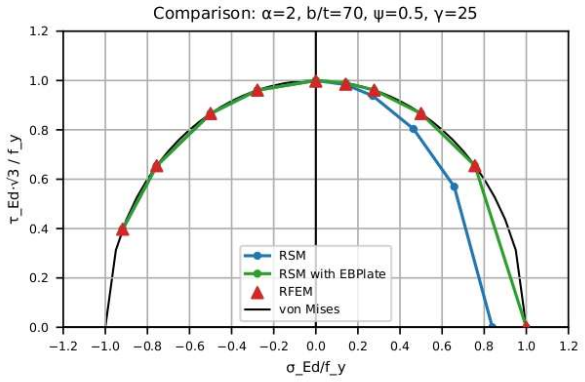
Comparison: α=2, b/t=70, ψ=0.5, γ=25
τ_Ed·√3 / f_y
σ_Ed/f_y
RSM
RSM with EBPlate
RFEM
von Mises

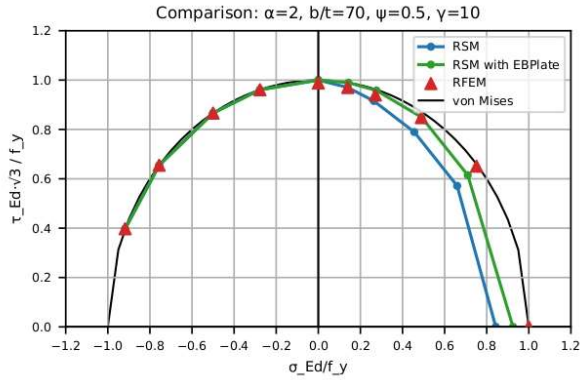
Comparison: α=2, b/t=70, ψ=0.5, γ=10
τ_Ed·√3 / f_y
σ_Ed/f_y
RSM
RSM with EBPlate
RFEM
von Mises

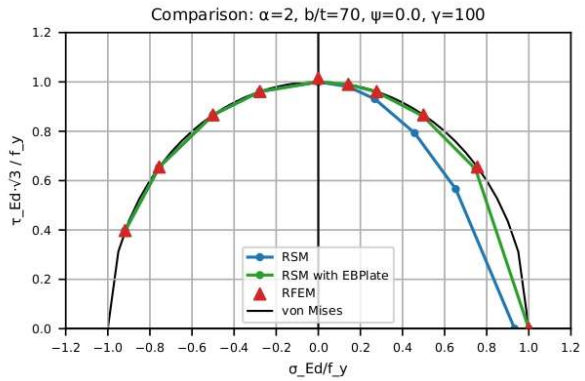
Comparison: α=2, b/t=70, ψ=0.0, γ=100
τ_Ed·√3 / f_y
σ_Ed/f_y
RSM
RSM with EBPlate
RFEM
von Mises

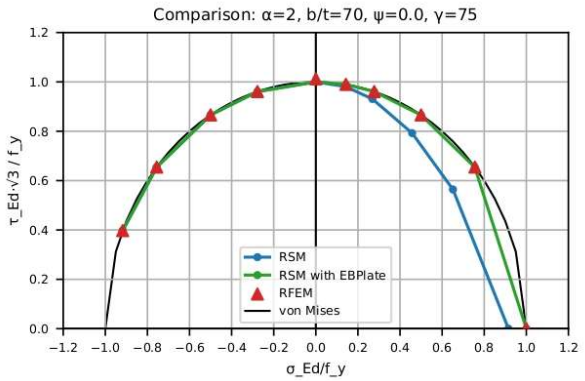
Comparison: α=2, b/t=70, ψ=0.0, γ=75
τ_Ed·√3 / f_y
σ_Ed/f_y
RSM
RSM with EBPlate
RFEM
von Mises

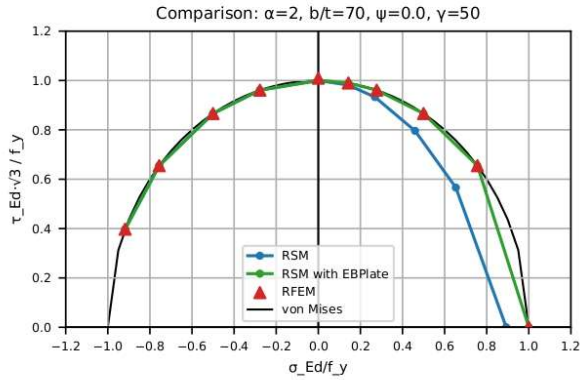
Comparison: α=2, b/t=70, ψ=0.0, γ=50
τ_Ed·√3 / f_y
σ_Ed/f_y
RSM
RSM with EBPlate
RFEM
von Mises

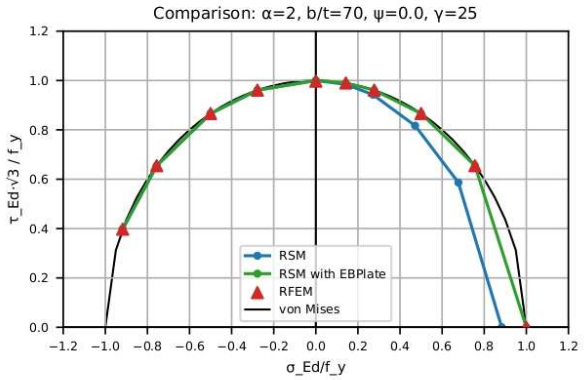
Comparison: α=2, b/t=70, ψ=0.0, γ=25
τ_Ed·√3 / f_y
σ_Ed/f_y
RSM
RSM with EBPlate
RFEM
von Mises

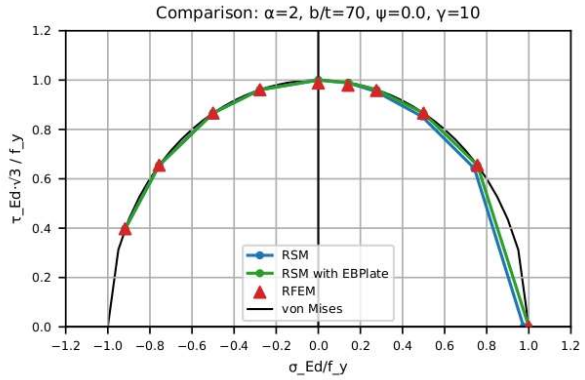
Comparison: α=2, b/t=70, ψ=0.0, γ=10
τ_Ed·√3 / f_y
σ_Ed/f_y
RSM
RSM with EBPlate
RFEM
von Mises

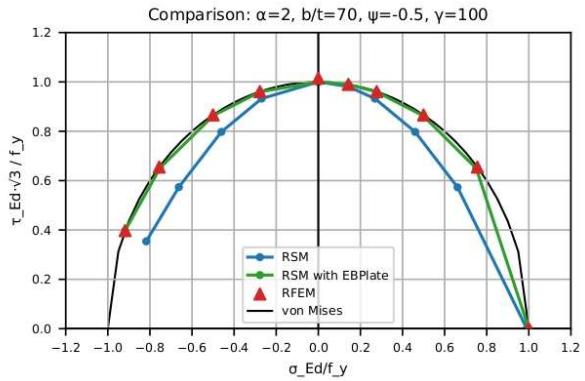
Comparison: α=2, b/t=70, ψ=-0.5, γ=100
τ_Ed·√3 / f_y
σ_Ed/f_y
RSM
RSM with EBPlate
RFEM
von Mises

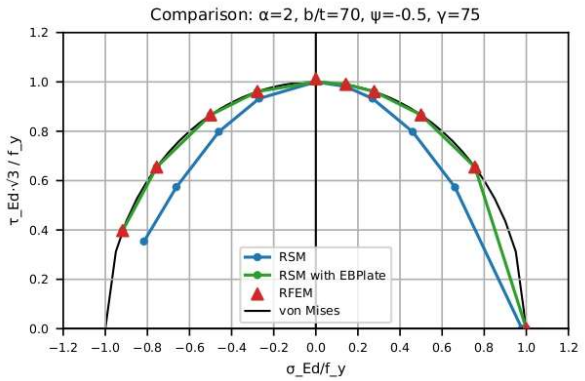
Comparison: α=2, b/t=70, ψ=-0.5, γ=75
τ_Ed·√3 / f_y
σ_Ed/f_y
RSM
RSM with EBPlate
RFEM
von Mises

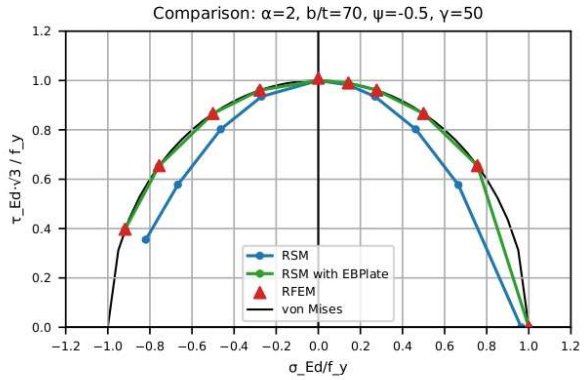
Comparison: α=2, b/t=70, ψ=-0.5, γ=50
τ_Ed·√3 / f_y
σ_Ed/f_y
RSM
RSM with EBPlate
RFEM
von Mises

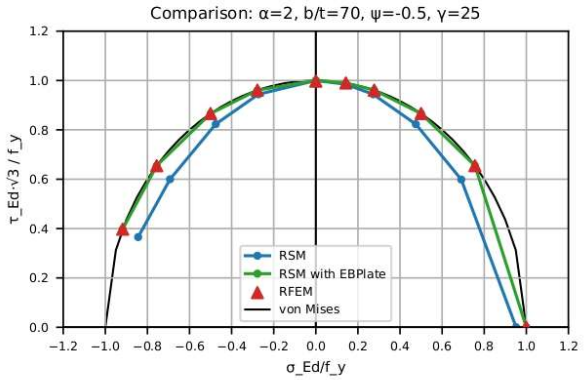
Comparison: α=2, b/t=70, ψ=-0.5, γ=25
τ_Ed·√3 / f_y
σ_Ed/f_y
RSM
RSM with EBPlate
RFEM
von Mises

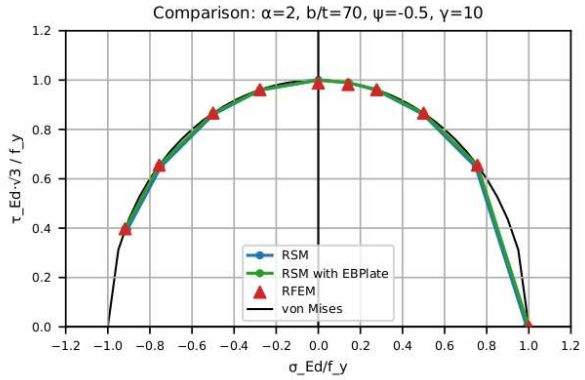
Comparison: α=2, b/t=70, ψ=-0.5, γ=10
τ_Ed·√3 / f_y
σ_Ed/f_y
RSM
RSM with EBPlate
RFEM
von Mises

Appendix C: Buckling resistance for stiffened plates - Approach 2 and 3, RF1, RF5 and RF10 side by side

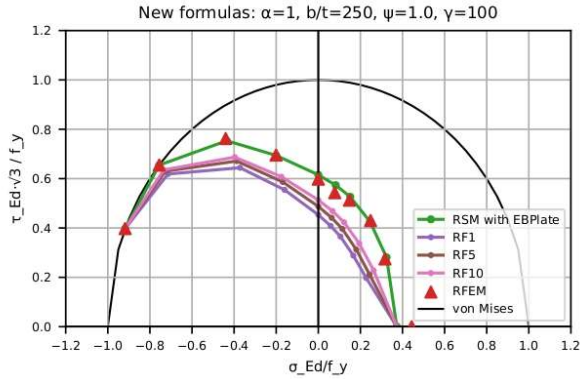
New formulas: α=1, b/t=250, ψ=1.0, γ=100
τ_Ed·√3 / f_y
σ_Ed/f_y
RSM with EBPlate
RF1
RF5
RF10
RFEM
von Mises

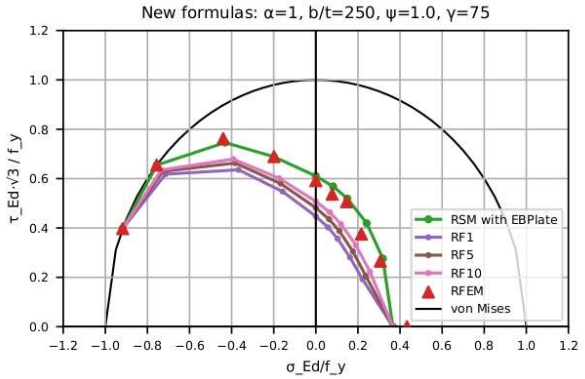
New formulas: α=1, b/t=250, ψ=1.0, γ=75
τ_Ed·√3 / f_y
σ_Ed/f_y
RSM with EBPlate
RF1
RF5
RF10
RFEM
von Mises

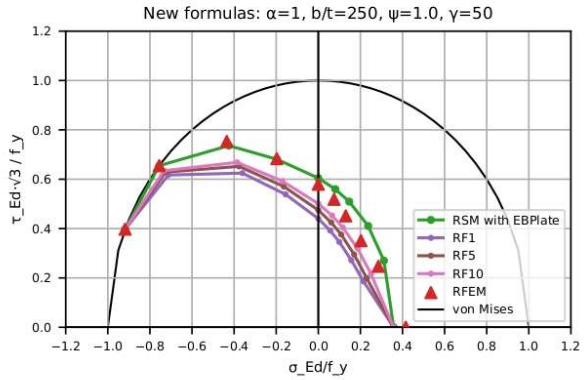
New formulas: α=1, b/t=250, ψ=1.0, γ=50
τ_Ed·√3 / f_y
σ_Ed/f_y
RSM with EBPlate
RF1
RF5
RF10
RFEM
von Mises

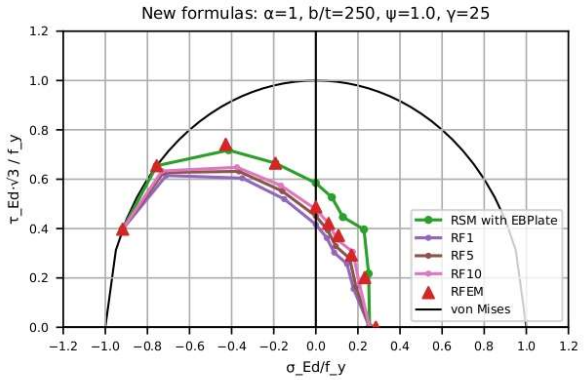
New formulas: α=1, b/t=250, ψ=1.0, γ=25
τ_Ed·√3 / f_y
σ_Ed/f_y
RSM with EBPlate
RF1
RF5
RF10
RFEM
von Mises

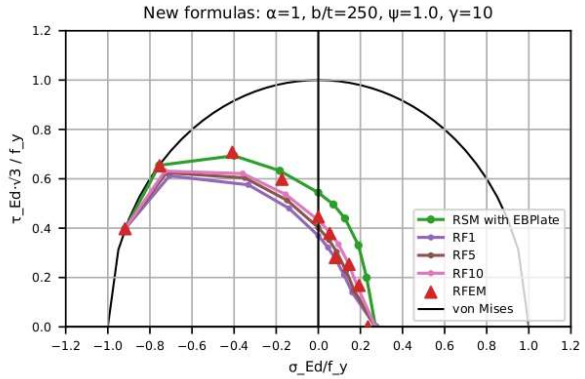
New formulas: α=1, b/t=250, ψ=1.0, γ=10
τ_Ed·√3 / f_y
σ_Ed/f_y
RSM with EBPlate
RF1
RF5
RF10
RFEM
von Mises

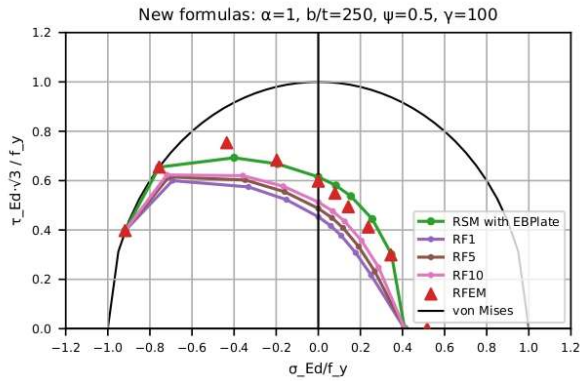
New formulas: α=1, b/t=250, ψ=0.5, γ=100
τ_Ed·√3 / f_y
σ_Ed/f_y
RSM with EBPlate
RF1
RF5
RF10
RFEM
von Mises

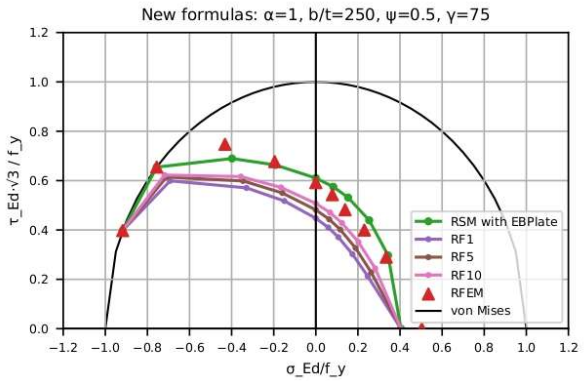
New formulas: α=1, b/t=250, ψ=0.5, γ=75
τ_Ed·√3 / f_y
σ_Ed/f_y
RSM with EBPlate
RF1
RF5
RF10
RFEM
von Mises

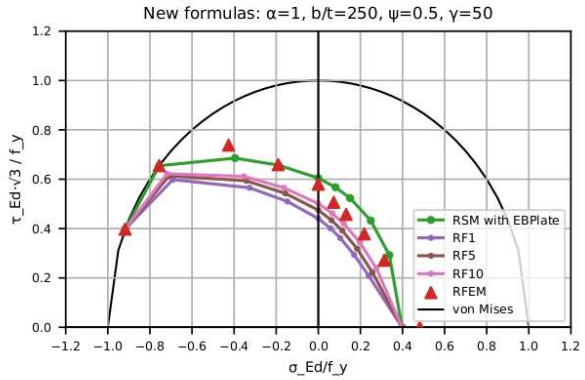
New formulas: α=1, b/t=250, ψ=0.5, γ=50
τ_Ed·√3 / f_y
σ_Ed/f_y
RSM with EBPlate
RF1
RF5
RF10
RFEM
von Mises

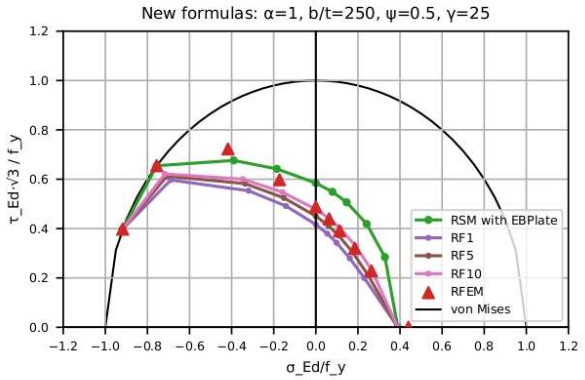
New formulas: α=1, b/t=250, ψ=0.5, γ=25
τ_Ed·√3 / f_y
σ_Ed/f_y
RSM with EBPlate
RF1
RF5
RF10
RFEM
von Mises

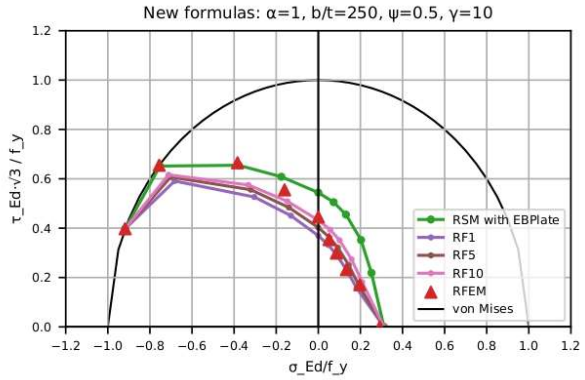
New formulas: α=1, b/t=250, ψ=0.5, γ=10
τ_Ed·√3 / f_y
σ_Ed/f_y
RSM with EBPlate
RF1
RF5
RF10
RFEM
von Mises

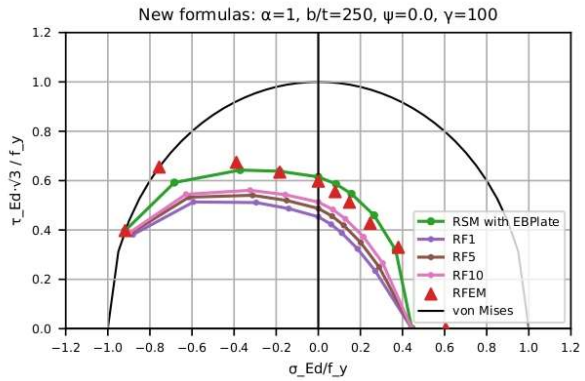
New formulas: α=1, b/t=250, ψ=0.0, γ=100
τ_Ed·√3 / f_y
σ_Ed/f_y
RSM with EBPlate
RF1
RF5
RF10
RFEM
von Mises

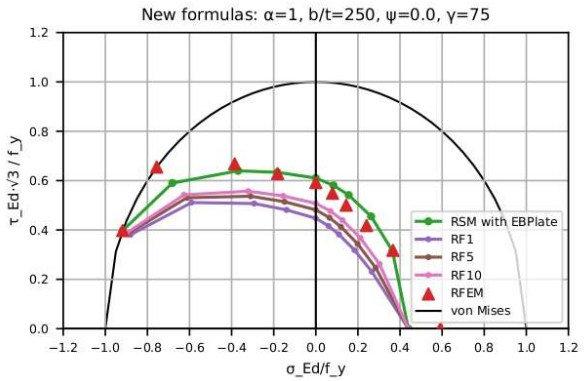
New formulas: α=1, b/t=250, ψ=0.0, γ=75
τ_Ed·√3 / f_y
σ_Ed/f_y
RSM with EBPlate
RF1
RF5
RF10
RFEM
von Mises

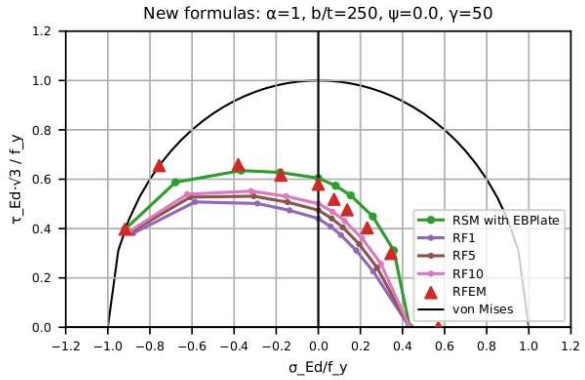
New formulas: α=1, b/t=250, ψ=0.0, γ=50
τ_Ed·√3 / f_y
σ_Ed/f_y
RSM with EBPlate
RF1
RF5
RF10
RFEM
von Mises

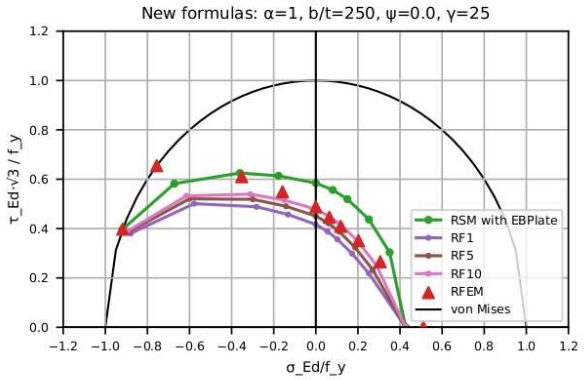
New formulas: α=1, b/t=250, ψ=0.0, γ=25
τ_Ed·√3 / f_y
σ_Ed/f_y
RSM with EBPlate
RF1
RF5
RF10
RFEM
von Mises

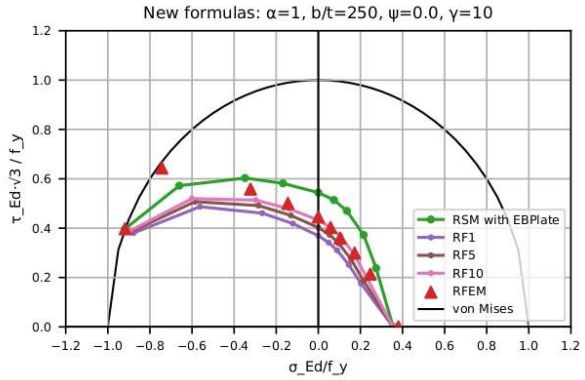
New formulas: α=1, b/t=250, ψ=0.0, γ=10
τ_Ed·√3 / f_y
σ_Ed/f_y
RSM with EBPlate
RF1
RF5
RF10
RFEM
von Mises

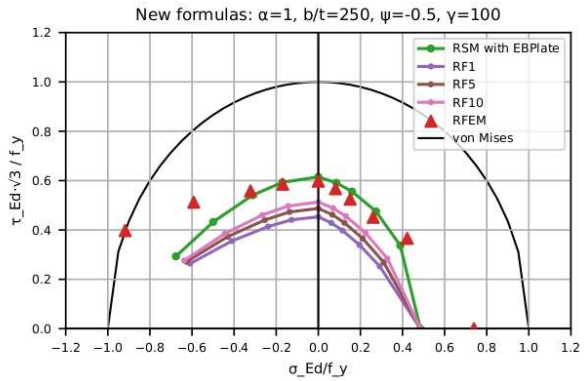
New formulas: α=1, b/t=250, ψ=-0.5, γ=100
RSM with EBPlate
RF1
RF5
RF10
RFEM
von Mises
τ_Ed·√3 / f_y
σ_Ed/f_y

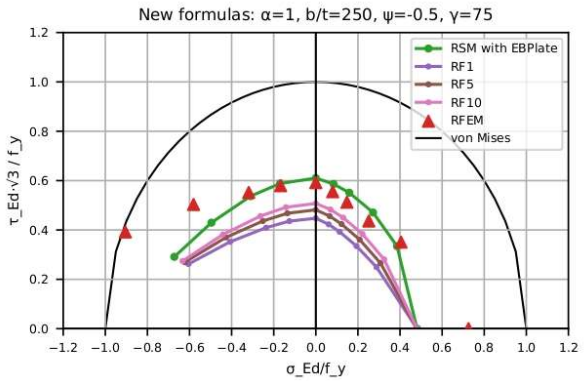
New formulas: α=1, b/t=250, ψ=-0.5, γ=75
RSM with EBPlate
RF1
RF5
RF10
RFEM
von Mises
τ_Ed·√3 / f_y
σ_Ed/f_y

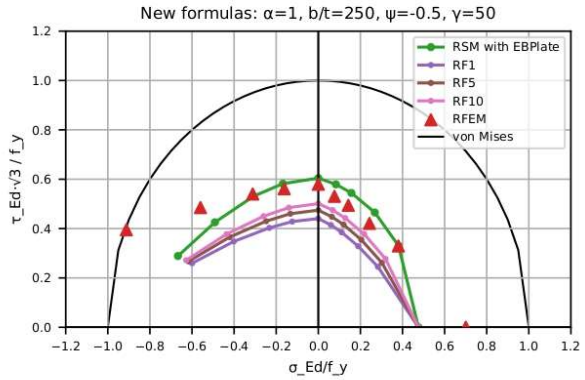
New formulas: α=1, b/t=250, ψ=-0.5, γ=50
RSM with EBPlate
RF1
RF5
RF10
RFEM
von Mises
τ_Ed·√3 / f_y
σ_Ed/f_y

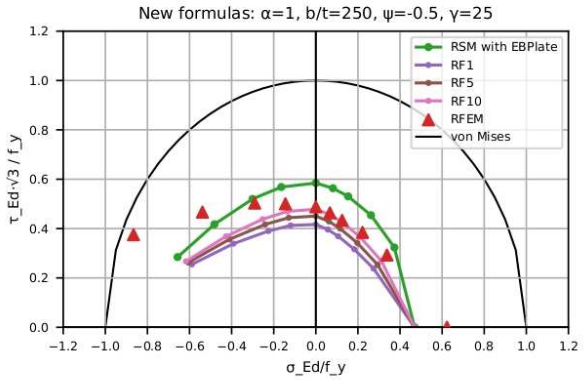
New formulas: α=1, b/t=250, ψ=-0.5, γ=25
RSM with EBPlate
RF1
RF5
RF10
RFEM
von Mises
τ_Ed·√3 / f_y
σ_Ed/f_y

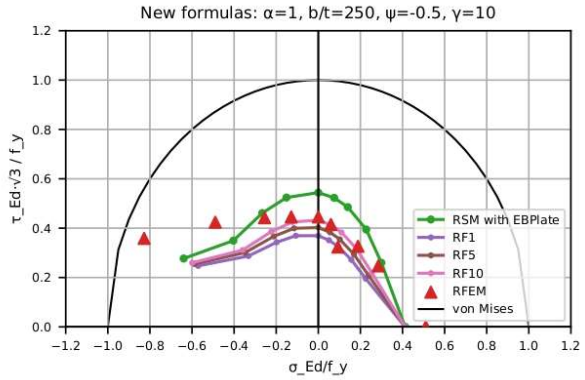
New formulas: α=1, b/t=250, ψ=-0.5, γ=10
RSM with EBPlate
RF1
RF5
RF10
RFEM
von Mises
τ_Ed·√3 / f_y
σ_Ed/f_y

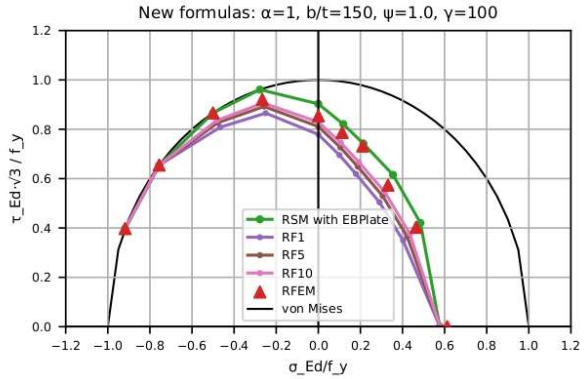
New formulas: α=1, b/t=150, ψ=1.0, γ=100
τ_Ed·√3 / f_y
σ_Ed/f_y
RSM with EBPlate
RF1
RF5
RF10
RFEM
von Mises

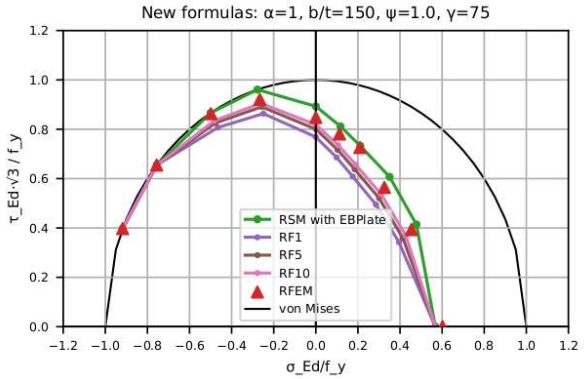
New formulas: α=1, b/t=150, ψ=1.0, γ=75
τ_Ed·√3 / f_y
σ_Ed/f_y
RSM with EBPlate
RF1
RF5
RF10
RFEM
von Mises

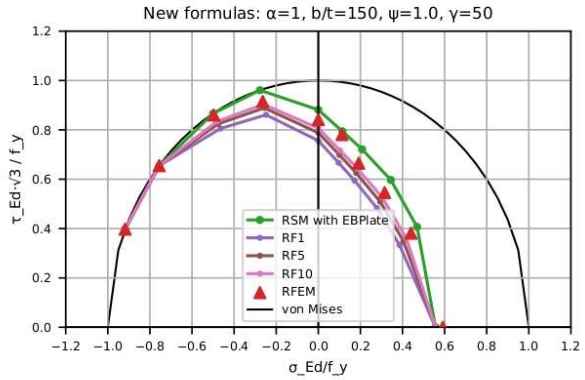
New formulas: α=1, b/t=150, ψ=1.0, γ=50
τ_Ed·√3 / f_y
σ_Ed/f_y
RSM with EBPlate
RF1
RF5
RF10
RFEM
von Mises

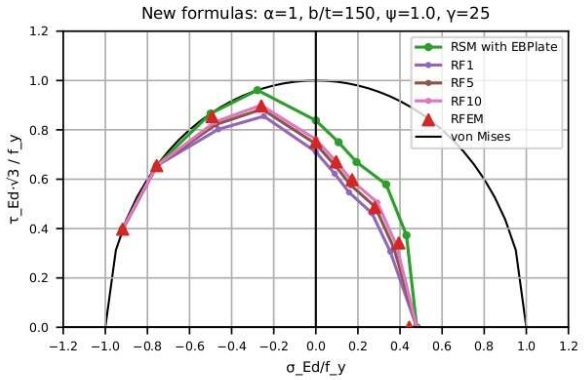
New formulas: α=1, b/t=150, ψ=1.0, γ=25
τ_Ed·√3 / f_y
σ_Ed/f_y
RSM with EBPlate
RF1
RF5
RF10
RFEM
von Mises

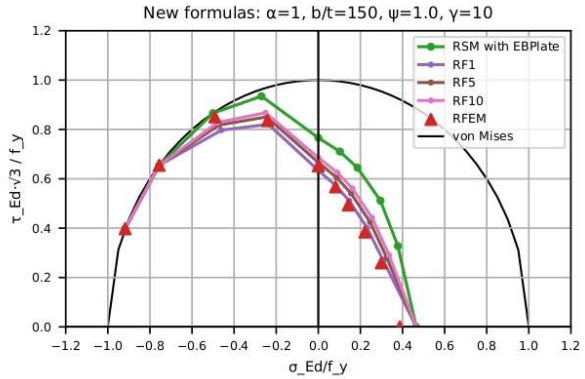
New formulas: α=1, b/t=150, ψ=1.0, γ=10
τ_Ed·√3 / f_y
σ_Ed/f_y
RSM with EBPlate
RF1
RF5
RF10
RFEM
von Mises

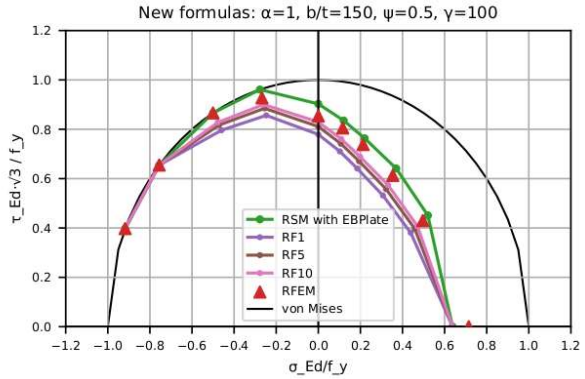
New formulas: α=1, b/t=150, ψ=0.5, γ=100
τ_Ed·√3 / f_y
σ_Ed/f_y
RSM with EBPlate
RF1
RF5
RF10
RFEM
von Mises

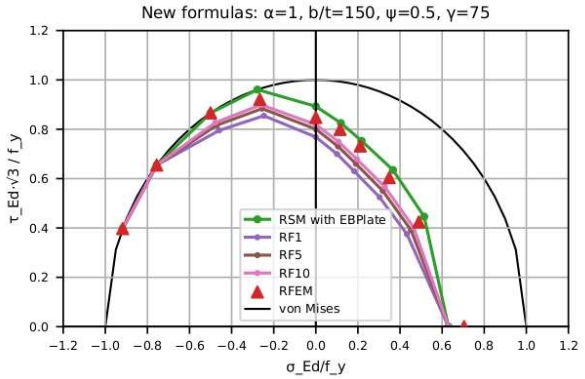
New formulas: α=1, b/t=150, ψ=0.5, γ=75
τ_Ed·√3 / f_y
σ_Ed/f_y
RSM with EBPlate
RF1
RF5
RF10
RFEM
von Mises

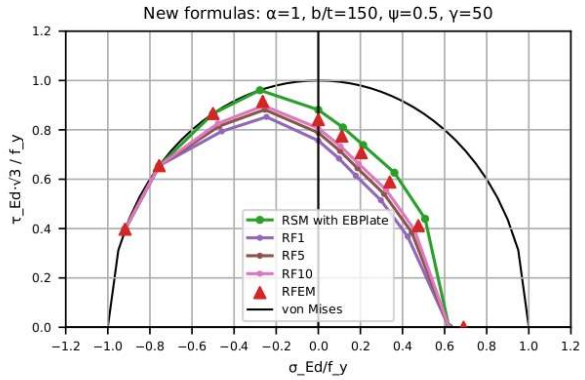
New formulas: α=1, b/t=150, ψ=0.5, γ=50
τ_Ed·√3 / f_y
σ_Ed/f_y
RSM with EBPlate
RF1
RF5
RF10
RFEM
von Mises

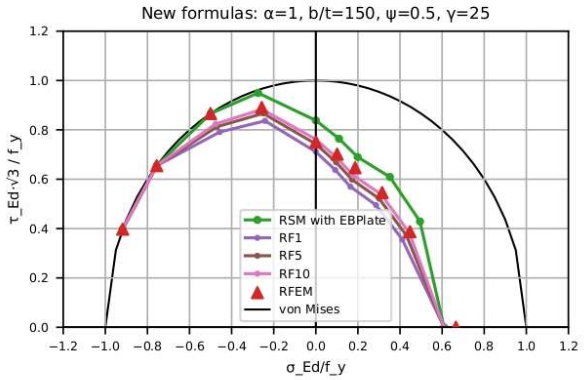
New formulas: α=1, b/t=150, ψ=0.5, γ=25
τ_Ed·√3 / f_y
σ_Ed/f_y
RSM with EBPlate
RF1
RF5
RF10
RFEM
von Mises

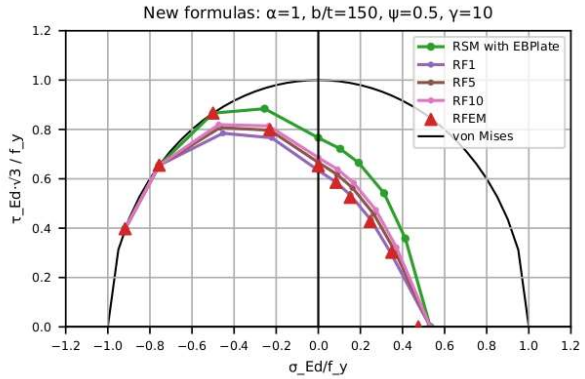
New formulas: α=1, b/t=150, ψ=0.5, γ=10
τ_Ed·√3 / f_y
σ_Ed/f_y
RSM with EBPlate
RF1
RF5
RF10
RFEM
von Mises

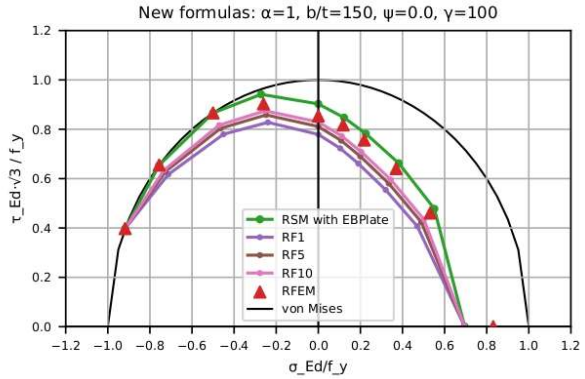
New formulas: α=1, b/t=150, ψ=0.0, γ=100
τ_Ed·√3 / f_y
σ_Ed/f_y
RSM with EBPlate
RF1
RF5
RF10
RFEM
von Mises

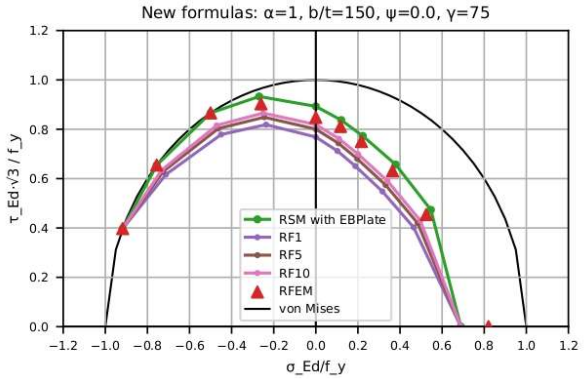
New formulas: α=1, b/t=150, ψ=0.0, γ=75
τ_Ed·√3 / f_y
σ_Ed/f_y
RSM with EBPlate
RF1
RF5
RF10
RFEM
von Mises

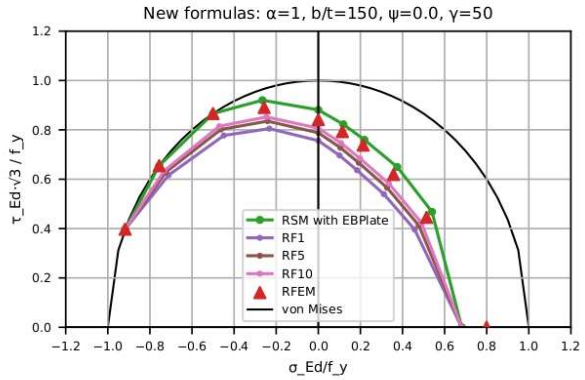
New formulas: α=1, b/t=150, ψ=0.0, γ=50
τ_Ed·√3 / f_y
σ_Ed/f_y
RSM with EBPlate
RF1
RF5
RF10
RFEM
von Mises

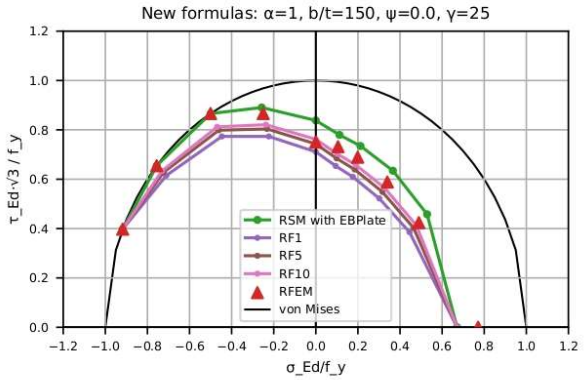
New formulas: α=1, b/t=150, ψ=0.0, γ=25
τ_Ed·√3 / f_y
σ_Ed/f_y
RSM with EBPlate
RF1
RF5
RF10
RFEM
von Mises

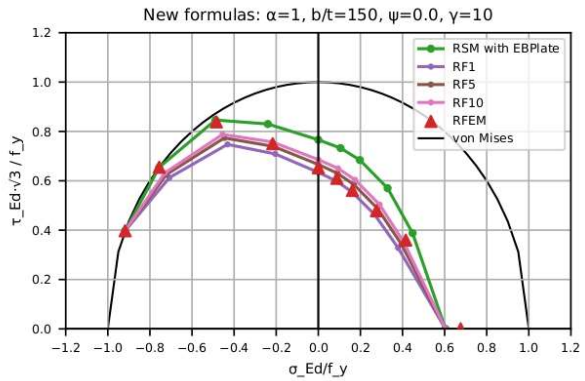
New formulas: α=1, b/t=150, ψ=0.0, γ=10
τ_Ed·√3 / f_y
σ_Ed/f_y
RSM with EBPlate
RF1
RF5
RF10
RFEM
von Mises

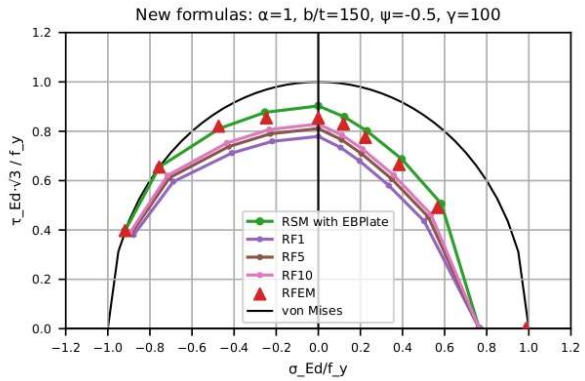
New formulas: α=1, b/t=150, ψ=-0.5, γ=100
τ_Ed·√3 / f_y
σ_Ed/f_y
RSM with EBPlate
RF1
RF5
RF10
RFEM
von Mises

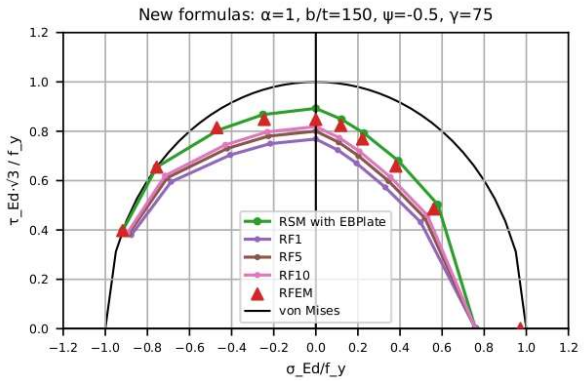
New formulas: α=1, b/t=150, ψ=-0.5, γ=75
τ_Ed·√3 / f_y
σ_Ed/f_y
RSM with EBPlate
RF1
RF5
RF10
RFEM
von Mises

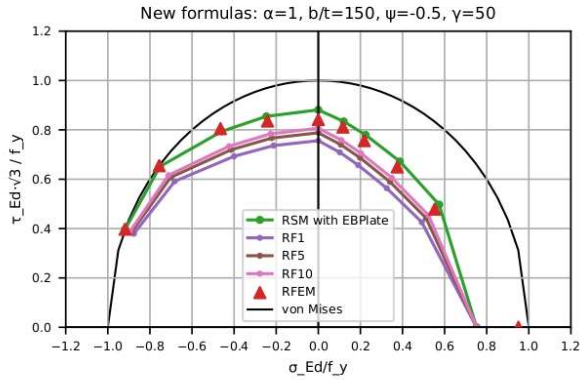
New formulas: α=1, b/t=150, ψ=-0.5, γ=50
τ_Ed·√3 / f_y
σ_Ed/f_y
RSM with EBPlate
RF1
RF5
RF10
RFEM
von Mises

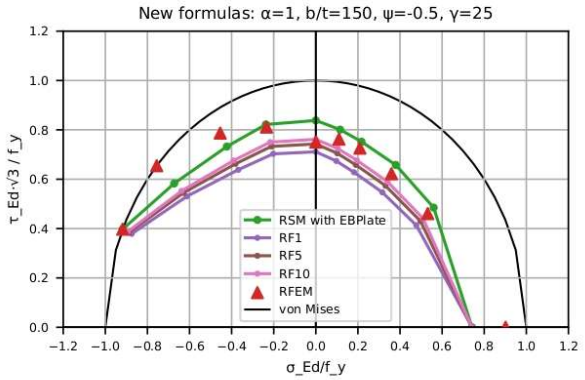
New formulas: α=1, b/t=150, ψ=-0.5, γ=25
τ_Ed·√3 / f_y
σ_Ed/f_y
RSM with EBPlate
RF1
RF5
RF10
RFEM
von Mises

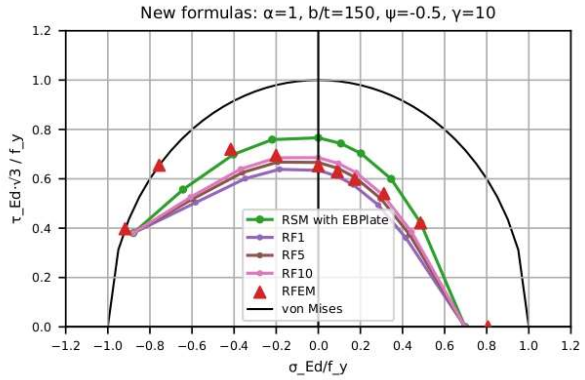
New formulas: α=1, b/t=150, ψ=-0.5, γ=10
τ_Ed·√3 / f_y
σ_Ed/f_y
RSM with EBPlate
RF1
RF5
RF10
RFEM
von Mises

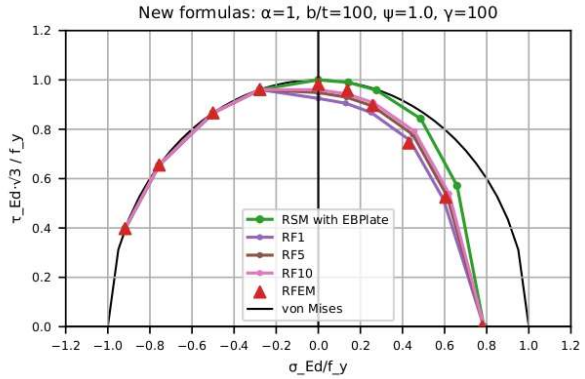
New formulas: α=1, b/t=100, ψ=1.0, γ=100
τ_Ed·√3 / f_y
σ_Ed/f_y
RSM with EBPlate
RF1
RF5
RF10
RFEM
von Mises

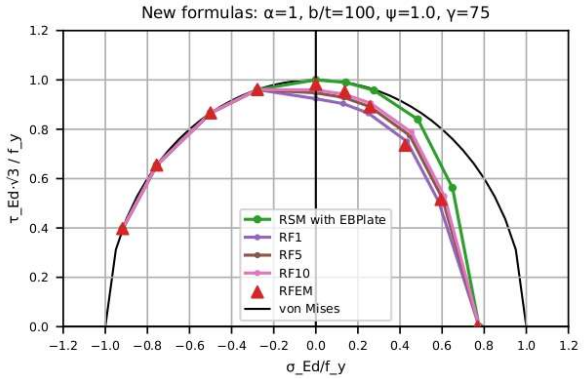
New formulas: α=1, b/t=100, ψ=1.0, γ=75
τ_Ed·√3 / f_y
σ_Ed/f_y
RSM with EBPlate
RF1
RF5
RF10
RFEM
von Mises

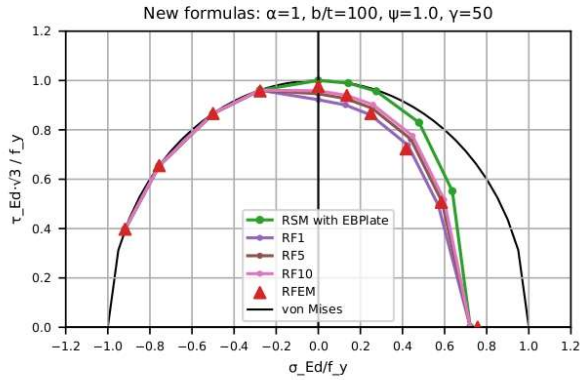
New formulas: α=1, b/t=100, ψ=1.0, γ=50
τ_Ed·√3 / f_y
σ_Ed/f_y
RSM with EBPlate
RF1
RF5
RF10
RFEM
von Mises

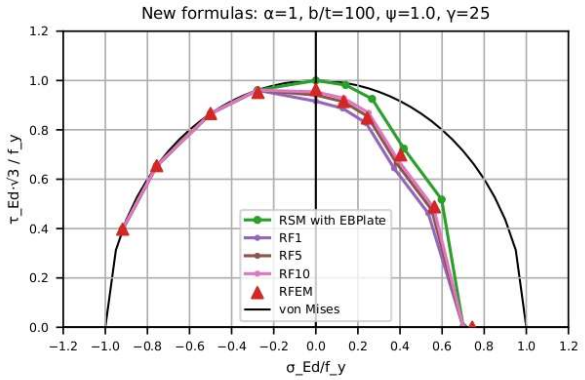
New formulas: α=1, b/t=100, ψ=1.0, γ=25
τ_Ed·√3 / f_y
σ_Ed/f_y
RSM with EBPlate
RF1
RF5
RF10
RFEM
von Mises

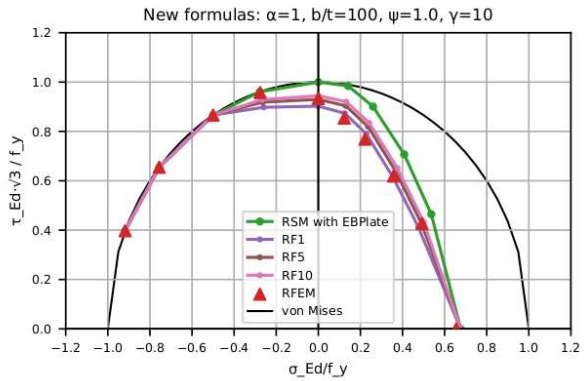
New formulas: α=1, b/t=100, ψ=1.0, γ=10
τ_Ed·√3 / f_y
σ_Ed/f_y
RSM with EBPlate
RF1
RF5
RF10
RFEM
von Mises

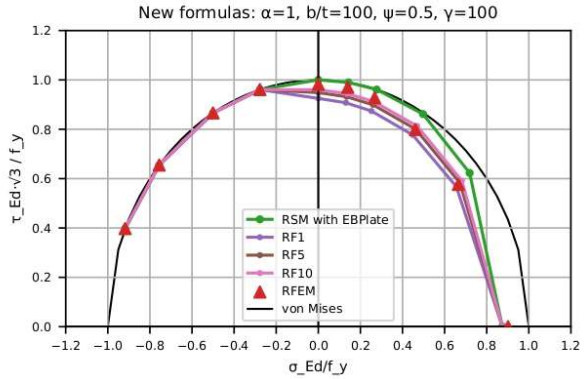
New formulas: α=1, b/t=100, ψ=0.5, γ=100
τ_Ed·√3 / f_y
σ_Ed/f_y
RSM with EBPlate
RF1
RF5
RF10
RFEM
von Mises

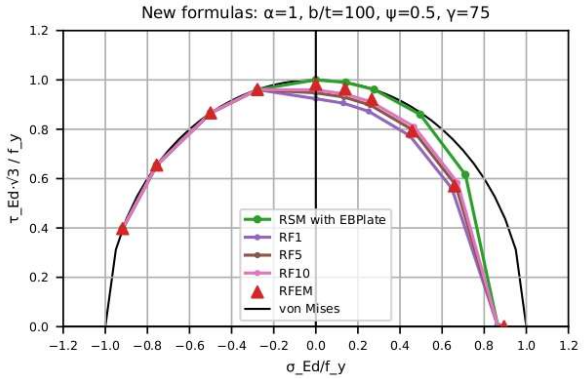
New formulas: α=1, b/t=100, ψ=0.5, γ=75
τ_Ed·√3 / f_y
σ_Ed/f_y
RSM with EBPlate
RF1
RF5
RF10
RFEM
von Mises

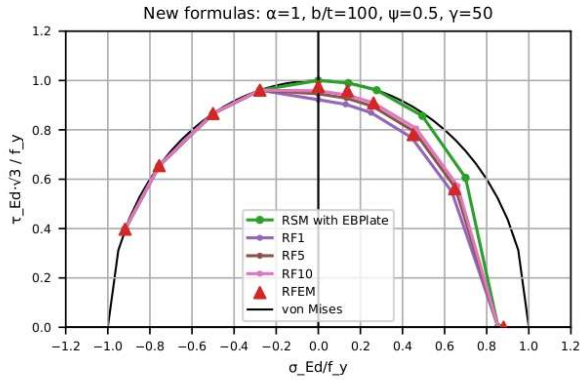
New formulas: α=1, b/t=100, ψ=0.5, γ=50
τ_Ed·√3 / f_y
σ_Ed/f_y
RSM with EBPlate
RF1
RF5
RF10
RFEM
von Mises

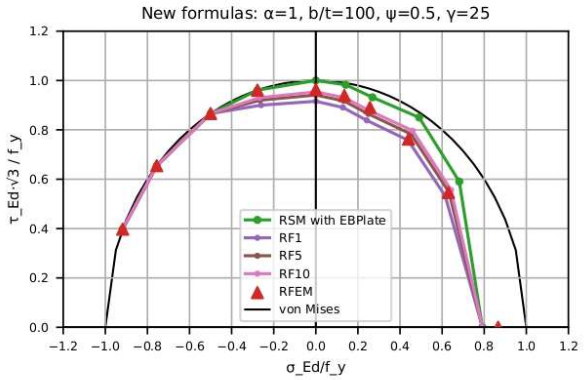
New formulas: α=1, b/t=100, ψ=0.5, γ=25
τ_Ed·√3 / f_y
σ_Ed/f_y
RSM with EBPlate
RF1
RF5
RF10
RFEM
von Mises

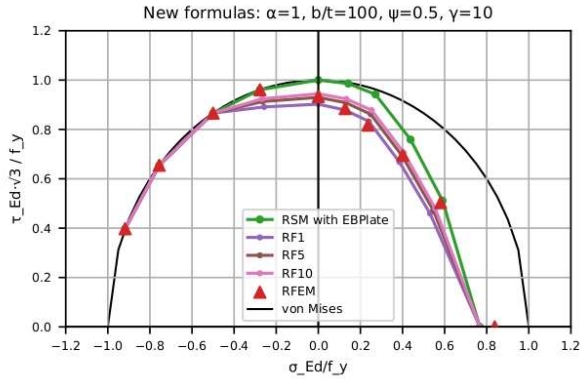
New formulas: α=1, b/t=100, ψ=0.5, γ=10
τ_Ed·√3 / f_y
σ_Ed/f_y
RSM with EBPlate
RF1
RF5
RF10
RFEM
von Mises

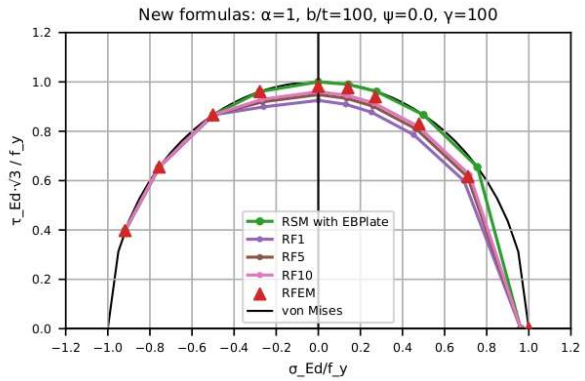
New formulas: α=1, b/t=100, ψ=0.0, γ=100
τ_Ed·√3 / f_y
σ_Ed/f_y
RSM with EBPlate
RF1
RF5
RF10
RFEM
von Mises

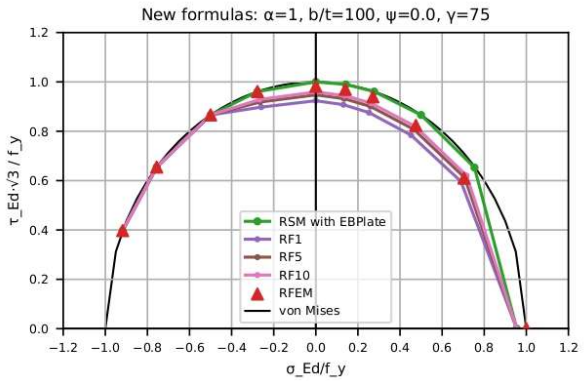
New formulas: α=1, b/t=100, ψ=0.0, γ=75
τ_Ed·√3 / f_y
σ_Ed/f_y
RSM with EBPlate
RF1
RF5
RF10
RFEM
von Mises

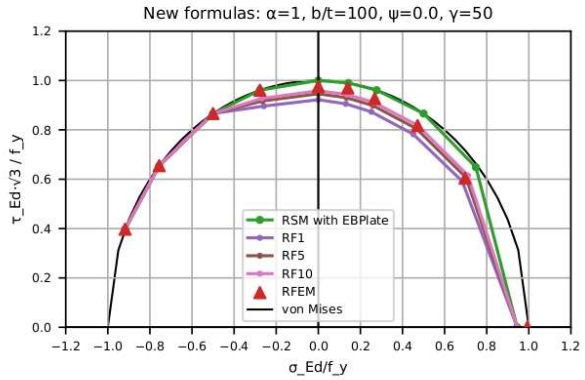
New formulas: α=1, b/t=100, ψ=0.0, γ=50
τ_Ed·√3 / f_y
σ_Ed/f_y
RSM with EBPlate
RF1
RF5
RF10
RFEM
von Mises

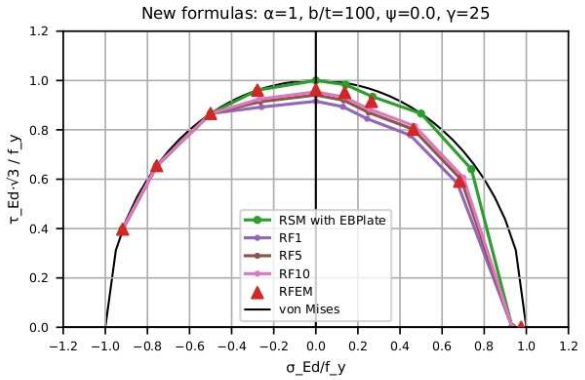
New formulas: α=1, b/t=100, ψ=0.0, γ=25
τ_Ed·√3 / f_y
σ_Ed/f_y
RSM with EBPlate
RF1
RF5
RF10
RFEM
von Mises

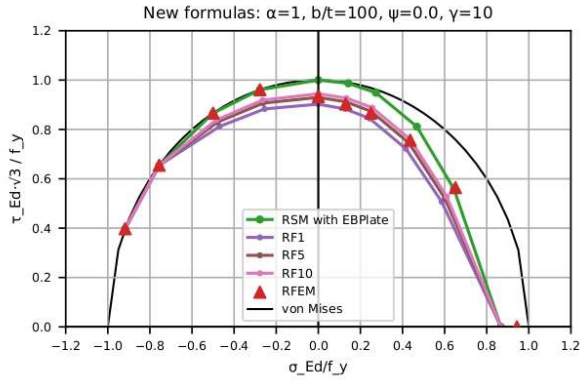
New formulas: α=1, b/t=100, ψ=0.0, γ=10
τ_Ed·√3 / f_y
σ_Ed/f_y
RSM with EBPlate
RF1
RF5
RF10
RFEM
von Mises

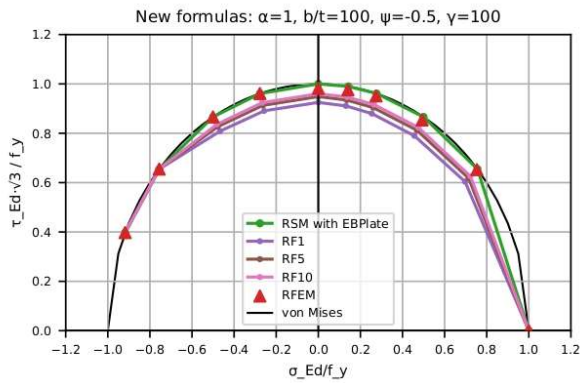
New formulas: α=1, b/t=100, ψ=-0.5, γ=100
τ_Ed·√3 / f_y
σ_Ed/f_y
RSM with EBPlate
RF1
RF5
RF10
RFEM
von Mises

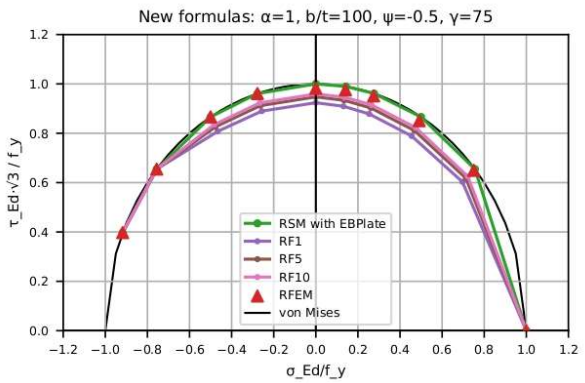
New formulas: α=1, b/t=100, ψ=-0.5, γ=75
τ_Ed·√3 / f_y
σ_Ed/f_y
RSM with EBPlate
RF1
RF5
RF10
RFEM
von Mises

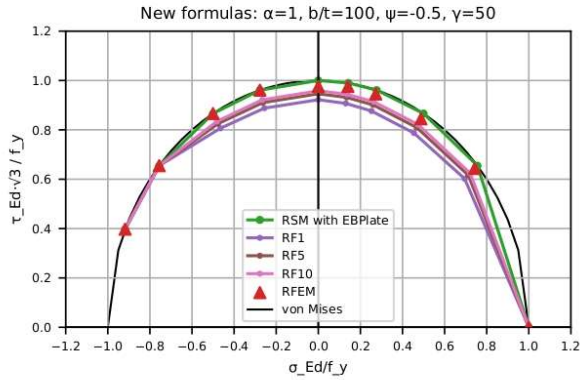
New formulas: α=1, b/t=100, ψ=-0.5, γ=50
τ_Ed·√3 / f_y
σ_Ed/f_y
RSM with EBPlate
RF1
RF5
RF10
RFEM
von Mises

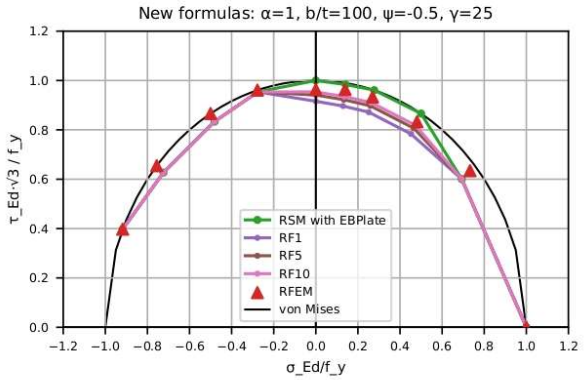
New formulas: α=1, b/t=100, ψ=-0.5, γ=25
τ_Ed·√3 / f_y
σ_Ed/f_y
RSM with EBPlate
RF1
RF5
RF10
RFEM
von Mises

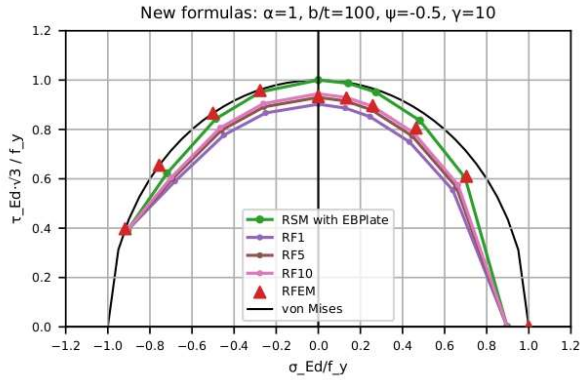
New formulas: α=1, b/t=100, ψ=-0.5, γ=10
τ_Ed·√3 / f_y
σ_Ed/f_y
RSM with EBPlate
RF1
RF5
RF10
RFEM
von Mises

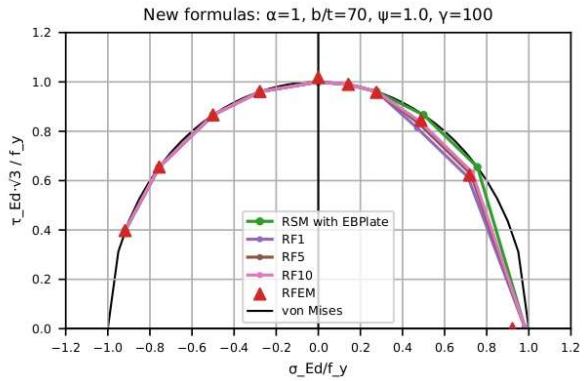
New formulas: α=1, b/t=70, ψ=1.0, γ=100
τ_Ed·√3 / f_y
σ_Ed/f_y
RSM with EBPlate
RF1
RF5
RF10
RFEM
von Mises

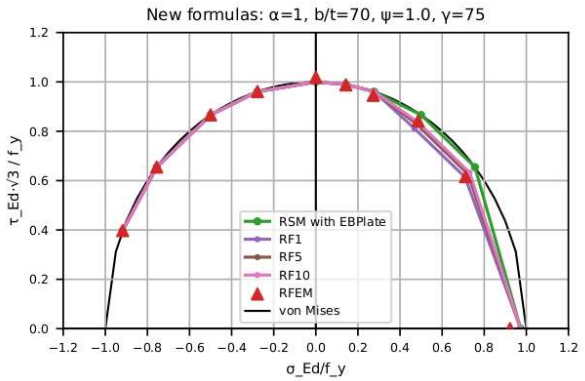
New formulas: α=1, b/t=70, ψ=1.0, γ=75
τ_Ed·√3 / f_y
σ_Ed/f_y
RSM with EBPlate
RF1
RF5
RF10
RFEM
von Mises

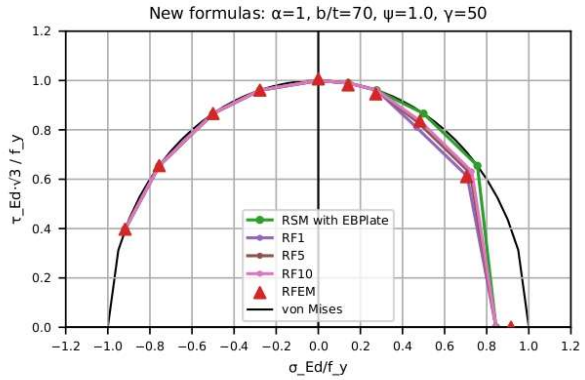
New formulas: α=1, b/t=70, ψ=1.0, γ=50
τ_Ed·√3 / f_y
σ_Ed/f_y
RSM with EBPlate
RF1
RF5
RF10
RFEM
von Mises

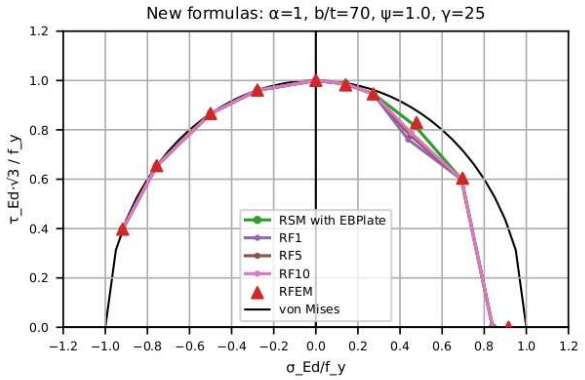
New formulas: α=1, b/t=70, ψ=1.0, γ=25
τ_Ed·√3 / f_y
σ_Ed/f_y
RSM with EBPlate
RF1
RF5
RF10
RFEM
von Mises

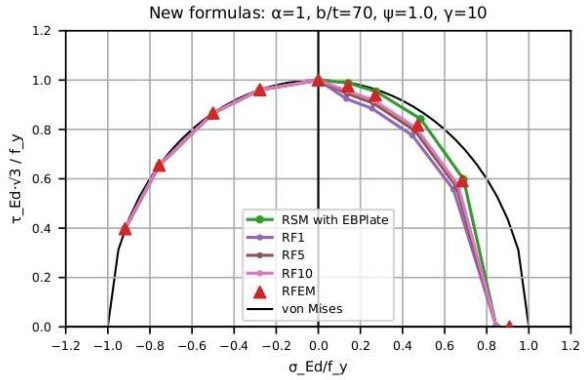
New formulas: α=1, b/t=70, ψ=1.0, γ=10
τ_Ed·√3 / f_y
σ_Ed/f_y
RSM with EBPlate
RF1
RF5
RF10
RFEM
von Mises

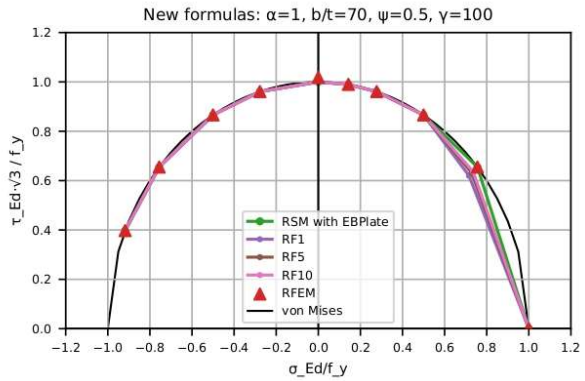
New formulas: α=1, b/t=70, ψ=0.5, γ=100
τ_Ed·√3 / f_y
σ_Ed/f_y
RSM with EBPlate
RF1
RF5
RF10
RFEM
von Mises

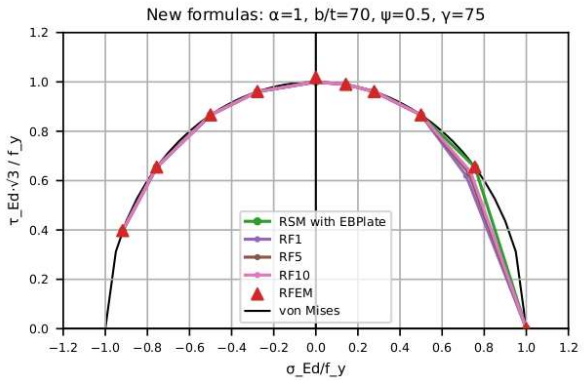
New formulas: α=1, b/t=70, ψ=0.5, γ=75
τ_Ed·√3 / f_y
σ_Ed/f_y
RSM with EBPlate
RF1
RF5
RF10
RFEM
von Mises

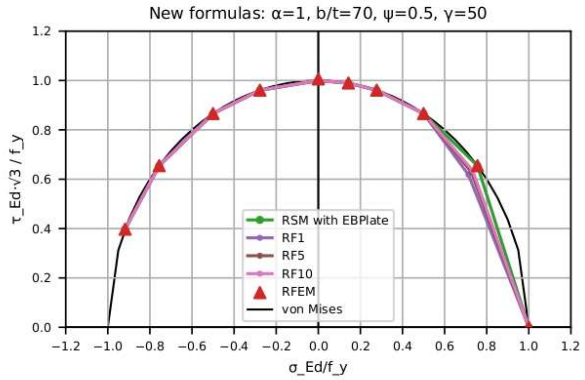
New formulas: α=1, b/t=70, ψ=0.5, γ=50
τ_Ed·√3 / f_y
σ_Ed/f_y
RSM with EBPlate
RF1
RF5
RF10
RFEM
von Mises

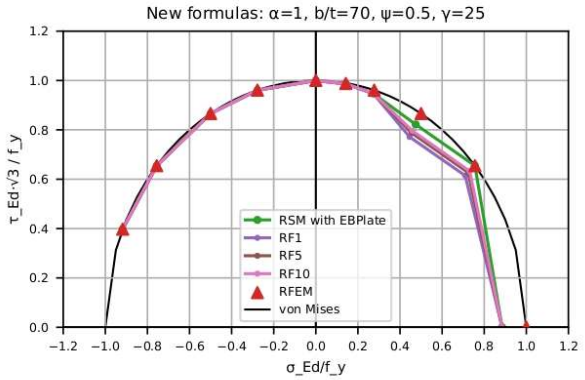
New formulas: α=1, b/t=70, ψ=0.5, γ=25
τ_Ed·√3 / f_y
σ_Ed/f_y
RSM with EBPlate
RF1
RF5
RF10
RFEM
von Mises

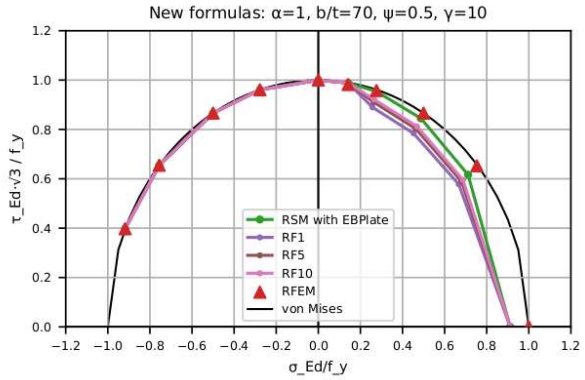
New formulas: α=1, b/t=70, ψ=0.5, γ=10
τ_Ed·√3 / f_y
σ_Ed/f_y
RSM with EBPlate
RF1
RF5
RF10
RFEM
von Mises

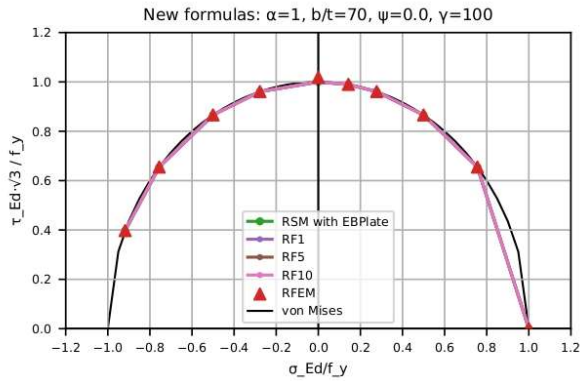
New formulas: α=1, b/t=70, ψ=0.0, γ=100
τ_Ed·√3 / f_y
σ_Ed/f_y
RSM with EBPlate
RF1
RF5
RF10
RFEM
von Mises

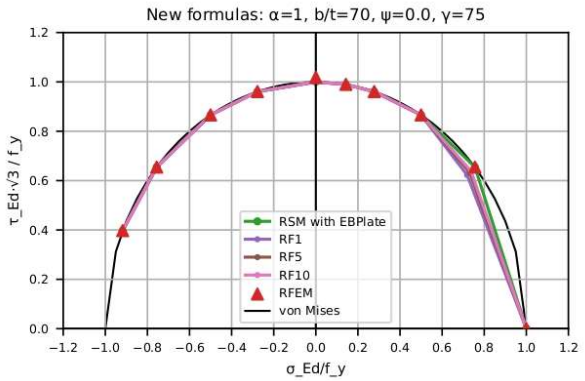
New formulas: α=1, b/t=70, ψ=0.0, γ=75
τ_Ed·√3 / f_y
σ_Ed/f_y
RSM with EBPlate
RF1
RF5
RF10
RFEM
von Mises

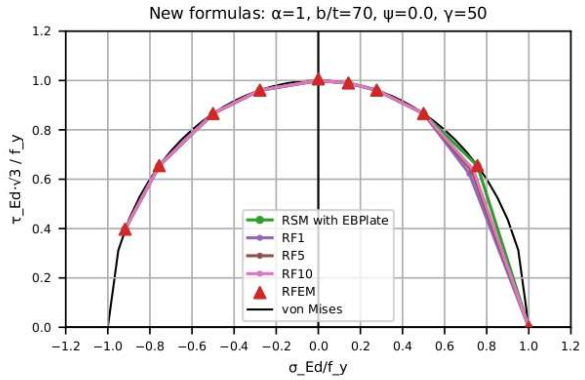
New formulas: α=1, b/t=70, ψ=0.0, γ=50
τ_Ed·√3 / f_y
σ_Ed/f_y
RSM with EBPlate
RF1
RF5
RF10
RFEM
von Mises

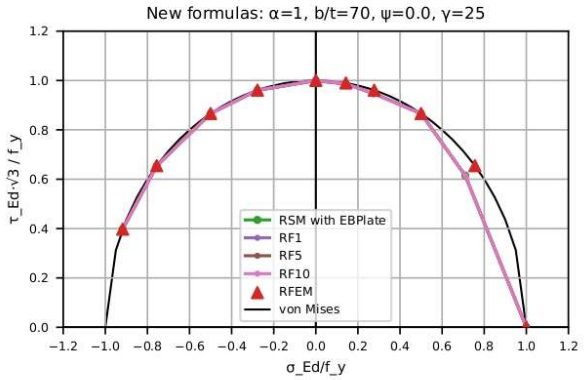
New formulas: α=1, b/t=70, ψ=0.0, γ=25
τ_Ed·√3 / f_y
σ_Ed/f_y
RSM with EBPlate
RF1
RF5
RF10
RFEM
von Mises

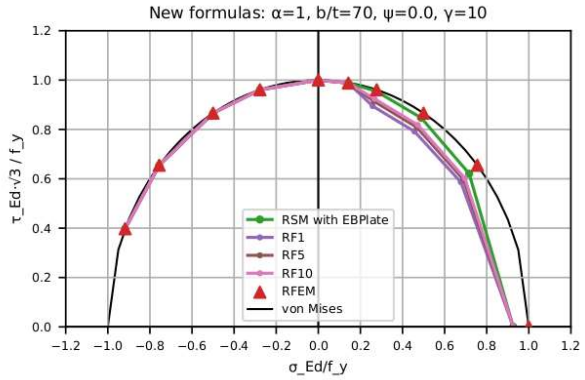
New formulas: α=1, b/t=70, ψ=0.0, γ=10
τ_Ed·√3 / f_y
σ_Ed/f_y
RSM with EBPlate
RF1
RF5
RF10
RFEM
von Mises

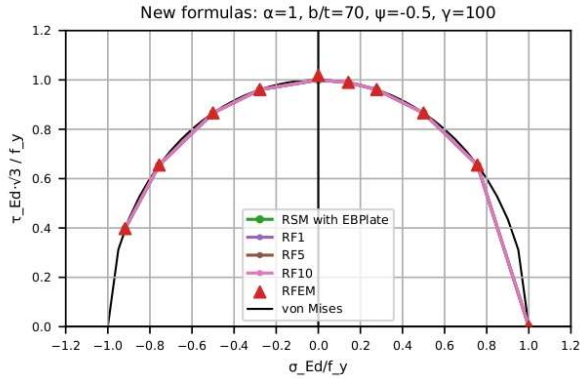
New formulas: α=1, b/t=70, ψ=-0.5, γ=100
τ_Ed·√3 / f_y
σ_Ed/f_y
RSM with EBPlate
RF1
RF5
RF10
RFEM
von Mises

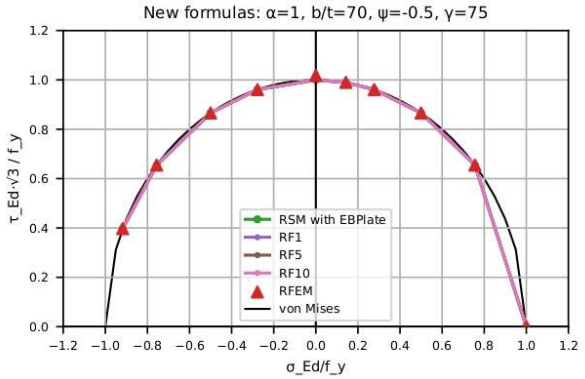
New formulas: α=1, b/t=70, ψ=-0.5, γ=75
τ_Ed·√3 / f_y
σ_Ed/f_y
RSM with EBPlate
RF1
RF5
RF10
RFEM
von Mises

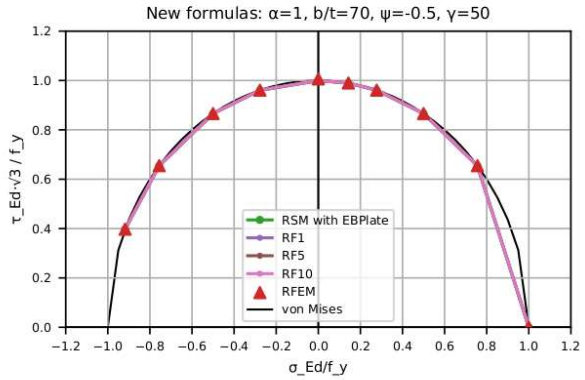
New formulas: α=1, b/t=70, ψ=-0.5, γ=50
τ_Ed·√3 / f_y
σ_Ed/f_y
RSM with EBPlate
RF1
RF5
RF10
RFEM
von Mises

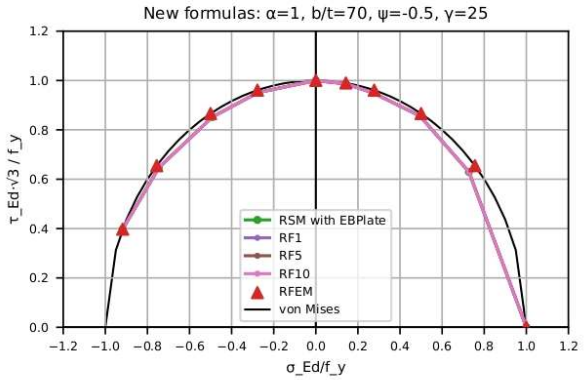
New formulas: α=1, b/t=70, ψ=-0.5, γ=25
τ_Ed·√3 / f_y
σ_Ed/f_y
RSM with EBPlate
RF1
RF5
RF10
RFEM
von Mises

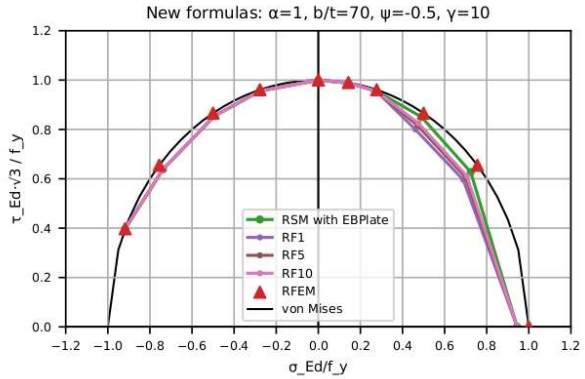
New formulas: α=1, b/t=70, ψ=-0.5, γ=10
τ_Ed·√3 / f_y
σ_Ed/f_y
RSM with EBPlate
RF1
RF5
RF10
RFEM
von Mises

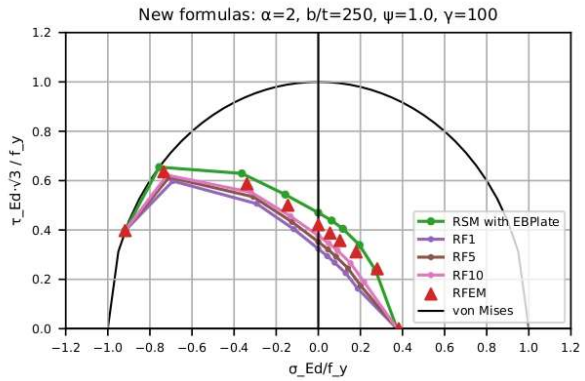
New formulas: α=2, b/t=250, ψ=1.0, γ=100
τ_Ed·√3 / f_y
σ_Ed/f_y
RSM with EBPlate
RF1
RF5
RF10
RFEM
von Mises

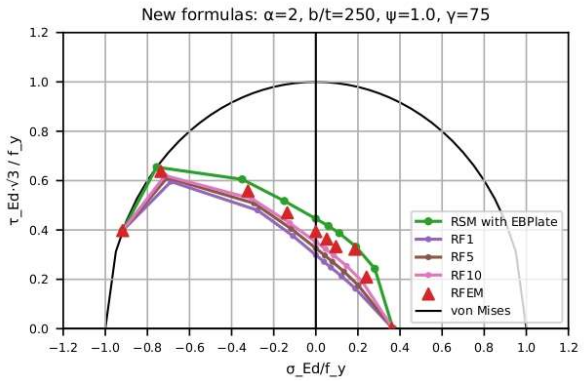
New formulas: α=2, b/t=250, ψ=1.0, γ=75
τ_Ed·√3 / f_y
σ_Ed/f_y
RSM with EBPlate
RF1
RF5
RF10
RFEM
von Mises

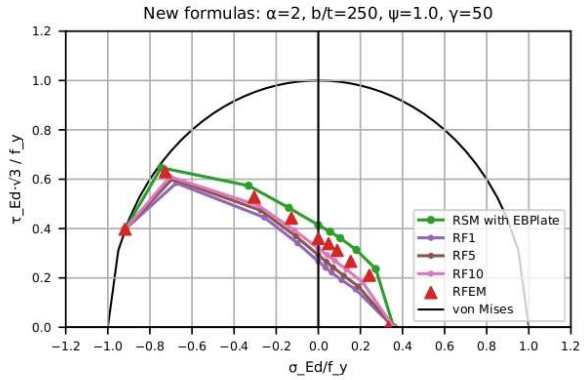
New formulas: α=2, b/t=250, ψ=1.0, γ=50
τ_Ed·√3 / f_y
σ_Ed/f_y
RSM with EBPlate
RF1
RF5
RF10
RFEM
von Mises

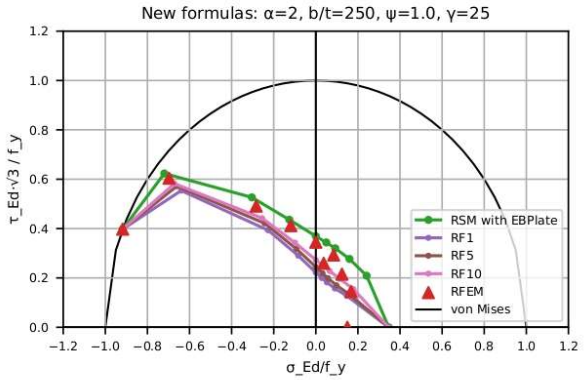
New formulas: α=2, b/t=250, ψ=1.0, γ=25
τ_Ed·√3 / f_y
σ_Ed/f_y
RSM with EBPlate
RF1
RF5
RF10
RFEM
von Mises

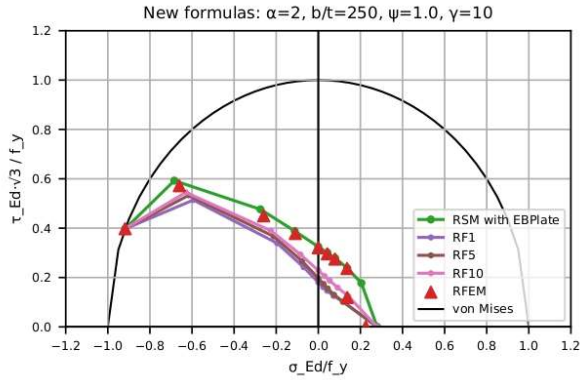
New formulas: α=2, b/t=250, ψ=1.0, γ=10
τ_Ed·√3 / f_y
σ_Ed/f_y
RSM with EBPlate
RF1
RF5
RF10
RFEM
von Mises

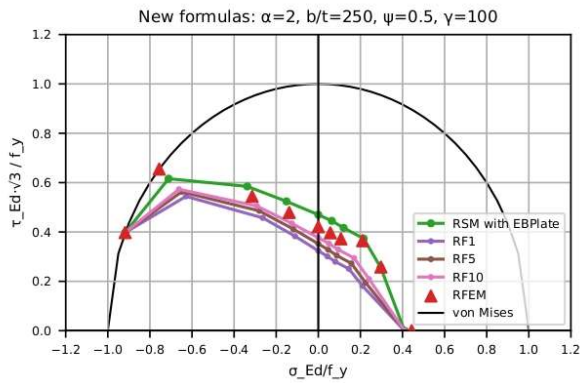
New formulas: α=2, b/t=250, ψ=0.5, γ=100
τ_Ed·√3 / f_y
σ_Ed/f_y
RSM with EBPlate
RF1
RF5
RF10
RFEM
von Mises

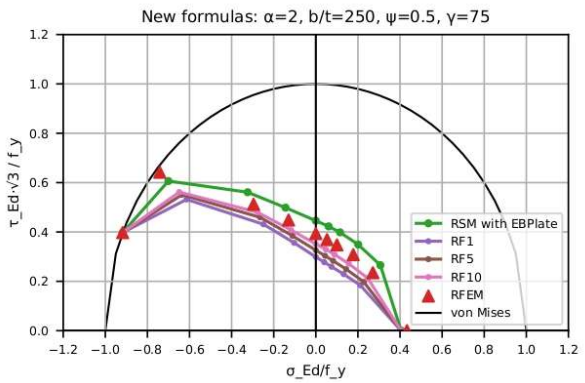
New formulas: α=2, b/t=250, ψ=0.5, γ=75
τ_Ed·√3 / f_y
σ_Ed/f_y
RSM with EBPlate
RF1
RF5
RF10
RFEM
von Mises

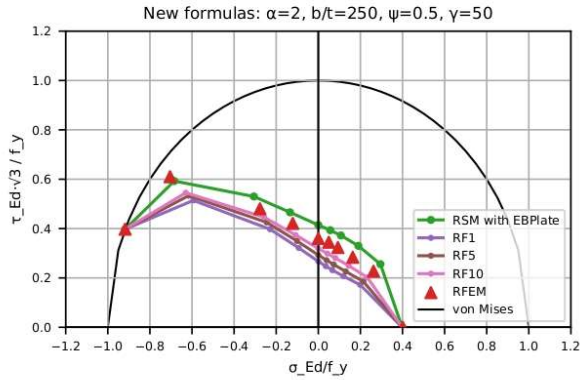
New formulas: α=2, b/t=250, ψ=0.5, γ=50
τ_Ed·√3 / f_y
σ_Ed/f_y
RSM with EBPlate
RF1
RF5
RF10
RFEM
von Mises

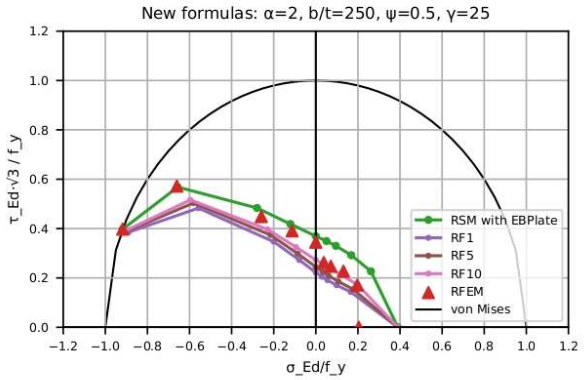
New formulas: α=2, b/t=250, ψ=0.5, γ=25
τ_Ed·√3 / f_y
σ_Ed/f_y
RSM with EBPlate
RF1
RF5
RF10
RFEM
von Mises

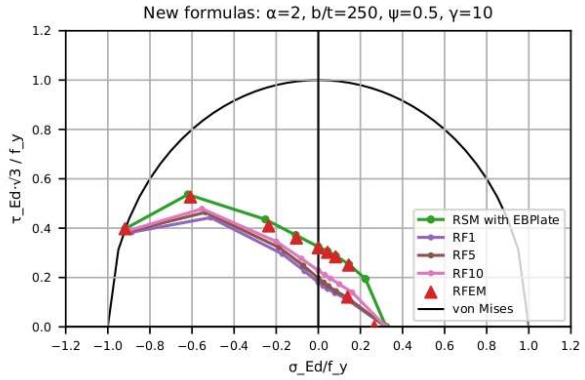
New formulas: α=2, b/t=250, ψ=0.5, γ=10
τ_Ed·√3 / f_y
σ_Ed/f_y
RSM with EBPlate
RF1
RF5
RF10
RFEM
von Mises

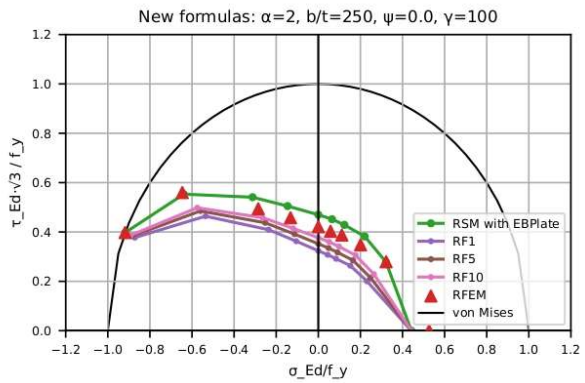
New formulas: α=2, b/t=250, ψ=0.0, γ=100
τ_Ed·√3 / f_y
σ_Ed/f_y
RSM with EBPlate
RF1
RF5
RF10
RFEM
von Mises

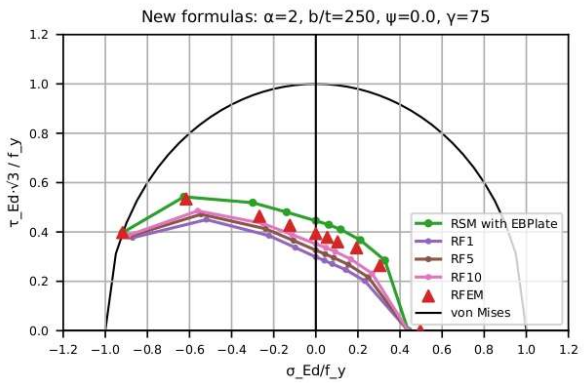
New formulas: α=2, b/t=250, ψ=0.0, γ=75
τ_Ed·√3 / f_y
σ_Ed/f_y
RSM with EBPlate
RF1
RF5
RF10
RFEM
von Mises

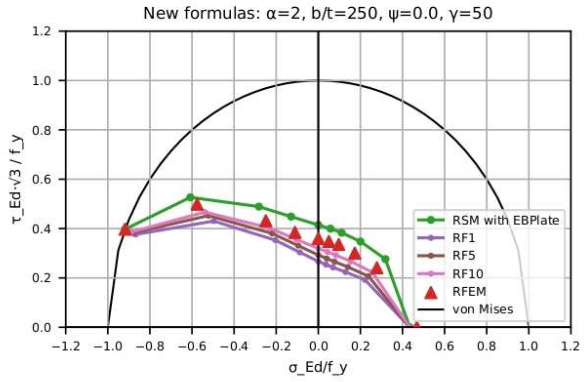
New formulas: α=2, b/t=250, ψ=0.0, γ=50
τ_Ed·√3 / f_y
σ_Ed/f_y
RSM with EBPlate
RF1
RF5
RF10
RFEM
von Mises

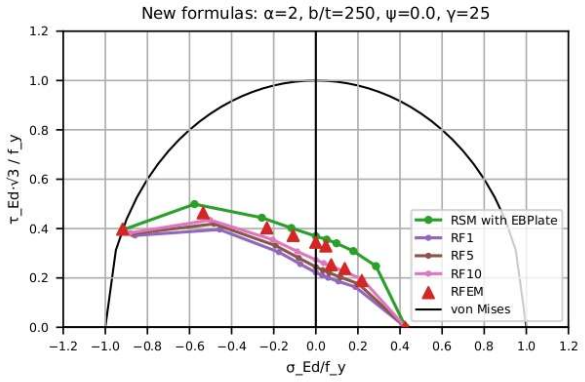
New formulas: α=2, b/t=250, ψ=0.0, γ=25
τ_Ed·√3 / f_y
σ_Ed/f_y
RSM with EBPlate
RF1
RF5
RF10
RFEM
von Mises

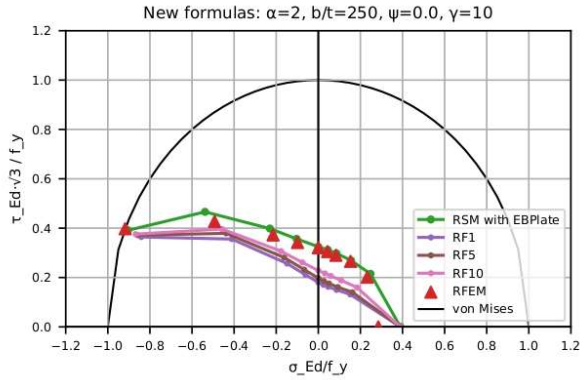
New formulas: α=2, b/t=250, ψ=0.0, γ=10
τ_Ed·√3 / f_y
σ_Ed/f_y
RSM with EBPlate
RF1
RF5
RF10
RFEM
von Mises

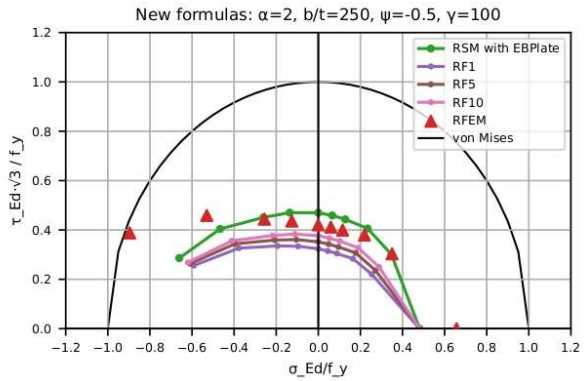
New formulas: α=2, b/t=250, ψ=-0.5, γ=100
RSM with EBPlate
RF1
RF5
RF10
RFEM
von Mises
τ_Ed·√3 / f_y
σ_Ed/f_y

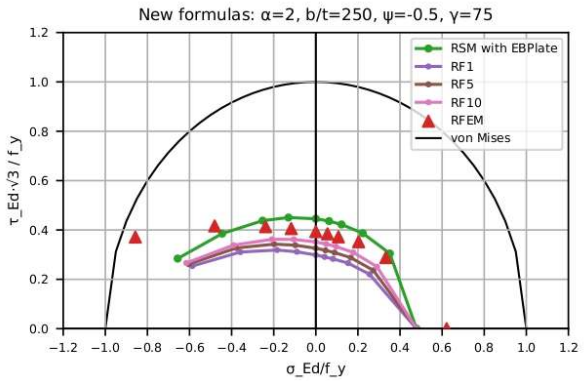
New formulas: α=2, b/t=250, ψ=-0.5, γ=75
RSM with EBPlate
RF1
RF5
RF10
RFEM
von Mises
τ_Ed·√3 / f_y
σ_Ed/f_y

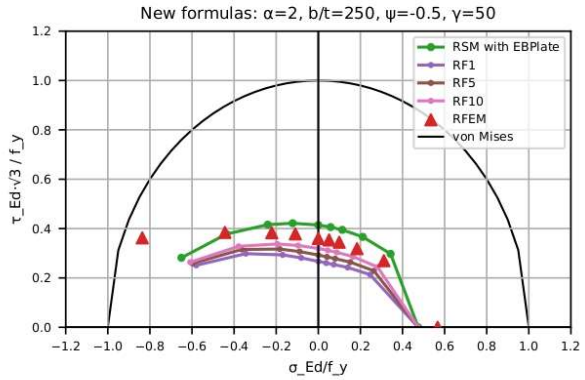
New formulas: α=2, b/t=250, ψ=-0.5, γ=50
RSM with EBPlate
RF1
RF5
RF10
RFEM
von Mises
τ_Ed·√3 / f_y
σ_Ed/f_y

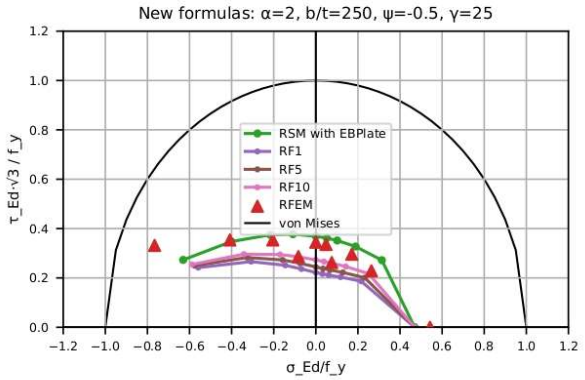
New formulas: α=2, b/t=250, ψ=-0.5, γ=25
RSM with EBPlate
RF1
RF5
RF10
RFEM
von Mises
τ_Ed·√3 / f_y
σ_Ed/f_y

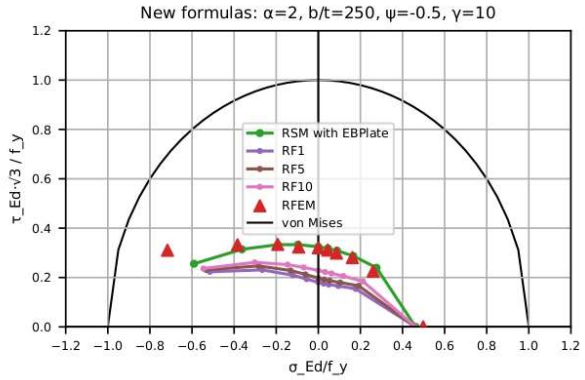
New formulas: α=2, b/t=250, ψ=-0.5, γ=10
RSM with EBPlate
RF1
RF5
RF10
RFEM
von Mises
τ_Ed·√3 / f_y
σ_Ed/f_y

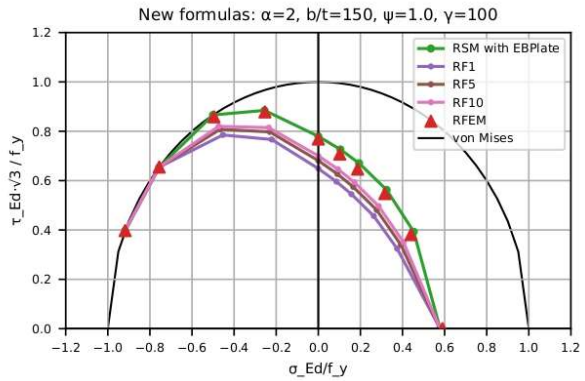
New formulas: α=2, b/t=150, ψ=1.0, γ=100
RSM with EBPlate
RF1
RF5
RF10
RFEM
von Mises
τ_Ed·√3 / f_y
σ_Ed/f_y

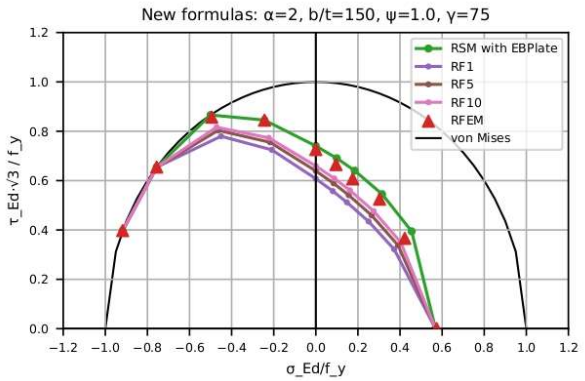
New formulas: α=2, b/t=150, ψ=1.0, γ=75
RSM with EBPlate
RF1
RF5
RF10
RFEM
von Mises
τ_Ed·√3 / f_y
σ_Ed/f_y

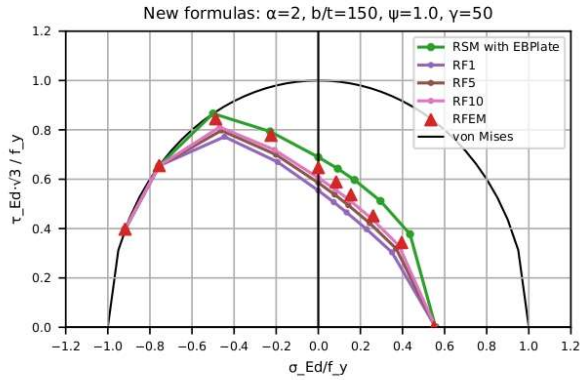
New formulas: α=2, b/t=150, ψ=1.0, γ=50
RSM with EBPlate
RF1
RF5
RF10
RFEM
von Mises
τ_Ed·√3 / f_y
σ_Ed/f_y

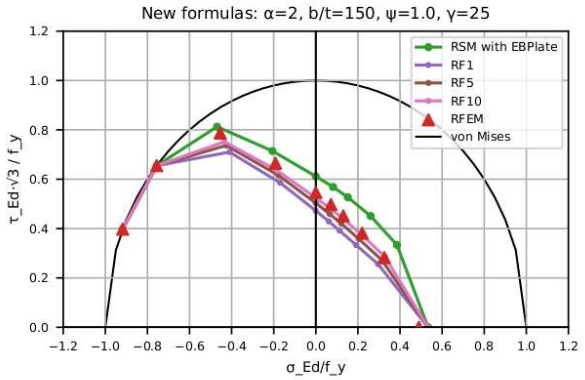
New formulas: α=2, b/t=150, ψ=1.0, γ=25
RSM with EBPlate
RF1
RF5
RF10
RFEM
von Mises
τ_Ed·√3 / f_y
σ_Ed/f_y

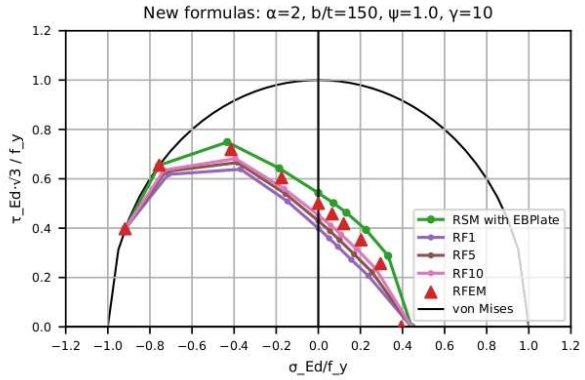
New formulas: α=2, b/t=150, ψ=1.0, γ=10
RSM with EBPlate
RF1
RF5
RF10
RFEM
von Mises
τ_Ed·√3 / f_y
σ_Ed/f_y

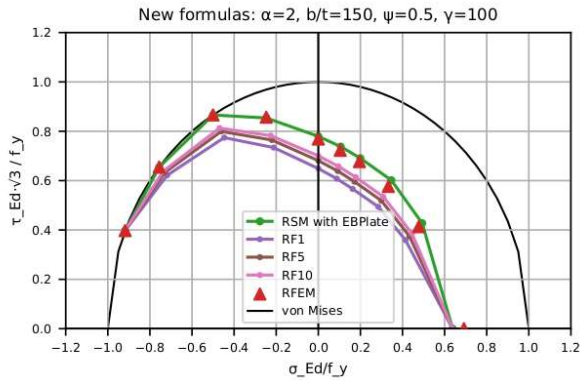
New formulas: α=2, b/t=150, ψ=0.5, γ=100
τ_Ed·√3 / f_y
σ_Ed/f_y
RSM with EBPlate
RF1
RF5
RF10
RFEM
von Mises

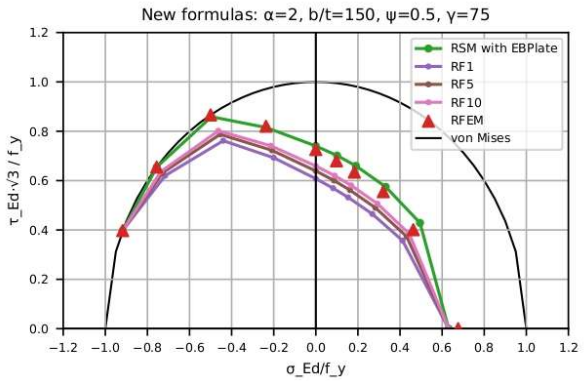
New formulas: α=2, b/t=150, ψ=0.5, γ=75
τ_Ed·√3 / f_y
σ_Ed/f_y
RSM with EBPlate
RF1
RF5
RF10
RFEM
von Mises

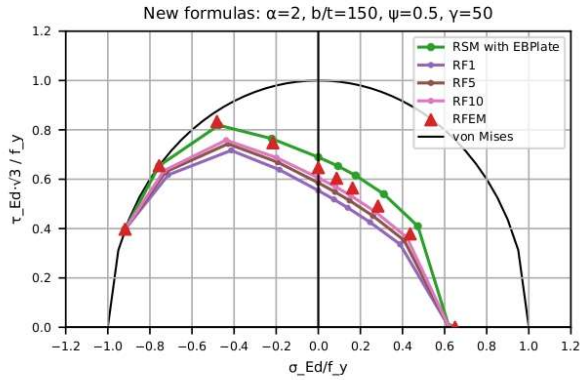
New formulas: α=2, b/t=150, ψ=0.5, γ=50
τ_Ed·√3 / f_y
σ_Ed/f_y
RSM with EBPlate
RF1
RF5
RF10
RFEM
von Mises

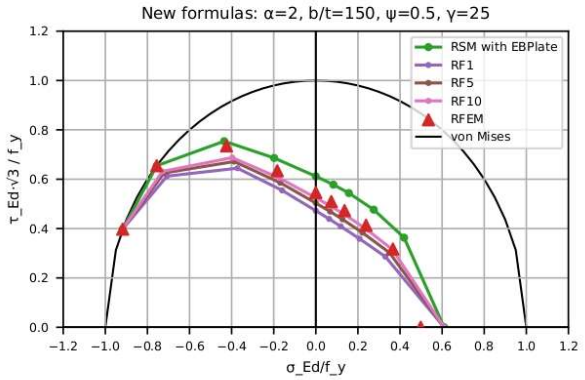
New formulas: α=2, b/t=150, ψ=0.5, γ=25
τ_Ed·√3 / f_y
σ_Ed/f_y
RSM with EBPlate
RF1
RF5
RF10
RFEM
von Mises

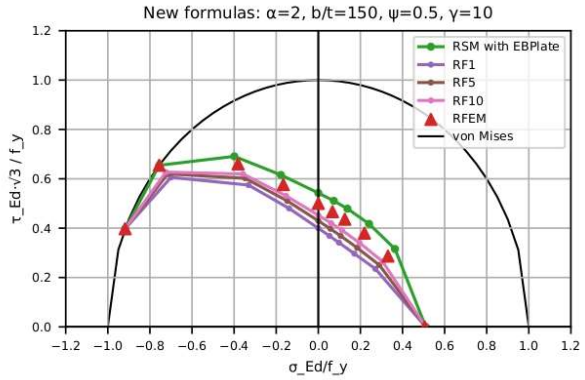
New formulas: α=2, b/t=150, ψ=0.5, γ=10
τ_Ed·√3 / f_y
σ_Ed/f_y
RSM with EBPlate
RF1
RF5
RF10
RFEM
von Mises

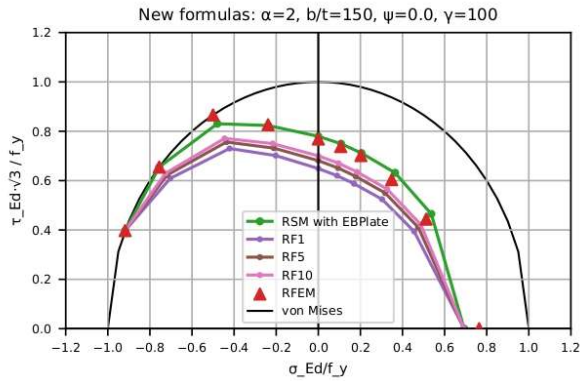
New formulas: α=2, b/t=150, ψ=0.0, γ=100
τ_Ed·√3 / f_y
σ_Ed/f_y
RSM with EBPlate
RF1
RF5
RF10
RFEM
von Mises

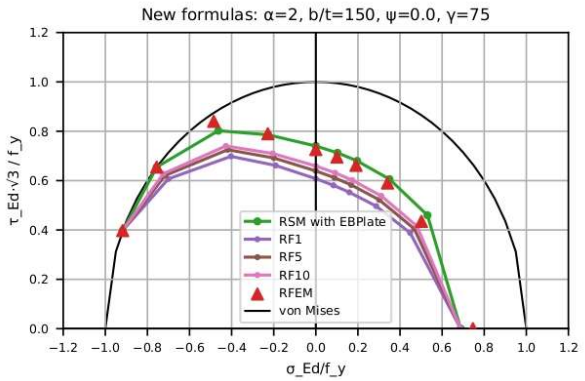
New formulas: α=2, b/t=150, ψ=0.0, γ=75
τ_Ed·√3 / f_y
σ_Ed/f_y
RSM with EBPlate
RF1
RF5
RF10
RFEM
von Mises

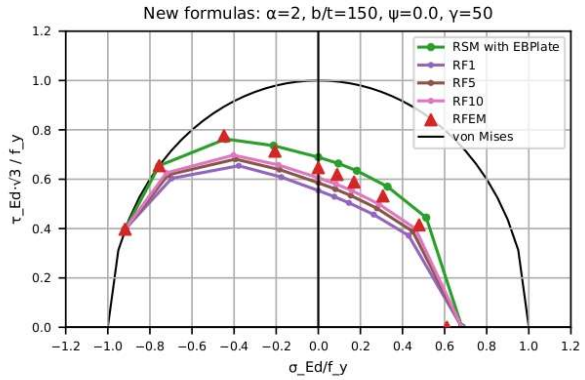
New formulas: α=2, b/t=150, ψ=0.0, γ=50
τ_Ed·√3 / f_y
σ_Ed/f_y
RSM with EBPlate
RF1
RF5
RF10
RFEM
von Mises

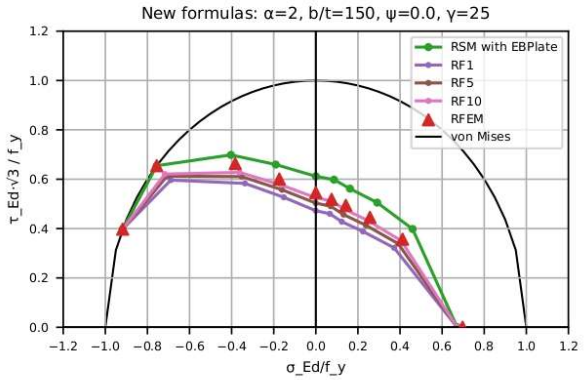
New formulas: α=2, b/t=150, ψ=0.0, γ=25
τ_Ed·√3 / f_y
σ_Ed/f_y
RSM with EBPlate
RF1
RF5
RF10
RFEM
von Mises

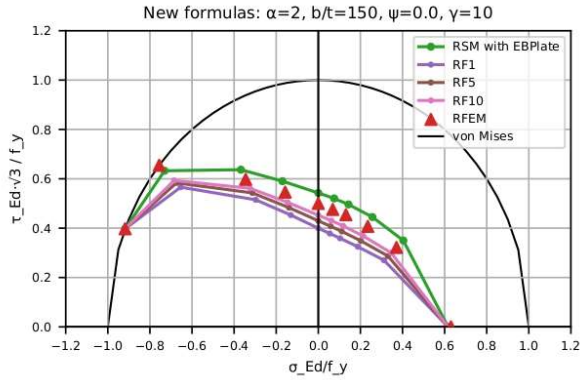
New formulas: α=2, b/t=150, ψ=0.0, γ=10
τ_Ed·√3 / f_y
σ_Ed/f_y
RSM with EBPlate
RF1
RF5
RF10
RFEM
von Mises

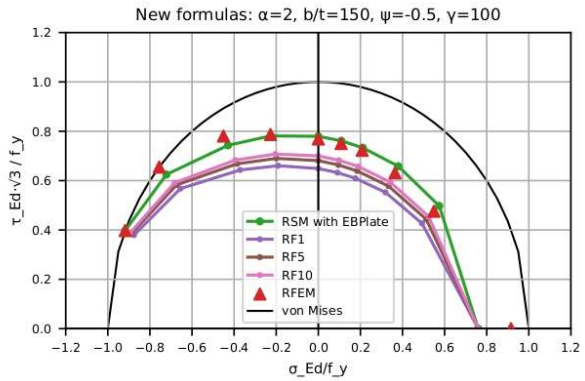
New formulas: α=2, b/t=150, ψ=-0.5, γ=100
τ_Ed·√3 / f_y
σ_Ed/f_y
RSM with EBPlate
RF1
RF5
RF10
RFEM
von Mises

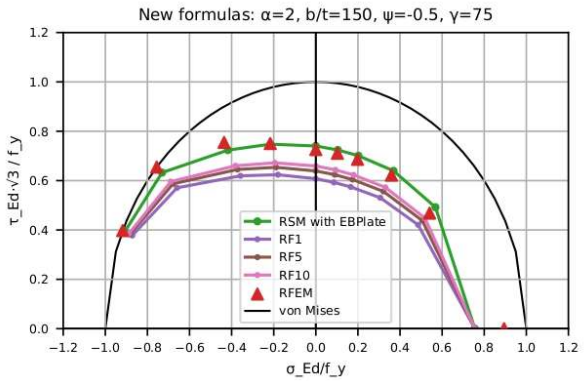
New formulas: α=2, b/t=150, ψ=-0.5, γ=75
τ_Ed·√3 / f_y
σ_Ed/f_y
RSM with EBPlate
RF1
RF5
RF10
RFEM
von Mises

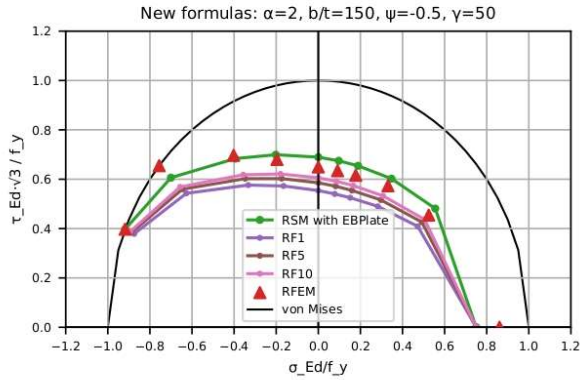
New formulas: α=2, b/t=150, ψ=-0.5, γ=50
τ_Ed·√3 / f_y
σ_Ed/f_y
RSM with EBPlate
RF1
RF5
RF10
RFEM
von Mises

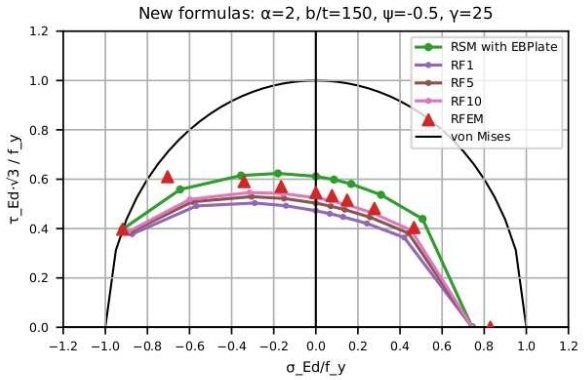
New formulas: α=2, b/t=150, ψ=-0.5, γ=25
τ_Ed·√3 / f_y
σ_Ed/f_y
RSM with EBPlate
RF1
RF5
RF10
RFEM
von Mises

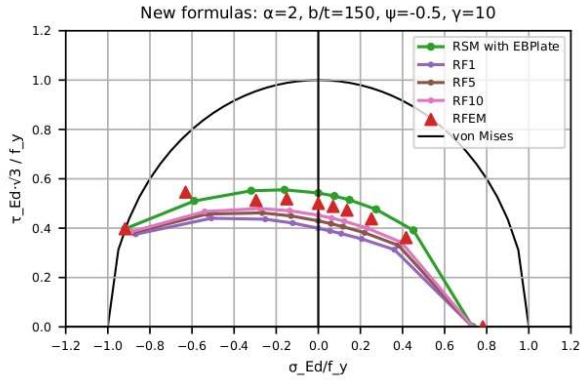
New formulas: α=2, b/t=150, ψ=-0.5, γ=10
τ_Ed·√3 / f_y
σ_Ed/f_y
RSM with EBPlate
RF1
RF5
RF10
RFEM
von Mises

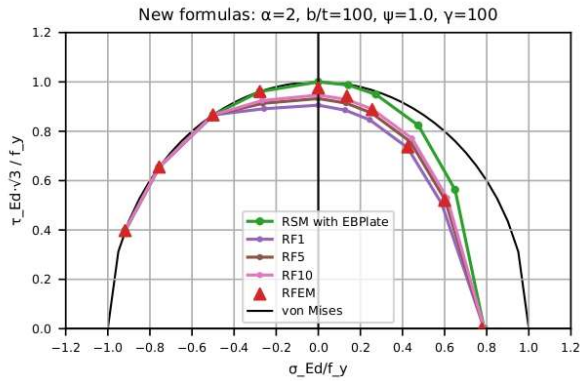
New formulas: α=2, b/t=100, ψ=1.0, γ=100
τ_Ed·√3 / f_y
σ_Ed/f_y
RSM with EBPlate
RF1
RF5
RF10
RFEM
von Mises

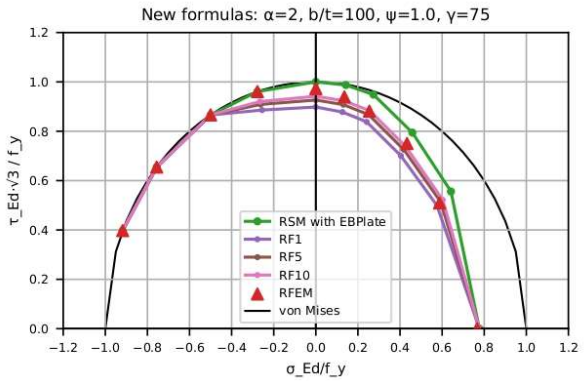
New formulas: α=2, b/t=100, ψ=1.0, γ=75
τ_Ed·√3 / f_y
σ_Ed/f_y
RSM with EBPlate
RF1
RF5
RF10
RFEM
von Mises

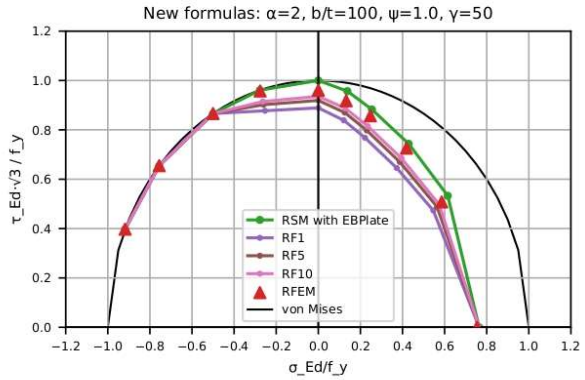
New formulas: α=2, b/t=100, ψ=1.0, γ=50
τ_Ed·√3 / f_y
σ_Ed/f_y
RSM with EBPlate
RF1
RF5
RF10
RFEM
von Mises

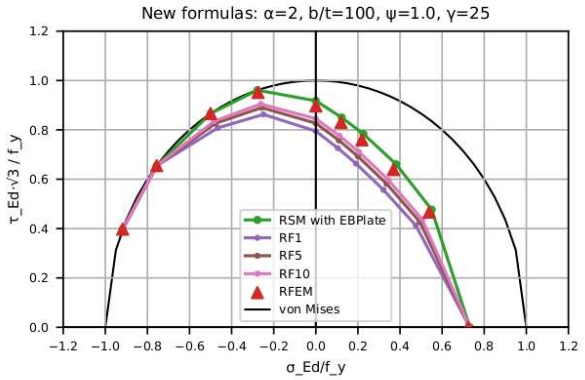
New formulas: α=2, b/t=100, ψ=1.0, γ=25
τ_Ed·√3 / f_y
σ_Ed/f_y
RSM with EBPlate
RF1
RF5
RF10
RFEM
von Mises

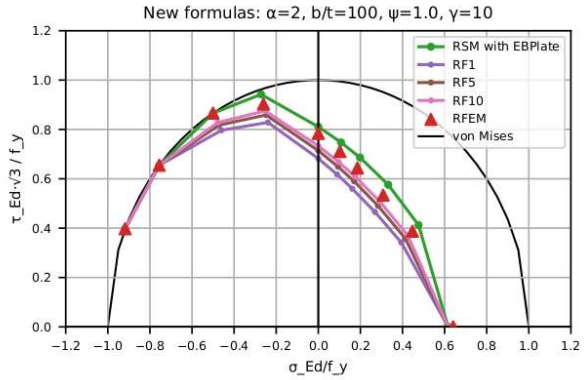
New formulas: α=2, b/t=100, ψ=1.0, γ=10
τ_Ed·√3 / f_y
σ_Ed/f_y
RSM with EBPlate
RF1
RF5
RF10
RFEM
von Mises

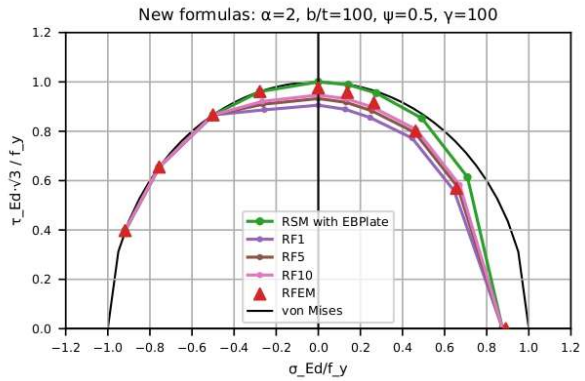
New formulas: α=2, b/t=100, ψ=0.5, γ=100
τ_Ed·√3 / f_y
σ_Ed/f_y
RSM with EBPlate
RF1
RF5
RF10
RFEM
von Mises

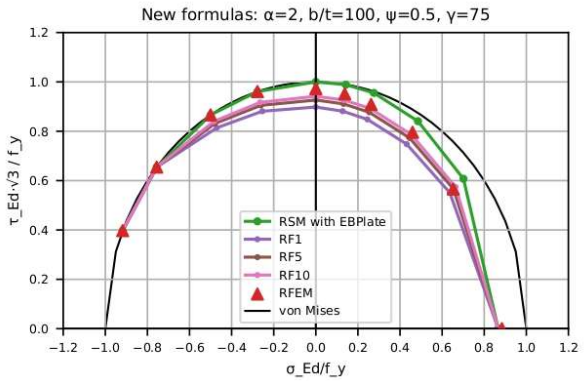
New formulas: α=2, b/t=100, ψ=0.5, γ=75
τ_Ed·√3 / f_y
σ_Ed/f_y
RSM with EBPlate
RF1
RF5
RF10
RFEM
von Mises

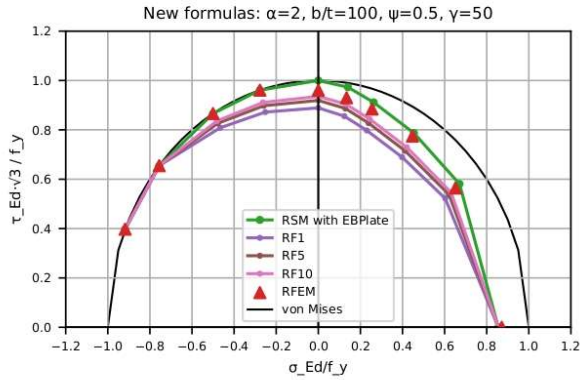
New formulas: α=2, b/t=100, ψ=0.5, γ=50
τ_Ed·√3 / f_y
σ_Ed/f_y
RSM with EBPlate
RF1
RF5
RF10
RFEM
von Mises

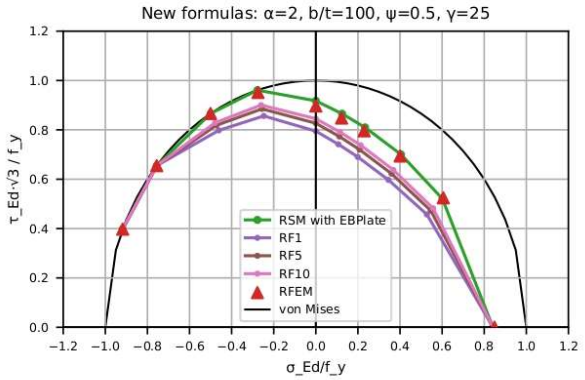
New formulas: α=2, b/t=100, ψ=0.5, γ=25
τ_Ed·√3 / f_y
σ_Ed/f_y
RSM with EBPlate
RF1
RF5
RF10
RFEM
von Mises

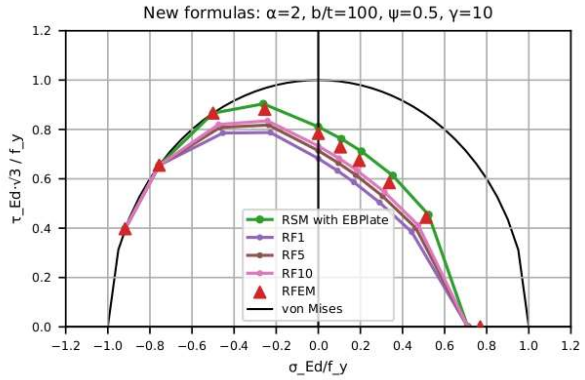
New formulas: α=2, b/t=100, ψ=0.5, γ=10
τ_Ed·√3 / f_y
σ_Ed/f_y
RSM with EBPlate
RF1
RF5
RF10
RFEM
von Mises

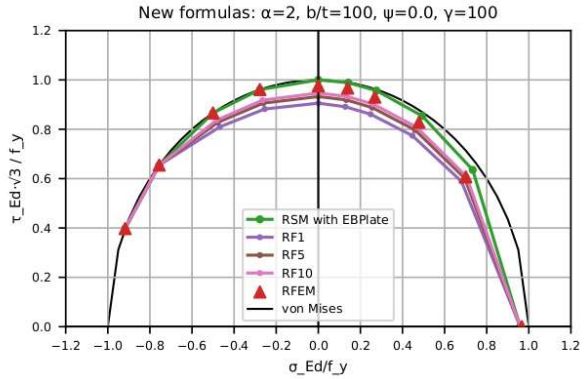
New formulas: α=2, b/t=100, ψ=0.0, γ=100
τ_Ed·√3 / f_y
σ_Ed/f_y
RSM with EBPlate
RF1
RF5
RF10
RFEM
von Mises

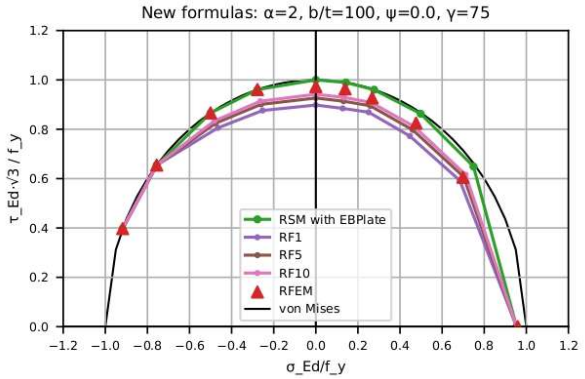
New formulas: α=2, b/t=100, ψ=0.0, γ=75
τ_Ed·√3 / f_y
σ_Ed/f_y
RSM with EBPlate
RF1
RF5
RF10
RFEM
von Mises

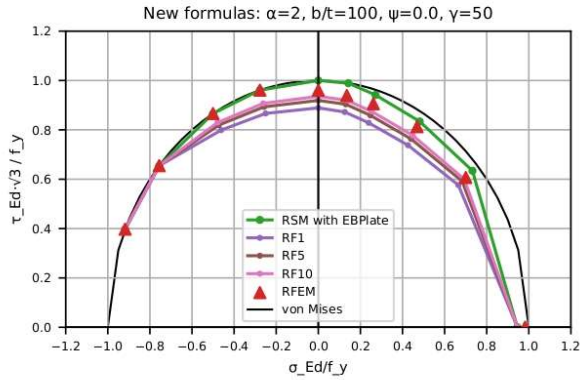
New formulas: α=2, b/t=100, ψ=0.0, γ=50
τ_Ed·√3 / f_y
σ_Ed/f_y
RSM with EBPlate
RF1
RF5
RF10
RFEM
von Mises

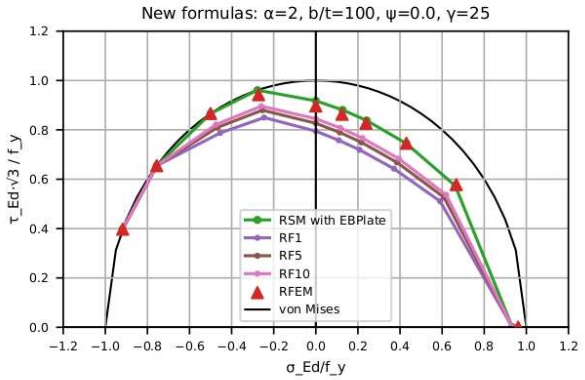
New formulas: α=2, b/t=100, ψ=0.0, γ=25
τ_Ed·√3 / f_y
σ_Ed/f_y
RSM with EBPlate
RF1
RF5
RF10
RFEM
von Mises

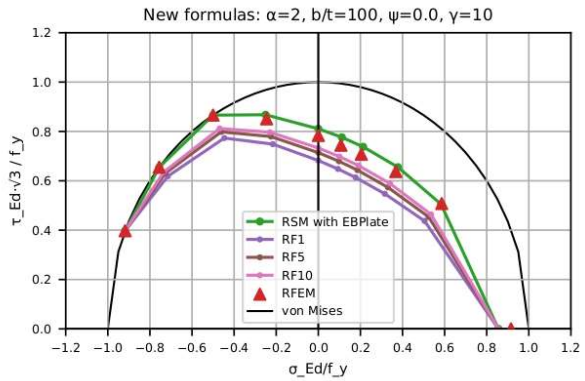
New formulas: α=2, b/t=100, ψ=0.0, γ=10
τ_Ed·√3 / f_y
σ_Ed/f_y
RSM with EBPlate
RF1
RF5
RF10
RFEM
von Mises

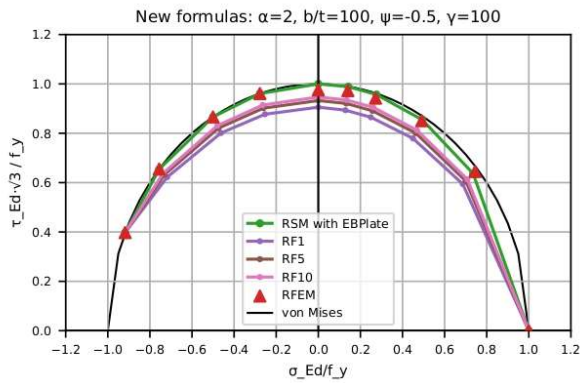
New formulas: α=2, b/t=100, ψ=-0.5, γ=100
τ_Ed·√3 / f_y
σ_Ed/f_y
RSM with EBPlate
RF1
RF5
RF10
RFEM
von Mises

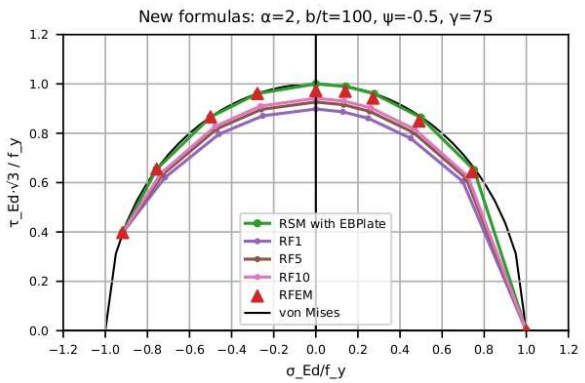
New formulas: α=2, b/t=100, ψ=-0.5, γ=75
τ_Ed·√3 / f_y
σ_Ed/f_y
RSM with EBPlate
RF1
RF5
RF10
RFEM
von Mises

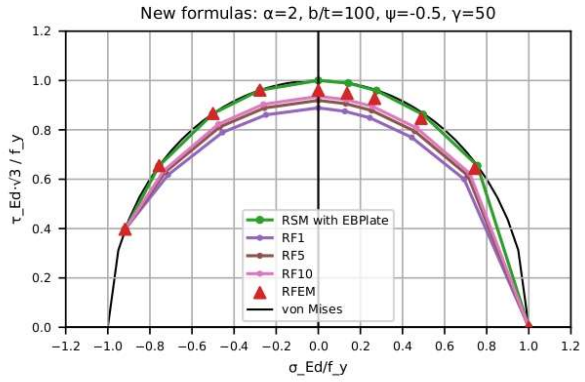
New formulas: α=2, b/t=100, ψ=-0.5, γ=50
τ_Ed·√3 / f_y
σ_Ed/f_y
RSM with EBPlate
RF1
RF5
RF10
RFEM
von Mises

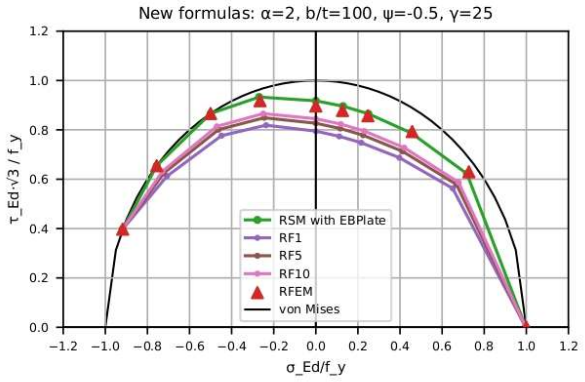
New formulas: α=2, b/t=100, ψ=-0.5, γ=25
τ_Ed·√3 / f_y
σ_Ed/f_y
RSM with EBPlate
RF1
RF5
RF10
RFEM
von Mises

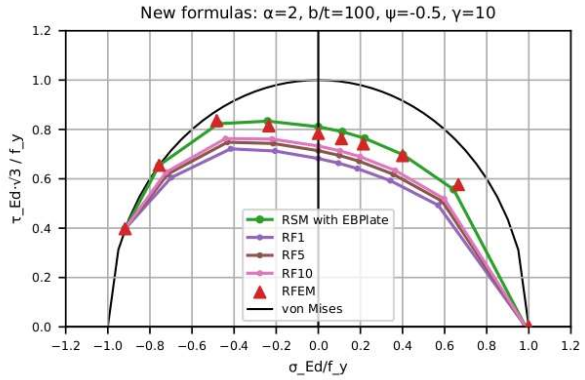
New formulas: α=2, b/t=100, ψ=-0.5, γ=10
τ_Ed·√3 / f_y
σ_Ed/f_y
RSM with EBPlate
RF1
RF5
RF10
RFEM
von Mises

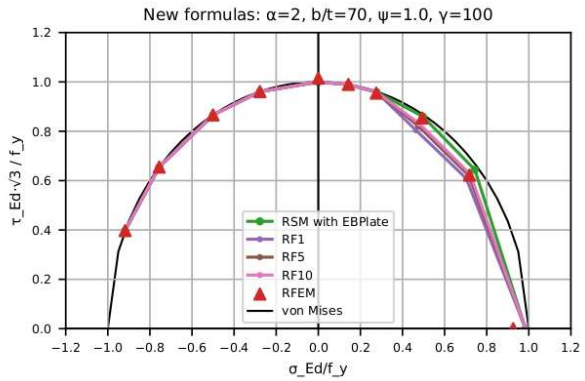
New formulas: α=2, b/t=70, ψ=1.0, γ=100
τ_Ed·√3 / f_y
σ_Ed/f_y
RSM with EBPlate
RF1
RF5
RF10
RFEM
von Mises

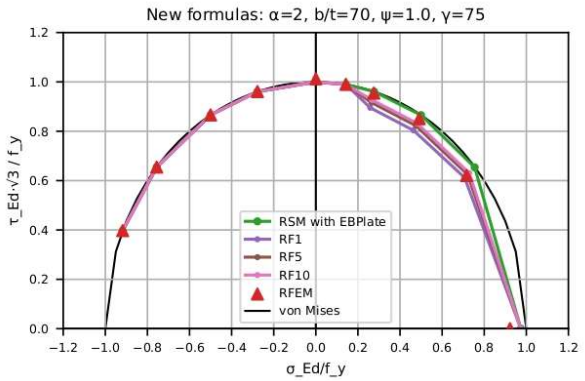
New formulas: α=2, b/t=70, ψ=1.0, γ=75
τ_Ed·√3 / f_y
σ_Ed/f_y
RSM with EBPlate
RF1
RF5
RF10
RFEM
von Mises

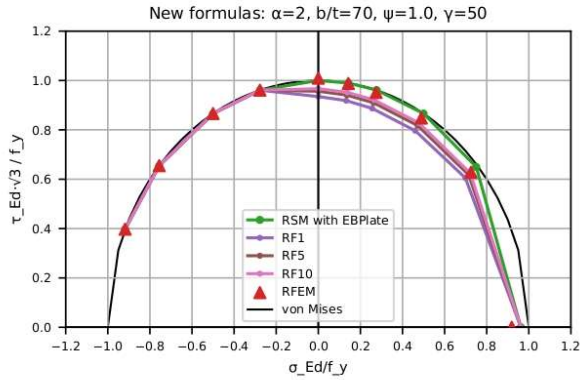
New formulas: α=2, b/t=70, ψ=1.0, γ=50
τ_Ed·√3 / f_y
σ_Ed/f_y
RSM with EBPlate
RF1
RF5
RF10
RFEM
von Mises

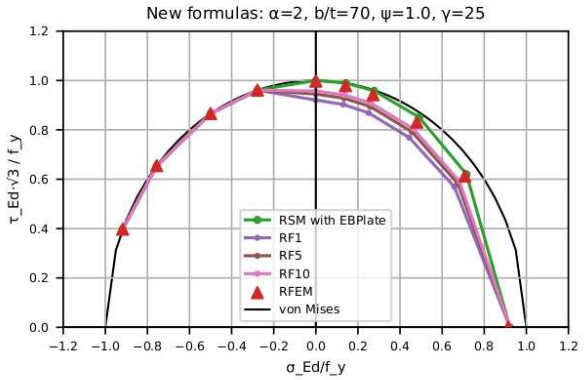
New formulas: α=2, b/t=70, ψ=1.0, γ=25
τ_Ed·√3 / f_y
σ_Ed/f_y
RSM with EBPlate
RF1
RF5
RF10
RFEM
von Mises

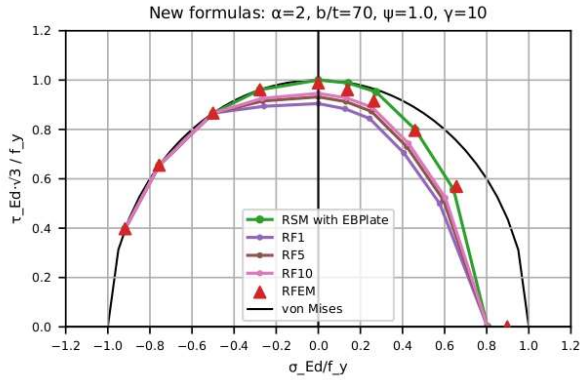
New formulas: α=2, b/t=70, ψ=1.0, γ=10
τ_Ed·√3 / f_y
σ_Ed/f_y
RSM with EBPlate
RF1
RF5
RF10
RFEM
von Mises

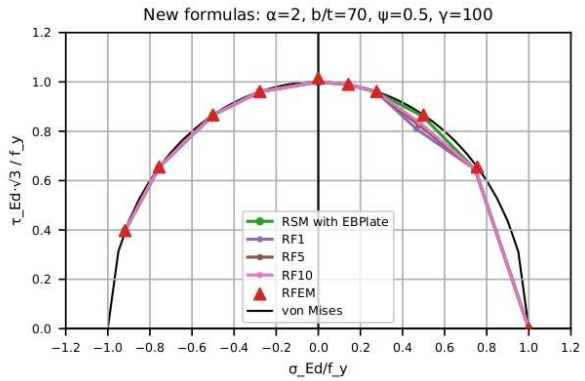
New formulas: α=2, b/t=70, ψ=0.5, γ=100
τ_Ed·√3 / f_y
σ_Ed/f_y
RSM with EBPlate
RF1
RF5
RF10
RFEM
von Mises

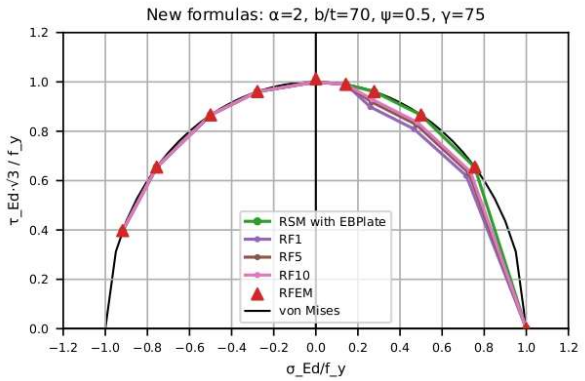
New formulas: α=2, b/t=70, ψ=0.5, γ=75
τ_Ed·√3 / f_y
σ_Ed/f_y
RSM with EBPlate
RF1
RF5
RF10
RFEM
von Mises

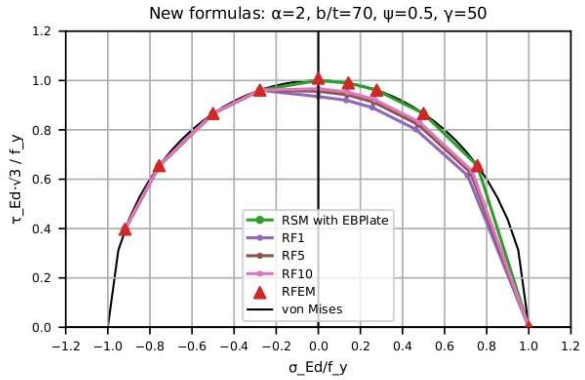
New formulas: α=2, b/t=70, ψ=0.5, γ=50
τ_Ed·√3 / f_y
σ_Ed/f_y
RSM with EBPlate
RF1
RF5
RF10
RFEM
von Mises

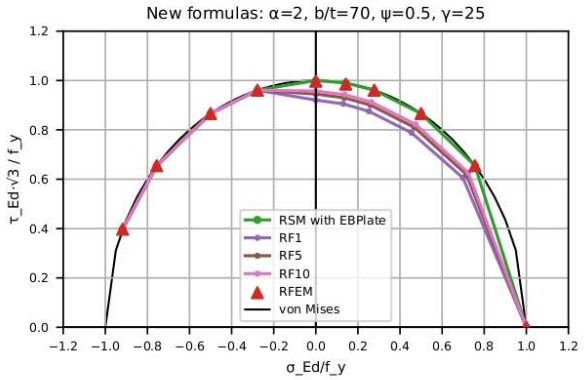
New formulas: α=2, b/t=70, ψ=0.5, γ=25
τ_Ed·√3 / f_y
σ_Ed/f_y
RSM with EBPlate
RF1
RF5
RF10
RFEM
von Mises

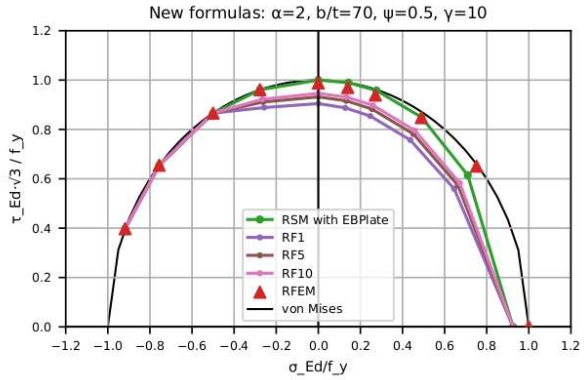
New formulas: α=2, b/t=70, ψ=0.5, γ=10
τ_Ed·√3 / f_y
σ_Ed/f_y
RSM with EBPlate
RF1
RF5
RF10
RFEM
von Mises

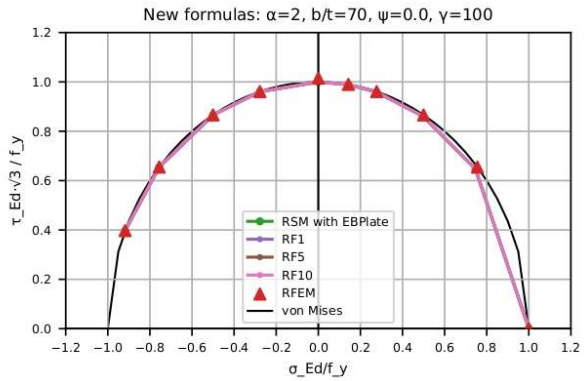
New formulas: α=2, b/t=70, ψ=0.0, γ=100
τ_Ed·√3 / f_y
σ_Ed/f_y
RSM with EBPlate
RF1
RF5
RF10
RFEM
von Mises

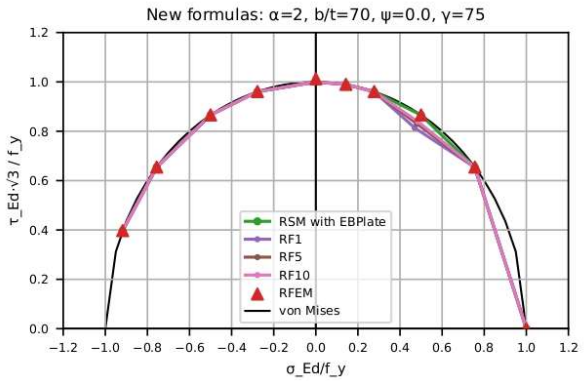
New formulas: α=2, b/t=70, ψ=0.0, γ=75
τ_Ed·√3 / f_y
σ_Ed/f_y
RSM with EBPlate
RF1
RF5
RF10
RFEM
von Mises

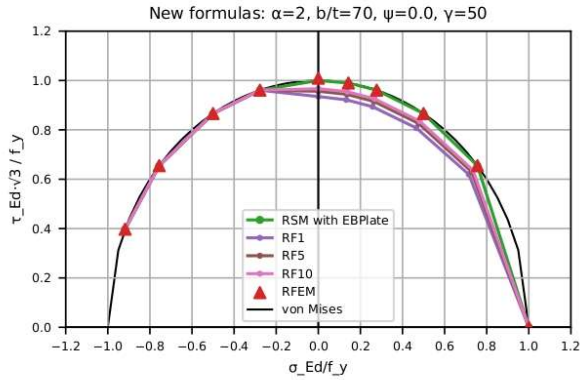
New formulas: α=2, b/t=70, ψ=0.0, γ=50
τ_Ed·√3 / f_y
σ_Ed/f_y
RSM with EBPlate
RF1
RF5
RF10
RFEM
von Mises

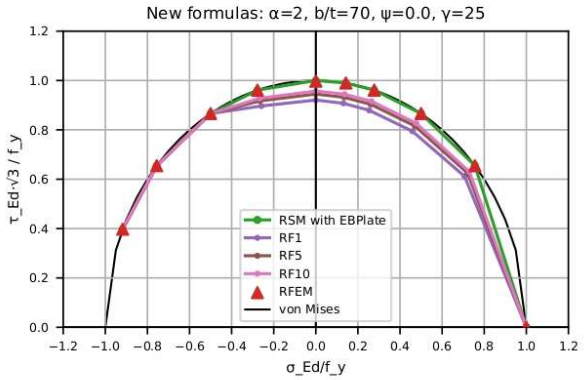
New formulas: α=2, b/t=70, ψ=0.0, γ=25
τ_Ed·√3 / f_y
σ_Ed/f_y
RSM with EBPlate
RF1
RF5
RF10
RFEM
von Mises

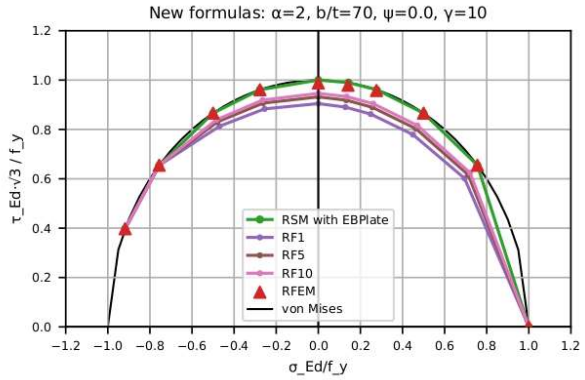
New formulas: α=2, b/t=70, ψ=0.0, γ=10
τ_Ed·√3 / f_y
σ_Ed/f_y
RSM with EBPlate
RF1
RF5
RF10
RFEM
von Mises

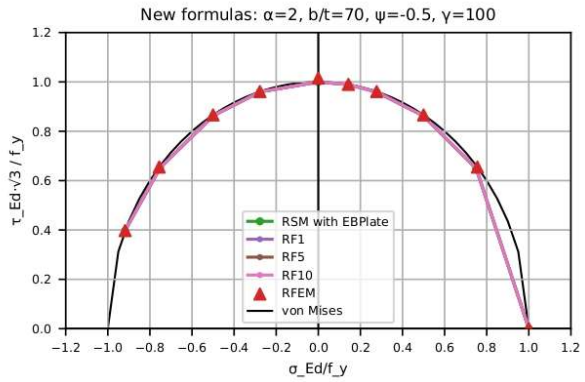
New formulas: α=2, b/t=70, ψ=-0.5, γ=100
τ_Ed·√3 / f_y
σ_Ed/f_y
RSM with EBPlate
RF1
RF5
RF10
RFEM
von Mises

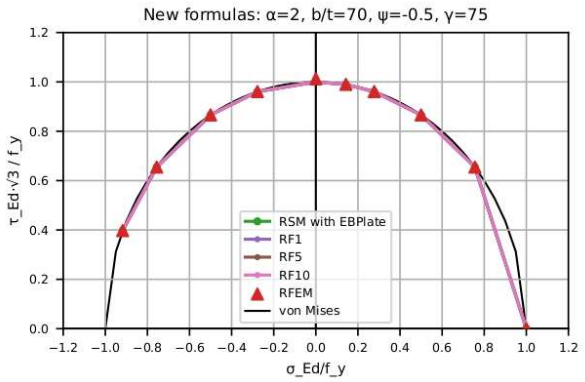
New formulas: α=2, b/t=70, ψ=-0.5, γ=75
τ_Ed·√3 / f_y
σ_Ed/f_y
RSM with EBPlate
RF1
RF5
RF10
RFEM
von Mises

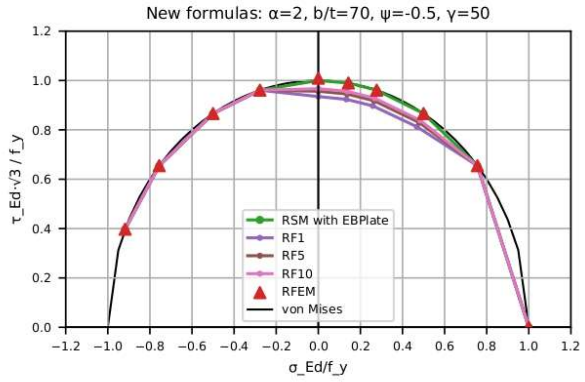
New formulas: α=2, b/t=70, ψ=-0.5, γ=50
τ_Ed·√3 / f_y
σ_Ed/f_y
RSM with EBPlate
RF1
RF5
RF10
RFEM
von Mises

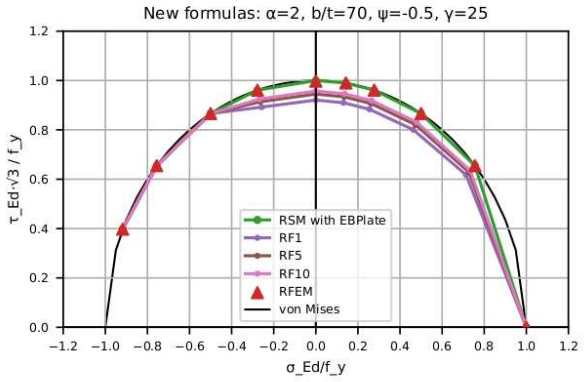
New formulas: α=2, b/t=70, ψ=-0.5, γ=25
τ_Ed·√3 / f_y
σ_Ed/f_y
RSM with EBPlate
RF1
RF5
RF10
RFEM
von Mises

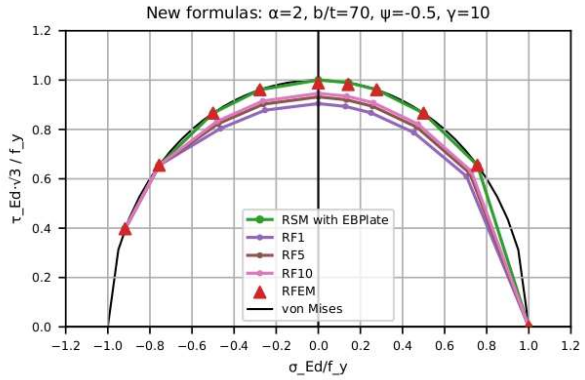
New formulas: α=2, b/t=70, ψ=-0.5, γ=10
τ_Ed·√3 / f_y
σ_Ed/f_y
RSM with EBPlate
RF1
RF5
RF10
RFEM
von Mises

Appendix D: Global vs local buckling classification of stiffened steel plate (α=2, t=6mm, ψ=-0.5, γ=10, and τ/σ=0.5)

1 Basic Objects

1.1 THICKNESSES

Thick. No.	Type	Assigned to Surface No.	Material	Symbol	Thickness Value	Unit	Nodes	Direction
1	Plate | d : 6 mm | Material S355							
	Uniform	10	2	d	6.0	mm		
2	Stiffener | d : 5.6 mm | Material S355							
	Uniform	11	2	d	5.6	mm		

2 Loads

2.1 MODEL

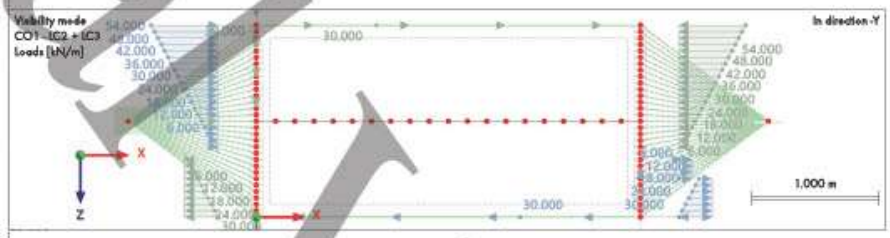

3 Stability Analysis Results

3.1 CRITICAL LOAD FACTORS

Stability Analysis

Mode No.	Critical Load Factor f [–]	Magnification Factor α [–]
	CO1 - LC2 + LC3	
1	4.652	1.274
2	6.308	1.186
3	6.768	1.173
4	7.158	1.162
5	7.923	1.144
6	8.945	1.126
7	10.280	1.108
8	11.513	1.095
9	12.793	1.085
10	13.698	1.079

3.2 MODEL

Stability Analysis

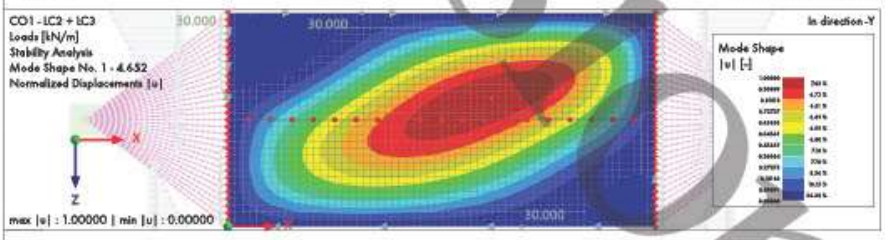

3.3 MODEL — Stability Analysis

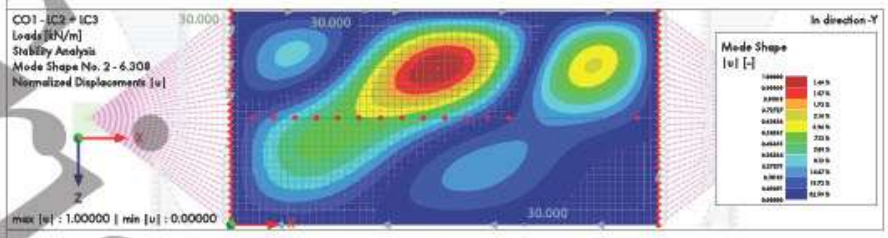

3.4 MODEL — Stability Analysis

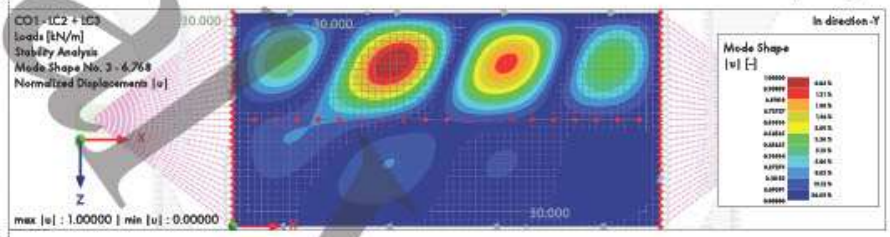

3.5 MODEL — Stability Analysis

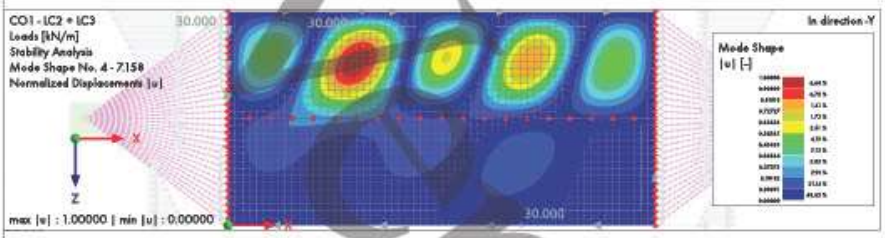

3.6 MODEL — Stability Analysis

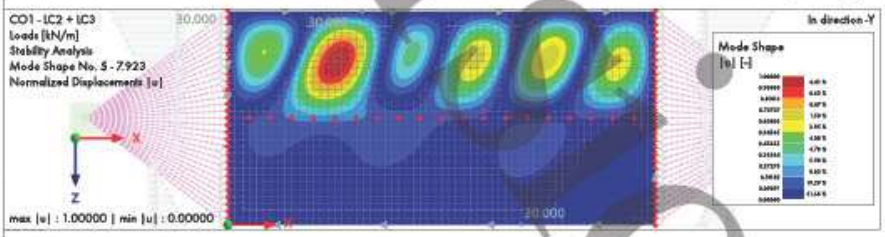

3.7 MODEL — Stability Analysis

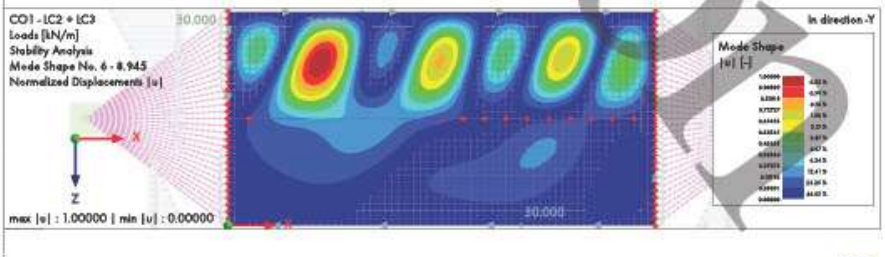

3.8 **MODEL** — **Stability Analysis**

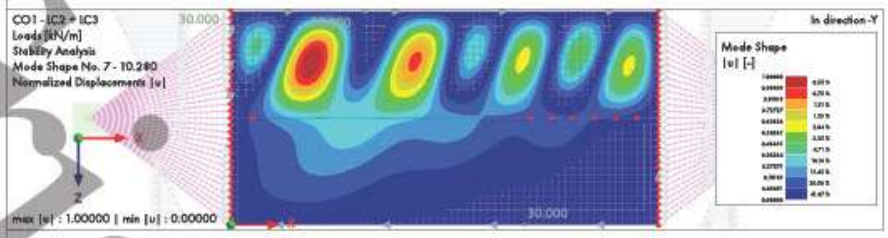

3.9 **MODEL** — **Stability Analysis**

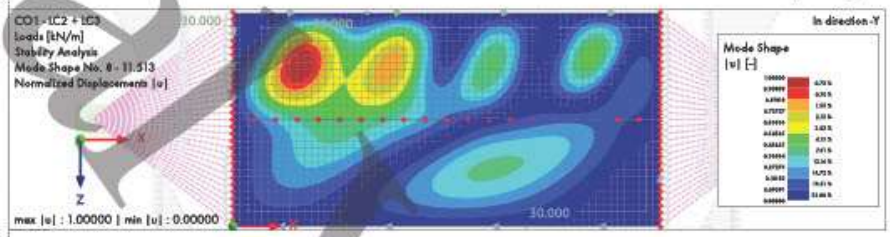

3.10 **MODEL** — **Stability Analysis**

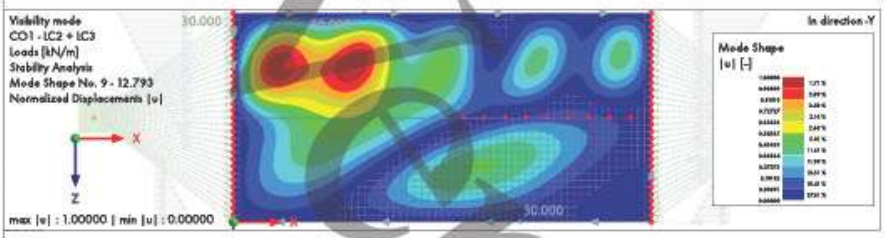

3.11 **MODEL** — **Stability Analysis**

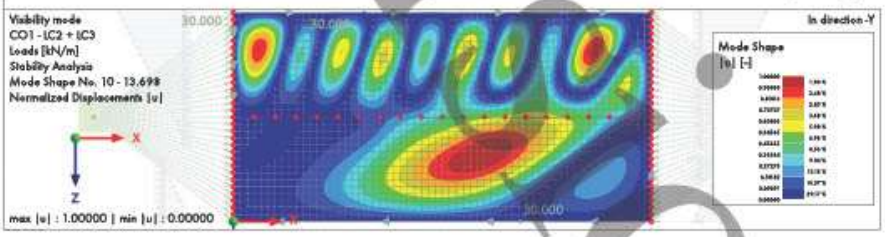

3.12 **NODES - NODES BY MODE SHAPE** — **Stability Analysis**

Mode No.	Node No.	Normalized Displacements [–] ux	uy	uz	Normalized Rotations [–] φx	φy	φz	Node Comment
		CO1 - LC2 + LC3						
1	72	0.00024	-0.15461	0.00001	-0.53502	-0.00180	1.03053	
	73	0.00038	-0.30802	0.00001	-0.97533	-0.00142	1.01077	
	74	0.00042	-0.45813	0.00001	-1.26293	-0.00080	0.95862	
	75	0.00034	-0.59373	0.00001	-1.38055	-0.00016	0.87089	
	76	0.00017	-0.71559	0.00001	-1.34676	0.00038	0.74950	
	77	-0.00008	-0.81715	0.00001	-1.19852	0.00078	0.60093	
	78	-0.00034	-0.89483	0.00001	-0.97497	0.00103	0.43229	
	79	-0.00064	-0.94820	0.00001	-0.70856	0.00117	0.25136	
	80	-0.00095	-0.97001	0.00001	-0.42285	0.00122	0.06586	

3.12 NODES - NODES BY MODE SHAPE

Stability Analysis

Mode No.	Node No.	Normalized Displacements [–] u_X	u_Y	u_Z	Normalized Rotations [–] φ_X	φ_Y	φ_Z	Node Comment
1	81	-0.00125	-0.98612	0.00001	-0.13399	0.00121	-0.11667	
	82	-0.00153	-0.93554	0.00001	0.14845	0.00115	-0.28906	
	83	-0.00178	-0.88029	0.00001	0.40853	0.00105	-0.44465	
	84	-0.00198	-0.80334	0.00001	0.64154	0.00090	-0.57752	
	85	-0.00211	-0.70848	0.00001	0.83200	0.00068	-0.68294	
	86	-0.00218	-0.60006	0.00001	0.96222	0.00038	-0.75789	
	87	-0.00217	-0.48275	0.00001	1.01002	-0.00001	-0.80174	
	88	-0.00208	-0.36103	0.00001	0.95064	-0.00048	-0.81717	
	89	-0.00194	-0.23873	0.00001	0.76224	-0.00100	-0.81092	
	90	-0.00178	-0.11828	0.00001	0.43630	-0.00140	-0.79463	
	CO1 - LC2 + LC3							
2	72	-0.00052	0.08049	-0.00001	0.53775	0.00184	-0.52505	
	73	-0.00060	0.15380	-0.00001	1.00646	0.00137	-0.43797	
	74	-0.00033	0.20755	-0.00001	1.25450	0.00025	-0.26988	
	75	0.00024	0.23091	-0.00001	1.16084	-0.00116	-0.03315	
	76	0.00098	0.21553	-0.00001	0.71124	-0.00241	0.24096	
	77	0.00175	0.16891	-0.00001	-0.00321	-0.00316	0.51020	
	78	0.00240	0.09507	-0.00001	-0.82651	-0.00325	0.73113	
	79	0.00280	-0.05594	-0.00001	-1.58636	-0.00268	0.86800	
	80	0.00290	-0.18970	-0.00001	-2.13450	-0.00161	0.89903	
	81	0.00266	-0.31979	-0.00001	-2.37271	-0.00027	0.81952	
	82	0.00217	-0.43037	-0.00001	-2.26419	0.00111	0.64182	
	83	0.00147	-0.50858	-0.00001	-1.83392	0.00226	0.39259	
	84	0.00070	-0.54632	-0.00001	-1.16147	0.00301	0.10793	
	85	-0.00002	-0.54121	-0.00001	-0.36865	0.00321	-0.17295	
	86	-0.00059	-0.49656	-0.00001	0.39796	0.00280	-0.41459	
	87	-0.00091	-0.42029	-0.00001	0.96980	0.00184	-0.59174	
	88	-0.00096	-0.32302	-0.00001	1.26341	0.00050	-0.69419	
	89	-0.00077	-0.21561	-0.00001	1.20579	-0.00097	-0.72897	
	90	-0.00044	-0.10663	-0.00001	0.74986	-0.00217	-0.71984	
	CO1 - LC2 + LC3							
3	72	0.00027	-0.02664	0.00001	-0.51596	-0.00177	0.16835	
	73	0.00018	-0.04756	0.00001	-0.96575	-0.00114	0.10196	
	74	-0.00022	-0.05425	0.00001	-1.11277	0.00042	-0.01949	
	75	-0.00079	-0.04029	0.00001	-0.77795	0.00226	-0.16739	
	76	-0.00133	-0.00538	0.00001	-0.00331	0.00347	-0.29087	
	77	-0.00159	0.04276	0.00001	0.94150	0.00336	-0.33686	
	78	-0.00141	0.08977	0.00001	1.67169	0.00182	-0.27332	
	79	-0.00080	0.11914	0.00001	1.85446	-0.00066	-0.10500	
	80	0.00008	0.11801	0.00001	1.35634	-0.00314	0.12494	
	81	0.00096	0.08207	0.00001	0.30637	-0.00464	0.34869	
	82	0.00155	0.01750	0.00001	-0.93881	-0.00457	0.49761	
	83	0.00167	-0.06074	0.00001	-1.95125	-0.00293	0.52662	
	84	0.00130	-0.13375	0.00001	-2.38276	-0.00033	0.42963	
	85	0.00060	-0.18474	0.00001	-2.10958	0.00222	0.23999	
	86	-0.00019	-0.20404	0.00001	-1.27355	0.00381	0.01636	
	87	-0.00081	-0.19122	0.00001	-0.21798	0.00389	-0.17997	
	88	-0.00110	-0.15384	0.00001	0.65279	0.00254	-0.30694	
	89	-0.00102	-0.10340	0.00001	1.02456	0.00094	-0.35464	
	90	-0.00073	-0.05042	0.00001	0.76922	-0.00180	-0.34618	
	CO1 - LC2 + LC3							
4	72	-0.00034	0.03508	-0.00001	0.64001	0.00196	-0.21931	
	73	-0.00015	0.06173	-0.00002	1.07483	0.00056	-0.12507	
	74	0.00038	0.06933	-0.00002	0.94794	-0.00187	0.02983	
	75	0.00099	0.05253	-0.00002	0.16349	-0.00379	0.19048	
	76	0.00134	0.01562	-0.00001	-0.93160	-0.00381	0.28897	
	77	0.00122	-0.02860	-0.00001	-1.73113	-0.00165	0.28526	
	78	0.00069	-0.06524	-0.00001	-1.74914	0.00158	0.19365	
	79	0.00007	-0.08542	-0.00001	-0.93738	0.00402	0.07652	
	80	-0.00028	-0.09100	-0.00002	0.26208	0.00420	0.00874	
	81	-0.00014	-0.09312	-0.00002	1.16568	0.00197	0.03323	
	82	0.00042	-0.10513	-0.00002	1.24994	-0.00141	0.13461	
	83	0.00108	-0.13401	-0.00002	0.46302	-0.00399	0.24688	
	84	0.00145	-0.17540	-0.00001	-0.74283	-0.00429	0.29107	
	85	0.00129	-0.21506	-0.00001	-1.67868	-0.00217	0.22047	
	86	0.00067	-0.23601	-0.00001	-1.82495	0.00109	0.04707	
	87	-0.00010	-0.22714	-0.00001	-1.13281	0.00357	-0.16606	
	88	-0.00066	-0.18837	-0.00001	-0.04413	0.00384	-0.34119	
	89	-0.00078	-0.12957	-0.00002	0.77056	0.00176	-0.42929	
	90	-0.00050	-0.06397	-0.00002	0.79162	-0.00131	-0.43618	
	CO1 - LC2 + LC3							
5	72	0.00029	-0.04187	0.00002	-0.86391	-0.00251	0.26424	
	73	0.00000	-0.07499	0.00002	-1.36864	-0.00029	0.16610	

3.12 NODES - NODES BY MODE SHAPE

Stability Analysis

Mode No.	Node No.	Normalized Displacements [–] u_x	u_y	u_z	Normalized Rotations [–] φ_x	φ_y	φ_z	Node Comment
5	74	-0.00061	-0.08894	0.00002	-1.03242	0.00289	0.01686	
	75	-0.00114	-0.08170	0.00002	0.05952	0.00440	-0.10360	
	76	-0.00117	-0.06345	0.00001	1.14884	0.00272	-0.12285	
	77	-0.00067	-0.05060	0.00001	1.40612	-0.00101	-0.03602	
	78	-0.00002	-0.05457	0.00002	0.64112	-0.00387	0.08858	
	79	0.00034	-0.07435	0.00002	-0.52121	-0.00362	0.16410	
	80	0.00021	-0.09907	0.00002	-1.15774	-0.00061	0.15413	
	81	-0.00016	-0.11811	0.00002	-0.81877	0.00251	0.09752	
	82	-0.00034	-0.12999	0.00002	0.10181	0.00305	0.06863	
	83	-0.00007	-0.14251	0.00001	0.71251	0.00056	0.10742	
	84	0.00046	-0.16404	0.00001	0.39245	-0.00279	0.17961	
	85	0.00081	-0.19358	0.00002	-0.67077	-0.00407	0.20165	
	86	0.00060	-0.21828	0.00002	-1.63111	-0.00206	0.11019	
	87	-0.00011	-0.22115	0.00002	-1.69625	0.00167	-0.08236	
	88	-0.00089	-0.19271	0.00002	-0.80238	0.00405	-0.29305	
	89	-0.00126	-0.13734	0.00001	0.30966	0.00305	-0.43087	
	90	-0.00108	-0.06905	0.00001	0.67961	-0.00044	-0.46645	
		CO1 - LC2 + LC3						
6	72	0.00039	-0.04827	0.00002	-0.82027	-0.00200	0.29977	
	73	0.00003	-0.08448	0.00002	-1.08999	0.00098	0.16975	
	74	-0.00063	-0.09662	0.00002	-0.35176	0.00410	-0.00882	
	75	-0.00102	-0.08462	0.00002	0.92082	0.00403	-0.13903	
	76	-0.00088	-0.06030	0.00001	1.62251	0.00055	-0.17192	
	77	-0.00049	-0.03568	0.00002	1.17458	-0.00292	-0.15475	
	78	-0.00039	-0.01157	0.00002	0.16840	-0.00290	-0.17617	
	79	-0.00078	0.02109	0.00002	-0.26505	0.00033	-0.26700	
	80	-0.00130	0.06891	0.00002	0.32191	0.00303	-0.36536	
	81	-0.00142	0.12624	0.00001	1.22572	0.00218	-0.38400	
	82	-0.00106	0.17875	0.00001	1.39297	-0.00126	-0.30495	
	83	-0.00061	0.21626	0.00002	0.60192	-0.00340	-0.19663	
	84	-0.00054	0.24047	0.00002	-0.28444	-0.00178	-0.13499	
	85	-0.00084	0.25920	0.00002	-0.27393	0.00189	-0.11689	
	86	-0.00101	0.27349	0.00002	0.64886	0.00358	-0.06290	
	87	-0.00064	0.27243	0.00001	1.49259	0.00141	0.09212	
	88	0.00014	0.24188	0.00001	1.34529	-0.00226	0.31975	
	89	0.00076	0.17824	0.00002	0.38811	-0.00337	0.51780	
	90	0.00079	0.09242	0.00002	-0.28756	-0.00084	0.60969	
		CO1 - LC2 + LC3						
7	72	-0.00020	0.04359	-0.00003	1.01178	0.00252	-0.27621	
	73	0.00017	0.07873	-0.00003	1.35759	-0.00087	-0.18276	
	74	0.00068	0.09755	-0.00002	0.59511	-0.00373	-0.07237	
	75	0.00076	0.10493	-0.00002	-0.45233	-0.00236	-0.04125	
	76	0.00035	0.11482	-0.00002	-0.54839	0.00157	-0.09913	
	77	-0.00001	0.13448	-0.00002	0.30800	0.00293	-0.15659	
	78	0.00009	0.15796	-0.00003	0.87396	0.00013	-0.14720	
	79	0.00035	0.17742	-0.00002	0.37493	-0.00271	-0.11511	
	80	0.00021	0.19611	-0.00002	-0.43365	-0.00147	-0.14577	
	81	-0.00038	0.22452	-0.00002	-0.33602	0.00221	-0.23638	
	82	-0.00076	0.26478	-0.00002	0.63455	0.00325	-0.26782	
	83	-0.00058	0.30480	-0.00003	1.23176	0.00020	-0.23040	
	84	-0.00013	0.33054	-0.00002	0.72740	-0.00271	-0.10868	
	85	0.00002	0.33943	-0.00002	-0.07871	-0.00146	-0.01553	
	86	-0.00014	0.33703	-0.00002	0.01991	0.00213	0.04728	
	87	-0.00008	0.32237	-0.00003	0.94799	0.00296	0.16053	
	88	0.00054	0.28362	-0.00003	1.45239	-0.00019	0.36719	
	89	0.00128	0.21124	-0.00002	0.86279	-0.00296	0.59223	
	90	0.00151	0.11115	-0.00002	0.03872	-0.00172	0.72434	
		CO1 - LC2 + LC3						
8	72	-0.00039	0.06218	-0.00001	0.44917	0.00046	-0.39307	
	73	-0.00014	0.11329	-0.00002	0.26729	-0.00214	-0.27789	
	74	0.00023	0.14400	-0.00001	-0.57863	-0.00325	-0.13159	
	75	0.00041	0.15418	-0.00001	-1.29903	-0.00156	-0.00843	
	76	0.00051	0.14710	-0.00001	-1.33485	0.00039	0.10402	
	77	0.00082	0.12126	-0.00001	-1.12071	0.00004	0.24508	
	78	0.00130	0.07273	-0.00001	-1.31396	-0.00129	0.39976	
	79	0.00159	0.00389	-0.00001	-1.71870	-0.00071	0.50786	
	80	0.00160	-0.07595	-0.00001	-1.63696	0.00137	0.54823	
	81	0.00161	-0.15919	-0.00001	-1.05606	0.00191	0.59024	
	82	0.00179	-0.24394	-0.00001	-0.72053	0.00018	0.56744	
	83	0.00191	-0.32696	-0.00001	-0.96343	-0.00103	0.52864	
	84	0.00166	-0.39745	-0.00001	-1.20225	0.00009	0.39749	
	85	0.00115	-0.44236	-0.00001	-0.92060	0.00143	0.19501	
	86	0.00073	-0.45534	-0.00001	-0.52945	0.00049	-0.02135	
	87	0.00041	-0.43591	-0.00001	-0.69852	-0.00148	-0.23951	

3.12 NODES - NODES BY MODE SHAPE

Stability Analysis

Mode No.	Node No.	Normalized Displacements [–] u_X	u_Y	u_Z	Normalized Rotations [–] φ_X	φ_Y	φ_Z	Node Comment
8	88	-0.00008	-0.38158	-0.00001	-1.24532	-0.00140	-0.49051	
	89	-0.00078	-0.28732	0.00000	-1.37875	0.00082	-0.78534	
	90	-0.00125	-0.15497	-0.00001	-0.83973	0.00255	-0.98410	
		CO1 - LC2 + LC3						
9	72	0.00024	-0.04332	-0.00001	0.35603	0.00141	0.28229	
	73	0.00038	-0.08380	-0.00001	0.71920	0.00093	0.25442	
	74	0.00040	-0.11786	-0.00001	0.80221	0.00031	0.19215	
	75	0.00013	-0.13797	0.00000	0.89154	0.00115	0.09665	
	76	-0.00035	-0.13559	-0.00001	1.36723	0.00206	-0.10056	
	77	-0.00072	-0.10850	-0.00001	1.86958	0.00101	-0.25627	
	78	-0.00097	-0.05993	-0.00001	1.84583	-0.00076	-0.38903	
	79	-0.00134	0.00846	0.00000	1.52026	-0.00078	-0.52321	
	80	-0.00179	0.09852	0.00000	1.47509	0.00022	-0.64550	
	81	-0.00204	0.19854	-0.00001	1.80068	-0.00022	-0.70195	
	82	-0.00199	0.30251	-0.00001	1.35306	-0.00162	-0.67305	
	83	-0.00187	0.39766	-0.00001	0.83010	-0.00147	-0.58969	
	84	-0.00176	0.47719	-0.00001	0.65896	0.00015	-0.46292	
	85	-0.00142	0.53243	-0.00001	0.88755	0.00065	-0.29089	
	86	-0.00078	0.55099	-0.00001	0.95907	-0.00029	0.02234	
	87	-0.00005	0.52425	-0.00001	0.77431	-0.00026	0.33360	
	88	0.00051	0.45197	-0.00001	0.87559	0.00112	0.62614	
	89	0.00104	0.33714	-0.00001	1.32492	0.00093	0.90289	
	90	0.00155	0.18251	-0.00002	1.25519	-0.00228	1.14908	
		CO1 - LC2 + LC3						
10	72	0.00069	-0.17009	0.00006	-1.88030	-0.00308	1.10357	
	73	0.00024	-0.32227	0.00006	-1.70454	0.00474	0.90494	
	74	-0.00033	-0.43994	0.00004	0.31473	0.00701	0.66864	
	75	-0.00042	-0.52625	0.00004	1.62166	0.00226	0.48736	
	76	-0.00072	-0.58382	0.00005	1.48789	0.00023	0.26706	
	77	-0.00165	-0.60119	0.00005	1.82856	0.00337	-0.04106	
	78	-0.00238	-0.57449	0.00004	3.04932	0.00295	-0.29507	
	79	-0.00228	-0.52081	0.00004	3.15235	-0.00266	-0.40194	
	80	-0.00217	-0.45573	0.00005	1.80607	-0.00431	-0.46879	
	81	-0.00252	-0.37799	0.00005	1.14184	-0.00019	-0.56791	
	82	-0.00260	-0.28967	0.00004	1.64791	0.00063	-0.58947	
	83	-0.00196	-0.20874	0.00004	1.36114	-0.00361	-0.47576	
	84	-0.00144	-0.14676	0.00005	-0.03217	-0.00396	-0.36131	
	85	-0.00157	-0.09545	0.00005	-0.45408	0.00110	-0.33143	
	86	-0.00159	-0.04882	0.00004	0.45723	0.00240	-0.27827	
	87	-0.00104	-0.01700	0.00004	0.64478	-0.00168	-0.13859	
	88	-0.00067	-0.00527	0.00005	-0.26241	-0.00226	-0.03224	
	89	-0.00090	-0.00169	0.00005	-0.34727	0.00163	-0.02534	
	90	-0.00102	0.00164	0.00003	0.41276	0.00101	-0.01093	